UNIVERSITY OF SOUTHAMPTON.

BASE ANALOGUES AND LIGANDS FOR STABILISING TRIPLE HELICAL NUCLEIC ACIDS.

Richard Anthony James Darby.

Thesis submitted for the degree of

Doctor of Philosophy

Division of Biochemistry & Molecular Biology,

Faculty of Science.

May 2002

UNIVERSITY OF SOUTHAMPTON
ABSTRACT
FACULTY OF SCIENCE
SCHOOL OF BIOLOGICAL SCIENCES

Doctor of Philosophy
Base Analogues and Ligands for Stabilising Triple Helical Nucleic Acids.
Richard Anthony James Darby

Triplex formation offers the opportunity to develop sequence specific oligonucleotides for regulating gene activity or for use as biomolecular tools. In this strategy a synthetic oligonucleotide binds within the major groove of duplex DNA, where it makes specific contacts with substituents of the bases. Although these complexes form with high sequence specificity, their use is limited by several factors including their low stability, a requirement for low pHs, and the requirement for oligopurine tracts. The work presented in this thesis examines several DNA base analogues which might be used to overcome these restrictions.

DNase I footprinting has demonstrated that the thymidine analogues 5-propargylamino dU, 2'-aminoethoxy T, 5-propynyl dU, and 5-aminopropyl dU, do not significantly increase triplex stability when incorporated at only two positions within a 9-mer oligonucleotide. More stable triplexes are generated using oligonucleotides substituted at four positions and examined at pH 5. However oligonucleotides substituted with the bis-modified thymidine analogue 2'-aminoethoxy-5-propargylamino U form stable triplexes at both pH 5 and 7.5, with only three substitutions. Furthermore 5-propargylamino dU cannot be used to stabilise GT containing triplexes formed in either the parallel or antiparallel orientation. Similarly the cytidine analogue 5-aminohexyl dC does not appear to enhance parallel triplex formation.

The requirement for recognition of an uninterrupted polypurine tract has been examined using two charged abasic analogues, 1'-β-hexylaminoribose, and 1'-methoxy, 2'-aminoethoxyribose. However these do not increase the stability of parallel triplexes across a central pyrimidine base compared to the abasic analogue 1',2-H-dideoxyribose.

Triplex stability may also be enhanced by the use of triplex binding ligands. It is demonstrated that some proflavine derivatives stabilise triplexes containing adjacent T·AT triplets. Furthermore it is shown that the alpha anomer of naphthoflavone stabilises parallel triplexes independent of the DNA sequence. It appears that positively charged ligands are selective for T·AT triplets, while neutral ligands bind to both T·AT and C^+·GC.

This thesis also describes a novel method for measuring DNA thermal denaturation profiles. This technique uses synthetic oligonucleotides containing a fluorophore and quencher which are positioned so that folded complexes have weak fluorescence, which is greatly enhanced upon denaturation. The fluorescent melting profiles are measured using a Roche LightCycler. This technique has been successfully employed for examining the stabilising effect of base analogues and triplex stabilising ligands.

Contents.

Chapter 2 - Materials & Methods.

Chapter 3 - Base Analogues to Stabilise Triplex DNA.

Chapter 4 - Triple Helical DNA Stabilising Ligands.

Chapter 5 - Triplex and Duplex DNA Thermal Denaturation Profiles Measured using Fluorescently Labelled Oligonucleotides.

Chapter 6 - Conclusions.

References.

Figure List.

Table List.

<u>Preface.</u>

Abbreviations.

A	Adenine
AMPs	20 % Ammonium Persulphate
ATP	Adenosine Triphosphate
C	Cytosine
DNA	Deoxyribonucleic Acid
DNase I	Deoxyribonuclease I
EDTA	Ethylenediaminetetracetic Acid
G	Guanine
IPTG	Isopropyl β D-thiogalactopyranoside
NaOAc	Sodium Acetate
OD	Optical Density
R	Purine
RNA	Ribonucleic Acid
T	Thymine
TBE	Tris, Borate, EDTA; 5 x buffer
TEMED	N,N,N',N'-Tetramethylethylenediaamine
TFO	Triplex Forming Oligonucleotide
Tm	Melting Temperature
Tris	Tris-Hydroxymethyl-aminomethane
UV	Ultra Violet
X-Gal	5-Bromo-4-chloro-3-indolyl β-D-galactoside
Y	Pyrimidine

The notation used throughout this thesis for triplexes is as follows; the third strand oligonucleotide is represented by the first letter, the Hoogsteen hydrogen bonds are designated by ·, the second and third letters represent the purine and pyrimidine strands of the duplex respectively.

Chapter 1 - Introduction.

(1.1) The Genome and Genetic Diseases.

Genetic diseases are caused by alteration to the genetic sequence of a genome and these mutations can be either acquired or inherited. The human genome is comprised of approximately 6×10^9 base pairs per diploid cell, and many mutations occur within this most of which do not cause any effects. However some mutations result in alteration to the coding sequence or in control regions producing non-functional or inappropriately expressed proteins, which may manifest as a disease. Mutations can also result in the chromosomes themselves being broken, lost, or multiplied, all of which can result in disease states including Downs syndrome, and cancer.

It has been estimated that approximately one person in five world wide will suffer from cancer and this rate is increasing due to increasing longevity. During the last century much research has been carried out to identify potential causes of cancer and to understand the modes of action of carcinogens. This increase in our knowledge of the causes of cancer has not been matched by improvements in treatment, with cancer therapy still a relatively blunt instrument which merely kill rapidly dividing cells, as discussed below. There is therefore a need for developing novel gene specific agents directed at particular disease processes. This thesis describes *in vitro* studies on one strategy for targeting specific regions of duplex DNA with triplex forming oligonucleotides.

(1.1.1) What Is Cancer?

Cells of a multicellular organism, unlike those of single celled organisms such as bacteria grow and divide in a controlled fashion and are organised to achieve prosperity for the entire organism. Cellular mutations that result in uncontrolled cell growth in which individual cells prosper at the expense of other cells within the organism leads to

the formation of cancer. Cancers can be found in almost any part of the body and range benign tumours to malignant tumours. They can spread with speed or remain undetected for years. Some individuals are predisposed towards specific cancers, and many proto-oncogenes have been identified that when mutated to oncogenes, play a role in cancer formation. These mutated genes cause an increase in cellular growth by stimulating autocrine growth factor production, cell proliferation pathways, and causing abnormal growth factor receptors to be produced (Alberts *et al* 1994). From a histological prospective cancerous tissue is often seen to regress to a state of undifferentiation, similar to that seen in embryo-genesis, and it is due to this that recognition by the immune system is compromised. A number of treatments have been devised to combat cancer, most of which are highly cytotoxic agents that inhibit cell replication and are not selective for tumour cells.

Early prognosis of cancer is critical, and if it is detected before the tumour can metastasize then it may be possible to remove it via surgery depending upon its position and size. However even the removal of the tumour and some surrounding tissue may not guarantee against secondary tumour formation. This is because if even a single cancerous cell remains, it possesses the ability to initiate tumour formation.

(1.1.2)   Chemotherapy.

Cancer is usually treated by a combination of surgery, radiotherapy and chemotherapy; the later of which is related to the subject matter of this thesis.

Chemotherapy is based on the use of drugs to target and kill tumour cells. However most of these agents are not selective for cancerous cells and are merely cytotoxic agents that act against all rapidly dividing cells. Many tumours have higher than normal cell turnover, explaining the selectivity of these drugs. However these drugs are not tumour specific and they are toxic to normal fast dividing cells such as those of the gut lining, hair follicles, and the haemopoietic system, resulting nausea, hair loss, and anaemia. Some of these agents directly inhibit DNA replication, preventing cell growth,

but there is now considerable evidence that many compounds act by activating apoptotic pathways, particularly those involving p53. However many tumours have inactivated genes within the p53 pathway (Jones 2001) resulting in a poor response to these drugs.

(1.1.2.1)   Antimetabolites.

These are compounds that inhibit essential metabolic pathways, often involved in nucleic acid synthesis. Three classes of antimetabolites are used for cancer therapy; antifolates, pyrimidine and purine antimetabolites.

The original antifolate was 4-aminofolate, (Farber *et al* 1948) but has since been superseded by methotrexate. Methotrexate is an antagonist of folate metabolism acting via the inhibition of dihydrofolate reductase, resulting in an intracellular decrease in the level of tetrahydrofolate (Futterman *et al* 1957). This in turn causes a decrease in the production of thymidylate and purines thereby preventing DNA synthesis and cellular division. However methotrexate has no selectivity for cancer cells, and its action is dependent upon cell proliferation rates, with its cytotoxic effects being concentrated in cells with high rates of DNA synthesis.

6-Mercaptopurine is an example of a purine antimetabolite that is an analogue of hypoxanthine in which the exocyclic oxygen atom is replaced with sulphur. This compound prevents purine synthesis and interconversion of purine nucleosides once phosphorylated to thioinosinate via hypoxanthine-guanine phosphoribosyltransfrease. Thioinosinate acts as a competitive inhibitor preventing the production of inosinate, which in turn prevents the production of xanthine monophosphate and AMP. Once 6-mercaptopurine has been metabolised it has also been shown to be incorporated into DNA and may prevent further DNA replication.

5-fluorouracil was developed as a pyrimidine analogue, with a fluorine atom substituted at the C5 position of uracil. This is converted to 5-fluorodeoxyuridine monophosphate which efficiently inhibits the production of thymidine monophosphate

by thymidylate synthase.

(1.1.2.2) Alkylating Compounds.

These compounds are highly reactive nucleophiles which generate covalently bound alkylated products. The use of alkylating agents as anticancer drugs followed the observation that sulphur mustard displayed cytotoxicity towards the lyphoid vessels and organs (Gilman *et al* 1946). Since then several such agents have been developed and clinically applied to a wide variety of tumours including; melphalan, chlorambucol, cyclophosphamide, busuplhan, triethylenethiophosphoramide, and dicarbazine. Each of these agents is a bifunctional DNA alkylator causing interstrand cross-linking, thereby preventing separation of the two DNA strands.

(1.1.2.3) Platinum Compounds.

Since the initial discovery by Rosenberg *et al* 1965 that the cis isomer of dichlorodiamineplatinum (cisplatin) could prevent cell division, much research has been conducted into organoplatinum compounds. It was later shown that cisplatin had anticancer activity towards a variety of cancers (Rosenberg *et al* 1969) including testicular, ovarian, and cancer of the bladder. It acts like an alkylating agent reacting with nucleophiles in DNA causing inter- and intrastrand cross-linking probably between the O6 and N7 of adjacent guanine molecules (Pinto & Lippard 1985). More recently cisplatin has been shown to have an effect on cervical cancer when used in conjunction with radiotherapy. Cisplatin is believed to inhibit the repair of radiation induced damage, shrinking the tumour and further sensitising it towards radiation (Rose *et al* 1999, Thomas 1999, Morris *et al* 1999). However cisplatin has also been shown to react with sulphur containing nucleophiles, and may explain its high nephrotoxic effects, by binding to the SH groups in the kidney tubules. Furthermore cisplatin causes severe nausea and vomiting, and as such treatment with cisplatin requires the administration of diuretics and drugs to control the nausea and vomiting.

(1.1.2.4)   Topoisomerase Inhibitors.

Topoisomerase I is a ubiquitous DNA-cleaving enzyme that generates single strand breaks in the double helix in order relax DNA supercoiling. The reaction of topoisomerase I with duplex DNA produces a covalent 3'-phosphotyrosine linkage that is usually religated in a fast step following relaxation of the DNA (Wang 1996). Derivatives of the antitumor alkolid camptothecin (CPT), including Irinotecan and Hycamtin are used to treat colon and ovarian cancers respectively, and prevent the religation step. These drugs prevent DNA relaxation and enhance the production of DNA strand breaks, leading to cell death (Pommier *et al* 1998). Furthermore the antibiotic Rebeccamycin (RBC) and its indolocarbazole derivatives have been shown to enhance topoisomerase I cleavage (Anizon *et al* 1997, Bailly *et al* 1997, Moreau *et al* 1998). RBC and indolocarbazole conjugated oligonucleotides have also been shown to increase the effects of the compounds in a sequence specific manner by generating triplex structures (Arimondo *et al* 2000, 2001).

Topoisomerase II is an enzyme that transiently cleaves and reseals both DNA strands simultaneously, and allows passage of a separate double helix through the break site. Therefore topoisomerase II may be involved in i) separating entwined DNA strands, ii) removing excessive supercoiling, and iii) catenating double-stranded DNA circles (Liu *et al* 1980, Baldi *et al* 1980, Hsieh & Brutlag, 1980). The antitumor agents, Etoposide and *m*-AMSA, have been shown to stabilise the topoisomerase II-DNA cleavage complex by preventing the religation step (Osheroff 1989, Nelson *et al* 1984, Tewey *et al* 1984, Pommier *et al* 1985). It has also been suggested that daunomycin, adriamycin, and mitoxantrone also act through topoisomerase inhibition (Gupta 1983, Glisson *et al* 1985)

(1.1.2.5) Inhibitors of Mitosis & Antibiotics.

Some alkaloid compounds, including vincristine and vinblastine, have been shown to disrupt metaphasic activity by preventing the formation of microtubules, and subsequently the mitotic spindle (Bensch & Malawista 1969, Marantz & Shelanski 1970, David-Pfeuty *et al* 1979, Safa *et al* 1987). These two compounds are believed to bind to tubulin (George *et al* 1965, Safa *et al* 1987), an active component of the microtubules, with the loss of spindle formation leading to unorganised segregation of the genetic material during cell division. Taxol is another agent which acts on microtubules, promoting their aggregation (Schiff & Horwitz 1980, Manfredi *et al* 1982).

A wide variety of antibiotics are used as anticancer agents. These include daunomycin and adriamycin which are DNA intercalators, bleomycin which promotes DNA cleavage (Umezawa *et al* 1966, 1968), mithramycin which binds to DNA preventing RNA synthesis (Kersten *et al* 1966), and actinomycin D which also binds to DNA (Gale *et al* 1981).

(1.1.2.6) Limitations With Cancer Therapy.

As can be seen there are limitations with all forms of cancer therapy and it is for these reasons that cancers are usually treated using combination therapy such as surgery or radiotherapy to remove/destroy the majority of the tumour, followed by a course of chemotherapy to attempt to eradicate any lingering abnormal cells. In addition chemotherapeutic regimes usually employ a cocktail of drugs with the aim of increasing their therapeutic effects whilst limiting their toxicity.

A fundamental problem associated with the design of anticancer drugs is the requirement for sequence specificity. That is to say that a drug must be able to distinguish between genetic sequences of similar composition *in vivo* and bind only to the target sequence in cancer cells so as to limit/prevent normal cell toxicity. Many drugs are known to interact with DNA but generally tend to have short recognition sequences
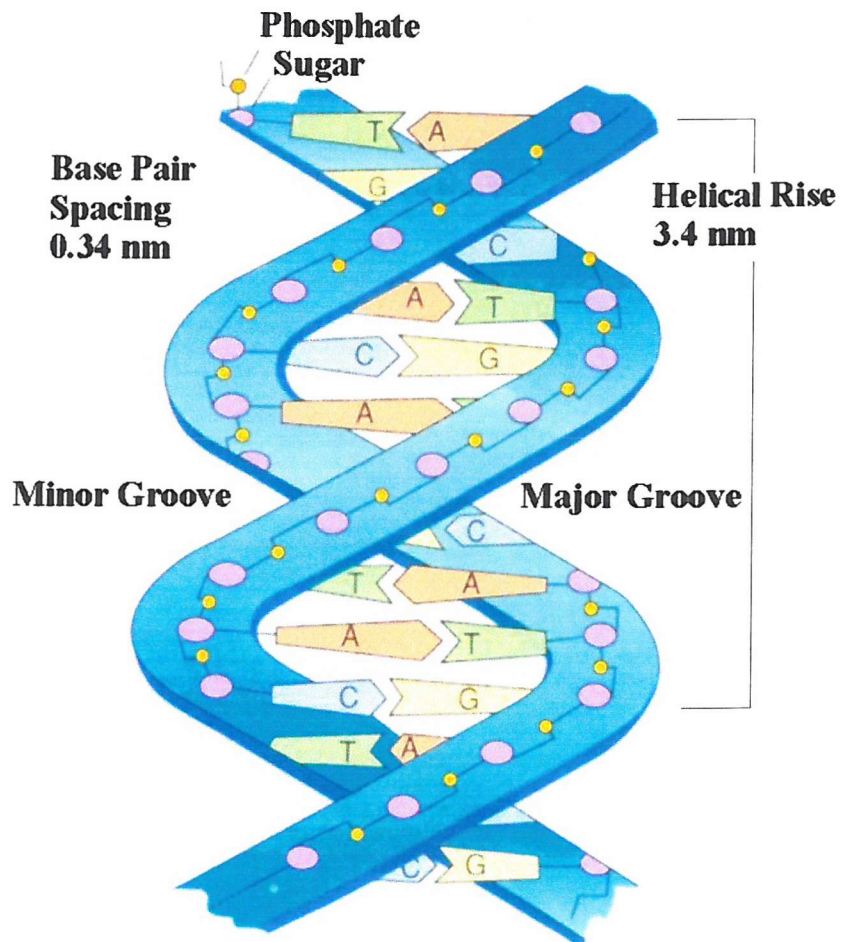
Figure 1.1: A ribbon model representing B-DNA The ribbons correspond to the antiparallel sugar phosphate backbones with the purple and yellow dots representing the sugar moieties and phosphate molecules respectively. The major and minor grooves are highlighted, and the base pairing scheme illustrated. The helical rise and base pair spacing is also shown. Reproduced from Zubay, G. - Biochmistry 3rd Ed.

(a)

Minor Groove

Major Groove

B-DNA

Minor Groove

Major Groove

A-DNA

(b)

C-5′   O   C-2′   Base   C-2′-endo

C-4′   C-1′

C-3′

C-5′   C-3′   O   Base   C-3′-endo

C-4′   C-1′

C-2′

(c)

Minor Groove

Major Groove

Z-DNA

B-DNA

Figure 1.2: (a) shows the A and B forms of DNA with the major and minor grooves illustrated. Diagram (b) shows the C-2'-endo and C-3'-endo sugar puckers of B-DNA and A-DNA respectively. Diagram (c) shows the space filled models of Z and B-DNA. The irregularity of Z-DNA, compared to B-DNA is illustrated by the solid black line adjoining the phosphate molecules. Reproduced from Zubay, G., - Biochemistry 3rd Ed.

of between 2-4 base pairs, examples include actinomycin (GpC), echinomycin (CpG), distamycin (A/T)$_4$, and Hoechst 33258 (A)$_4$. However in order to recognise a unique genetic sequence within the human genome, requires sequence recognition of a 17 base pair region (Thuong *et al* 1993). Thus in order to recognise these longer genetic sequences the antisense and antigene strategies are being developed.

(1.2.) Deoxyribonucleic Acid (DNA).

Double-stranded DNA is a polymorphic molecule which encompasses three distinct structural forms A, B, and Z-DNA (Figs. 1.1 - 1.2). The flexibility of the furanose ring of the sugar moiety and several rotational bonds within the sugar phosphate backbone give rise to the various conformations of duplex DNA. The B and A-forms are both right handed helices with 10 and 11 base pairs per helical turn which form under conditions of high and low humidity respectively. Cellular DNA is believed to be predominantly in the B-conformation, with a C-2'-endo sugar pucker (Fig. 1.2), however dehydrating the DNA forces the DNA helices closer together and the sugar pucker changes to C-3'-endo, known as A-DNA (Fig. 1.2). Z-DNA is a left handed helix with twelve base pairs per helical turn that is usually composed of alternating purine and pyrimidine residues in *Anti* and *Syn* conformations respectively. This results in the sugar-phosphate backbone adopting a zigzag nature (Fig. 1.2).

The 3.4Å distance between the planes of B-DNA allows favourable stacking interactions between the base pairs. These interactions include Van der Waals forces and dipole-dipole interactions producing stacking energies comparable to the base pair hydrogen bonds and therefore results in maximised stacking within the duplex. The nucleotide bases are conserved towards the centre of the duplex, with the negatively charged phosphate groups located on the outer surface of the helix where they have minimum electrostatic repulsion and can be further neutralised via interaction with chromosomal proteins, cations, and polyamines.

(1.2.1) Triplex DNA.

Triple helices were again discovered over 40 years ago (Felsenfeld *et al* 1957), but remained little more than a laboratory based abnormality until 1987. The first triplex discovered was formed using a RNA polyadenine·polyuracil duplex (A·U) which was associated with a RNA polyuracil third strand. The bonds within this triplex consisted of the usual Watson & Crick hydrogen bonds between the adenine and uracil bases in the duplex, with a further two hydrogen bonds formed to the N7 and N4 atoms of the adenine residues from the N3 and O4 atoms of the uracils in the third strand. These were later termed Hoogsteen hydrogen bonds (Fig. 1.3), and are also formed in the C^+·GC, and T·AT triplets discussed in section 1.3.1

It was not until 1987 when the potential of triple helix DNA was realised (Moser & Dervan 1987) when experiments showed that sequence specific cleavage of dsDNA was possible via the formation of a triplex. In this study, polypyrimidine oligonucleotides were prepared with a single thymidine-EDTA·Fe at the 5' terminal position. The EDTA·Fe moiety caused cleavage of the duplex backbone via hydroxyl radical action therefore producing sequence specific ds-breaks. Specificity was demonstrated as an oligonucleotide with a single base mismatch generated significantly weaker cleavage patten maps.

At the same time a separate group demonstrated that the α-anomers of thymidylate could recognise an 8 base pair A·T tract within a 27 base pair duplex. The third strand was again covalently linked to a cleaving agent at the 5' terminal base (3-azideproflavine derivative). The third strand was photocross-linked to the duplex using visible light and treated with piperidine to induce cleaving at the cross-linked sites. The results showed cleavage at well defined sites only, and indicated sequence specific binding of the oligonucleotide to the 8 base pair A·T tract.
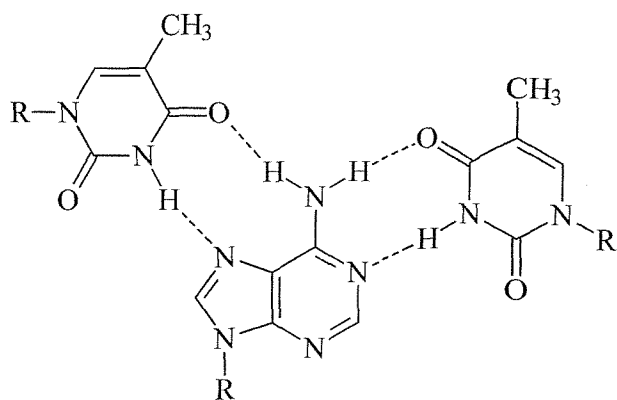
T·AT Triplet
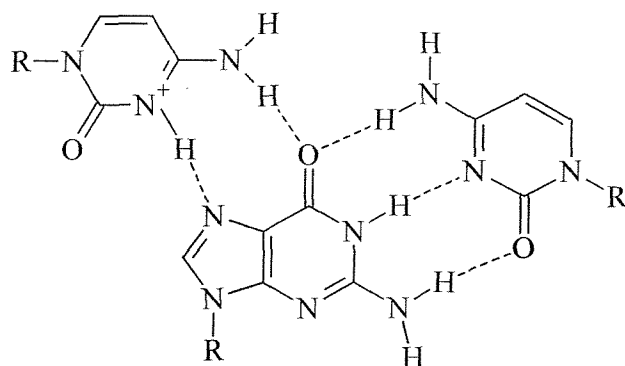
C⁺·GC Triplet
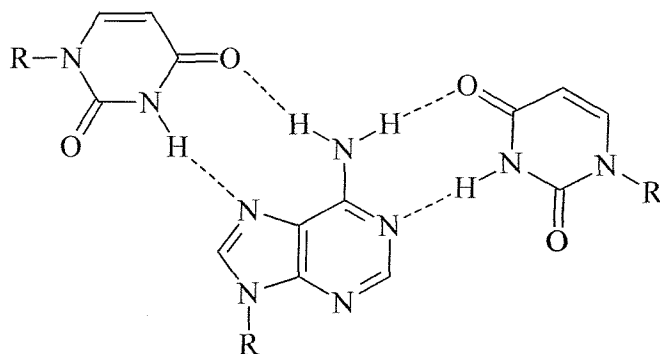
U·AU Triplet

Figure 1.3: Diagrams representing the hydrogen bonding schemes of parallel triplets. The base to the left in each diagram represents the Hoogsteen hydrogen bonded base of the third strand. The central base is that of the purine base in the duplex, with the right-hand base representing the pyrimidine base of the duplex. Note that the third strand cytosine in the C⁺·GC triplet is in its protonated state.

The results of both experiments contributed to the theory that triplex formation may be used to target specific DNA sequences. This theory was further validated in 1988 when Coony *et al* demonstrated down regulation of c-myc transcription *in vitro* at physiological pH. This was achieved via the formation of a 27mer antiparallel triplex 115 base pairs upstream of the P1 origin of transcription site (Coony *et al* 1988).

(1.2.2) Oligonucleotides As Sequence Specific Agents.

Within the last ten to fifteen years there has been an explosion of interest in oligonucleotides as therapeutic agents. The majority of research falls into two main categories; antisense and antigene studies. For every protein to be made a unique sequence of the genome must be transcribed from double stranded DNA into single stranded messenger RNA. These mRNA molecules are then translated into the specific protein.

The antisense strategy has evolved ever since the discovery in the 1980's that certain bacterial strains produced natural antisense RNA as a means of regulating gene expression. The antisense RNA could complex with the complement (sense) mRNA to form a duplex, thereby causing down regulation of protein expression. The antisense strategy is to design specific oligonucleotides to sequence specifically bind to mRNA molecules, thereby causing a decrease in the process of translation, and/or degradation of the target mRNA by RNase A.

The antigene theory stems back to 1957 when Felsenfeld *et al* discovered the first triple helix. However it was not until the late 1980's that the first natural gene region was successfully targeted with a triplex forming oligonucleotide (Cooney *et al* 1988). In this strategy a third strand oligonucleotide binds in the major groove of the target DNA sequence, and is held in place by the formation of separate hydrogen bonds between the third strand and the substituents on the purine strand of the target DNA.

Both strategies can be seen in principle to decrease the production of specific protein. However the antigene strategy will in theory allow a lower concentration of drug to be used as each gene target should only have 2 copies in each diploid cell. In contrast the process of transcription results in the production of many mRNA molecules from a single gene sequence, producing thousands of target sites. Another advantage of the antigene strategy is that once the gene is down regulated no transcription will occur until the triplex is destabilised, or the third strand is degraded. In contrast the antisense strategy targets in the products of transcription without altering the rate at which mRNA is produced, thus a continual supply of oligonucleotide is required to achieve down regulation, whereas a single application of triplex forming oligonucleotide (TFO) in the antigene strategy will prevent protein formation so long as the triplex is stable.

(1.2.3)   Triplex Applications.

The treatment of cancer is not the only application for triplex technology. Viral and bacterial infections such as HIV, hepatitis and bacterial multi-drug resistance tuberculosis (BMRTB), endocrine disorders and immunological diseases like arthritis could also in theory be treated with triplex technology.

Many viruses have been completely or partially sequenced increasing the potential possibility of TFO's as antiviral agents. Another advantage of their use as antiviral agents is that many viral genes have no host counterpart genes, thus eliminating the chance of non-specific binding of a TFO to an incorrect target sequence, and preventing adverse effects to normal healthy genes.

The formation of triplexes has potential applications in areas other than gene therapy, they may have potential as biomolecular tools. For example immobilised oligonucleotides have been used to sequence specifically bind plasmid DNA via triplex formation under acidic conditions (Schluep & Cooney 1998). The plasmid can be eluted from the column in a purified state by increasing the pH of the wash buffer, thus disrupting the Hoogsteen hydrogen bonds of the triplex. Therefore it is possible to

produce pharmaceutical quality plasmid DNA via affinity chromatography alone, via the incorporation of triplex technology.

(1.2.4) Orientation of the Third Strand.

DNA triple helices can exist in one of two forms; in which the third strand runs either parallel or antiparallel to the purine strand of the duplex target (Fig. 1.5). Affinity cleavage studies demonstrated that pyrimidine containing third strands run parallel to the duplex purine strand (Moser & Dervan 1987). Early experiments revealed pyrimidine rich third strands formed T·AT and C$^+$·GC triplets (Fig. 1.3) (Lipsett 1964, Riley *et al* 1966, Lee *et al* 1979). Studies have since demonstrated the formation of G·TA and T·CG triplets (Griffen & Dervan 1989, Yoon *et al* 1992). Both the T·AT and the C$^+$·GC triplets are stabilised by the formation of two Hoogsteen hydrogen bonds between the bases of the third strand and the duplex purine strand (De los Santos *et al* 1989, Rajagopal & Feigon 1989). The requirement for cytosine protonation is covered in section 1.3.2.

Purine containing third strands run in an antiparallel orientation (Beal & Dervan 1991). NMR studies with intramolecular triplexes also concluded that purine rich third strands align themselves in the major groove in an antiparallel orientation, generating G·GC, A·AT, and T·AT triplets (Fig. 1.4) (Radhakrishnan *et al* 1991, Pilch *et al* 1991). These studies supported the initial affinity cleavage experiments of Beal & Dervan (1991). All three triplets are stabilised by reverse Hoogsteen bonding between the bases of the third strand and the purine strand of the duplex (Radhakrisnan *et al* 1991, 1993). GT containing third strands however can be either parallel or antiparallel with respect to the duplex purine strand (Sun *et al* 1991, Giovannangeli *et al* 1992).

(1.2.5) The Structure of Triplex DNA.

Early fibre diffraction studies on the structure of triplex DNA suggested that it resembled A-DNA, with the sugars in the C3'-endo (N-type) conformation (Fig. 1.2b) (Arnott & Bond 1973, Arnott & Selsing 1974, Arnott *et al* 1976). However this would
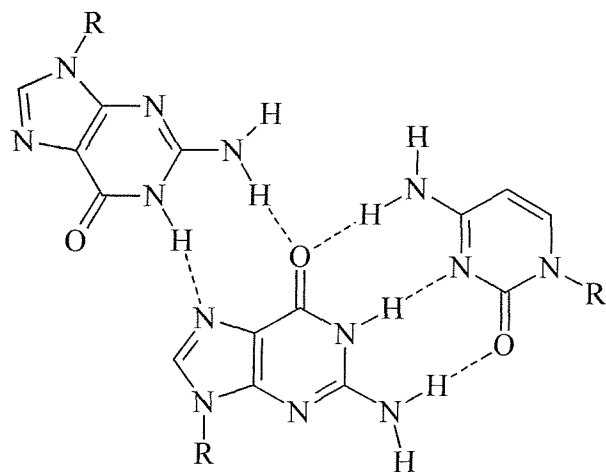
G·GC Triplet
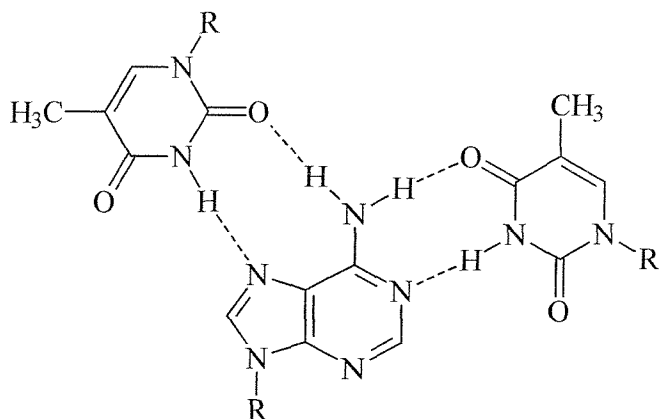
T·AT Triplet
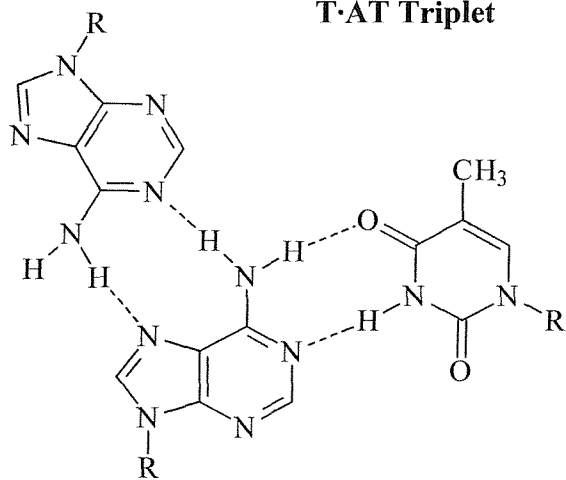
A·AT Triplet

Figure 1.4: Diagrams representing the hydrogen bonding schemes of antiparallel triplets. The base to the left in each diagram represents the third strand base reverse Hoogsteen hydrogen bonded in the major groove. The central and right-hand bases represent the purine and pyrimidine bases of the duplex respectively.
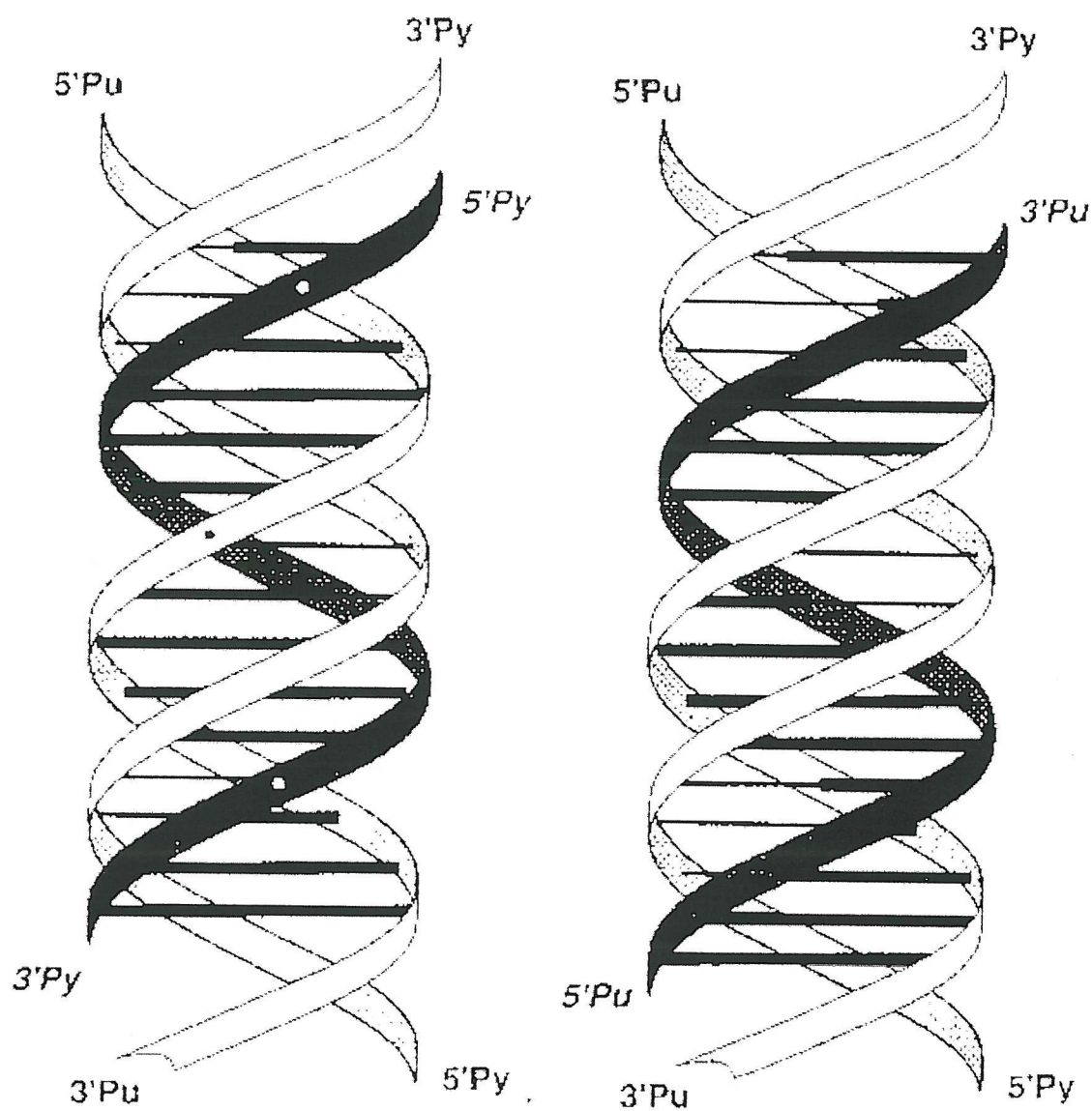
Figure 1.5: Ribbon models of (left) a parallel intermolecular triplex, and (right) an antiparallel intermolecular triplex. In both the diagrams the black strand represents the third oligonucleotide strand located in the major groove of the duplex.

require a change in the duplex structure to an N-type sugar conformation in order to accommodate the third strand in the major groove which would be energetically un-favourable. Subsequent NMR, Fourier transform infared (FTIR), and molecular modelling studies suggested that triplex DNA contained sugar puckers predominantly in the C2'-endo (S-type) conformation (Fig. 1.2b) which more closely resembled B-DNA (Rajagopal & Feigon 1989, Macaya *et al* 1992, Howard *et al* 1992, Liquier *et al* 1991, Raghunathan *et al* 1993). Further studies demonstrated that T·AT/C⁺·GC triplex DNA contain both N-type (C⁺·GC) and S-type (T·AT) sugar puckers (Macaya *et al* 1992, Ouali *et al* 1993). This suggests that the structure of triplex DNA is neither true A or B-DNA but that it forms an intermediate structure between the two types, requiring a separate classification. Triplexes formed by third strand RNA oligonucleotides with duplexes containing DNA purine strands are more stable than if the third strand was DNA, and stability is further enhanced by replacing the 2'-OH groups with 2'-OCH$_3$ (Escaudé *et al* 1993). The geometry of RNA·2DNA triplexes has been shown to be changed form S-type sugar conformation to N-type sugar conformation, resembling A-DNA (Dagneaux *et al* 1995).

The crystal structure of a short parallel triplex (3 base triplets) has been resolved to 1.8 Å (Rhee *et al* 1999). The Hoogsteen strand is positioned in the major groove of the DNA duplex and most of the nucleotides were found to adopt C2'-endo sugar conformations, except for the two 5'-terminal Hoogsteen bases which were shown to be in equilibrium between the C2'-endo and C3'-endo conformation, supporting the studies of Rajagopal & Feigon (1989), Macaya *et al* (1992), Howard *et al* (1992), Liquier *et al* (1991), Raghunathan *et al* (1993), Ouali *et al* (1993). In addition the base pairs of the duplex portion of the triplex DNA were found to be more perpendicular to the helical axis and displaced towards the minor groove and that the transition from triplex to duplex DNA results in a partial unwinding of the DNA as initially shown by Radhakrishnan *et al* (1994). The overall triplex dimensions differ from those of B and A-DNA, but the overall topology is more similar to B-DNA, supporting the findings of Macaya *et al* (1992) and Ouali *et al* (1993) that suggested that triplex DNA generates an intermediate structure. The third strand cytosine residues were shown to require

protonation at the N3 atom in order to generate a second hydrogen bond to the N7 atom of guanine residues (covered in section 1.3.2), and that there is a narrowing of the groove between the Hoogsteen and duplex purine strand in the vicinity of the C^+ base. The narrowing of the groove is believed to be due to electrostatic interactions between the positive charge of the cytosine residues and the phosphate groups of the phosphodiester backbone, as suggested by Asensio *et al* (1998c).

It has also been shown that there is structural asymmetry between 5' and 3' triplex junctions (Asensio *et al* 1998b,c). The 5' triplex-duplex junction demonstrates greater distortions than the 3' junction that extend into the duplex, generating a narrower minor groove. These differences in the local structure of triplex-duplex junctions may explain the differences observed in DNase I cleavage of triplex DNA and ligand intercalation at triplex boundaries (Cassidy *et al* 1994, Collier *et al* 1991).

A 2PNA·DNA complex has also been crystallised to a 2.5 Å resolution that shows the overall structure is neither B or A-DNA and has been assigned P-form (Betts *et al* 1995). The helix is underwound with a base tilt similar to that of B-DNA, but the bases are displaced from the helical axis more than in the A-form and the sugars have a C3'-endo pucker. Furthermore hydrogen bonding was observed between the Hoogsteen PNA backbone and the phosphodiester backbone, and may explain the high stability of 2PNA·DNA complexes (PNA is covered in greater detail in section 1.4.3.4).

(1.2.6)   Intermolecular & Intramolecular Triplexes.

Triplexes can be formed as both intermolecular and intramolecular structures. Intermolecular triplexes are produced when a polypurine·polypyrimidine region within a duplex is bound to a separate oligonucleotide strand. Intramolecular triplexes are formed by the disproportionation of mirror repeats of polypurine and polypyrimidine sequences. The process of formation involves a partial melting of the DNA duplex thus enabling one of the two strands to fold back on itself and form a triplex by bringing into close proximity the mirror repeats on the complementary strands. Again the triplex is stabilised

via the formation of Hoogsteen hydrogen bonds. Intramolecular triplexes are also known as H-DNA and may exists *in vivo* where they are postulated to be involved in the replication and transcription processes.

(1.2.7)   Evidence for the *in vivo* Existence of Triplex DNA.

Several potential roles for triplex DNA have been suggested and these include influencing transcription, replication, and recombination (Agazie *et al* 1996, Cooney *et al* 1988, Kohwi *et al* 1991, Baran *et al* 1987, and Rooney & Moore 1995).

Further evidence supporting the theory of a biological role for triplexes has been the discovery of proteins that specifically bind triplex DNA. Two studies isolated 55 KDa proteins from human HeLa cell lines that recognised intermolecular and intramolecular Y·RY triplexes (Kiyama *et al* 1991, and Guieysse *et al* 1997). The proteins had a high affinity for the parallel triplexes, whilst duplex, single strand and other forms of triplex DNA were poor substrates. Three further proteins have been purified from HeLa cells and shown to recognise R·RY motif triplexes (Musso *et al* 1998), as well as having a weak affinity for G-rich oligonucleotides capable of forming G-quartets. Both these structures have high electro-negativity and Hoogsteen hydrogen bonds, and it is possible that either one, or a combination of both these factors, enables recognition by the proteins.

Triplex binding proteins have also been isolated from other eukaryotic organisms including *Drosophila* (Jiménez-García *et al* 1998) and the yeast *Saccharomyces cerevisiae* (Nelson *et al* 2000). It was found that the GAGA factor in *Drosophila* could bind to $d[CT(GA \cdot TC)]_{22}$ intermolecular triplexes with an affinity comparable to that of its native double stranded $(GA \cdot TC)_{22}$ target sequence. GAGA binding sites are located at the promoters of several *Drosophila* genes and its function is believed to be involved in transcription regulation. The interaction of GAGA with triplex DNA, contrary to that of duplex DNA, did not lead to transcription *in vitro*, highlighting the effect of DNA structure on biological processes. The yeast gene product, stm1, is a 35 KDa protein that

has previously been identified as a G-quartet binding protein, G4p2, (Frantz & Gilbert 1995). Its biological function is a multicopy suppressor of mutations in genes involved in mitosis. However it has also been shown to selectively bind to antiparallel triplex DNA, and not the pyrimidine motif (Nelson *et al* 2000). Whether this is related to its biological function is as yet unknown, but it does implement structural changes in DNA influencing replication.

More recent studies have demonstrated that prokaryotic systems may also possess triplex binding proteins in the form of transposons. Rao *et al* (2000), demonstrated that the transposon Tn7 preferentially inserted adjacent to triplex DNA. With a cross-linked intermolecular triplex, 70% of all insertions occurred within 40 bp of the 5' terminal of the triplex, and 98 % of these insertions had the right end of Tn7 located closet to the triplex. However with an intramolecular triplex only 25% of insertions occurred within 50 bp of the triplex and were located at both the 3' and the 5' terminals. These results could be biassed however as the intermolecular triplex was cross-linked with psoralen generating a significantly more stable triplex than the H-DNA structure. Further studies demonstrated that the pyrimidine motif was preferentially recognised over that of the purine motif (Rao & Craig 2001). This discovery can be seen to have potential applications in gene therapy, as Tn7 can be engineered to carry a gene of interest. It can be envisaged that the gene can then be delivered to a specific location within a genome that has the ability to generate a triplex.

Notwithstanding all the circumstantial evidence suggesting potential biological roles for triplex DNA, and with triplex binding proteins shown to exist, there is to date no direct evidence for the existence of triple helical structures *in vivo*.

(1.2.8)   Triplex Limitations.

i) One of the major limiting factors associated with triplex formation is the requirement for an uninterrupted polypurine tract as the target site. To date there are no specific methods for the recognition of pyrimidine residues, despite extensive research.

This is mainly due to the fact that pyrimidine residues only present one possible Hoogsteen hydrogen bonding site in the major groove, and therefore the natural base triplets, G·TA, T·CG, A·TA, and G·CG are less stable than the standard triplets (Fig. 1.6).

Some base analogues have been designed to enhance the stability of the single Hoogsteen hydrogen bond, whereas other analogues have been designed to recognise the base pair. However to date the design of novel base analogues for specific recognition of pyrimidine residues lacks a definitive solution (Gowers & Fox 1999a). Base analogues are discussed in further detail in section 1.4.1.

An alternative method for overcoming polypurine limitation is that of alternate strand recognition. This method does not require the recognition of pyrimidine residues, but instead involves the simultaneous recognition of adjacent polypurine tracts on opposite strands of the duplex, using a single polypyrimidine third strand (Horne *et al* 1990). This is generally achieved by joining two separate polypyrimidine tracts in a 3'-3' or 5'-5' orientation via linker molecules such as dideoxyribose (Horne *et al* 1990). This linker unit introduces a change in strand orientation. Another means is to combine both parallel and antiparallel triplexes within the same molecule, which then allows the third strand to cross the major groove of the duplex without changing its orientation as the individual orientations of the polypyrimidine tracts are opposite (Marchand *et al* 1998). Alternate strand recognition is discussed in greater detail in section 1.2.9. An alternative method for recognising polypurine tracts on alternate strands of a DNA duplex has been recently proposed (Ihara *et al* 2001). In this method glutamate is conjugated to the 5' terminus of complementary oligonucleotides and cooperative binding achieved via coordination of Cu^{2+} generating a oligonucleotide dimer. The coordinated dimer was shown to be 10 times more stable than the independent triplexes produced in the absence of Cu^{2+}.

ii) Cell uptake of oligonucleotides presents a problem for the *in vivo* use of both antigene and antisense agents since oligonucleotides are large polyanionic molecules they would not be expected to cross the cell membrane. However it has been shown that oligonucleotides not only cross the lipid membrane (Zamecnik *et al* 1986) but that when

a) **G·TA Triplet**

b) **T·CG Triplet**

c) **A·TA Triplet**
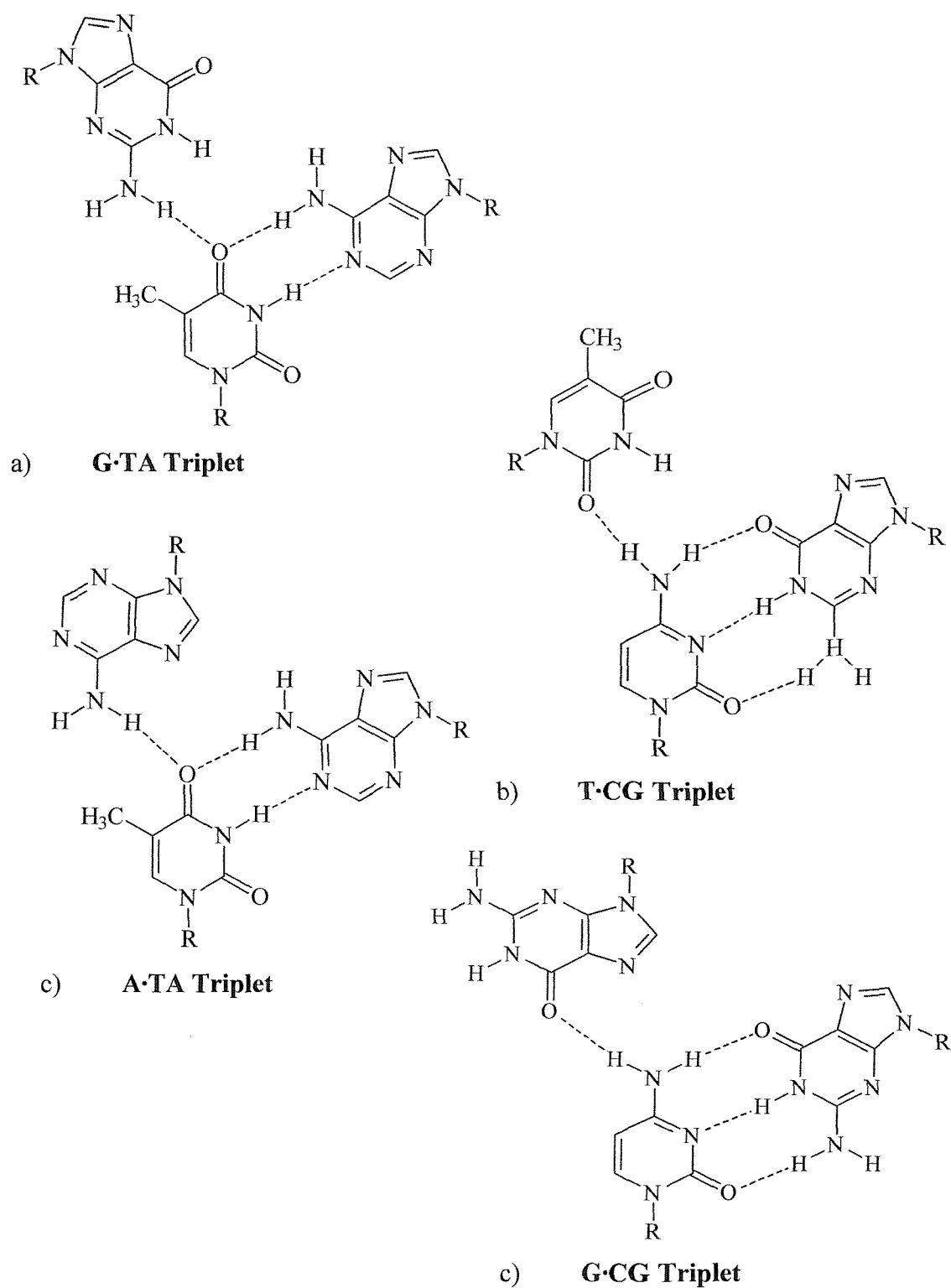
c) **G·CG Triplet**

Figure 1.6: The Hoogsteen hydrogen bonding pattern of the a) parallel G·TA triplet, b) parallel T·CG triplet, c) antiparallel A·TA triplet, d) the antiparallel G·CG triplet. In each case the target base is a pyrimidine residue, and as such only presents a single bond.

internalised, they are concentrated in the nucleus via diffusion (Leonetti *et al* 1991). The cellular uptake of oligonucleotides was shown to be an endocytic process that was saturable and oligonucleotide length dependent (Loke *et al* 1989). However it has also been shown that the intracellular concentration of oligonucleotide was approx. $^{1}/_{10}$ that of the extracellular concentration, indicating that the process of oligonucleotide uptake is inefficient.

iii) Another consideration is that oligonucleotides are sensitive to degradation by endonucleases and exonucleases and various modifications of oligonucleotide structure have been made to prevent this degradation. Backbone modifications have included phosphoramidate and phosphorothioate analogues (Escudé *et al* 1996, Hacia *et al* 1994) (section 1.4.3). Modifying the 3'-end of oligonucleotides has also been shown to prevent their degradation. These modifications have enhanced the cellular half-life of the synthetic oligonucleotides but as yet only one modification, that of PNA, has afforded complete protection (see section 1.4.3.5.).

However a side-effect of some modifications is decreased target specificity, as demonstrated with phosphorothioate oligonucleotides. These have been shown to bind to several proteins thereby altering their activity. DNA polymerase has been shown to be non-specifically inhibited by these types of oligonucleotides (Gao *et al* 1988).

(1.2.9) Alternate Strand Recognition.

Alternate strand recognition (Horne & Dervan 1990) investigates the recognition of homopurine tracts located on opposite strands of a duplex using a single third strand. This was achieved by employing a third strand containing a 3'-3' phosphodiester link using a 1,2-dideoxy-D-ribose linker unit (Fig. 1.7). Subsequent studies demonstrated that 5'-5' linkage at the strand switch site was also possible (Ono *et al*, 1991) and that multiple strand switching could be achieved. Several alternative linker units have also been designed to permit strand switching (Froehler *et al* 1992, Ono *et al*, 1991).

Figure 1.7: Diagram a) represents a bidirectional pyrimidine oligonucleotide bound to both purine strands of a DNA duplex in opposite orientations. The strand switch is stablised via the incorporation of a 1',2-dideoxy-D-ribose linker unit. Reproduced from Horne & Dervan *J. Am. Chem. Soc.* **112**, 2435-2437 (1990).Diagram b) demonstrates the overlaping target tracts at a RpY switching junction (left), and the gap generated at a YpR switching junction (right). Reproduced from Beal & Dervan *Nuc. Acid Res.* **20**, 2773-2776 (1992).

Strand switching can also be achieved by targeting the two purine tracts with parallel and antiparallel triplexes maintaining the natural 3'-5' phosphodiester backbone (Beal & Dervan, 1992, Jayasena & Johnston 1992a,b, Washbrook & Fox 1994). The formation of both parallel and antiparallel structures eliminates the necessity for a linker group to enable switching between strands. However the composition of the crossover junction influences the stability of an alternate strand triplex. The initial study (Beal & Dervan, 1992) concluded that in RpY junctions the two central bases are skipped by the third strand due to the target tracts overlapping, whereas for YpR junctions two nucleotide linker units are required to permit triplex formation crossing the major groove (Fig. 1.7). Further experiments showed that certain YpR junctions do not permit triplex formation and the results suggested that the composition of the targeted tracts may influence the stability (Jayasena & Johnston, 1993). Another study demonstrated a difference between CpG and between GpC junctions. CpG junctions require an additional cytosine residue in the third strand to act as a linker and facilitate the strand crossover. In contrast the GpC junctions do not require any additional bases or linker groups, and that removal of a base facing the junction increases the triplex stability (Marchand *et al*, 1998). This study supported conclusions drawn by Beal & Dervan (1992) by demonstrating that RpY junctions facilitate a more stable switch strand triplex than YpR, due to the more favourable steric contacts and a concomitant increase in the base stacking interactions

(1.3) Factors Affecting Triplex Stability.

There are several extrinsic and intrinsic factors that can influence the stability of triplexes some of which are described below.

(1.3.1) Hoogsteen Hydrogen Bonds.

The formation of Hoogsteen hydrogen bonds is one of the most important factors for forming stable and selective triplexes. All the stable triplets in the parallel or antiparallel orientation have two hydrogen bonds between the third strand base and the

duplex purine residue. The formation of these hydrogen bonds is the major determinant of triplex sequence specificity, with a single mismatch within a triplex resulting in a dramatic loss in stability, equivalent to that seen for mismatches in duplex DNA (Roberts & Crothers 1991).

This is not to say that single Hoogsteen hydrogen bonded triplets are not stable, because experiments have shown A·GC, T·CG, and C·AT triplets (Fig. 1.6), can be incorporated within stable triplexes (Beal & Dervan 1992). However incorporation of even one of these single triplets into a relatively stable triplex has been shown to reduce the overall stability dramatically (Beal & Dervan 1992, Yoon *et al* 1992).

One of the other factors associated with the formation of Hoogsteen hydrogen bonds is that C^+·GC, & A^+·GC triplets require protonation for the formation of one of the bonds. Without protonation the N3 atom of cytosine will not carry a hydrogen atom and thus can not donate the second Hoogsteen hydrogen bond to the formation of a stable triplet. This results in a decrease in triplex stability with increasing numbers of C·GC triplets at physiological pH.

(1.3.2)   pH Dependence.

The bases that contribute to the formation of all nucleic acids contain several nitrogen atoms which can either accept or donate protons depending upon the pH. At low pHs these are protonated and act as hydrogen bond donors, whilst they are hydrogen bond acceptors at high pHs. All of the common natural bases are not protonated at a neutral or physiological pH, and T·AT, U·AU, A·AT, and G·GC triplets will form readily. However the C^+·GC and A^+·GC triplets require protonation as previously mentioned. Therefore parallel triplexes containing C^+·GC triplets and antiparallel triplexes containing A^+·GC triplets require a pH < 6.0 to ensure protonation and triplex stabilisation (Lipsett 1963, 1964, Lyamichev *et al* 1988, Malkov *et al* 1993). The first conclusive evidence for the protonation of third strand cytosine residues was obtained from NMR studies (Rajagopal & Feigon 1989). In this study a DNA

homopurine·homopyrimidine duplex was targeted with a homopyrimidine CT oligonucleotide forming a parallel triplex. The results showed evidence for C^+ imino protons in the Hoogsteen strand.

The pKa of free cytosine is approximately 4.3, however when cytosine is incorporated into a polynucleotide the pKa increases to approximately 5.5 (Xodo *et al* 1991, Singleton & Dervan 1992). Despite this increase in the pKa value, triplex formation is still unfavourable at physiological or neutral pH (Lipsett 1963, Lee *et al* 1979, Mirkin *et al* 1987, & Malkov *et al* 1993). It has also been shown that the pKa of protonated cytosine is approximately 9.5 at internal positions (Asensio *et al* 1998a). Regions of contiguous C^+·GC triplets have been demonstrated to decrease triplex stability (Kiessling *et al* 1992, Roberts & Crothers 1996) and indicates the requirement for C^+·GC triplets to be separated by at least one T·AT triplet to prevent unfavourable charge interactions. The C^+·GC triplet has also been shown to impart a greater stabilising effect upon a parallel triplex than T·AT at low pH and that variations in the width of the CT triplex groove is associated with the positive charge of protonated cytosine (Roberts & Crothers 1996, Asensio *et al* 1998a,b,c). Furthermore $(CT)_n$ triplexes are thought to be the most stable triplex (Roberts & Crothers 1996). In contrast unprotonated C·GC is less stable than T·AT. The increased stability as a result of protonation is too great to be accounted for by the formation of the second hydrogen bond, and must result from increased electrostatic interactions with the phosphodiester backbone or enhanced base stacking with neighbouring bases, possibly between the positive charge and the π-stack (Asensio *et al* 1998a). Furthermore parallel triplexes have also been shown to be more stable when they incorporate terminal cytosine residues, compared to terminal thymine residues (Asensio *et al* 1999). This is postulated to be due to the greater stability of C^+·GC triplets preventing the terminal regions of the oligonucleotide fraying from the DNA duplex. Cytosine analogues designed to overcome the limitation of pH are discussed in section 1.4.1

(1.3.3)   Length Dependence And Interstrand Repulsion.

It is widely accepted that increasing the length of the TFO will enhance the overall triplex stability due to increasing the hydrogen bonding (Lipsett *et al* 1960, Raae & Kleppe 1978), and base stacking interactions, with the minimum length of the third strand being no less than nine bases long (Moser & Dervan 1987, Lyamichev *et al* 1990, 1991, Rubin *et al* 1993). Stability is also influenced by any requirement to adjust the conformation of the target duplex or the third strand TFO. If the conformations of the duplex and third strand do not exactly match then there will be an increase in deformation as successive third strand residues wind around the duplex as the two become out of register. Ultimately this deformation will increase to the point where the winding about the duplex of the third strand becomes unfavourable and hence triplex formation is prevented (Broitman *et al* 1987).

Since triplex formation involves the association of two polyanionic molecules it is profoundly affected by the presence of metal cations (Letai *et al* 1988) which mask the charges on the sugar-phosphate backbones. Monovalent cations can stabilise triplex formation, though much higher concentrations are required compared to divalent cations (1M and 1-10 mM respectively) (Felsenfeld & Rich 1957, Krakauer & Sturtevant 1968). Since monovalent and divalent cations bind to the same sites, but with different affinities, addition of sodium ions can result in the destabilisation of triplexes formed in the presence of magnesium. It has also been postulated that triplex stability is dependent upon the specific cation bound to the phosphate groups, and the effect of different diavalent cations bound to intermolecular antiparallel triplexes has been demonstrated to affect the stability of the complex (Malkov *et al* 1993). These studies showed that Mg^{2+} and Ca^{2+} stabilise triplexes composed solely of G·GC triplets, whereas Mn^{2+}, Ni^{2+}, Zn^{2+}, Cd^{2+}, Co^{2+} stabilise all antiparallel triplets. The differences in the stabilising properties were postulated to be due to cations binding at different positions; the alkali-earth metals may bind to the phosphate groups, whilst the transition metals are thought to bind to the bases themselves (Malkov *et al* 1993).

The formation of antiparallel triplexes is also inhibited by the presence of physiological concentrations of potassium (Cheng & Van Dyke, 1993). Potassium ions are known to stabilise the formation of tetraplex structures from the self-association of GT rich oligonucleotides (Williamson *et al* 1989, Sen & Gilbert 1990). Therefore it was thought that inhibition of the purine motif was due to potassium ions stabilising an intermediate tetraplex formed by the self association of the GT rich and GA rich 19 mer oligonucleotides. However it may also be caused by the formation hairpin duplex structures (Cheng & Van Dyke 1993).

This presents a potential problem for use of the purine motif, and several methods have been investigated in an attempt to overcome this shortcoming. Tetraplex formation has been overcome via the addition of millimolar concentrations of manganese, colbalt, and nickel demonstrating that formation of the various multistranded nucleic acid complexes may be governed by the presence of different cations (Blume *et al,* 1997). The transition metal ions are believed to compensate for tetraplex formation via their co-ordination to the N7 of the guanine residues where they are believed to enhance hydrogen bond formation between the third strand and its duplex target and prevent G-quartet formation (Floris *et al,* 1999). Another study indicated that inhibition of triplex formation via the presence of potassium ions may be overcome by designing the synthetic oligonucleotides to be zipper molecules. Zipper molecules are where the 5' or the 3' ends of the synthetic oligonucleotides are partially duplexed in an attempt to prevent their self-association. Upon these molecules associating with their duplex targets the full length triplex is formed and the partial duplexes are unzipped (Svinarchuk *et al,* 1996). Base analogues have also been designed so as to prevent the formation of tetraplexes and are further discussed in section 1.4.1.

A recent study has indicated that tetraplex formation is not solely dependent on potassium ions, but that the concentration of the oligonucleotide also plays a part (Aich *et al,* 2000). They demonstrated that up to a oligonucleotide concentration of 10 nM, little if any tetraplex formation occurred, whilst at a concentration of 1 μM self-association of the oligonucleotide was complete. This was interpreted by suggesting that

the kinetics of triplex formation are probably first order with respect to the oligonucleotide, whereas that of tetraplex formation is probably second order. Further to this they also calculated that for a cell with a radius of 20 μm, and volume 2 x 10^{-14} m^3, a single duplex target sequence would have a concentration of approximately 10^{-13} M, which is lower than the maximum permissible concentration of oligonucleotide (1 μM) in the presence of potassium. Therefore it would theoretically be possible to form an *in vivo* purine motif triplex with a stoichiometric excess of synthetic oligonucleotide even in the presence of potassium ions. Thus it can be seen that the inhibition of antiparallel triplex formation may not be as detrimental to the potential applications of the purine motif in the antigene strategy as was initially believed.

The relative stability of triplexes containing protonated bases differs in that C$^+$·GC triplets are inherently more stable than T·AT triplets at sodium concentrations below 0.4 M. This trend is reversed when sodium concentrations are elevated above 0.4 M with the T·AT triplets becoming more stable than the C$^+$·GC triplets (Völker & Klump 1994). However the addition of magnesium eliminates the destabilising effect associated with C$^+$·GC triplets at a high sodium concentration (Lyamichev *et al* 1991, & Soyfer *et al* 1992).

Another way of reducing interstrand repulsion is via the use of polyamines, where again the efficiency is influenced by the net charge carried by the molecule. Again the higher the charge on the polyamine, the higher the resulting stabilisation of the triplex (Thomas & Thomas 1993). Parallel triplex formation can be enhanced by the addition of sub-millimolar concentrations of spermine which carries a 4$^+$ charge; this polyamine also enhances antiparallel triplexes to some extent (Raae & Kleppe 1978, Soyfer *et al* 1992, Beal & Dervan 1991). The stabilising effect of polyamines is somewhat dependent on the composition of the polyamine used, and the distance between the multiple charges influences the degree of stabilisation. Tethered polyamines have also been used to overcome interstrand repulsion and are discussed in section 1.4.4.

(1.3.4)   Stacking Interactions.

The importance of base stacking interactions in triplex formation has been demonstrated by experimental studies, from which it has been possible to establish that a single base mismatch within a triplex results in a 2.5-6.0 Kcalmol^{-1} free energy change, which compares to a value of 2-3 Kcalmol^{-1} for dsDNA (Roberts & Crothers 1991, Rougée *et al* 1992, Xodo *et al* 1993, Gralla & Crothers 1973, Tibanyenda *et al* 1984). It was shown that mismatched bases are either completely or partially expelled from their helical positions, which then results in a loss of Hoogsteen hydrogen bonding. Not only is there a loss of bonding between the mismatched bases, but that there is also a distortion in the backbone bi-directionally from the mismatch to the adjacent bases. Thus a single mismatched base also causes the loss of two stacking interactions resulting in a substantially decreased affinity for triplex formation (Horne & Dervan 1991).

Base stacking interactions can be enhanced by incorporating favourable stacking groups onto the bases. One example is the use of methyl-cytosine as a replacement for cytosine (section 1.4.1). It is known that enhancing the terminal base stacking interactions enhances the triplex association constant, in a sequence dependent fashion (Colocci *et al* 1993). Furthermore novel extended bases have been developed to increase stacking interactions within the third strand by extending the ring system. Quinazoline-2,4(1H,3H)-dione and various cholro, fluoro, and nitro substituted quinazoline compounds have been designed, (Michel *et al* 1996, 1997), but shown to bind preferentially to single stranded DNA and only mildly stabilise triplex formation. Pyrido [2,3-d] pyrimidine, (F), was shown to bind to guanine in duplex DNA, whereas in a Hoogsteen strand it was demonstrated to bind to adenine residues, and was attributed to F having two tautomeric forms (Staubli & Dervan 1994). They also demonstrated that the incorporation of F did not increase the favourable stacking interactions and actually decreased the stability of triplex formation.

(1.3.5)   Effects Of Hydration.

It has long been established that there is a primary hydration shell that surrounds a DNA molecule comprised of several water molecules per nucleotide (Tao *et al* 1989). This water is not evenly distributed along the length of a polynucleotide, and polypurine tracts are hydrated to a much higher degree than alternating polypurine·polypyrimidine sequences (Marky & Macgregor 1990, Rentzeperis *et al* 1992). It has also been shown that AT base pairing will result in a higher hydration than GC base pairing, and that bound polyvalent ligands cause an overall re-organisation of the water molecules resulting in them becoming polarised. This polarisation leads to increased hydration effects (Rau & Parsegian 1992).

Water molecules are located within the three grooves of both parallel and antiparallel triplexes, causing an increase in the solvation of the molecule which may aid triplex stabilisation. Water molecules may also mask the electrostatic repulsion produced by the close proximity of phosphate groups across the narrow groove between the duplex purine strand and the third strand (Radhakrishan & Patel 1994a,b).

Highly hydrated nucleotide sequences such as those of AT base pairing produce what is known as outer-sphere complexes, and these can prevent divalent cations from penetrating the shell. Whereas less hydrated nucleotide sequences like those of GC pairing regions produce an inner-sphere complex, and conversely allow divalent cations to penetrate the shell Therefore it can be seen that the overall hydration state of a triplex can be influenced by the base sequence composition.

(1.3.6)   Base Sequence Composition.

Several studies have examined the effects of sequence composition on triplex stability (Völker & Klump 1994, Keppler & Fox 1997, Asensio *et al* 1998a,b, 1999). It has been shown that sequences containing large numbers of C^+·GC triplets produce more stable triplexes at pH 5.0 than sequences containing fewer C^+·GC triplets. A 9mer third

strand with a single $C^+ \cdot GC$ triplet produced a dissociation constant of $>30 \mu M$, whereas a 9mer third strand with 4 $C^+ \cdot GC$ triplets had a dissociation constant of $0.13 \mu M$, a 230 fold increase in affinity (Keppler & Fox 1997). Since $T \cdot AT$ and $C^+ \cdot GC$ triplets are isostructural their different stabilising properties must be due to the presence of the positive charge on the cytosine. It is believed that the charge on the protonated cytosine increases stabilisation by either masking the polyanionic charge of the backbones, or interacting with the stacked π system (Keppler & Fox 1997, Völker & Klump 1994). It should be remembered that adjacent $C^+ \cdot GC$ triplets always destabilise triplex formation, and upon increasing the pH this trend reverses so that the triplexes with higher numbers of $C^+ \cdot GC$ triplets are less stable than triplexes with fewer $C^+ \cdot GC$ triplets. This is due to the loss of protonation, as previously discussed.

It has been shown that the position of the Hoogsteen strand in the Watson-crick major groove can vary, affecting the width of the two triplex grooves. This is believed to be caused by the interaction of the positive charge of cytosine residues with the phosphodiester bonds, and is therefore sequence dependent (Asensio *et al* 1999). These authors also demonstrated that the incorporation of terminal cytosine residues at either the 3' or 5' triplex·duplex junction increased the stability of the complex (Asensio *et al* 1998a, 1999). Furthermore it was shown that the asymmetry of the 5' and the 3' junctions were different and may explain the preference for intercalation of ligands at the 5' terminus and enhanced DNase I cleavage at the 3' terminus (Asensio *et al* 1998b)

(1.4) Improving The Stability Of Triplexes.

Despite triplex formation being sequence selective several factors limit the stability of these complexes. As discussed above, these factors include the local DNA structure, the temperature and pH of the environment, electrostatic interactions and the oligonucleotide length. Several strategies have been developed to minimise or overcome these limitations.

(1.4.1)   Base Modifications.

As previously mentioned there is a requirement of an acidic environment for formation of the $C^+\cdot GC$ triplet, and several base analogues have been prepared to overcome this limitation. Novel base analogues have also been prepared to extend the triplex recognition code to include pyrimidine residues.

When designing base analogues several factors must be taken into consideration. The hydrogen bonding surface must first be compatible with the mode of recognition, base stacking must be maximised and backbone distortions between adjacent triplets kept to a minimum.

(1.4.1.1)   5-Methyl-cytosine.

The first cytosine analogue produced was 5-methyl-cytosine (Fig. 1.8), which stabilised triplexes at elevated pHs. Lee *et al* (1984) demonstrated that it is possible to form stable parallel triplexes below pH 8 when methyl-cytosine replaces cytosine. This was intriguing because addition of the methyl group only causes a small increase in the pKa value. Subsequent studies however demonstrated that methyl-cytosine increases triplex stability by about 1 pH unit, and does not afford stabilisation at physiological pH (Xodo *et al* 1991). The increase in stability is probably due to the spine of methyl groups in the major groove which either displaces water molecules, producing a positive entropy change, or enhances base stacking interactions with neighbouring bases, rather than as a direct reflection of its slightly elevated pKa value. Frohler *et al* (1992) demonstrated that the carbocyclic analogue of methyl-cytosine had a higher pKa than that of the furanosyl nucleoside and increases the stability of triplex formation 100-fold when incorporated into a TFO.

a) $^mC^+\cdot GC$ Triplet

b) $^{6ox}C\cdot GC$ Triplet

c) $m^5C^{6ox}\cdot GC$ Triplet
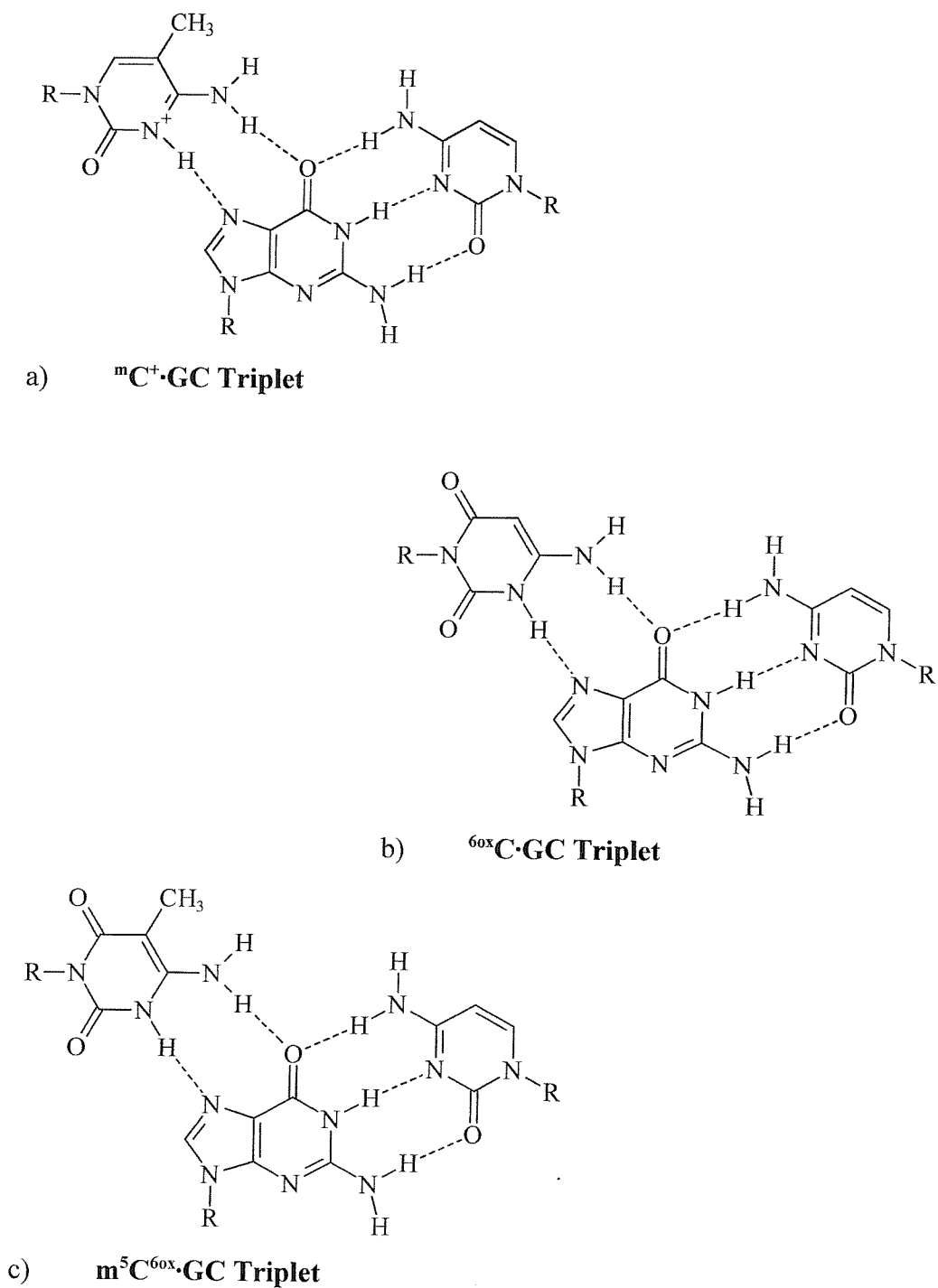
Figure 1.8: Hoogsteen hydrogen bonding of the parallel triplets formed incorporating the cytosine analogues; a) 5-methyl-cytosine, b) 6-oxo-cytosine, and c) 5-methyl-6-oxo-cytosine

(1.4.1.2)   5-Methyl-6-oxo-cytosine & 6-Oxo-cytosine.

m^5C^{6ox} is a 6-keto derivative of 5-methyl-cytosine (Fig. 1.8). Of the possible tautomers the N3 protonated version was shown to enable pH-independent recognition of GC base pairs, whilst the tautomer containing a protonated O6 atom did not (Xiang *et al* 1994). The N3 protonated tautomer enables a hydrogen bond to be formed between the N3 of m^5C^{6ox} and the N7 of the duplex guanine residue at a neutral pH. However in a mildly acidic environment the stability of triplexes containing the m^5C^{6ox} analogue was lower than that achieved by either natural cytosine or methyl-cytosine containing third strands. However m^5C^{6ox} produced more stable triplexes at pH's between 8.0-8.5 than cytosine or methyl-cytosine (Xiang *et al* 1994). However continuous GC base pairs could still not be recognised using m^5C^{6ox}.

6-Oxo-cytosine is a similar pyrimidine analogue (Fig. 1.8), which also allows pH-independent recognition of guanine. However as for m^5C^{6ox} triplex stability was lower than that of cytosine and 5-methyl-cytosine at low pH (Xiang *et al* 1994,Berressem *et al* 1995). The low stability of $m^5C^{6ox}\cdot GC$ and $^{6ox}C\cdot GC$ triplets compared to $C^+\cdot GC$ is thought to be due to the lack of a positive charge on the analogue. These triplets are therefore similar to the less stable T·AT.

(1.4.1.3)   2'-O-methylpseudoisocytidine.

This base was designed as a cytosine analogue to enable the recognition of GC base pairs at physiological pH via hydrogen bonding of N7 of guanine with the hydrogen at position N3 on the pseudo-base (Fig. 1.9), (Ono *et al* 1991). In the initial study the oligonucleotide TTXTTXTT (where X was the pseudo-base) was targeted to the duplex AAGAAGAAGAA-TTCTTCTTCTT and the stability of the triplex was studied by thermal melting. The results demonstrated two transitions; one at $42\,^{\circ}C$ corresponding to the duplex melt, with the second at $12\,^{\circ}C$ corresponding to the triplex melt. Control oligonucleotides TTCTTCTT and TT^mCTT^mCTT gave only one transition corresponding to that of the duplex melt, indicating a failure of triplex formation (Ono *et al* 1991).
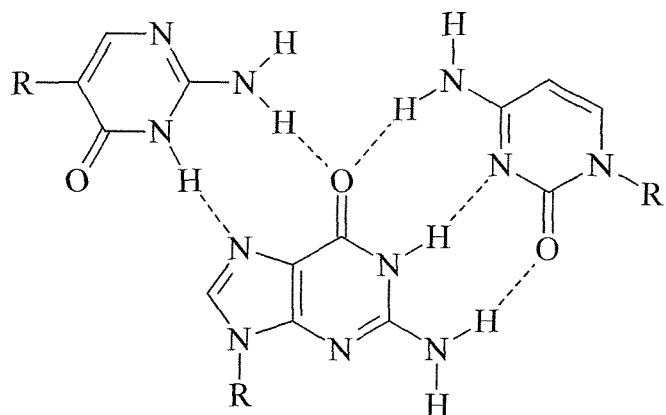
a) $^{\Psi}$C·GC Triplet
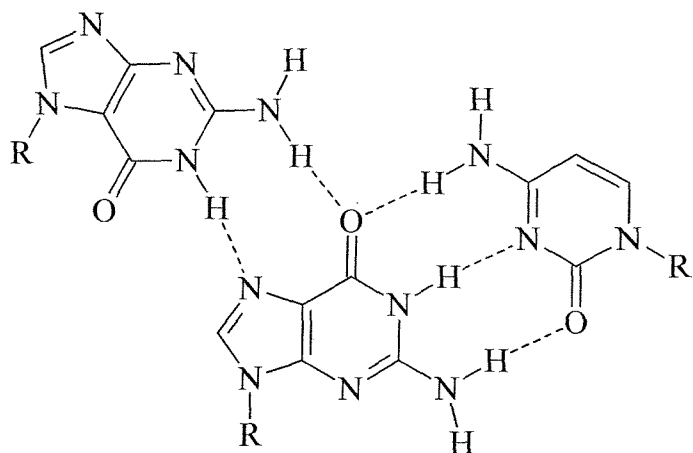
b) ^{7}G·GC Triplet

Figure 1.9: Diagrams representing the Hoogsteen hydrogen bonding schemes for the parallel triplets containing the cytosine analogues; a) 2' O-methylpseudoisoctosine, and b) 7-deoxyguanine.

Whilst the incorporation of this pseudo-base results in an improvement in triplex stability over that of cytosine and methyl-cytosine at physiological pH, the overall stability of the resulting complex was still relatively low. However this low stability may have been due to in part the short length of the third strand oligonucleotide (8 bases).

A separate study investigated the potential of this base for recognising contiguous GC base pairs. Thermal melting studies showed that replacement of cytosine residues with the pseudo-base in the oligonucleotide TTTTXTTTTXXXXXXT (where X is the pseudo-base) gave two transitions. The first transition at $20\,^{\circ}C$ resulted from the triplex melt, whereas the second transition at $72\,^{\circ}C$ corresponded to the duplex melt. The results of the ^{m}C substituted third strand showed a partial transition relating to the dissociation of the third strand at a temperature below $0\,^{\circ}C$ (Ono *et al* 1992). This increase in stability is presumably because this unprotonated pseudo-base does not suffer from the unfavourable charge repulsions with either that of cytosine or methyl-cytosine. Thus these results indicate that stable recognition of continuous GC residues was possible when substituting 2'-O-methylpseudoisocytidine for cytosine, but that the resulting stability of the triplex was still relatively low. Once again the low stability may be because this is a uncharged base analogue.

(1.4.1.4)   7-Deoxyguanine.

The deoxyribose group of this analogue was attached to the guanine base at the N7 position instead of N9 and as a result this analogue mimics protonated cytosine (Fig. 1.9), allowing recognition of GC base pairs in a parallel orientation, in contrast to guanine which recognises GC base pairs in an antiparallel orientation. When it was incorporated into the sequence (TTTTT^{7}GT^{7}GT^{7}GT^{7}GA^{7}GA) it associated with the target sequence (AAAAAGAGAGAGAGA) with an affinity three orders of magnitude less than the oligonucleotide (TTTTT^{m}CT^{m}CT^{m}CT^{m}CT^{m}CT). This decrease in affinity is believed to be due to the lack of structural isomorphism between ^{7}G·GC and T·AT triplets, therefore A$_{p}$G and G$_{p}$A steps would cause unfavourable distortions in the backbone of the molecule (Helmut & Dervan 1996). However TTTT^{m}CTTTT ^{7}G ^{7}G ^{7}G

^{7}G ^{7}G ^{7}GT bound to a target purine sequence (AAAAGAAAACCCCCCA) with an affinity five orders of magnitude higher than TTTT^{m}CTTTT ^{m}C^{m}C^{m}C^{m}C^{m}CT. The large difference in the affinities in this case is believed to be a direct result of electrostatic repulsions between the adjacent protonated ^{m}C bases which was alleviated via their replacement with ^{7}G bases (Brunar & Dervan 1996). In addition there are no structural distortions between adjacent ^{7}G·GC triplets. Thus the results indicate that ^{7}G binds continuous GC base pairs with a higher affinity than ^{m}C, but that isolated GC base pairs are bound with a higher affinity by ^{m}C. The same study also indicated that triplexes containing ^{7}G bases were able to form independently of pH, but as demonstrated were dependent upon the target base sequence composition.

(1.4.1.5) 2-Aminopyridine.

2-aminopyridine (2AP) is a structural analogue of cytosine, however it is much more basic with a pKa value of 6.86 as opposed to that of cytosine at 4.3 (Fig. 1.11). This therefore results in triplexes containing this analogue being protonated at higher pH's compared to cytosine containing triplexes (Bates *et al* 1996).

2AP is an isostructural analogue of cytosine and therefore incorporation of this into a triplex causes minimal structural distortions of the phosphate backbone, thus allowing the generation of continuous 2AP·GC stretches at pHs as high as 7.0 (Cassidy *et al* 1997). Whilst it can be seen that this would have an advantage over some of the other nucleoside analogues, its potential *in vivo* use is limited in, like all the analogues previously mentioned, β-nucleosides are susceptible to nuclease degradation. This can be potentially overcome by preparing the analogue in an α anomeric configuration. Initial studies with an oligonucleotide containing α-AP suggested that it could be used to target GC. However these studies used psoralen to form a covalent triplex adduct and subsequent footprinting studies showed that it does not stabilise triplexes to the same degree as β-AP (Cassidy *et al* 1997).
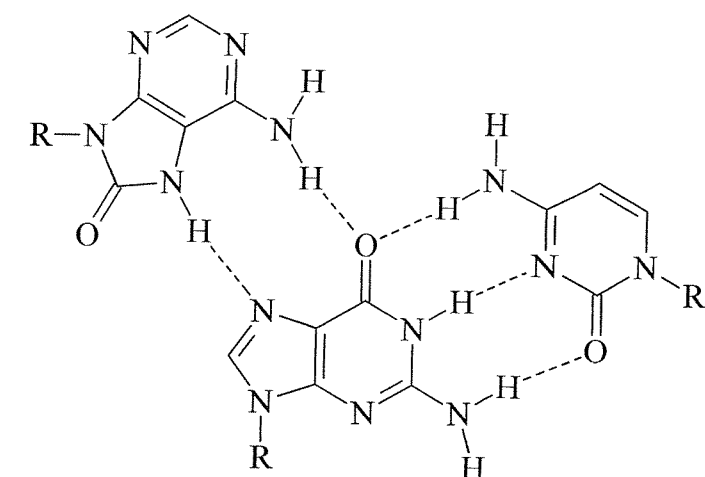
a) **^{oxo}A·GC Triplet**
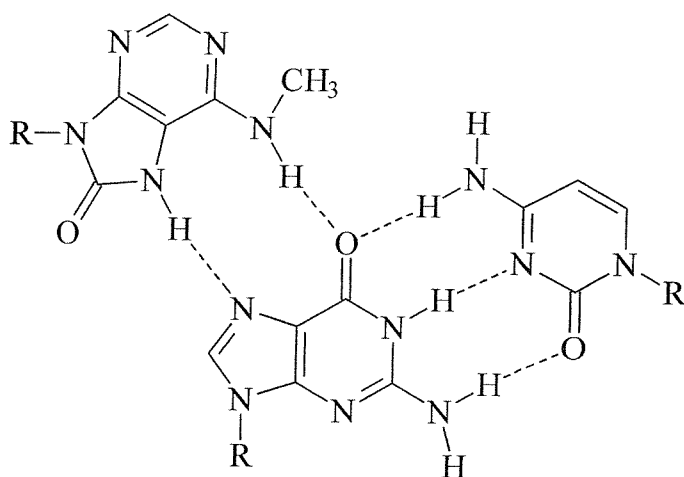
b) **M·GC Triplet**

Figure 1.10: Diagrams representing the Hoogsteen hydrogen bonding of the parallel triplets formed incorporating the cytosine analogues; a) 8-oxo-adenine, and b) N6-methyl-8-oxo-adenine.

(1.4.1.6)   8-Oxo-adenine and N6-Methyl-8-oxo-adenine.

8-oxo-adenine is a modified purine base that was designed to recognise GC base pairs in a parallel orientation within a pyrimidine oligonucleotide (Fig. 1.10). The initial study (Miller *et al* 1992) demonstrated that replacement of cytosine with 8-oxo-adenine in the sequence CTTCTTTTTTATTTT resulted in stable triplex formation at neutral pH. This was due to 8-oxo-adenine generating two hydrogen bonds from positions N7 and N6, with the hydrogen atom at position N7 having a pKa value of 8.7 (Cho & Evens 1991). A series of thermal melting studies showed that 8-oxo-adenine substituted into the above sequence interacted almost exclusively with GC base pairs at pH 7 with a T_m value of 29 °C, whilst the same sequence substituted with ^mC resulted in a T_m value of 32 °C. However increasing the pH to 8.0 resulted in the 8-oxo-adenine substituted oligonucleotide destabilising the triplex by 7 °C, whereas as the ^mC substituted oligonucleotide destabilised the triplex by 12 °C compared to the Tm values at pH 7 (Miller *et al* 1992).

Whilst this analogue improves the stability of parallel triplexes at near physiological pH, the level of stability achieved is still lower than with either protonated cytosine or methyl cytosine at low pHs. A later study concluded that at pHs above 7.4, an oligonucleotide substituted with 8-oxo-adenine in place of cytosine had a greater affinity for its native duplex target than an unmodified oligonucleotide containing cytosine residues. However when the pH was decreased below 7.4 then the affinity of the native oligonucleotide was found to be greater than the 8-oxo-adenine modified oligonucleotide (Davison & Johnson 1993). Oligonucleotides containing 8-oxo-adenine modifications bound in a pH independent manner to their duplex targets. The relatively low affinity could be due to the lack of charge on the OA·GC triplet and because it is not isostructual with T·AT and C^+·GC.

N6- methyl-8-oxo-adenine (M) is a similar purine derivative which was designed to interact with GC when in the *syn* conformation (Krawczyk *et al* 1992) (Fig. 1.10). It was found that M gave superior triplex stabilisation to $m^{5ox}C$ at physiological pH and that
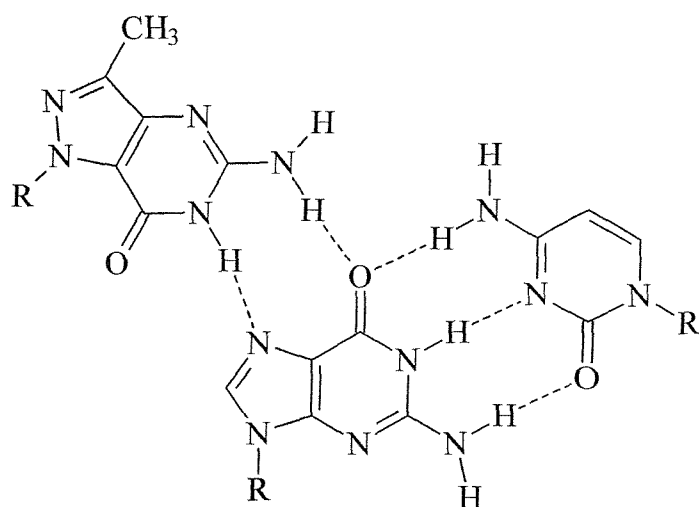
a) **P1·GC Triplet**
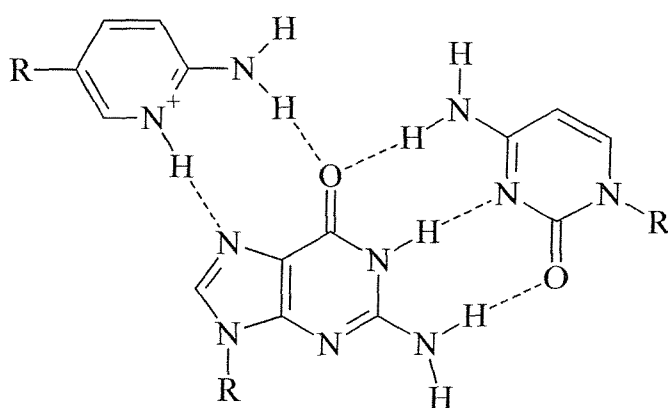
b) **β-2AP·GC Triplet**
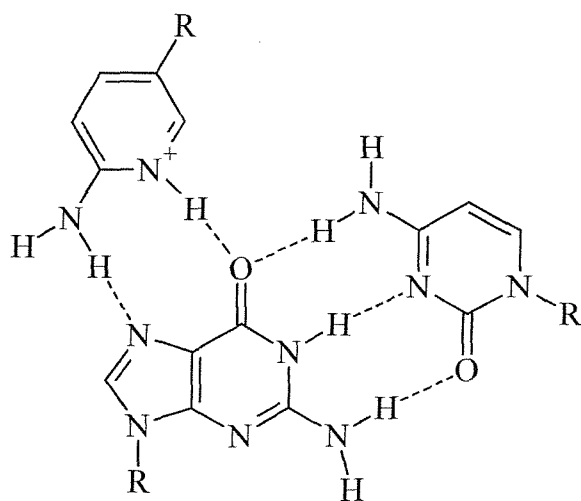
c) **α-2AP·GC Triplet**

Figure 1.11: Hoogsteen hydrogen bonding of the parallel triplets formed containing a) P1, and b) β-2-aminopyridine as cytosine analogues. Figure c) represents an antiparallel triplet incorporating the cytosine analogue α-2-aminopyrimidine.

the affinity was pH independent. However since it is a purine analogue incorporation into pyrimidine third strands causes backbone distortions, not only at the GC target sites but also at adjacent AT sites.

(1.4.1.7)   P1.

Another example of a purine analogue is P1 (Fig. 1.11), which binds to GC in an *anti* configuration, with one edge mimicing the N3 protonation of cytosine (Koh & Dervan 1992). Single P1·GC triplets have been found to have the same stability as ^{5m}C·GC triplets, however alternating AG sites are bound with lower affinity than with ^{5m}C. This may be due to structural deformations arising at each ApG and GpA step as P1·GC is not isostructual with T·AT (Radhakrishnan *et al* 1993).

(1.4.1.8)   5(1-Propynyl)-2-deoxyuridine.

This analogue was one of several C5 substituted uracil bases (Fig. 1.12), designed initially as potential antiviral/ anticancer agents (De Clercg *et al* 1983, & Goodchild *et al* 1983). It was initially trialed as a potential antisense agent and was shown to bind to a RNA target with a high affinity when incorporated into a phosphothioate oligonucleotide (Wagner *et al* 1993). This subsequently caused gene-specific inhibition at an oligonucleotide concentration of 5nM. Phosphothioate modified oligonucleotides without the C5-propyne group exhibited a much lower inhibitory effect. However the addition of cell permeablizing agents or their direct micro-injection into the cells was required for the oligonucleotides to exert their antisense effects (Wagner *et al* 1993 & Wagner 1994).

This base was subsequently incorporated into TFO's (Lacroix *et al* 1999) and shown to produce more stable triplexes than thymidine and the stability is retained even at a neutral pH and at physiological magnesium concentrations. The increase in triplex stability imparted by the incorporation of propynyl deoxyuridine was postulated to be due to entropic stabilisation and enhanced base stacking as compared to that of thymidine. A 2-D-NMR study (Phipps *et al* 1998) concluded that the enhanced stability was due to

a) $_p$U·AT Triplet

b) ^{P}U·AT Triplet

c) ^{7}X·AT Triplet
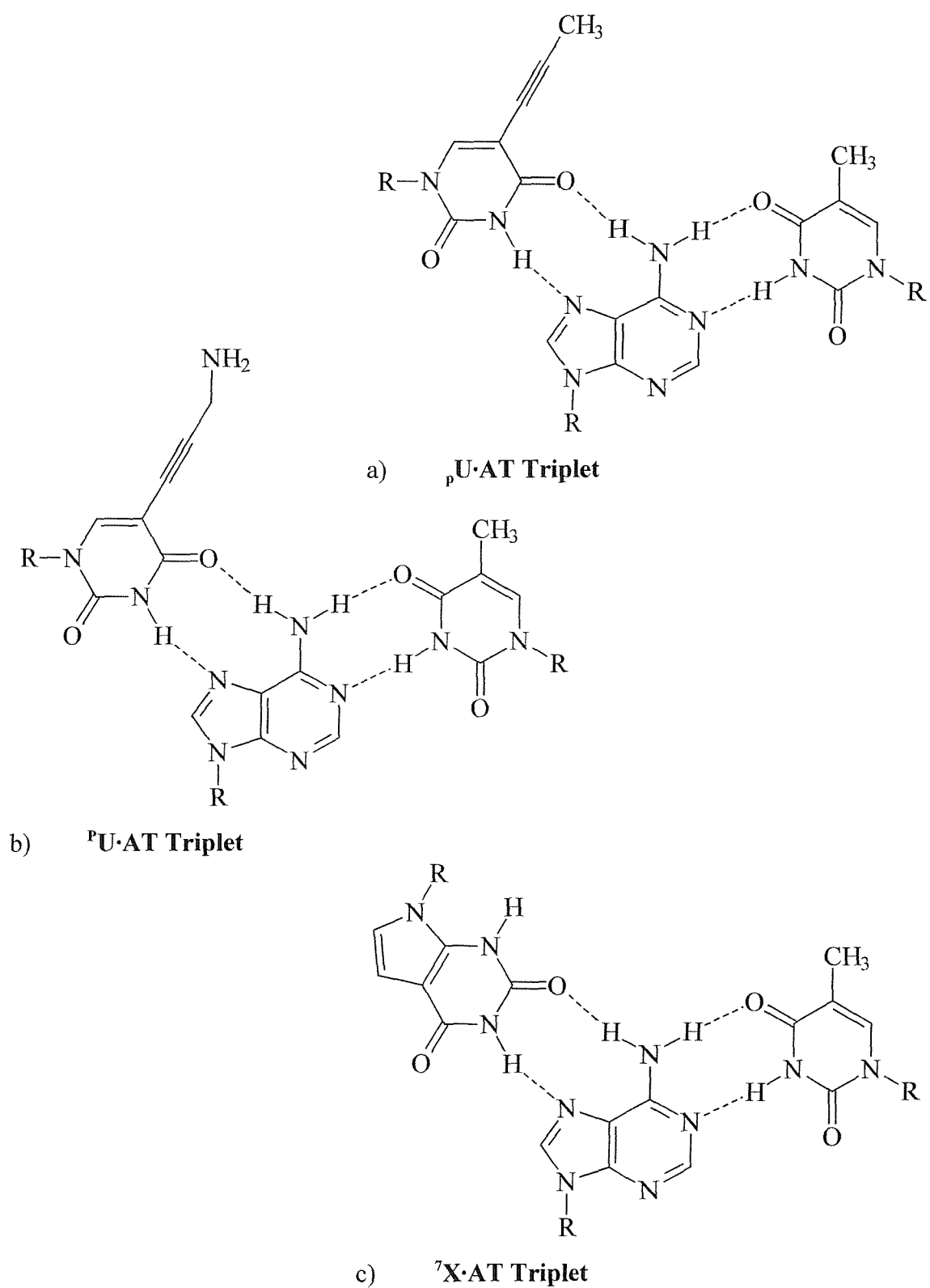
Figure 1.12: Hoogsteen hydrogen bonding of the parallel triplets containing the thymine analogues; a) 5-propynyl deoxyuridine, and b) 5-propargylamino deoxyuridine. Figure c) represents the antiparallel triplet containing the 7-deaza-2-deoxyxanthine thymine analogue.

increased base stacking interactions and local hydrophobicity of the propynyl group. These results demonstrated that the electron cloud of propynyl deoxyuridine stacked over the 5' neighbouring bases.

(1.4.1.9)   **5(1-Propargylamino) deoxyuridine.**

This base was designed as a specific protonated thymine analogue (Fig. 1.12), following reports that the positive charge on cytosine bases imparted a higher stability at low pH on parallel triplexes than did T·AT triplets (Volker & Klump 1994, Keppler & Fox 1997, Gowers & Fox 1998) and the early results achieved with 5(1-propynyl)-2-deoxyuridine. 5(1-Propargylamino) deoxyuridine (^{P}U) substitution has subsequently been shown to enhance parallel triplex stability across a range of pH's and a fully substituted TFO at pH 5.0 bound at least 4 orders of magnitude greater than its unmodified counterpart (Bijapur *et al* 1999).

The increased stability is thought to be due to favourable interactions between the charged amino groups and the phosphodiester backbone. However the generation of the charged amino group is pH dependent and it has been shown to bind with a lower affinity at pH 7.0 than at pH 5.0. However this results in a more stable complex than the unmodified oligonucleotide (Bijapur *et al* 1999). While ^{P}U has a stabilising influence on triplex stability, dependent on pH, the stabilisation has also been shown to be influenced by the base sequence composition. If ^{P}U is placed adjacent to a protonated cytosine the triplex is less stable than that observed when ^{P}U and protonated cytosine residues are separated by one uncharged nucleotide (Gowers *et al* 1999b).

(1.4.1.10)   **7-Deaza-2-deoxyxanthosine.**

This compound was designed as an analogue of thymine for recognition of AT base pairs (Fig. 1.12). Substitution of dzaX for T into a TFO with guanine resulted in a high affinity for its duplex target in an antiparallel orientation above that of the native TG containing TFO (Milligan *et al* 1993). The same study also showed that the destabilising

effect of physiological concentrations of potassium upon antiparallel triplex formation (Cheng & Van Dyke 1993 and Olivas & Maher 1995) could be alleviated by substituting dzaX for thymine. A 100-fold increase in the affinity of GGXGGXGGXXGXGGX (where X is either T or dzaX) for its duplex target was observed under physiological conditions when substituted with dzaX. The increase in affinity was postulated to be because dzaX is a purine base whereas thymine is a pyrimidine base. dzaX would cause less structural distortions in the phosphodiester backbone than in a GT containing oligonucleotide, as a continuous purine TFO would have a more regular geometry than a TFO contain both pyrimidines and purines.

A further study has demonstrated the potential of dzaX in stabilising antiparallel triplex formation *in vitro* and *in vivo* in a series of gene directed experiments (Faruqi *et al* 1997). These studies demonstrated that dzaX substituted oligonucleotides could target a duplex in the presence of 140 mM KCl, whereas unsubstituted oligonucleotides could not. The same oligonucleotides were also shown to give approximately a five fold increase in the *in vivo* mutation frequency relative to the unmodified oligonucleotides.

(1.4.1.11)   3-Benzamido phenylimidazole (D₃)

The non-natural deoxyribonucleoside 1-(2-deoxy-β-D-ribofuranosyl)-4-(3-benzamidophenyl) imidazole (D₃) has a single bond that joins two aromatic rings resulting in the structure having a high degree of rotational flexibility (Fig.1.13), and therefore permits it to have an interchangeable geometry. As a result it was thought that it might allow the interaction with pyrimidine·purine base pairs preferentially over purine·pyrimidine base pairs at physiological pH (Griffin *et al* 1992). This base analogue when used in combination with thymine and cytosine, allowed recognition of DNA sequences containing all 4 bases. However this non-natural base cannot distinguish between CG or TA base pairs. Recognition of TA and CG was found to be strongly dependent on the 3' neighbouring triplet, but only weakly dependent on the 5' triplet (Griffen *et al* 1992). D₃ has three chemical groups that can potentially form Hoogsteen hydrogen bonds; a carbonyl oxygen, a N3 imidazole nitrogen, and an amide proton.
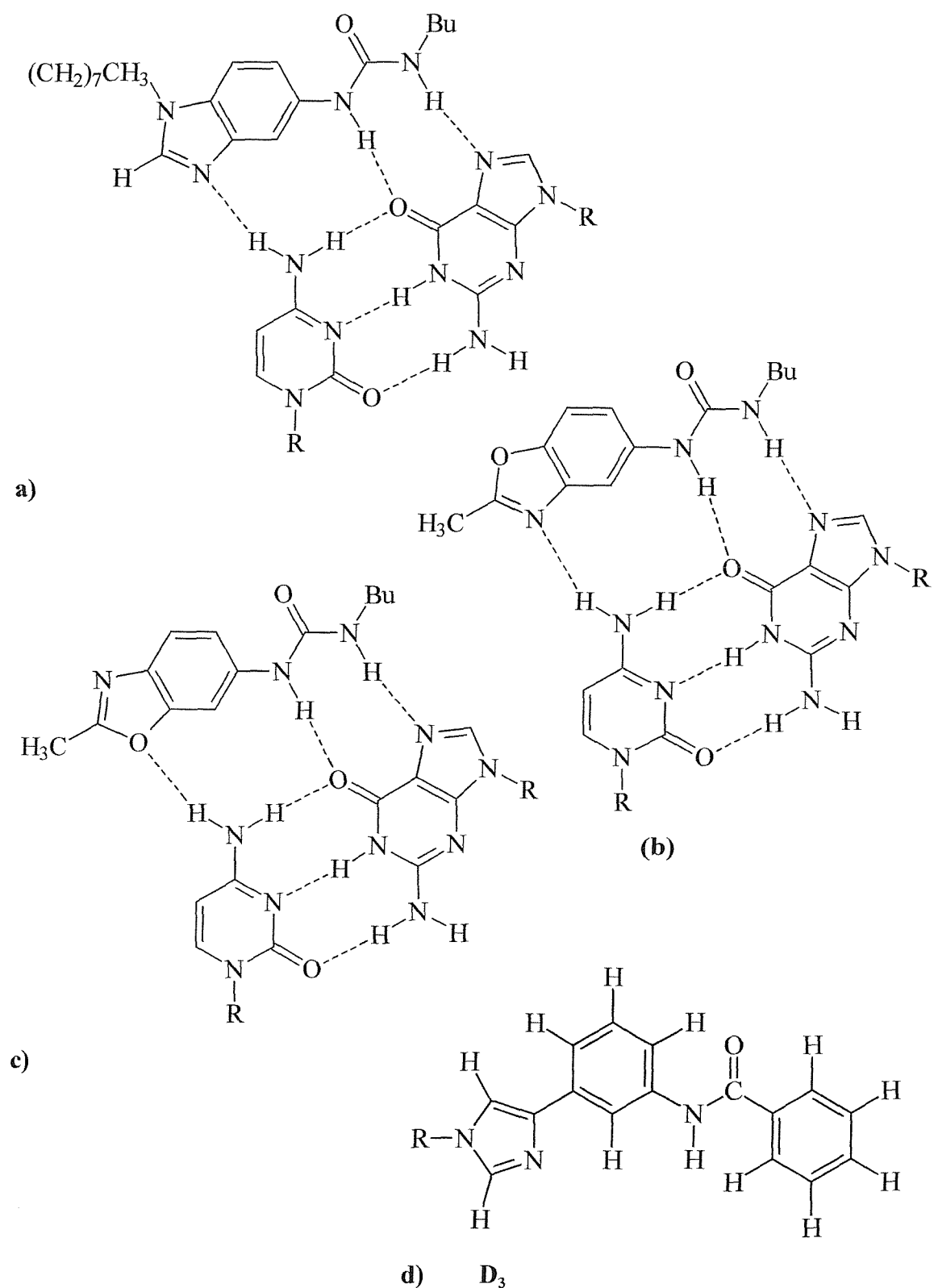
Figure 1.13: Un-natural base analogues designed to enhance the stability of the single hydrogen bond presented by the pyrimidine residues. Diagrams a) - c) represent the benzimidazole and benzoxazole derived heterobicyclic analogues bound to CG base pairs. Diagram d) represents the 3-benzamido phenylimidazole deoxyribonucleoside in its free state.

Despite this D_3 shows no evidence for specific hydrogen bond formation. An additional NMR study demonstrated that D_3 actually intercalates between TA base pairs and the adjacent 3' T·AT triplet (Koshlap *et al* 1993). YpR steps have long been known as good sites for intercalation and the D_3 base forms a structure imitating a single base triplet, in that each ring lies in a position within the triplex similar to that of each base within a natural triplet. This causes a general unwinding of the helix at the D_3 site and its 3' neighbour enabling accommodation of the D_3 base by increasing the helical rise (Wang *et al* 1996). Furthermore it was shown that D_3 mimics a triplet and changes the DNA conformation so that it is more similar to B-DNA, rather than A-DNA. (Wang *et al* 1996). These changes in structure are a direct result of D_3 intercalating, skipping a potential base pair, and results in other bases being forced out of plane. Therefore pyrimidine bases within a duplex purine strand are skipped via the use of D3, resulting in a step towards mixed sequence recognition (Koshlap *et al* 1993).

(1.4.1.12)   2'-deoxynebularine.

This artificial base (deoxypurine) was designed to recognise pyrimidine bases of a duplex with the N1 atom acting as a hydrogen bond acceptor forming a single hydrogen bond to the pyrimidine target (Fig. 1.14). Experiments confirmed the formation of N·CG triplets but showed that N·AT triplets were formed with comparable stability (Stilz & Dervan, 1993). The stability of both these triplets was higher than either N·TA or N·GC, however the stability of the N·CG triplet was comparable to that of A·CG and significantly less stable than G·GC, A·AT, and T·AT. The lower stability of N·AT and N·CG compared to the conventional triplets was due to the formation of only a single hydrogen bond, and that no other stabilising interactions occurred between the N base and either the CG or AT base pairs.

a)   **N·CG Triplet**

b)   **N·AT Triplet**

c)   **N^9-2-aminopurine**

d)   **N^7-2-aminopurine**

e)   **WNA-7βG**
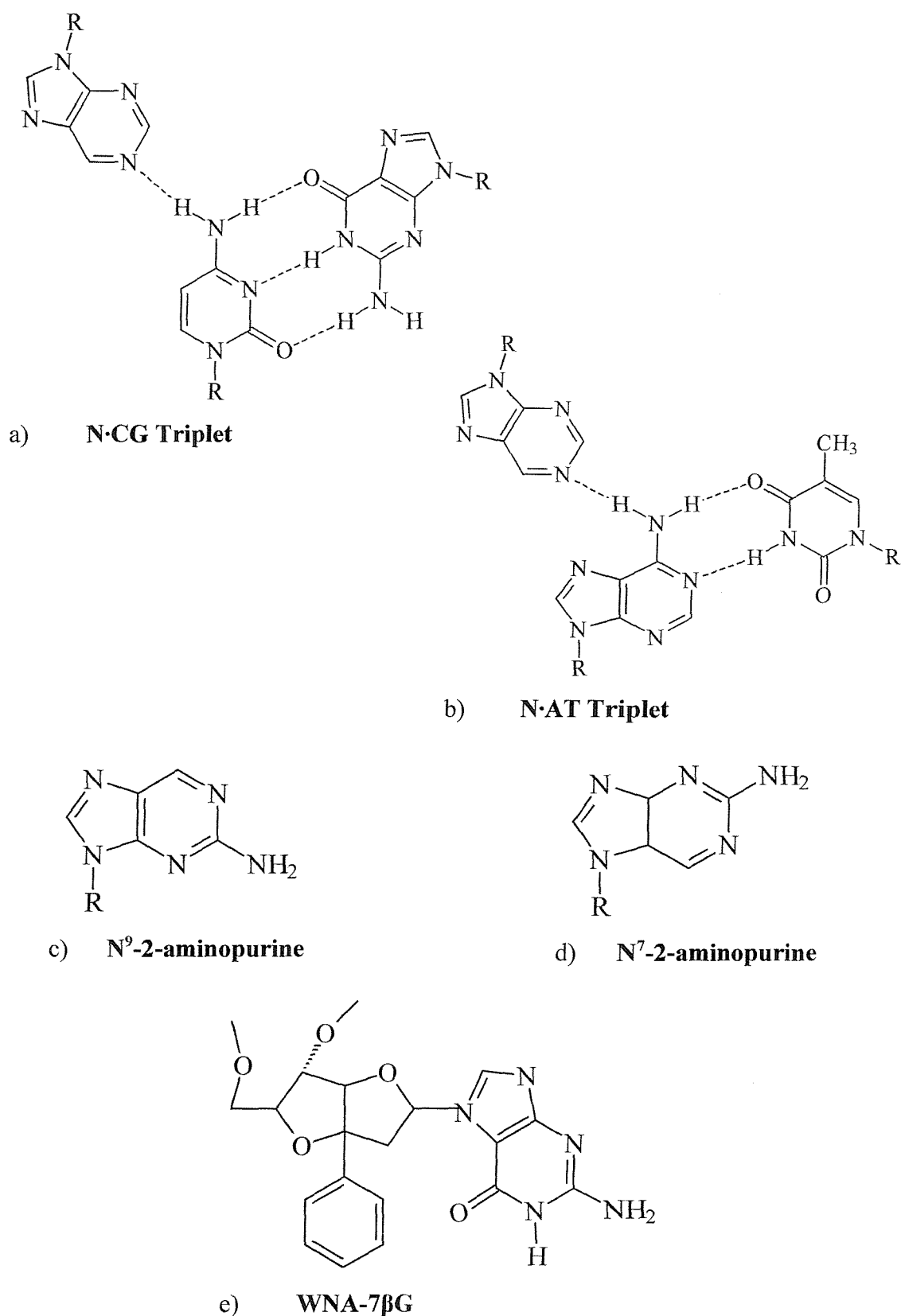
Figure 1.14: Diagram a) represents the artificial base 2'-deoxynebularine bound to cytosine, whilst diagram b) represents the base bound to adenine. Diagrams c) and d) represent beta anomers of N^9- and N^7-2-aminopurine respectively. Diagram e) shows the structure of the W-shaped nucleic acid 7 β-guanine.

(1.4.1.13)   N⁹-aminopurine & N⁷-aminopurine.

The alpha and beta anomers (Fig.1.14) of these analogues were designed to overcome pyrimidine interruptions within antiparallel triplexes. It was shown that $\beta N^7 ap$ can replace T or A in recognising an AT base pair, whereas $\alpha N^7 ap$ could recognise a TA inversion. However the triplex with generated with a single $\alpha N^7 ap$ residue was 4 fold less stable than the canonical triplex with an AT base pair (Parel & Leumann 2001). Furthermore these studies demonstrated that $\alpha N^9 ap$ poorly discriminated between all four potential base pairs indicating it may have a potential role as a universal triplex base. In contrast $\beta N^9 ap$ preferentially recognised the CG base pair. Therefore $\beta N^9 ap$ may be a potential base analogue for guanine, not only to overcome pyrimidine recognition, but also to prevent the formation of G-quadruplex structures within G-rich oligonucleotides.

(1.4.1.14)   Other analogues.

Benzimidazole and benzoxazole derived heterobicyclic compounds have been reported to recognise CG base pairs (Lecubin *et al* 1999). Studies demonstrated that recognition is due to interaction with the 4-amino group of cytosine and the O4 and N7 groups of guanine. However these results were obtained with free bases in chloroform and have not been incorporated within an oligonucleotide third strand (Fig. 1.13).

A nucleoside analogue incorporating a benzene ring and a purine base has been reported to recognise a TA base pair in an antiparallel orientation (Sasaki *et al* 2001). The bicyclic structure is believed to fix the conformation of the non-natural nucleoside in a W shape, and has been subsequently termed W-shaped nucleic acid (WNA) (Fig 1.14). Attachment of guanine at the N-7 position to the WNA in the beta conformation (WNA-7βG) was demonstrated to recognise a TA base pair via the guanine base forming two hydrogen bonds to the adenine of the homopurine strand and the benzene ring opposite the thymidine base maintaining stacking interactions.

(1.4.2) Triple Helix Ligands.

Several compounds have been discovered which selectively bind to triple helical DNA. These compounds, which usually act via intercalation, stabilise triplexes by binding to triplex (not duplex) DNA, thereby perturbing the equilibrium in the direction of triplex formation. While most of these compounds are added as separate ligands, some have been covalently attached to triplex forming oligonucleotides (see section 1.4.4). Some ligands have been shown to stabilise triplex formation at sites containing a central triplex mismatch, and may therefore increase the range of triplex sites (Chandler *et al* 1995, Orson *et al* 1999). Many of the ligands used for stabilising triplexes have large aromatic planar groups so as to allow the molecules to intercalate with the DNA and therefore maximise the stacking interactions.

(1.4.2.1) Benzopyridoindole and derivatives.

Benzo(e)pyridoindole (BePI) (Fig. 1.15) was the first compound designed to stabilise triplex DNA. It has been shown to stabilise both parallel (Mergny *et al* 1992) and antiparallel triplexes (Escudé *et al* 1996), but does not affect GT parallel triplexes. This compound preferentially stabilises T·AT rather than C^+·GC triplets, presumably because of un-favourable charge interactions between the protonated cytosine and the cationic ligand. Selectivity is believed to result from the ring system of BePI stacking more efficiently within triplex rather than duplex DNA. Molecular modelling showed that the side chain of BePI lies within the major groove between the third strand and the duplex pyrimidine strand (Pilch *et al* 1993). This is located in a position which would be expected to reduce triplex stability. BePI has also been reported to block *E.coli* RNA polymerase by facilitating stable triplex formation downstream from the RNA polymerase binding site (Mergny *et al* 1992).

Benzo(g)pyridoindole (BgPI) is a derivative of BePI and has been shown to stabilise triplex DNA as well as BePI (Escudé *et al* 1995). Molecular modelling demonstrated that the side chain of BgPI was important for its triplex stabilisation, in
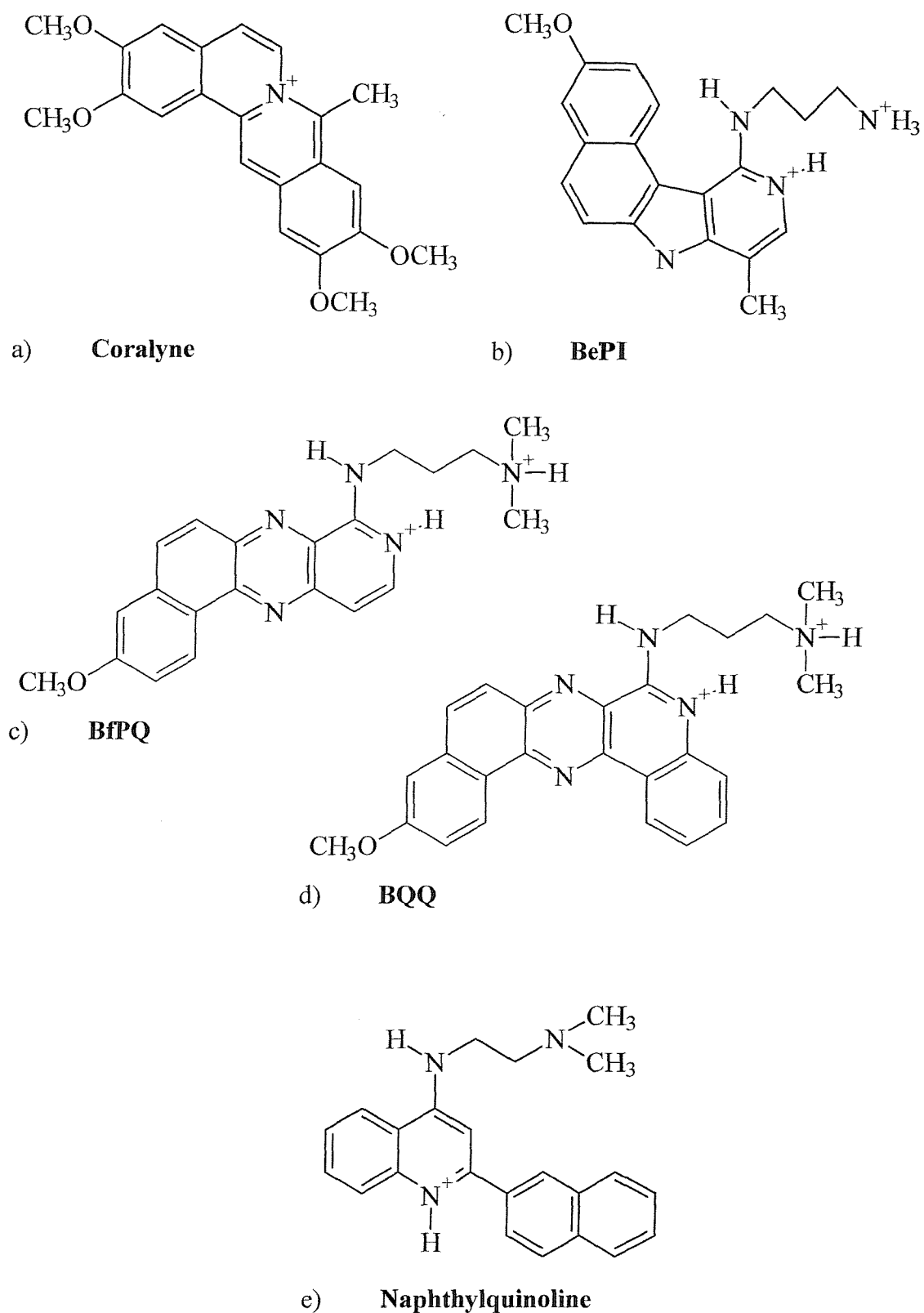
Figure 1.15: Structures of various triple helical DNA stabilising ligands. a) represents the ligand coralyne, b) - d) represent members of the benzopyridoindole family of compounds, e) represents the quinoline derivative, naphthylquinoline.

contrast to the side chain of BePI which forms un-favourable contacts with the triplex. It has therefore been suggested that the side chain of BgPI lies within the major groove between the third strand and the purine strand of the duplex (Escudé *et al* 1995). BgPI has a more linear structure than BePI, resulting in decreased base stacking; this may be overcome by increased electrostatic interactions.

A structurally related compound, benzo(f)pyridoquinoxaline (BfPQ) (Fig. 1.15), has also been reported to stabilise parallel triplexes (Escudé *et al* 1998). This ligand also stabilises a parallel triplex containing a bulge (Marchand *et al* 1996). BfPQ may therefore stabilise undesired triplexes, and thereby reduce the stringency of triplex formation. It has been suggested that BfPQ stacks with the Hoogsteen H-bond pairs and does not interact with the Watson stand of the triplex (Escudé *et al* 1998). Many derivatives of these ligands have been prepared in the search for a compound with improved triplex affinity. The next generation of ligands contained an additional ring adjacent to the pyridine ring of BfPQ giving rise to BQQ which is the best triplex binding agent described to date (Escudé *et al* 1998). Increasing the ring system from a tetracyclic to pentacyclic system presumably enhances triplex stability by improving stacking interactions.

(1.4.2.2) Coralyne.

This is a natural product that binds to DNA, containing 4 fused aromatic rings (Fig. 1.15). Initial reports claimed that it bound to triplexes much better than duplexes and that it had little sequence specificity and enhanced both T·AT and C^+·GC triplets (Lee *et al* 1993). However more recent studies have shown that coralyne preferentially stabilises T·AT triplets (Moraru-Allen *et al* 1997). This seems more reasonable as coralyne is positively charged and would be unlikely to intercalate adjacent to C^+·GC triplets. This seems to be a common feature of triplex binding ligands; those bearing a positive charge on the ring structure are selective for T·AT triplets.

Several coralyne derivatives have also been prepared, all of which have a lower affinity for triplex DNA, again exhibiting a preference for T·AT triplets (Latimer *et al* 1995).

(1.4.2.3)   Di-substituted Anthraquinones.

Anthraquinones possess a tricyclic ring system and it was demonstrated that bis-substituted versions stabilised triplexes in a manner dependent upon the position of substitution (Fig. 1.16). 1,4 di-substituted compounds showed preferential affinity for duplex DNA, whereas 2,6 di-substituted compounds bound selectively to triplex DNA (Fox *et al* 1995). A further study showed that the degree of triplex stabilisation was related to the position of substitution, with 2,7- disubstituted amidoanthraquinone displaying the greatest triplex affinity. The order of affinity with parallel triplexes decreases as follows; 2,7 > 1,8 = 1,5 > 2,6 (Keppler *et al* 1999a). Molecular modelling studies showed that all the ligands (except the 1,8 isomer) bound by intercalation with one substituent chain in the minor groove and the other substituent chain in the major groove (Fig. 1.17). The 1,8 disubstituted amidoanthraquinone could also bind by intercalation but inserted both side chains into the same triplex groove. (Keppler *et al* 1999a). However the order of stability is very different for antiparallel triplexes (Keppler *et al* 2001) with only the 2,7 and 1,8 isomers stabilising TG containing triplexes, whereas AG containing triplexes are only stabilised by 1,5 and 2,6 isomers. This must be due to differences in the ligand-base stacking interactions, as the various antiparallel triplets are not isomorphic.

Anthraquinone sulphonamides have also been shown to stabilise triplex DNA. Again the position of substitution influences triplex stabilisation (Kan *et al* 1997), with the 2,7 di-substituted anthraquinone sulphonamide again affording the best triplex stabilisation. It was further shown that greater triplex stabilisation was afforded by those ligands bearing higher numbers of positively charged substituents.
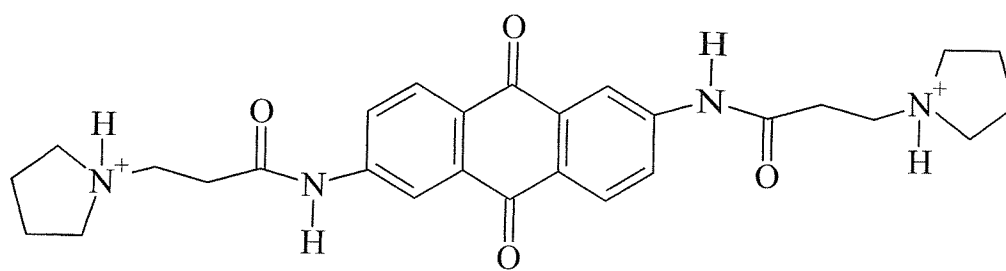
a) **2,6 Amidoanthraquinone**
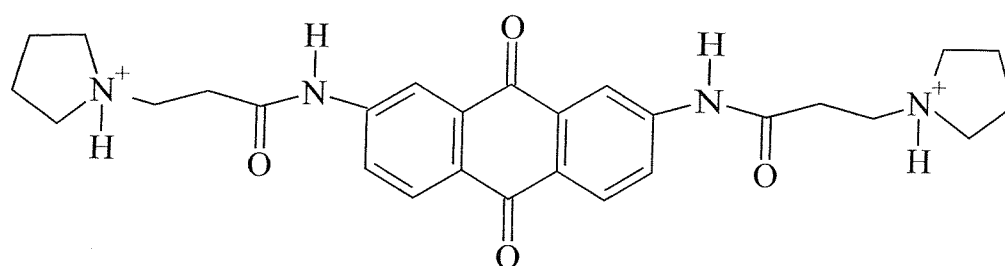
b) **2,7 Amidoanthraquinone**
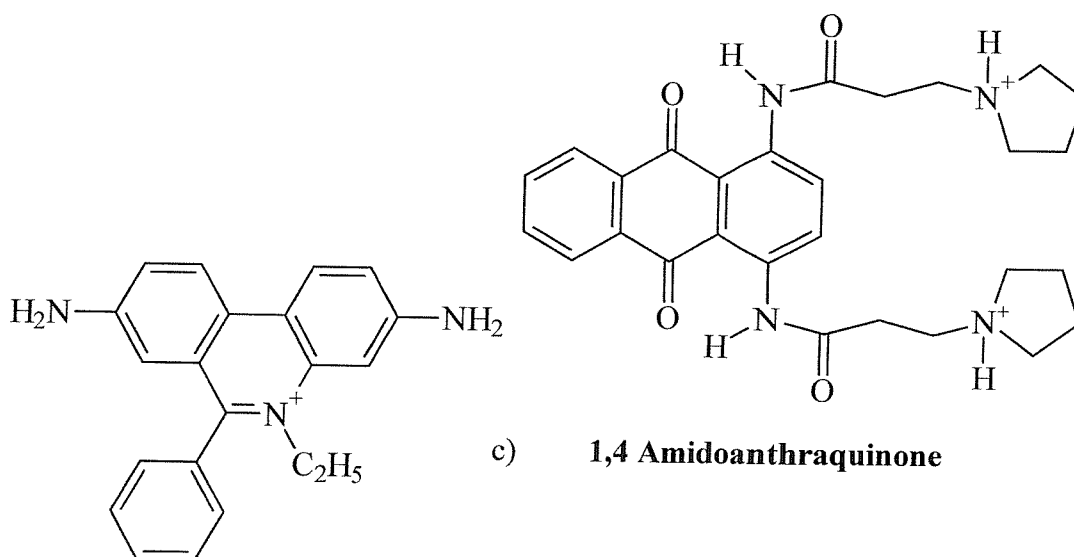
c) **1,4 Amidoanthraquinone**
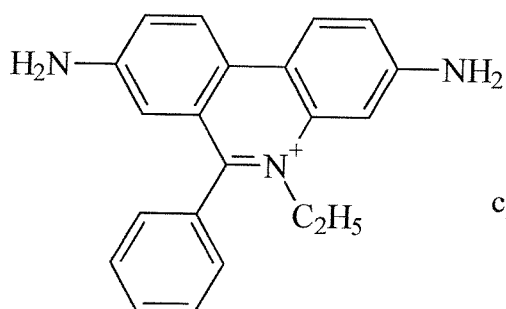
d) **Ethidium**

Figure 1.16: Diagrams a) - c) represent various di-substituted compounds from the anthraquinone family. Diagram d) shows the structure of ethidium.
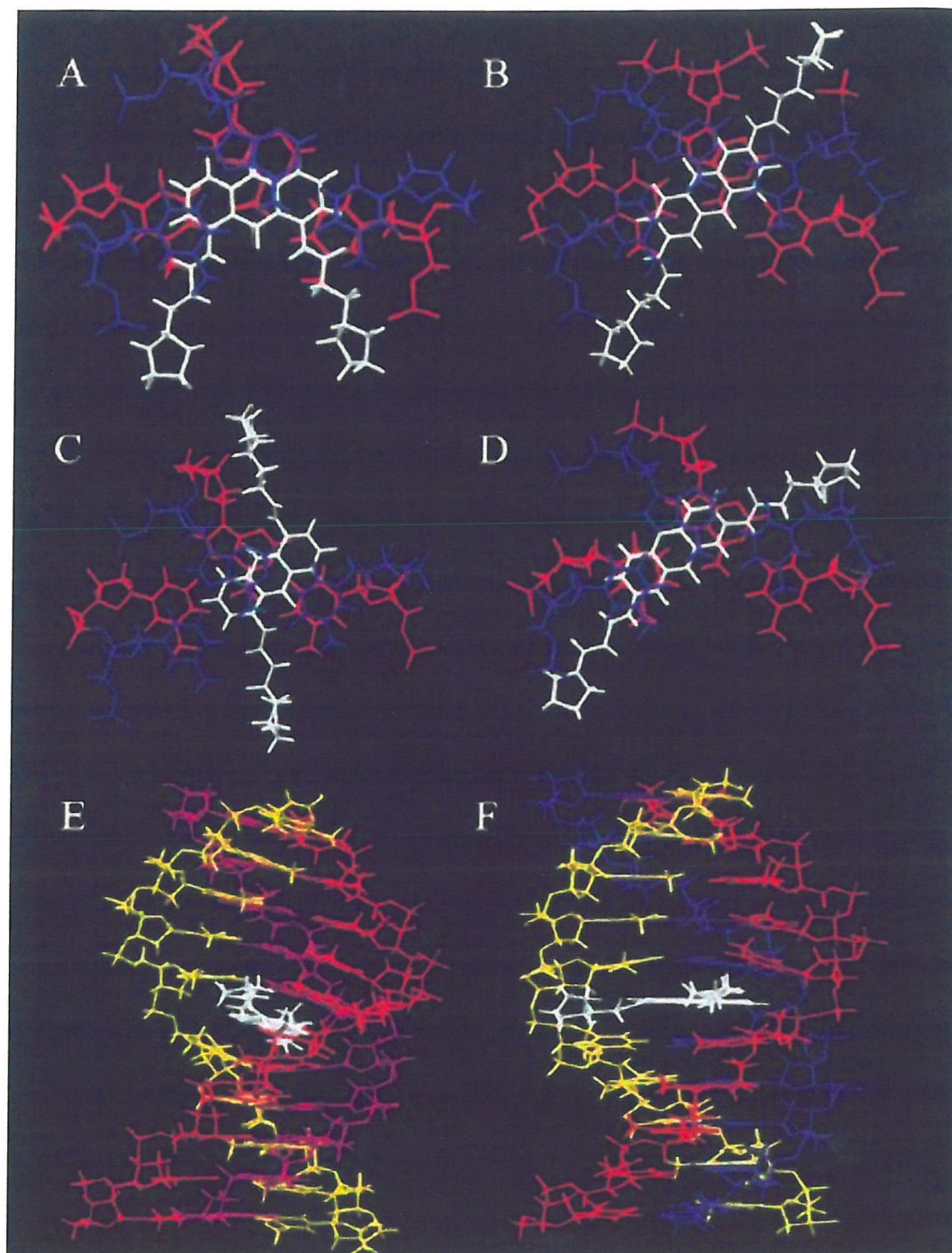
Figure 1.17: Molecular models of the interaction between $T_{(10)} \cdot A_{(10)} T_{(10)}$ triplex DNA and A) 1,8 bis-amidoanthraquinone, B) 2,6 bis-amidoanthraquinone, C) 1,5 bis-amidoanthraquinone, and D) 2,7 bis-amidoanthraquinone. In each case the base triplets immediately above the ligand are shown in blue and those below are shown in red; the ligand is also shown in white. E - F) show views of the entire complex with 2,6 bis-amidoanthraquinone and 1,8 bis-amidoanthraquinone respectively, with the third strand shown in red, illustrating the position and alignment of the intercalating ligand. Reproduced from Keppler *et al Eur. J. Biochem.* **263**, (1999)

(1.4.2.4)   Quinoline Derivatives.

The quinoline triplex stabilising ligands were designed to have an unfused aromatic system to enable flexibility and improve base stacking, a planar surface to promote intercalation, and a positive charge to counteract the negative density generated via the 3 phosphodiester backbones. In this serries of compounds the 2 naphthyl derivative (naphthylquinoline) afforded the greatest triplex stabilisation (Wilson *et al* 1993) (Fig. 1.15).

Footprinting studies later showed that 50 μM of this ligand enhanced triplex affinity by as much as 100-fold, and that it was also possible to stabilise triplexes with a central triplet mismatch (Chandler *et al* 1995). Further footprinting studies demonstrated that naphthylquinoline stabilised T·AT triplets to a greater degree than C^+·GC triplets (Cassidy *et al* 1996) and that naphthylquinoline could also be used to stabilise both parallel and antiparallel triplexes. Although antiparallel triplex formation is pH independent this ligand induced a greater increase in triplex affinity at low pH indicating that the active species is protonated (Cassidy *et al* 1996).

A further derivative in this serries is a naphthylquinoline dimer (bis-naphthylquinoline). Footprinting studies with this ligand demonstrated that it effectively stabilised 9mer parallel triplexes containing a single C^+·GC triplet approximately 30-fold more than the monofunctional naphthylquinoline at equivalent concentrations (Keppler *et al* 1999b). As well as increasing the binding affinity one other advantage of bis-intercalators is that they potentially enable a greater discrimination between triplex and duplex DNA and hence allows a lower concentration of ligand to be used (Keppler *et al* 1999b).

(1.4.2.5)   Ethidium Bromide.

Ethidium bromide (Fig. 1.16) is well known as a duplex DNA intercalating agent (Waring *et al* 1965, 1966). Early thermal denaturation studies demonstrated this ligand destabilised the triplex helix formed by poly(A)·2poly(U) (Wang *et al* 1974). However a later study showed that ethidium stabilised poly(A)·2poly(T) more than poly(A)·poly(T) (Scaria & Shafer 1991). This could be because ethidium binds only weakly to poly(A)·poly(T) because of its unusual conformation (Bresloff & Crothers 1981, Baguley & Falkenhaug 1978, Fox & Waring 1987, Nelson *et al* 1987). A separate study further demonstrated that parallel triplexes containing both C^+·GC and T·AT triplets were destabilised by ethidium, whereas mixed sequence duplexes were stabilised by ethidium (Mergny *et al* 1991, Fox & Waring 1987).

(1.4.2.6)   Other Ligands.

Aminoglycoside antibiotics are bacterial agents comprised of two or more amino sugars joined in glycosidic linkage to a hexose nucleus. It has been reported that the aminogylcoside, neomycin, significantly stabilises poly(dA)·2poly(dT) triplex DNA, while poly(dA)·poly(dT) duplex DNA is unaffected (Arya & Coffee Jr 2000, Arya *et al* 2001). The structure of neomycin prohibits intercalation as its mode of stabilisation and its triplex affinity is postulated to be due to neomycin binding to one of the triplex grooves (Arya & Coffee Jr 2000). Furthermore triplex stabilisation is sensitive to the charge and charge placement on the antibiotic, as related aminoglycosides were shown to have lower triplex stabilising properties (Arya *et al* 2001).

Recently diethyloxadicarbocyanine (DODC) has been reported to preferentially stabilise triplex DNA, but its mode of binding is unknown (Ren & Chaires 2000). It has also been reported that naphthoflavone exclusively stabilises triplex DNA (Prof. J.B. Chaires unpublished data). These findings were made using competition dialysis assays. Polycations such as polyamines, some oligopeptides (Potaman *et al* 1995), and comb-type polycations (Maruyama *et al* 1997) are also known to stabilise triplex DNA.

(1.4.3) Backbone Modifications.

As previously mentioned, native oligonucleotides are susceptible to degradation by cellular nucleases. The polyanionic charge of the phosphodiester backbone may also hinder their cellular uptake, as well as producing unfavourable interactions with the polyanionic backbones of the target duplex. In order to overcome these shortcomings several backbone modifications have been studied.

(1.4.3.1)   Phosphorothioates.

Replacement of one of the oxygen atoms in the phosphodiester backbone with sulphur gives rise to phosphorothioate (Fig. 1.18). These modifications have a similar charge density to normal phosphodiester backbones, are soluble in aqueous solvents and have increased resistance to many nucleases (Stein *et al* 1998). Purine strands containing stereoregular (Rp) or diastereoisomeric phosphothioate linkages demonstrate triplex affinity similar to that of phosphodiester linkages (Hacia *et al* 1994). In contrast pyrimidine strands containing stereoregular (Rp) or diastereoisomeric phosphothioate linkages do not form triplexes (Latimer *et al* 1989, Hacia *et al* 1994). Subsequent studies have demonstrated that antiparallel phosphorothioate GA oligonucleotides have a triplex affinity lower than that of phosphodiester oligonucleotides, but that 5' and 3' modification of GA oligonucleotides with phosphothioate increases nuclease resistance without reducing the binding affinity (Lacoste & Hélène 1997). Conversely phosphorothioate end modified GT oligonucleotides do not form triplexes in either orientation (Lacoste & Hélène 1997).

(1.4.3.2)   Phosphoramidates.

Phosphoramidates are formed when an oxygen atom in the phosphate group is replaced with a nitrogen atom. This replacement can occur at one of two positions, changing either the 3' or 5'-oxygen or one of the two phosphate oxygen atoms (Fig. 1.18). Parallel TFOs containing a N3' - P5' phosphoramidate show significantly enhanced
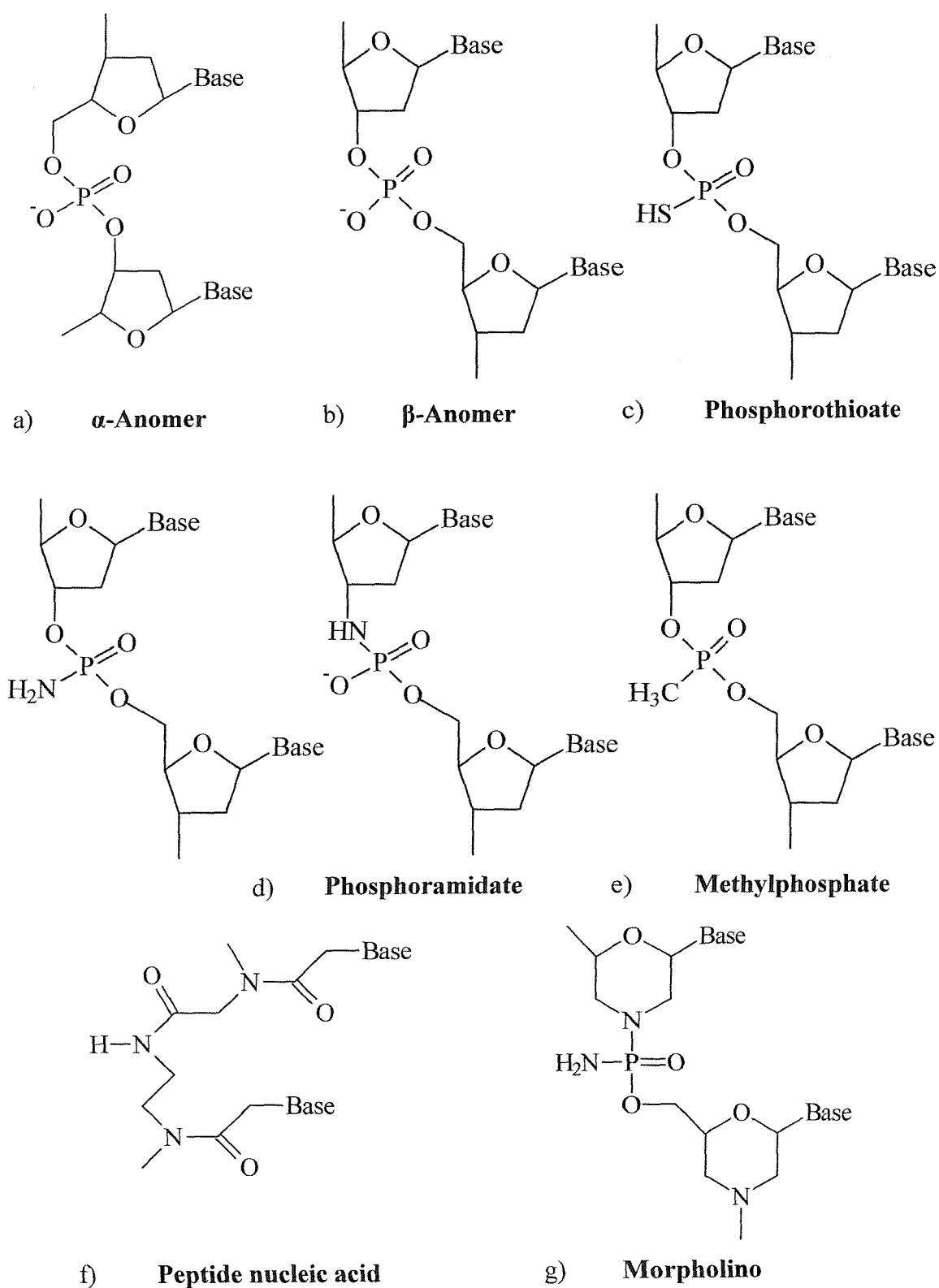
Figure 1.18: Diagrams a) and b) illustrate the two different anomers of the natural phosphodiester backbone. Diagrams c)-f) illustrate several backbone modifications discussed in section 1.4.3. Diagram g) illustrates a novel sugar modification (morpholino) again discussed in section 1.4.3.

triplex affinity when compared to their natural phosphodiester counterparts (Escudé *et al* 1996, Zhou-Sun *et al* 1997). This modification has been demonstrated to stabilise triplex formation with a target site containing 6 adjacent guanine residues at pH 7, and was shown to be more effective than 5-methyl-cytosine or conjugated acridine (Escudé *et al* 1996). Stabilisation was further enhanced by combining 5-methyl-cytosine and the N3'-P5' phosphoramidate modification. N3' - P5' phosphoroamidate oligonucleotides have been shown to inhibit transcription of proviral HIV at pH 7.0, whereas phosphodiester oligonucleotides had no effect. Further stability can be afforded by using an RNA phosphoramidate (Gryaznov & Winter 1998). Both of these studies demonstrated that phosphoramidates have an enhanced resistance to nucleases compared to the natural phosphodiester. The rationale for the increase in triplex stability afforded by N3' - P5' phosphoramidate is as yet unknown, however it is believed to result from the change in the backbone conformation.

Further studies have shown that introducing neutral charge groups into phosphoramidate backbones (2-methoxyethylamine phosphoramidate) gives rise to moderate triplex affinity compared to negatively charged phosphodiester backbones (Dagle & Weeks 1996). Furthermore it has been demonstrated that R isomers of the positively charged phosphoramidate backbone, N,N-dimethyl-ethylenediamine phosphoramidate, increase parallel triplex affinity compared to the S isomer and phosphodiester counterparts (Chaturvedi *et al* 1996, Dagle & Weeks 1996).

(1.4.3.3)   Methylphosphonate.

In this analogue a methyl group replaces an oxygen atom in the phosphoryl group (Fig. 1.18), resulting in a neutral backbone (Miller *et al* 1981). Short triplexes were reported when this modification was used, but with a similar affinity to the phosphodiester counterpart (Callahan *et al* 1990). However other studies suggested that longer triplexes were not produced using methylphosphonate oligonucleotides (Kibler-Herzog *et al* 1990).

(1.4.3.4)   Peptide Nucleic Acid (PNA).

One means of radically altering the backbone structure is to replace the sugar - phosphate groups with pseudopeptide moieties. The first of these to be reported was PNA (Nielsen *et al* 1991) and is made up of N-(2-aminoethyl)glycine units to which the nucleobases are attached with carbonyl methylene linkers to the nitrogen atom of the glycine (Egholm *et al* 1992a). The structure of PNA confers resistance to both nucleases and proteases and carries an overall neutral charge (Fig. 1.18).

Although PNA was designed to bind by triplex formation, thymine-rich PNAs were found to act via strand displacement whereby the PNA oligonucleotide binds to its complementary target DNA strand and displaces the non-complementary DNA strand causing it to loop out. A second PNA molecule then binds to the PNA·DNA duplex forming a 2PNA·DNA triplex (Cherny *et al* 1993, Nielsen *et al* 1994, Demidov *et al* 1995, Wittung *et al* 1996*)*. This mode of binding was initially demonstrated using a dT_{10} PNA oligonucleotide and a $dA_{10}·dT_{10}$ DNA duplex, with the displaced dT strand shown to be susceptible to nuclease digestion and chemical attack (Nielsen *et al* 1991). Subsequent studies showed that PNA oligonucleotides could also be designed to target mixed sequence DNA (Egholm *et al* 1992b, 1993) and operate via a mechanism of strand-displacement only. Cytosine-rich PNAs on the other hand have been shown to add to double stranded polynucleotide targets as Hoogsteen strands generating PNA·2DNA triplexes in a pH dependent fashion (Wittung *et al* 1997). Since pseudoisocytosine PNA also binds as a third strand, the presence of the positively charged cytosine is not sufficient to explain their different mode of binding (triplex vs. invasion) (Wittung *et al* 1997). A proposed explanation is that the duplex DNA targets, (A·T and G·C), form intrinsically different secondary structures, or that strand displacement at GC is less favourable.

Drawbacks with the use of PNA oligonucleotides *in vivo* arise due to the necessity for partially denaturing the duplex prior to strand invasion; this generally only occurs at low ionic strengths and not physiological pH (Cherny *et al* 1993). Another

potential problem arises when PNA is considered for use as an antisense molecule, as PNA/RNA complexes are not substrates for RNase H (Knudsen & Neilsen 1996). Furthermore there is no cellular uptake of PNA (Hanvey *et al* 1992), though it has been shown that PNA crosses the blood brain barrier when delivered by intraperitoneal injection (Tyler *et al* 1999). Linking PNA to the monoclonal antibody OX26 has also been show to enable it to cross the blood-brain barrier to a degree similar to that of morphine and decreases the clearance rate of PNA 7-fold (Boado 1995).

(1.4.3.5) Morpholino.

This novel sugar modification (Fig. 1.18), was originally demonstrated to be a promising modification for use in antisense applications (Summerton & Weller 1997). However a recent study (Lacroix *et al* 2000) has also shown this analogue can be used in the triplex strategy. The study demonstrated that a morpholino modified pyrimidine oligonucleotide formed a stable triplex with its duplex target in a near physiological environment in the absence of divalent magnesium cations. However under these conditions the resulting triplex dissociated at temperatures above 19 °C, though this low stability was probably due to the lack of protonation of the cytosine residue in the oligonucleotide 5'-TCCTCCTTTTCCTCCT-3'. Nevertheless when the morpholino modified oligonucleotide was compared with unmodified, methyl-cytosine modified, and phosphoramidate modified oligonucleotides it was the only one to give rise to triplex formation in physiological monovalent cation concentrations, at a pH of 7.0 in the absence of magnesium. However in the presence of magnesium cations the morpholino triplex was destabilised resulting in a lower triplex transition. At acidic pH's in the presence of magnesium, the morpholino modified oligonucleotide stabilised triplex formation to a similar extent to that achieved with methyl cytosine, but again higher stabilisation was found in the absence of magnesium.

The ability of morpholino to stabilise parallel triplex formation at neutral pH in the absence of magnesium ions has been postulated to be due to its uncharged nature. Therefore its incorporation into a triplex structure would alter the normal parameters of

stabilisation, as there would be no charge repulsion between the third strand oligonucleotide backbone and the duplex. However this charge effect is not sufficient to explain the overall stabilising effect of morpholino substitution, as several other neutral backbone modifications, such as phosphoroamidate, do not afford similar stability.

The early results of this novel sugar analogue indicate that it may have promising future applications in the design of analogues for use in the triplex strategy. It is the only analogue known which affords pyrimidine triplex stabilisation at a neutral pH in physiologically relevant monovalent cation concentrations, in the absence of magnesium.

(1.4.3.6)   α-Anomers.

Naturally occurring β-anomeric nucleotides are susceptible to both endonucleases and exonucleases. The first reported synthesis of α-oligonucleotides (Morvan *et al* 1987) allowed for the design of nuclease resistant molecules *in vitro* (Fig.1.18). Subsequent experiments showed that the α-anomers afforded nuclease protection when injected into Xenopus oocytes (Cazenave *et al* 1987) and therefore indicated potential *in vivo* uses.

Oligonucleotides made from α-anomers again bind by triple helix formation in the major groove of a duplex. However their orientation is opposite to that of their β-counterparts, and it was demonstrated that α-GT oligonucleotides formed parallel triplexes with a decreased affinity than when compared to that of their β-counterparts (Noonberg *et al* 1995). Neither parallel or antiparallel triplex formation was achieved using α-GA oligonucleotides, whereas the β-GA oligonucleotides give rise to strong antiparallel triplex formation.

(1.4.4) Conjugated Oligonucleotides.

Covalent modifications to the terminal regions of synthetic oligonucleotides have been synthesised in an attempt to improve the stability of triplexes and to widen the potential field of applications. The majority of modifications attach planar aromatic

molecules which act as nonspecific intercalating moieties. The conjugates generally enhance stability via intercalation of the planar groups, thus enhancing the binding affinities and increasing base stacking interactions. It is also possible to attach enzymes and DNA cross-linking agents to oligonucleotides thereby enabling the use of triplexes to induce DNA damage at specific sites.

(1.4.4.1)   Acridine.

Covalent attachment of 2-methoxy-6-chloro-9-amino acridine to the 3' end of a synthetic oligonucleotide (Fig. 1.19) increased stabilisation of poly T·AT, as shown by spectroscopic studies (Asseline *et al* 1984). Stabilisation is increased due to the acridine intercalating between the base pairs at the end of the triplex and maximising stacking interactions. Subsequent investigations revealed that an acridine tether could also enhance parallel triplex formation (Sun *et al* 1989) and that attachment to the 5' terminus and not the 3' terminus enhanced triplex stability (Sun *et al* 1989, Collier *et al* 1991). This suggests that the 5' terminus is a better site for intercalation, and highlights the structural differences between the 3' and 5' terminal regions.

Acridine failed to stabilise parallel G·GC and T·AT triplets (Fox 1994), and failed to increase the affinity of antiparallel triplex formation with phosphorothioate modified oligonucleotides (Lacoste *et al* 1997). Although GA phosphorothioate oligonucleotides were shown to only have low affinity for their duplex target sequences (section 1.4.3.1) (Lacoste *et al* 1997), tethering an acridine moiety to the 5' terminus of the GA phosphorothioate oligonucleotide increased the affinity above that of the native GA phosphodiester oligonucleotide (Lacoste *et al* 1997)

Acridine conjugated oligonucleotides have also been used to stabilise single and double mismatch sites. In these cases the acridine moiety was incorporated on either the 3' or 5' side of the third strand nucleotide facing the mismatch. The greatest stability was achieved when the acridine was 3' to a T or C and 5' to a G. Furthermore the flanking triplets also affect the extent of stability afforded (Kukreti *et al* 1997). Acridine has also
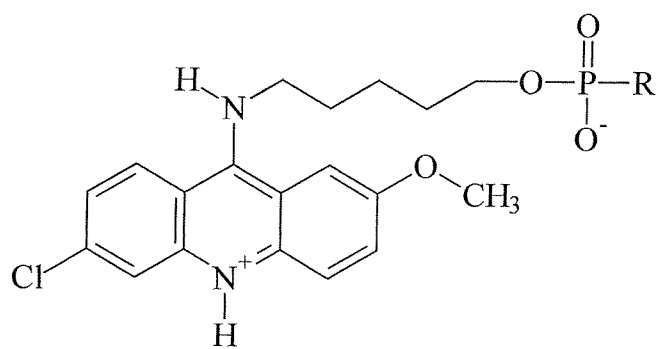
a) **Methoxy-6-chloro-9-amino-acridine**
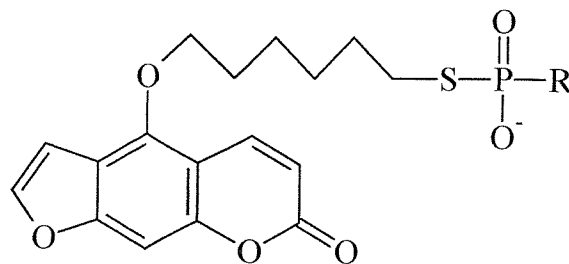
b) **Psoralen**
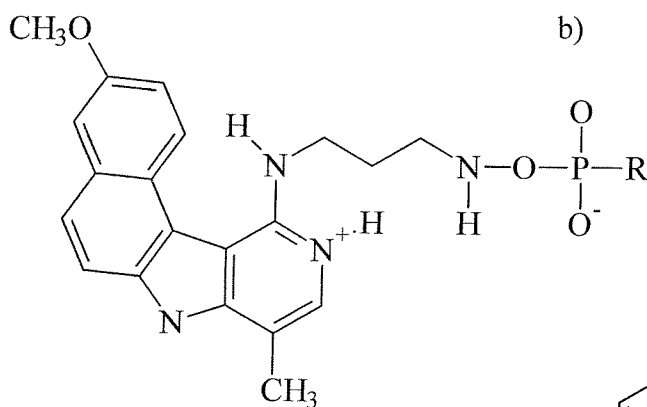
c) **Benzo(e)pyridoindole (BePI)**
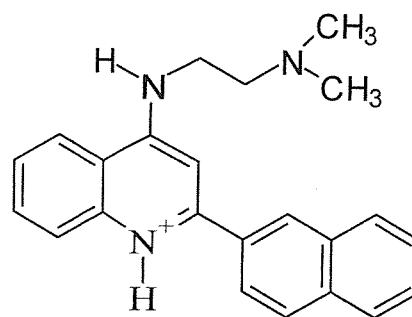
d) **Naphthylquinoline**
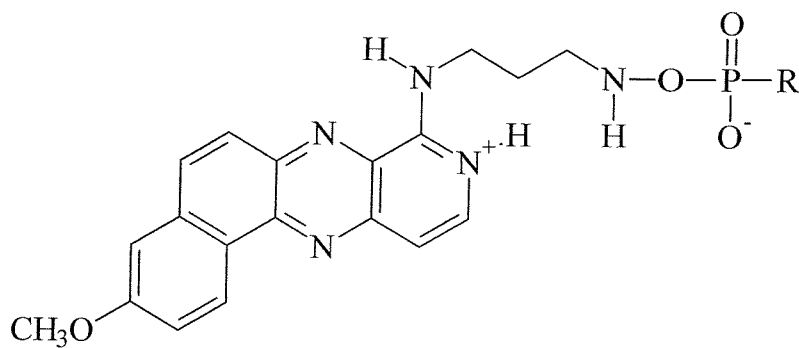
e) **Benzo(f)pyridoquinoxaline (BfPQ)**

Figure 1.19: Diagrams representing several of the conjugated triple helical nucleic acid ligands discussed in section 1.4.4.

been shown to facilitate the incorporation of modified bases opposite pyrimidine interruptions (Orson *et al* 1999), and the increase in stability was related to the distance of the interruption from the acridine moiety.

(1.4.4.2)   Psoralen.

Psoralens are photoreagents that form covalent bonds with pyrimidine residues upon induction with UV light. Psoralen intercalates at TpA sites and cross-links the two strands (Takasugi *et al* 1991). Psoralen tethered via its C5 atom to the 5' thiophosphate of a triplex forming oligonucleotide (Fig. 1.19), was shown to induce cross-links between the two strands at the T_pA triplex/duplex junction (Takasugi *et al* 1991). Psoralen tethered TFO's have also been used to achieve site specific mutagenesis (Harve *et al* 1993, Raha *et al* 1996, Wang *et al* 1995), in which the TFO delivers the psoralen to a unique site within the DNA and induces the formation of adducts at that site upon photoactivation.

Psoralen conjugated oligonucleotides have been shown to be effective in inhibiting specific gene activity, an example is psoralen tethered to a 20mer pyrimidine oligonucleotide, targeted to the cytochrome P_{450} gene *in vitro* (Macaulay *et al* 1995). *In vivo* psoralen oligonucleotides have been shown to persist for at least 72hrs, (Musso *et al* 1996) indicating that they may have potential in the antigene strategy. However it is not clear as to whether psoralen adducts may be repaired *in vivo* or not. Several papers have been published suggesting that repair pathways can not cope with this type of DNA damage (Sandor *et al* 1994), or that single adducts can be repaired whilst multiple adducts can not (Sandor & Bredberg 1995), or that the length of the psoralen tethered oligonucleotide influences the efficiency of the repair pathway (Wang & Glazer 1995).

(1.4.4.3)   Naphthylquinoline.

Tethering of the naphthylquinoline triplex binding ligand to the 5' terminus of oligonucleotides (Fig 1.19) increases the stability of both inter and intramolecular triplexes (Keppler *et al* 1999c). DNase I and UV melting studies demonstrated that 9mer intermolecular triplexes were stabilised between 15-60 fold when conjugated to naphthylquinoline, whilst naphthylquinoline conjugated intramolecular triplexes were stabilised by approximately 14K. These experiments also supported previous work demonstrating that the tethering of a ligand to an oligonucleotide confers greater stability than addition of free ligand.

(1.4.4.4)   Benzopyridoindole & Benzopyridoquinoxaline.

These triplex binding compounds (section 1.4.2.2) have also been conjugated to 14mer oligonucleotides at one of two positions; either at the 5' terminus (Fig. 1.19), or at an central internucleotide position (Silver *et al* 1997). The study demonstrated that when internally incorporated via a $(CH_2)_4$ linker arm to the phosphodiester backbone, the order of stability was; BfPQ $\geq$ BePI > BhPQ > BgPI. However when linked to the 5' terminus via the same linker arm, the order of stability changed to; BhPQ >> BfPQ $\geq$ BePI ~ BgPI. This is probably due to a change in the orientation of the intercalator with respect to the triplex, and that the 5' triplex/duplex junction is a good site for intercalation. The same study also demonstrated that specificity was not compromised when either 5' or internal incorporation was used, and that the linker arm length and charge affected the overall stability of triplex formation.

(1.4.4.5)   Additional Compounds.

Several other compounds have been conjugated to oligonucleotides; these include spermine (Tung *et al* 1993), 3'/5' cholesterol (Gryaznov & Lloyd 1993), oxazolopyridocarbazole (Mouscadet *et al* 1994), spermidine-cholesterol (Jayaramen *et al* 1995), Hoechst 33258 (Robles *et al* 1996), camptothecin (Matteucci *et al* 1997), and

rebeccamycin derivatives (Arimondo *et al* 2000, 2001).

(1.5) Methods for Studying Triplexes.

Numerous biophysical techniques for studying triplexes have been employed *in vitro*. These include footprinting, UV melting, circular dichromisum (CD) spectroscopy, nuclear magnetic resonance (NMR), crystallography, isothermal calorimetry, gel mobility. The two main techniques used in this thesis are footprinting and thermal denaturation, and are described below.

(1.5.1)   Footprinting.

Footprinting is a technique that was originally designed for studying the sequence specific binding of proteins to DNA (Galas & Schmitz, 1978). It was later shown to be a valid method for detecting drug DNA interactions (Van Dyke *et al*, 1982). The basis behind the technique is that the DNA binding compound physically prevents the access of a DNA degradation agent at its sites of interaction.

Prior to generating triplex footprints, one of the duplex DNA strands must first be labelled at either the 3' or 5' end. This is usually achieved by incorporating ^{32}P. The TFO is then annealed to the target site, and this target site can be either a synthetic DNA duplex or a restricted fragment. The DNA is then partially digested by a chemical or enzymic cleavage agent and the TFO affords protection at the target site. The products of digestion are then separated on the basis of size on a denaturing polyacrylamide gel. This generates a ladder of DNA bands in the control, with the triplex protected site being indicated by the absence of bands (Fig. 1.20).

As well as this qualitative assessment of ligand binding sites, footprinting can also be quantitative, often estimating ligand affinity. In this the TFO is applied in varying concentrations with the highest concentration of TFO affording complete protection, and the lower concentrations affording less protection. The intermediate concentrations are
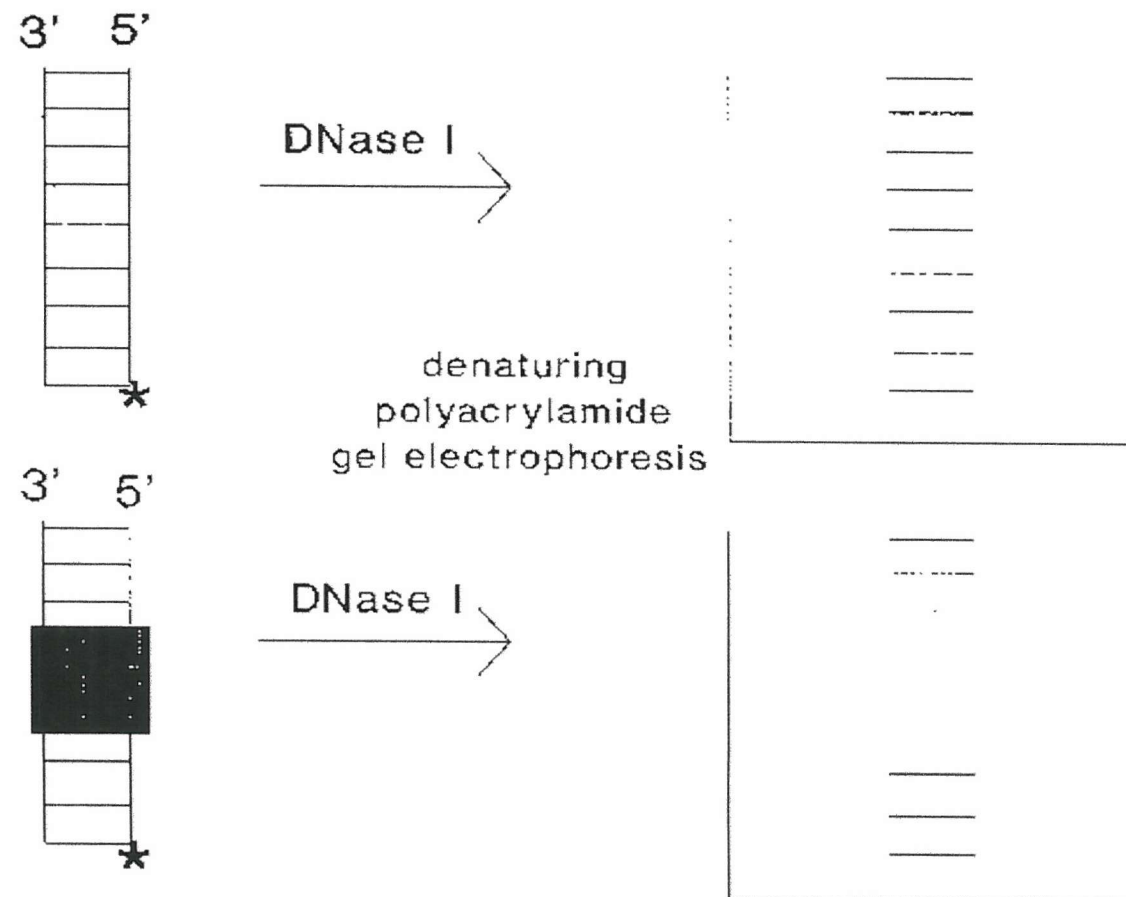
Figure 1.20: Diagramatic representation of DNase I footprinting. * designates the position of the radiolabel.

designed so as to show a gradual attenuation of the bands within the target site. The concentration dependency of this attenuation will be determined by the affinity of the ligand for its target. Analysis of this band attenuation allows the calculation of the oligonucleotide concentration required to achieve 50% protection of the duplex target (C_{50}). This value is equivalent to the triplex dissociation constant, so long as the target DNA concentration is much lower than the dissociation constant.

(1.5.1.1)   DNase I.

The bovine pancreatic glycoprotein, deoxyribonuclease I (DNase I) was the agent used in the original footprinting studies (Galas & Schmitz 1978). This enzyme requires calcium, manganese, or magnesium ions for activity. These ions act as co-factors enabling catalysis to proceed via a mechanism employing nucleophilic attack of a water molecule causing hydrolysis of the O3'-P bond (Fig. 1.21).

DNase I acts by inserting an exposed loop into the minor groove of DNA (Suck *et al* 1988, Hogan *et al* 1989). DNase I has its limitations in that its cleavage generates an uneven ladder of cleavage products (Bernardi *et al* 1973, 1975). Its activity is sequence specific, and $A_n \cdot T_n$ tracts are poor substrates (Drew & Travers 1984). This specificity has been attributed not to the sequence composition directly, but to variations in the local DNA structure. Regions with narrow mirror grooves exhibit lower cleavage as the enzyme cannot bind (Drew & Travers 1984). The crystal structure of the enzyme bound to short oligonucleotides (Fig. 1.21) revealed that the DNA bends away from the enzyme towards the major groove (Suck *et al* 1988). This bending may be an essential part of the catalytic mechanism, influencing the efficiency of cleavage. As a result less flexible sequences such as $G_n C_n$ will be poorly cleaved. DNase I produces footprints that are larger than the ligand size, and this is attributable to the large size of the protein (30.4 Kda). DNase I covers 10 base pairs explaining why it overestimates footprint sites by 2-3 bases. It binds across the minor groove, where it interacts with phosphates from opposing strands. Since closest phosphates across the minor groove are not attached to a individual base pairs, but are staggered by 2-3 bases the footprints are also staggered by
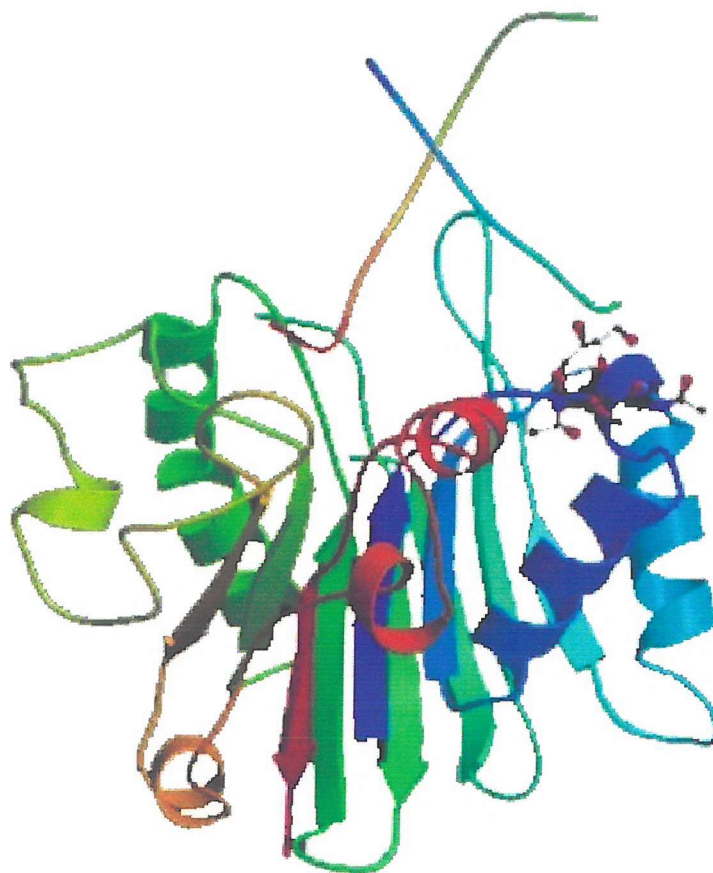
a) Crystal structure of DNase I

E75   H131   Water
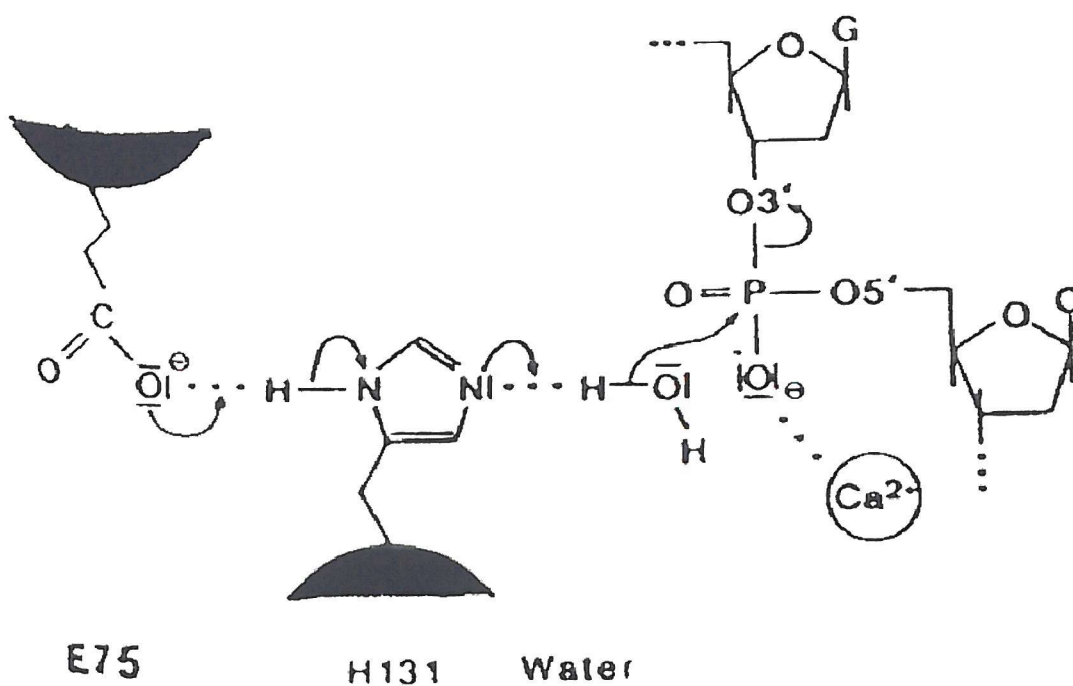
b) The proposed mechanism of DNase I cleavage.

Figure 1.21: Illustrated is a) the 2 angstrom crystal structure of the bovine pancreatic glycoprotein, deoxyribonuclease I (DNase I), complexed with (5'-D(GCGATCGC)-3') reproduced from Lahm & Suck, *J. Mol. Biol.* **222**, 645-667 (1991). Diagram b) shows the proposed mechanism by which the enzyme cleaves the phosphodiester backbone of DNA molecules. Reproduced from Suck *et al Nature*, **332**, 464-468 (1988)

2-3 bases in a 3'-direction. Since DNase I binds in the minor groove, while TFO's interact in the major groove, triplex footprints are not caused by direct stearic occlusion but must result from changes in the DNA structure and/or rigidity.

(1.5.1.2)   Methidiumpropyl-EDTA-Fe(II).

Methidiumpropyl-EDTA-Fe(II) (MPE) is a synthetic DNA cleavage agent, that is comprised of the DNA intercalator methidium tethered by a propyl linker to the metal chelator EDTA (Hertzberg & Dervan 1982, 1984). The EDTA group forms a very stable complex with Fe^{2+} that in the presence of oxygen can induce single strand breaks in DNA by oxidation of the deoxyribose moieties via the production of hydroxyl radicals (Hertzberg & Dervan 1982, 1984). MPE therefore induces cleavage of DNA at the site of intercalation several studies have showed that MPE has no base preference and little sequence selectivity though regions of $A_n{\cdot}T_n$ are cut less well as these are poor sites for intercalation. MPE cleaves DNA less efficiently than DNase I requiring more stringent conditions and it is rarely used as a quantitative footprinting probe. Despite this MPE is used as an alternative to DNase I (Van Dyke & Dervan 1983, 1984, Harshman & Dervan 1985), but rarely been used for footprinting since the intercalating moiety is based on ethidium, which can stabilise triplex DNA. Therefore the footprinting agent may actually enhance triplex formation.

(1.5.1.3)   Other Footprinting Agents.

A wide range of other cleavage agents have also been used as footprinting probes though none of these has been used in this study. Micrococcal nuclease (MNase) has been widely used in studies of chromatin structure and requires Ca^{2+} ions to attack the O5'-P bond. MNase has been shown to be sequence specific, and cuts exclusively at pA and pT (Hörz & Altenburger 1981, Dingwall *et al* 1981). It can be used for footprinting of ligands and is especially useful for AT selective compounds (Fox & Waring 1987). However MNase activity is also governed by the helical geometry as A_nT_n tracts are cut less well than $(AT)_n$. However footprints produced by MNase appeared bigger than those

produced by DNase I, demonstrating the importance of the DNA structure on MNase activity, and limiting its use for assessing triplex formation (Fox & Waring 1987).

Hydroxyl radicals are very small and attack the C4' bond via the minor groove (Tullius 1987). These produce the highest resolution footprinting pattens, however triplex formation does not prevent this attack and therefore this agent can not be used to produce triplex footprints. Dimethyl sulphate (DMS) is specific for the N7 position of guanine and the N3 of adenine. Therefore guanine residues bound in a triplet will be protected from its action via the formation of Hoogsteen hydrogen bonds. Thus DMS has not been used for probing triplex formation, as it can only be used to assess the guanine residue involved in triplex formation (Young *et al* 1991).

(1.5.2)   UV Melting Studies.

UV melting was the method used in the original study of Felsenfeld & Rich (1957) in which the triple helix was initially reported. It has since been used to characterise the stability and melting of an intermolecular parallel triplex (Plum *et al* 1990) and several modified triplexes (Amosova & Fresco 1999, Sollogoub *et al* 2000, Parel & Leumann 2001, Stein *et al* 1988, Latimer *et al* 1989, Torigoe 2001). The technique involves the gradual heating of triplex DNA in a controlled manner (usually $0.5\,^{\circ}C\ min^{-1}$) with a simultaneous measuring of UV absorbance at 260 - 280 nm to generate a melting profile. Nucleic acids have maximal absorption at 260 nm, and this is lower for duplexes and triplexes than the optical density of their individual components. This hypochromicity, is due to the stacking of the DNA bases. Denaturation of nucleic acids is therefore accompanied by an increase in UV absorbance (typically 25%), and the mid-point of the transition (Tm, melting temperature) is characteristic of the particular DNA and its physical environment. Triplex DNA melts in a biphasic manner, with the first transition being due to the melting of the third strand, producing duplex DNA and the oligonucleotide. The second transition is due to the melting of duplex DNA into single strand DNA. This technique has served as a platform for the evaluation of base analogues (Amosova & Fresco 1999, Sollogoub *et al* 2000, Parel & Leumann 2001), and

backbone modifications (Stein *et al* 1988, Latimer *et al* 1989, Torigoe 2001) as an increase in triplex stability results in the triplex melt shifting to higher temperatures. However the increase in triplex stability often results in the triplex-duplex and duplex-single strand transitions coalescing and accurate determination of the individual transitions is not possible. This technique is often used to initially estimate the degree of stability afforded by the modification before committing it to more labourious footprint studies (Sollogoub *et al* 2000). The application of this technique is restricted since antiparallel triplexes, and some parallel triplexes containing modified bases do not show any hypochromicity on melting (Faucon *et al* 1996, Arimondo *et al* 1998, Jetter & Hobbs 1993).

(1.6) Purpose of this Work.

The purpose of this work is to explore different means of stabilising triple helical DNA. This is achieved using novel base analogues as well as triplex binding ligands.

Quantitative DNase I footprinting is used to assess the stability of parallel and antiparallel triplexes incorporating base analogues in the third strand and/or stabilised by triplex binding ligands. The triplex stabilising properties of several base analogues, including the novel bis-modified thymidine analogue 2'-aminoethoxy-5-propargylamino uridine, have been investigated by assessing the ability of partially substituted oligonucleotides to generate stable triplexes with the DNA fragment *Tyr*T(43-59) . The triplex stabilising ligands investigated include acridine derivatives and naphthoflavone.

A novel high throughput method for measuring the thermal denaturation profiles of both triplex and duplex DNA has also been developed. Synthetic oligonucleotides containing appropriately positioned fluorophores and quenchers are used to assess the effects of several base analogues and triplex stabilising ligands in fluorescence-melting experiments using the Roche PCR LightCyler.

Chapter 2 - Materials & Methods.

(2.1) Oligonucleotides.

All of the oligonucleotides used in this study were purchased from Oswel DNA Services. They were supplied in sterile water and stored at -20°C. The 5-aminohexyl dC, 5-aminopropyl dU, 5-propargylamino dU, and 5-propynyl dU containing oligonucleotides were prepared by Dr. Jeevan Bijapaur & Prof. Tom Brown, Dept. of Chemistry, Southampton University, UK. The 2'-aminoethoxy-5-propargylamino dU containing oligonucleotides were prepared by Dr. Mattieu Sollogoub & Prof. Tom Brown, Dept. of Chemistry Southampton University, UK (Sollogoub *et al* 2000). The 1'-β-hexylaminoribose and 1'-methoxy-2'-aminoethoxyribose abaisc analogues were prepared by Dr. Beatriz Dominguez & Prof. Tom Brown, Dept. of Chemistry, Southampton University, UK. Fluorescein labelled oligonucleotides were synthesised by Dr. Catherine McKeen, Oswell DNA Services.

(2.2) Chemicals and Enzymes.

DNase I was purchased from SigmaAldrich and stored at a concentration of 7,200 units per ml at -20°C. AMV reverse transcriptase was also purchased from SigmaAldrich at a concentration of 20 units per μl and stored at -20°C, all of the restriction enzymes were supplied by Promega and again stored at -20°C. Redivue radioactive [α-^{32}P] dATP was purchased from Amersham international, Amersham, UK at a concentration of 3,000 Ci per mmol and stored at 4°C. The naphthylquinoline triplex binding ligand was a gift from Dr. L. Strekowski (Department of Chemistry, Georgia State University, Atlanta, GA). It was stored at a concentration of 10 mM at -20°C. The proflavine ligands were synthesised as part of a series of ligands by Prof. T. Jenkins (University of Bradford) and stored in dimethylsulphoxide at a concentration of 10 mM at -20°C. The anthraquinone and acridine derivatives were a gift from Prof. S. Neidle (CRC Biomolecular Structure Unit) and were stored in dimethylsulphoxide at concentrations of 10 mM and 5 mM

respectively. Alpha and beta naphthoflavone, ethidium bromide, and neomycin sulphate were purchased from Sigma-Aldrich.

(2.3) DNA Fragments.

The sequence *Tyr*T(43-59) contains a 17 base pair homopurine·homopyrimidine tract between positions 43 and 59. This was prepared by mutating positions 46, 55, 56, and 58 of the original *Tyr*T fragment using PCR site directed mutagenesis (Brown *et al* 1998). This was then cloned into pUC 18 between the *Sma*I and *Eco*RI sites. This plasmid was a gift from Prof. K. Fox and the sequence can be seen in Fig 2.1.

The *Tyr*T(35-59) sequence contains a 25 base pair homopurine·homopyrimidine tract and is a novel mutant of the original *Tyr*T fragment and was created using PCR site directed mutagenesis. The fragment was subsequently cloned into pUC 19 between the *Ava*I and the *Eco*RI sites (Keppler 1999). This plasmid was a gift from Dr. M. Keppler and Prof. K. Fox and the sequence can be seen in Fig 2.1.

The RAD1 sequence was designed to contain four thirteen base pair triplex target sites, each of which contained a different base at the centre (i.e. A, C, G, T). Both of the duplex strands were synthesised by Oswel DNA Services. These were annealed and cloned into pUC 18 as described below, the sequence can be seen in Fig 2.1.

(2.3.1)   Polynucleotide Kinase.

1 μl of T4 polynucleotide kinase (10 units), and 2 μl 10 x kinase buffer was used to catalyse the transfer of the γ phosphate of 1 μl of ATP (100 mM) in 10 μl of water to the 5' terminus of 1 μl of the individual oligonucleotide strands. Each reaction tube was incubated at 37°C for 30-60 min. The two strands were then mixed and annealed by placing in boiling water and allowing to cool to room temperature.

a) *Tyr*T(35-59)

AATTCCGGTTACCTTTAATCCGTTACGATGAAAATTACGCAACCCCCTCCTCCTTCCTTCTCTCTCTAACACTTTACAGCGGCGCGTCATTTGATATGATGCGCCCCGCTTC
3'-AGGCCAATGGAAATTAGGCAATGCTACTTTTAATGCGTT**GGGGGAGGAGGAAGGAAGAGAGAGA**TTGTGAAATGTCGCCGCGCAGTAAACTATACTACGCGGGGCGAAGGGCT-5'

b) **RAD1**

5'-GATC**AGAAGAGAAAGAA**TCAGTC**AGAAGACAAAGAA**TCAGTC**AGAAGATAAAGAA**TCAGTC**AGAAGAAAAAGAA**-3'
        TCTTCTCTTTCTTAGTCAGTCTTCTGTTTCTTAGTCAGTCTTCTATTTCTTAGTCAGTCTTCTTTTTCTTCTAG

c) *Tyr*T(43-59)

5'-AATTCCGGTTACCTTTAATCCGTTACGGATGAAAATTACGCAACCAGTTCTTTTTTCTCTTCCTAACACTTTACAGC
   0   10   20   30   40   50   60   70
   AAGGCCAATGGAAATTAGGCAATGCCTACTTTTAATGCGTTGGTC**AAGAAAAAAGAGAAGGA**TTGTGAAATGTCG

GGCGCGTCATTTGATATGAAGCGCCCCGCTTCCCGAGAAGGGAGCAGGCCAGTAAAAAGCATTACCCCGTGGTGGGGGTTC-3'
   80   90   100   110   120   130   140   150
CCGCGCAGTAAACTATACTTCGCGGGGCGAAGGGCTCTTCCCTCGTCCGGTCATTTTTCGTAATGGGGCACCACCCCCAAG

Figure 2.1: Diagram a) shows the *Tyr*T(35-59) sequence with the 25 base pair homopurine tract highlighted. Diagram b) shows the RAD1 insert with the four triplex target sites highlighted, and diagram c) shows the sequence of *Tyr*T(43-59) with the 17 base pair homopurine tract highlighted.

(2.3.2)   **DNA Ligation.**

1 μl of the above sample was mixed with 2 μl of 10x T4 DNA ligase buffer, (300 mM Tris-HCl (pH 7.8), 100 mM MgCl$_2$, 100 mM DTT, 1 mM ATP). 1 μl *Bam* H1 cut alkaline phosphatase treated pUC 18 (Pharmacia), 1.2 μl T4 DNA ligase (3.6 units) and 16 μl water. This was then left at room temperature overnight to maximise the ligation efficiency.

(2.3.3)   *E. coli* **TG2 Competent Cells.**

5 ml of 2YT media (16 g tryptone, 10 g yeast extract, 5 g NaCl per litre) was inoculated with *E. coli* TG2 cells and grown overnight. A 50 ml 2YT culture was then inoculated with 0.5 ml of the dense 5 ml 2YT culture and grown until an O.D. of 0.4-0.6 at 600 nm was achieved. The culture was then centrifuged at 5,000 rpm for 5 min at 4°C. The supernatant was decanted and the pellet resuspended in 20 ml of cold sterile transformation buffer (50 mM CaCl$_2$ 10 mM Tris-HCl pH 7.4) and left on ice for 30 min. The tube was then centrifuged again at 5,000 rpm, 4°C for 5 min and the supernatant discarded. The pellet was again resuspended in 3 ml of transformation buffer and stored at 4°C for no more than 2 weeks.

(2.3.4)   **Transformation.**

2 μl of the ligation mixture was added to 200 μl of competent cells and left on ice for 30 min. The cells were then heat shocked at 45°C for 1 min before being crash cooled on ice. 50 μl of the cells were then plated onto an agar plate, with a further 100 μl being plated onto a separate agar plate. Both plates were incubated overnight at 37°C with the remaining 50 μl of cells being stored at 4°C. The agar plates contained 0.5 mM isopropyl β D-thiogalactopyranoside (IPTG), 0.5 mM 5-bromo-4-chloro-3-indolyl β-D-galactosidase (X-gal), & 100 μgml^{-1} ampicillin. The plates were then stored at 4°C. Only white colonies were picked off using standard aseptic techniques

(2.4) Plasmid Preparation.

Plasmids were prepared using either Promega Wizard Miniprep kits, or Qiagen QIAprep kits. The latter was favoured as it did not involve the separate addition of DNA binding resin, but membrane filter elution instead.

(2.4.1)   Promega Wizard Miniprep.

5 ml 2YT cultures were inoculated with *E. coli* which had been transformed with either *Tyr*T(43-59), *Tyr*T(35-59), or RAD1, and ampicillin added to a final concentration of 100 μg ml^{-1}, and incubated at 37°C for eight hours or overnight. The cultures were then divided into three 1.5 ml eppendorf tubes and centrifuged at 7,000 rpm for 5 min. The supernatant was discarded and the pellet resuspended in cell resuspension buffer (100 μgml^{-1} RNase, 50 mM Tris-HCl pH 7.5, 10 mM EDTA) to a final volume of 200 μl. The cells were then lysed using 200 μl of cell lysis solution (0.2 M NaOH, 1% SDS) and mixed gently. 200 μl of neutralisation solution (2.55 M KOAc pH 4.8) was added and mixed prior to centrifugation at 10,000 rpm for 5 min. The supernatant was removed and added to 1 ml of vigorously mixed Wizard minprep resin from Promega, mixed well and applied to a Wizard miniprep column supplied by Promega. The solution was then drawn through the column under vacuum and washed with 2 ml of column wash solution (10 mM Tris, 0.1 M NaCl, 2.5 mM EDTA in 50% EtOH). The column was then dried under vacuum for 2-3 min and 40 μl of 65°C water added to the column, left for 30 sec and centrifuged for 30-60 sec at 10,000 rpm.

(2.4.2)   Qiagen QIAprep.

5 ml of 2YT media was inoculated with bacteria as described above. The culture was then divided into three 1.5 ml eppendorfs and centrifuged at 7,000 rpm for 5 min. The pelleted cells were then resuspended in 250 μl of buffer P1 (Qiagen) and lysed with 250 μl of buffer P2 (Qiagen) and gently mixed. Neutralisation was achieved using 350 μl of buffer P3 (Qiagen) and gentle mixing before centrifugation at 13,000 rpm for 10 min.

The supernatant was then transferred to a QIAprep spin column in a 2 ml collection tube and centrifuged for 1 min at 13,000 rpm. The flow through was discarded and the plasmid washed with 0.5 ml of buffer PB (Qiagen). It was then centrifuged again at 14,000 rpm for 1 min and the flow through discarded. The column was then washed with 0.75 ml of buffer PE (Qiagen), centrifuged at 13,000 rpm for 1 min and the flow through discarded. The column was then placed in a clean 1.5 ml eppendorf and the plasmid eluted with 50 µl of Quiagen buffer EB (10 mM Tris-HCl pH 8.5) via centrifugation at 13,000 rpm for 1 min.

(2.5) Sequencing of RAD1

40 µl of plasmid DNA was prepared as described above and denatured by adding 10 µl of 2 M NaOH for 10 min at room temperature. The DNA was then precipitated by the addition of 15 µl 3 M NaOAc (pH 4.8), 35 µl water, 300 µl absolute ethanol and stored on dry ice for 10 min. The sample was then centrifuged at 14,000 rpm, 4°C, for 10 min, the pellet washed in 70% ethanol and dried under vacuum in a SpeedVac Concentrator. Sequencing of the DNA was achieved using a T7 DNA sequencing kit purchased from AmershamPharmacia. The DNA was re-dissolved in 10 µl of water to which was then added 2 µl of annealing buffer (kit), and 2 µl of universal primer. This was then left for 20 min at 37°C, then 10 min at room temperature. For each template a polymerase mix was prepared using 3 µl label mix A, 1.5 µl water, 0.5 µl $\alpha[^{32}P]$ dATP, and stored on ice. T7 polymerase was diluted five-fold from the stock supplied and 2 µl per template added to the polymerase mix. To each tube of annealed template 6 µl of the polymerase mix was added and left at room temperature for 5 min. 4 tubes were prepared containing 2.5 µl of one of the dideoxy short mixes and warmed for 5 min at 37 °C. 4.5 µl of the reaction mixture was then added to each of the dideoxy mixes and left for 5 min. The reaction was terminated via the addition of 5 µl of the supplied stop solution and heating at 100°C for 3 min before crash cooling on ice. Approximately half the volume of the samples was then loaded onto a 10% (w/v) denaturing polyacrylamide gel and electrophoresed at 1,500 V for 2 hours. The gel was subsequently fixed in 10% (v/v) acetic acid for 10 min prior to drying under vacuum at 80°C for 90 min. The gel was

then exposed to X-ray film using an intensifying screen at room temperature for 2 hours.

(2.6) DNA Labelling.

10 μl of 5 x reverse transcriptase buffer (250 mM Tris-HCl, 250 mM KCl, 50 mM MgCl$_2$, 50 mM DTT, 2.5 mM spermidine pH 8.3) was added to 40 μl of plasmid DNA (prepared as described above). *Tyr*T(43-59) and *Tyr*T(35-59) were cut with 20 units of *Eco*RI and *Ava*I, at 37°C for a minimum of 2 hours. RAD1 was restricted using 20 units of *Hind*III and *Sac*I, at 37°C for a minimum of 2 hours. The restricted fragment was then radiolabelled at the 3' end of the *Eco*R1 or *Hind*III site with 1 μl α[^{32}P]dATP using 0.5 μl AMV reverse transcriptase at 37°C for a minimum 30 min. In each case this labels the polypurine strand of the fragment. The labelled fragment was then separated from the remainder of the plasmid on an 8% (w/v) non-denaturing polyacrylamide gel run at 800 V for 2 hours. The gel was then exposed to X-ray film for 10 min and the band corresponding to the labelled fragment excised. The DNA was eluted in 400 μl of 10 mM Tris-HCl pH 7.5, containing 0.1 mM EDTA, at 37°C overnight. The DNA was precipitated by adding $\frac{1}{9}$ volume of 3 M NaOAc (pH 7.4), three volumes of absolute ethanol and stored on dry ice for 10 min. The sample was then centrifuged at 14,000 rpm, 4°C for 10 min. The pellet was washed in 200 μl 70% ethanol and dried under vacuum in a SpeedVac concentrator. The pellet was finally dissolved in 10 mM Tris-HCl pH 7.5, containing 0.1 mM EDTA, to give approximately 10-20 cps per μl as estimated using a Geiger-Müller counter.

(2.7) Triplex Formation (Footprinting).

1.5 μl of radiolabelled DNA was mixed with 1.5 μl of appropriately diluted oligonucleotide and either 1.5 μl of buffer or ligand. The samples were then allowed to equilibrate for a minimum of 2 hours at room temperature, or at 20°C. The oligonucleotides were diluted appropriately with either 50 mM NaOAc (pH 5), and 10 mM MgCl$_2$, or 10 mM Tris-HCl (pH 7.5), 50 mM NaCl, and 10 mM MgCl$_2$. The ligand used was diluted from its stock concentration of 10 mM to a desired working

concentration using the same buffer as to dilute the oligonucleotides.

(2.8) DNase I Digestion.

A stock solution of DNase I (7,200 units per ml) was diluted to a working concentration of about 0.01 units per ml in DNase I buffer (20 mM NaCl, 2 mM $MgCl_2$, 2 mM $MnCl_2$). 2 μl of this dilution was added to the triplex samples, prepared as described above. The digestion was terminated after 1 minute by adding 3 μl of DNase I stop solution (80% formamide, 10 mM NaOH, 10 mM EDTA, 0.1% (w/v) bromophenol blue). The samples were then heated at 100°C for 4 min before crash cooling on ice. The samples were then loaded onto a 10% (w/v) denaturing polyacrylamide gel and electrophoresed at 1,500 V for 2 hours. The gel was subsequently fixed in 10% (v/v) acetic acid for 10 min before being dried under vacuum at 80°C for 90 min. The gel was then exposed to X-ray film using an intensifying screen and stored overnight at -80°C.

(2.9) Footprint Data Analysis.

Gels requiring data analysis were subjected to a Kodak phosphorimager screen overnight. The screen was then scanned using a Molecular Dynamics Storm 860 Phosphorimager. The intensity of bands within the footprint was estimated using ImageQuant software and normalised with respect to the corresponding area on the control lane. The oligonucleotide concentration was then plotted against the footprint intensity. C_{50} values, corresponding to the oligonucleotide concentration required to reduce intensity of bands within a footprint region by 50%, were calculated using the equation shown below using FigP for windows.

$$I / I_0 = C_{50} / (L + C_{50})$$

I and I_0 = Relative band intensity in the presence and absence of an oligonucleotide
L = The oligonucleotide concentration.
C_{50} = The oligonucleotide concentration required to reduce the intensity by 50%

However this is only valid if the DNA duplex concentration is very low, lower than the dissociation constant of the triplex. Under these conditions triplex formation is governed by equilibrium constant rather than the stoichiometric ratio of duplex DNA to oligonucleotide and the C_{50} value approximates to the dissociation constant. In these experiments we estimate the concentration of radiolabelled DNA to be about 1 nM so that dissociation constants above 10 nM are relatively accurate. Another assumption is that DNase I digestion results in each duplex being cut only once with little preference for specific sequences so as to produce an even digestion patten.

(2.10) Fluorescent Thermal Denaturation Studies.

Oligonucleotides containing fluorescein and methyl red as fluorophore and quencher respectively were diluted to a concentration of 5 μM. 1.0 μl of oligonucleotide was further diluted to 250 nM by mixing with 19 μl of buffer or buffer diluted ligand in LightCycler capillaries. The samples were then centrifuged at 1000 rpm for 30 sec. The oligonucleotides were diluted appropriately with either 50 mM NaOAc (pH 5), 0.1 M NaCl, and 1 mM EDTA or 50 mM HEPES (pH 7), 10 mM $MgCl_2$, and 1 mM EDTA. The ligands used were naphthylquinoline, naphthoflavone, neomycin sulphate, distamycin, Hoescht 33258, proflavine derivatives, acridine derivatives, and bis-amidoanthraquinone derivatives. All ligands were diluted from stock to desired working concentrations using the same buffer as to dilute the oligonucleotides. The samples were then placed in a Roche RT-PCR LightCycler, heated to 95°C at a rate of 20°C per second and held there for 5 min. The samples were then cooled to 27°C at a rate of 0.1°C per second and the fluorescence recorded continuously. The samples were then held at 27°C for 5 min before heating to 95°C at a rate of 0.1°C with the fluorescence continuously monitored. Tm values for the triplex-duplex and duplex-single strand transitions were determined from the first order derivatives of the melt profiles using Roche LightCycler3 software. The Tm values for both the annealing and melting experiments were compared to establish whether the samples were in thermodynamic equilibrium. Further details of these experiments are provided in chapter 6 of this thesis.

Chapter 3 - Results.

Base Analogues to Stabilise Triplex DNA.

(3.1) Foreword.

Triplex DNA is generated when a third oligonucleotide strand binds in the major groove of a DNA or RNA duplex. The third strand binding is primarily stabilised by hydrogen bonds between the bases of the third strand and the exposed faces of the purine bases in the duplex. These complexes are most stable when they are formed at homopurine·homopyrimidine regions within the duplex. The third strand can bind in one of two orientations with respect to the purine strand, determined by the composition of the third oligonucleotide strand. If the third strand is composed of cytosine and thymine residues then the strand will align itself in a parallel orientation with respect to the purine strand of the duplex, forming C^+·GC and T·AT triplets at low pH (Fig. 1.3). The stability of parallel triplexes is dependent upon the composition of the third strand, with C^+·GC triplets imparting a greater stabilising influence than T·AT triplets (Roberts & Crothers 1996). However adjacent C^+·GC triplets have been demonstrated to impart a strong destabilising force on a parallel triplex, due to the close proximity of the positive charges causing charge repulsion (Kiessling *et al* 1992). It has also been postulated that it is the positive charge on protonated cytosine residues that results in the higher stability of C^+·GC triplets, due to both C^+·GC and T·AT triplets being isohelical, and therefore any differences between the two triplets can only be accounted for by the positive charge (Roberts & Crothers 1996). The requirement to protonate the cytosine residues restricts the potential applications for parallel triplex formation, and the strong stabilising effect of protonated cytosine has yet to be fully reproduced in any of the cytosine base analogues.

a)

```
3'-TCCTTCTCTTTTTTCTT-5'   TyrT(43-59)
5'-AGGAAGAGAAAAAAGAA-3'
```

5'-TTTTTTCTT-3'	
5'-TTXTTXCTT-3'	**2^{P}U, 2^{AE}T, 2^{AP}U, 2P**
5'-XTTXTTCXT-3'	**3^{P}U, 3^{AE}T, 3^{AEP}U**
5'-XTXTXTCXT-3'	**4^{P}U, 4^{AE}T, 4^{AEP}U**
5'-TTTTTThTT-3'	**1h**
5'-TThThTTTT-3'	**2h**
5'-ThhTThThT-3'	**4h**
5'-XGGXXGXGXXXXXXGXT-3'	**17G^{P}UT**
5'-XGGXXGXGT-3'	**9^{P}UGT**
3'-TGGXXGXGXXXXXXGXX-5'	**17GGT (^{P}U)**
3'-TGGXXGXGX-5'	**9GGT (^{P}U)**
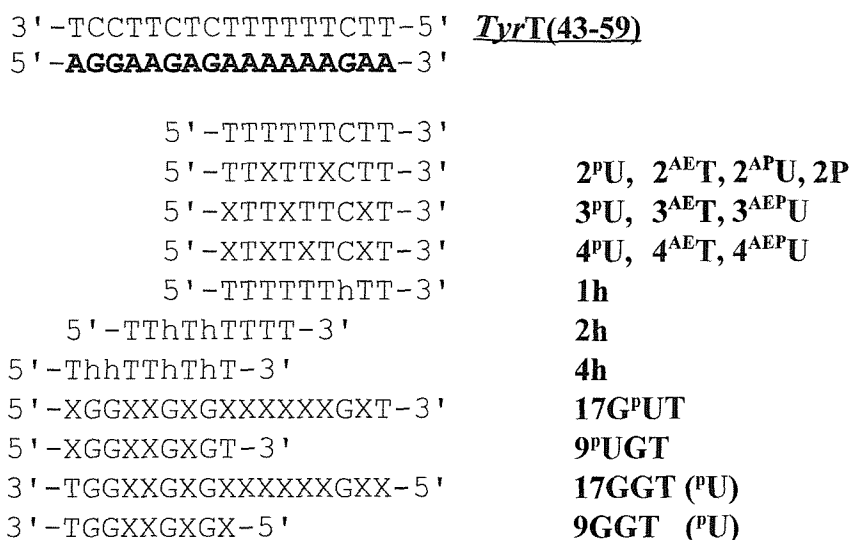
X indicates the position of substitution.

^{P}U	= 5-propargylamino dU
^{AE}T	= 2'-aminoethoxy T
^{AEP}U	= 2'-aminoethoxy-5-propargylamino U
^{AP}U	= 5-aminopropyl dU
P	= 5-propynyl dU
h	= 5-aminohexyl dC

b)

5-Propargylamino dU   2'-Aminoethoxy T   2'-aminoethoxy-5-
                                              propargylamino U

5-Propynyl dU   5-aminopropyl dU   5-aminohexyl dC
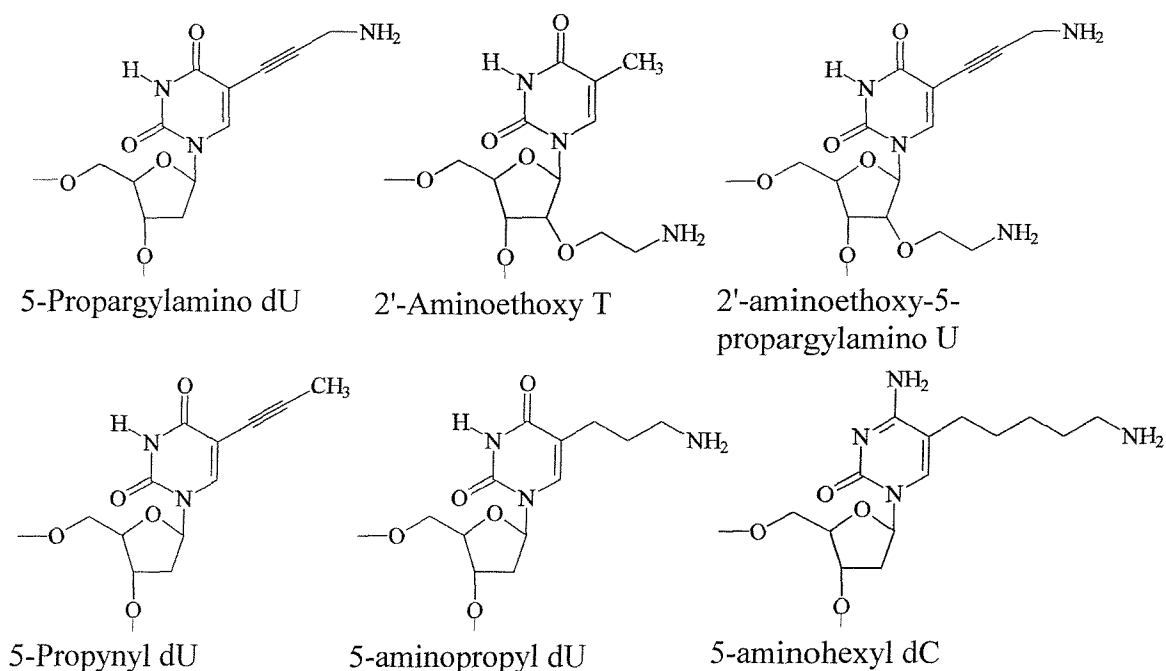
Figure 3.1: Diagram a) represents the homopurine·homopyrimidine tract in the DNA sequence TyrT(43-59). Also shown are the sequences of the oligonucleotides used, and their targets within the purine tract. Diagram b) illustrates the structures of the base analogues used in this chapter.

a)

```
3'CTAGTCTTCTCTTTCTTAGTCAGTCTTCTGTTTCTTAGTCAGTCTTCTATTTCTTAG
5'GATCAGAAGAGAAAGAATCAGTCAGAAGACAAAGAATCAGTCAGAAGATAAAGAATC
```

```
TCAGTCTTCTTTTTCTT-5'
AGTCAGAAGAAAAAGAA-3'          RAD 1
```

```
5'-TCTTCTXTTTCTT-3'
```

X indicates the site of substitution with;   **1',2-H-dideoxyribose**
1'-β-hexylamino deoxyribose
1'-methoxy-2'-aminoethoxyribose

b)
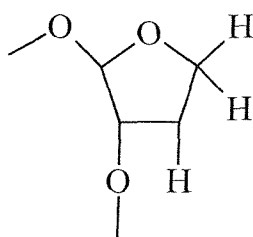
1',2-H-dideoxyribose
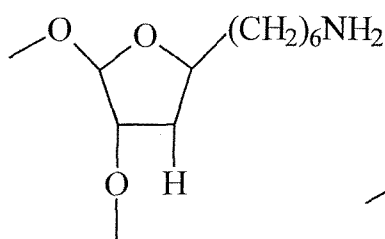
1'-β-hexylamino deoxyribose
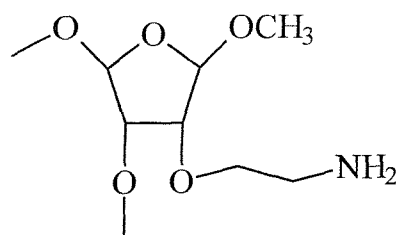
1'-methoxy-2'-aminoethoxyribose

Figure 3.2: Diagram a) shows the sequence of the RAD 1 fragment, with the bold letters illustrating the target sites for the abasic analogues. Also shown is the oligonucleotide sequence. Diagram b) shows the structures of the 1',2-H-dideoxyribose, 1'-β-hexylamino deoxyribose, and 1'-methoxy-2'-aminoethoxyribose abasic analogues.

If however the third strand is composed of guanine, adenine, or thymine residues then it binds in an antiparallel orientation generating G·GC, A·AT, and T·AT triplets (Fig 1.4). The lack of protonation permits triplex formation to occur over a much wider pH range.

Another limitation of both parallel and antiparallel triplex formation is the requirement for the targeting of an un-interrupted polypurine tract within a duplex. Whilst G·TA, and T·CG parallel triplets and a T·CG antiparallel triplet have described for the recognition of pyrimidine residues, they are less stable than the normal triplets as the structures only possess a single Hoogsteen hydrogen bond. One approach to overcome pyrimidine interruptions in an otherwise homopurine stretch involves the incorporation of an abasic residue in the oligonucleotide at a position opposite the Py·Pu step thereby skipping recognition of the pyrimidine base. An example of such a residue is 1',2-H-dideoxy-D-ribose, which theoretically enables pyrimidine residues to be skipped, allowing continuous triplex formation across pyrimidine sites (Fig. 3.2). However the incorporation of even a single abasic residue within an oligonucleotide significantly reduces triplex stability when compared to a perfectly matched triplex, with values comparable to mismatched natural base triplets (Horne & Dervan, 1991). It is thought that removal of a single base in the third strand reduces triplex stability as a result of a loss of base stacking interactions. Abasic sites can therefore not be used as "null" positions for recognition of mixed sequences.

(3.2) Base analogues.

The DNase I footprinting experiments presented in this chapter examine the properties of the thymidine analogues *5- propargylamino deoxyuridine, 2'-aminoethoxy thymidine, 2'-aminoethoxy-5-propargylamino uridine, 5-propynyl deoxyuridine, 5-aminopropyl deoxyuridine,* the cytidine analogue *5-aminohexyl deoxycytidine,* and the abasic residues *1',2-H-dideoxyribose, 1'-β-hexylamino deoxyribose,* and *1'-methoxy-2'-aminoethoxyribose* (Figs. 3.1 - 3.2) as DNA base analogues in triplex formation. Oligonucleotides containing these analogues were assessed by quantitative

DNase I footprinting.

(3.3) Thymidine analogues.

5-propargylamino deoxyuridine (Fig. 3.1), discussed in section 1.4.1.9, is a charged thymidine analogue which unlike cytosine has the positive charge attached to the 5 position, so as to interact with the phosphate backbone. This interaction should counteract some of the repulsive forces generated from the close proximity of three negatively charged phosphate backbones. 5-propargylamino dU has previously been demonstrated to increase the stability of triplexes over 1000 fold when used in an oligonucleotide in which it replaced every thymine residue (Bijapur *et al* 1999). In this study three oligonucleotides were partially substituted with 5-propargylamino deoxyuridine; 5'-TT^{P}UT^{P}UTCTT-3', 5'-TT^{P}UT^{P}UTC^{P}UT-3', and 5'-^{P}UT^{P}UT^{P}UTC^{P}UT-3' (where ^{P}U indicates the positions of substitution, and subsequently these oligonucleotides are termed 2^{P}U, 3^{P}U, and 4^{P}U respectively). Two further oligonucleotides were synthesised containing guanine in which every thymidine residue was replaced with 5-propargylamino dU, 5'-^{P}UGG^{P}U^{P}UG^{P}UGT-3' and 5'-^{P}UGG^{P}U^{P}UG^{P}UG^{P}U^{P}U^{P}U^{P}U^{P}UG^{P}UT-3'. These oligonucleotides are termed 9^{P}UGT and 17G^{P}UT respectively in the remainder of this chapter. Two additional 5-propargylamino dU containing oligonucleotides were prepared for antiparallel triplex formation; 5'-^{P}UG^{P}UG^{P}U^{P}UGGT-3' and 5'-^{P}U^{P}UG^{P}U^{P}U^{P}U^{P}U^{P}U^{P}UG^{P}UG^{P}U^{P}UGGT-3', subsequently termed 9GGT and 17GGT respectively.

2'-aminoethoxy thymidine (Fig. 3.1) has been reported to stabilise triplex formation when used in place of dT for recognising AT base pairs (Blommers *et al* 1998, & Cuenoud *et al* 1998). The analogue incorporates the aminoethoxy modification at the 2' position of the ribose moiety, and was a gift from Dr. B. Cuenoud, *Novartis*. Three oligonucleotides were synthesised which are partially substituted with this analogue; 5'-TT^{AE}TTT^{AE}TCTT-3', 5'-TT^{AE}TT^{AE}TTC^{AE}TT-3', and 5'-^{AE}TT^{AE}TT^{AE}TTC^{AE}TT-3', (where ^{AE}T represents the site of substitution and are subsequently termed 2^{AE}T, 3^{AE}T, and 4^{AE}T respectively).

2'-aminoethoxy-5-propargylamino uridine (Fig. 3.1) is a novel thymidine analogue designed to incorporate the sugar modification, aminoethoxy at the 2' position of the ribose moiety and the propargylamino side chain at position 5 of the uridine base. Two oligonucleotides were synthesised which were partially substituted with this analogue; 5'-TT^{AEP}UT^{AEP}UTC^{AEP}UT-3', and 5'-^{AEP}UT^{AEP}UT^{AEP}UTC^{AEP}UT-3' (where ^{AEP}U represents the position of substitution, and are subsequently termed 3^{AEP}U and 4^{AEP}U respectively).

Both 5-propynyl dU and 5-aminopropyl dU were designed to increase the stability of parallel T·AT triplets. It was postulated that the side chain of 5-aminopropyl dU may interact with the DNA backbone in a similar fashion to that of 5-propargylamino dU producing comparable effects. Whereas 5-propynyl dU has previously been reported to enhance triplex stability presumably due to increased stacking interactions (Lacroix *et al* 1999, Phipps *et al* 1998). Both analogues were substituted into oligonucleotides with the sequence 5'-TT^{AP}UT^{AP}UTCTT-3' and 5'-TTPTPTCTT-3' (where ^{AP}U and P represent the site of substitution by 5-aminopropyl dU and 5-propynyl dU respectively) and are subsequently termed 2^{AP}U and 2P respectively.

Footprints generated by DNase I cleavage usually extend beyond the length of the oligonucleotide binding site to cover an additional couple of bases, and this can in turn be used to assess the ability of an oligonucleotide to form a stable triplex. The DNase I cleavage patten is not even, with some bonds being cleaved more readily than others to produce an uneven ladder of cleavage products. An example of a strong cleavage site can be seen at position 53 of *Tyr*T(43-59) (see Fig. 3.3). Digestion is generally very poor within the polypurine tract, with the exception of band 53, which is cut much more efficiently.

Unmodified Oligonucleotide.
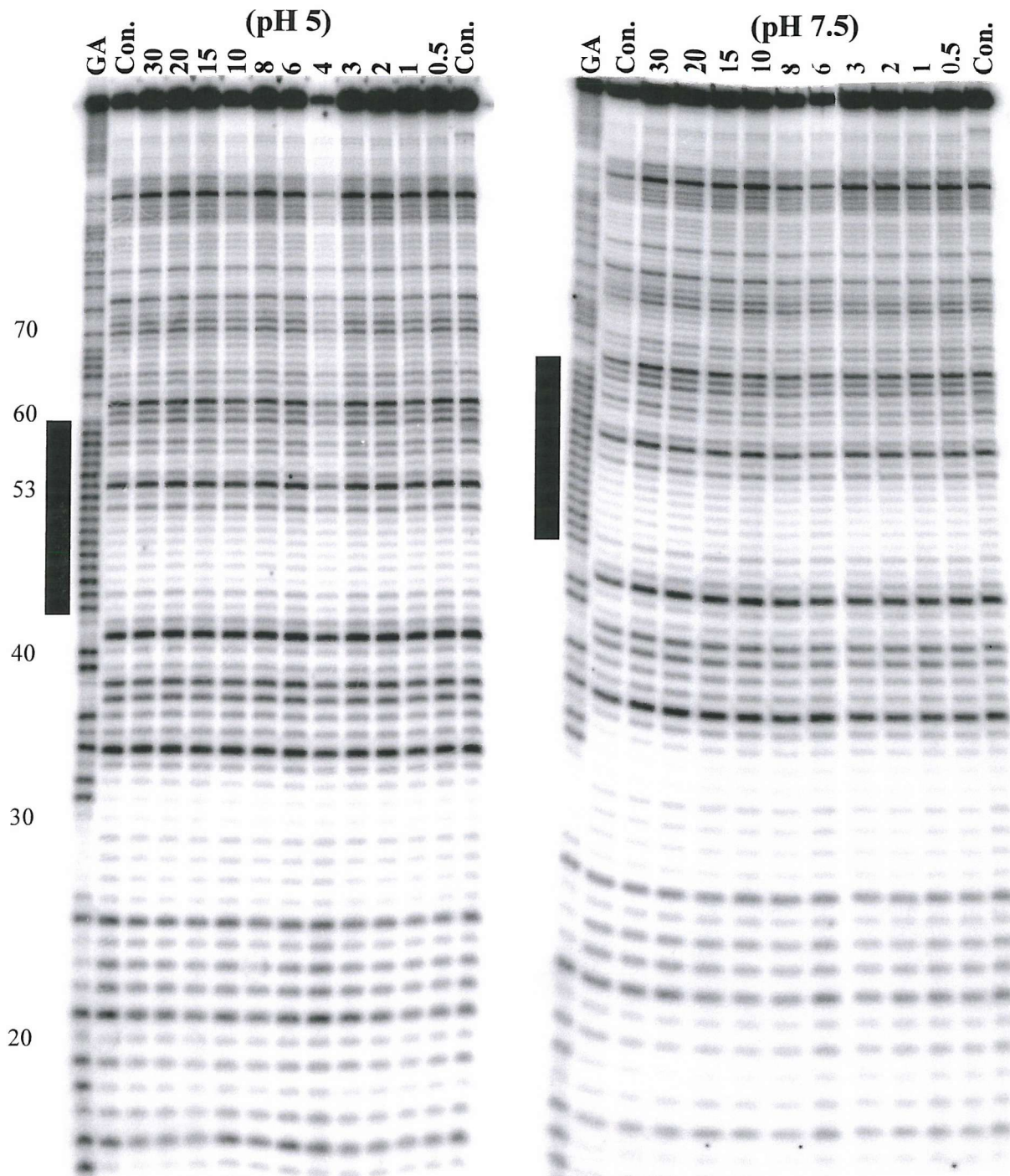
Figure 3.3 DNase I footprints showing the interaction of the oligonucleotide 5'-TTTTTTCTT-3' with ^{32}P labeled *Tyr*T(43-59). The left hand panel shows the digestion pattern in 50 mM sodium acetate (pH 5), 10 mM MgCl$_2$. The right hand panel shows the results obtained in 50 mM Tris-HCl (pH 7.5), 10 mM MgCl$_2$. Oligonucleotide concentrations (μM) are indicated at the top of the lanes. "GA" tracts are Maxam-Gilbert markers specific for purine residues. Lanes labeled Con. show the digestion pattern in the absence of oligonucleotide. The solid rectangular boxes to the left of each gel indicate the 17 base pair homopurine tract. The numbers indicate the sequence numbering scheme.

(3.3.1)   Unmodified oligonucleotides.

The gels shown in Fig. 3.3 demonstrate the DNase I digestion pattern of

*Tyr*T(43-59) in the presence of the unmodified oligonucleotide 5'-TTTTTTCTT-3'. The

left hand panel shows the results obtained in 50 mM sodium acetate (pH 5), 10 mM

$MgCl_2$. The lane labelled GA is a DNA marker specific for purine residues, whilst the

lane labelled Con. shows the DNase I digestion patten obtained in the absence of

oligonucleotide. It can be seen that no footprint is generated within the triplex target site

(positions 43 - 51). The right hand panel of Fig. 3.3 shows the result obtained in 10 mM

Tris-HCl (pH 7.5), 10 mM $MgCl_2$ and again demonstrates a lack of footprinting at the

triplex target site. Furthermore in contrast to the results presented below, no band

enhancement is produced at the 3'-end of the triplex target site in either gel (position 43).

These results confirm previous studies that show an unmodified oligonucleotide

containing a single cytosine residue does not stabilise triplex formation at either pH.

(3.3.2)   5-Propargylamino deoxyuridine.

The left hand panel of Fig. 3.4 shows the DNase I digestion of *Tyr*T(43-59) in the

presence of 5'-TT^{P}UT^{P}UTCTT-3' (2^PU) at pH 5.0. No footprint is apparent at the

expected target site (position 43 - 51) under these conditions even at the highest

oligonucleotide concentrations. However it can be seen that cleavage of the band at

position 43 is slightly enhanced above oligonucleotide concentrations of 3 μM,

indicating a weak interaction between the oligonucleotide and the DNA duplex.

Quantitative analysis of the band at position 43 revealed that the enhancement had a C_{50}

value of 7.9 ± 1.7 μM (Fig. 3.9b and Table 3.1).

The central panel of Fig. 3.4 shows the DNase I digestion pattern of *Tyr*T(43-59)

in the presence of oligonucleotide 5'-^{P}UTT^{P}UTTC^{P}UT-3' (3^PU) in 50 mM sodium acetate

(pH 5), 10 mM $MgCl_2$. No footprint is apparent at the expected target site

(position 43 - 51). However it can be seen that the band at position 43 is enhanced at

oligonucleotide concentrations of 4 μM and above, indicating a weak interaction between
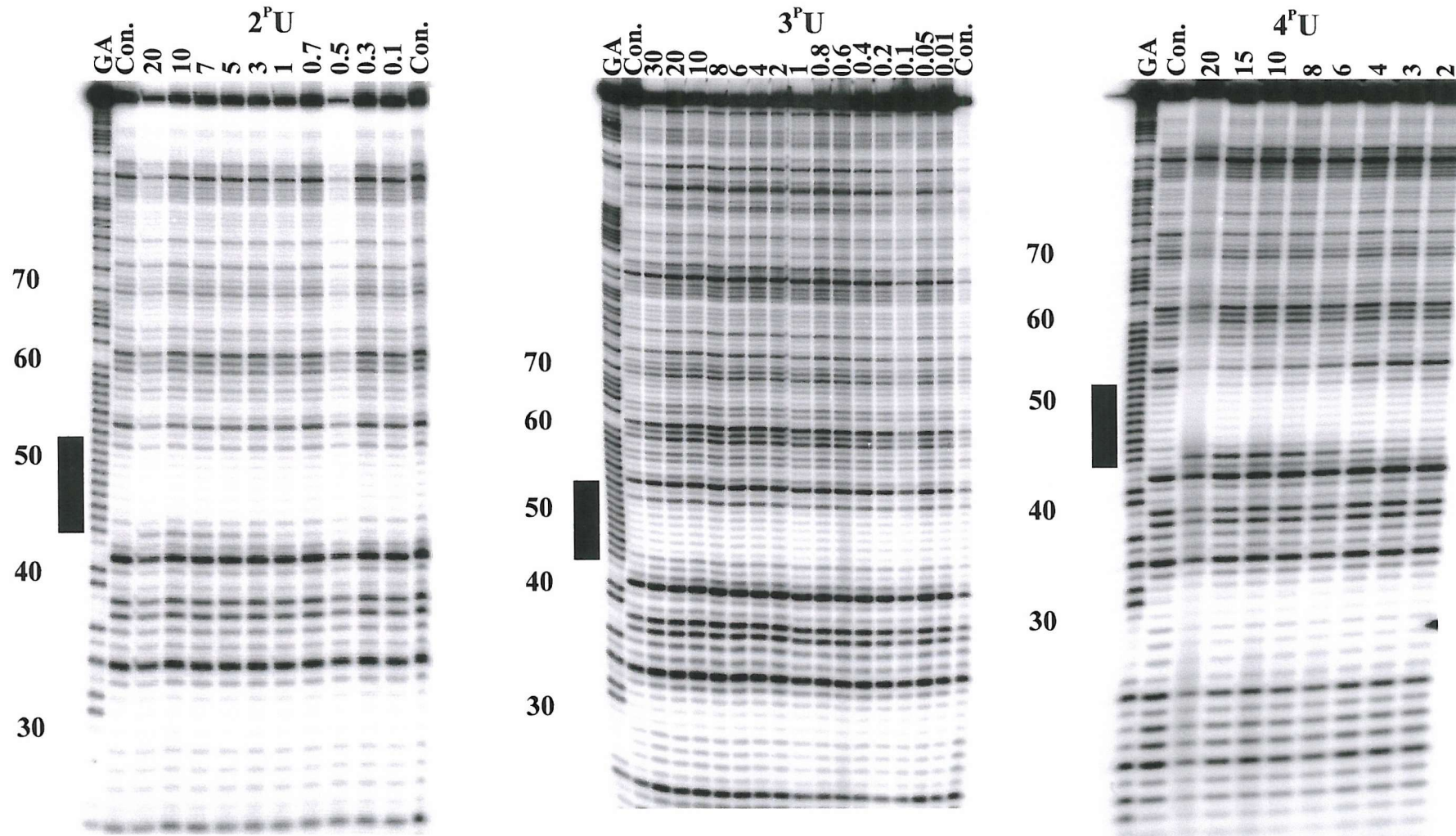
Figure 3.4: DNase I footprinting gels showing the interaction of 5'-TT^PUT^PUTCTT-3' (left hand panel), 5'-T^PUT^PUTTC^PUT-3' (middle panel), 5'-^PUT^PUT^PUTC^PUT-3' (right hand panel), with *Tyr*T(43-59) in 50 mM sodium acetate (pH5), 10 mM MgCl_2. Oligonucleotide concentrations (μM) are indicated at the top of the lanes. "GA" tracts are Maxam-Gilbert markers specific for purine residues. Lanes labelled Con. show the digestion of *Tyr*T(43-59) in the absence of oligonucleotide. The solid rectangular boxes to the left of each gel indicate the 9-base pair target sites. The numbers to the left of the gels designate the numbering scheme of the DNA sequence.

the oligonucleotide and the DNA duplex. However this interaction was too weak to quantify.

The right hand panel of Fig. 3.4 illustrates the DNase I digestion of *Tyr*T(43-59) in the presence of oligonucleotide 5'-^{P}UT^{P}UT^{P}UTC^{P}UT-3' (4^{P}U) at pH 5. It can be seen that, at oligonucleotide concentrations of 4 μM and above the intensity of the bands between positions 43 - 53 are attenuated, particularly band 53. Furthermore band enhancement can be observed at position 43 that persists to an oligonucleotide concentration of 4 μM. Quantitative analysis yielded C_{50} values of 7.3 ± 1.5 μM for the enhancement and 8.6 ± 3.8 μM for the footprint (Fig. 3.9b and Table 3.1).

These DNase I footprinting experiments demonstrate that the triplex stability afforded by 5-propargylamino dU is dependent upon the number of base substitutions in the TFO. Two and three substitutions do not yield a footprint, while the substitution produces a weak interaction as evidenced by the enhancement at position 43. In contrast 4^{P}U generates a footprint at the expected target site as evidenced by band attenuation between positions 43 - 53 (Figs. 3.4 & 3.9b).

(3.3.3) 2'-Aminoethoxy thymidine.

The left hand panel of Fig. 3.5 shows the DNase I digestion pattern of *Tyr*T(43-59) in the presence of oligonucleotide 2^{AE}T. This was performed at pH 5.0, ensuring protonation of the cytosine residue and the aminoethoxy side chains. It can be seen that no footprint is generated between positions 43 - 51, but enhancement of cleavage is evident at position 43 at concentrations of 4 μM and above. Quantitative analysis of this band yielded a C_{50} value of 19.1 ± 4.8 μM (Fig. 3.9a and Table 3.1).

The central panel of Fig. 3.5 shows the DNase I digestion of *Tyr*T(43-59) in the presence of 3^{AE}T at pH 5.0. The oligonucleotide was designed to generate a triplex with *Tyr*T(43-59) DNA between positions 43 - 51. No footprint can be seen between these positions, however enhancement is evident at position 43 persisting to approximately

2'-aminoethoxy T Modified Oligonucleotides (pH 5).
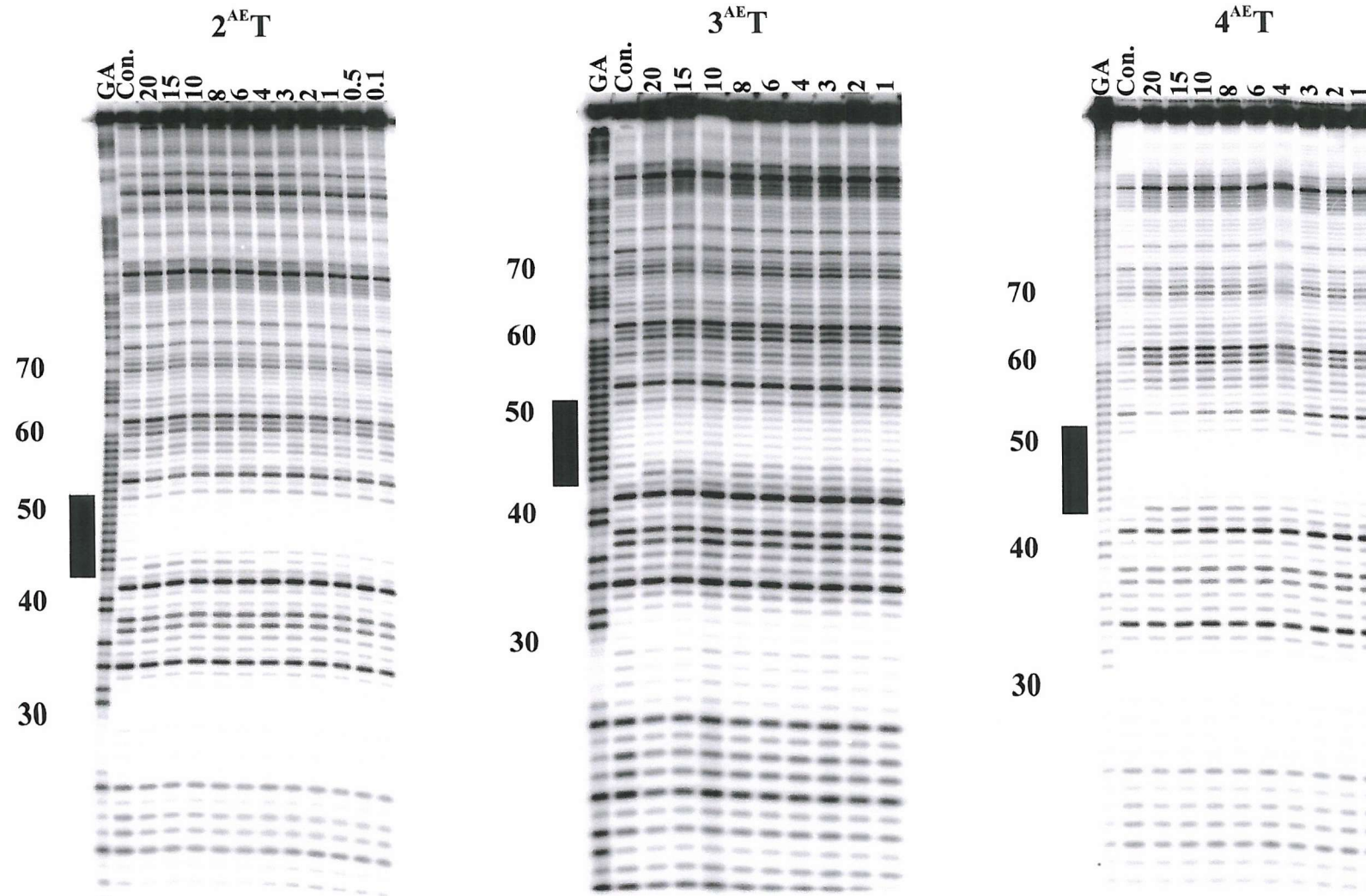
Figure 3.5: DNase I footprinting gels showing the results obtained with *Tyr*T(43-59) in the presence of varrying concentrations of 5'-TT^{EA}TT^{EA}TTCTT (left hand Panel), 5'-T^{EA}TT^{EA}TTTC^{EA}TT-3' (middle panel), 5'-^{EA}TT^{EA}TT^{EA}TTC^{Ea}TT-3' (right hand panel), in 50 mM sodium acetate (pH 5), 10 mM MgCl$_2$. Oligonucleotide concentrations are indicated at the top of the lanes. "GA" tracts are Maxam-Gilbert markers specific for purine residues. Lanes labelled Con. show the digestion pattern of *Tyr*T(43-59) in the absence of oligonucleotide. The solid rectangular boxes to the left of each gel indicates the 9-base pair triplex target site, and the numbers designate the numbering scheme of the DNA sequence.
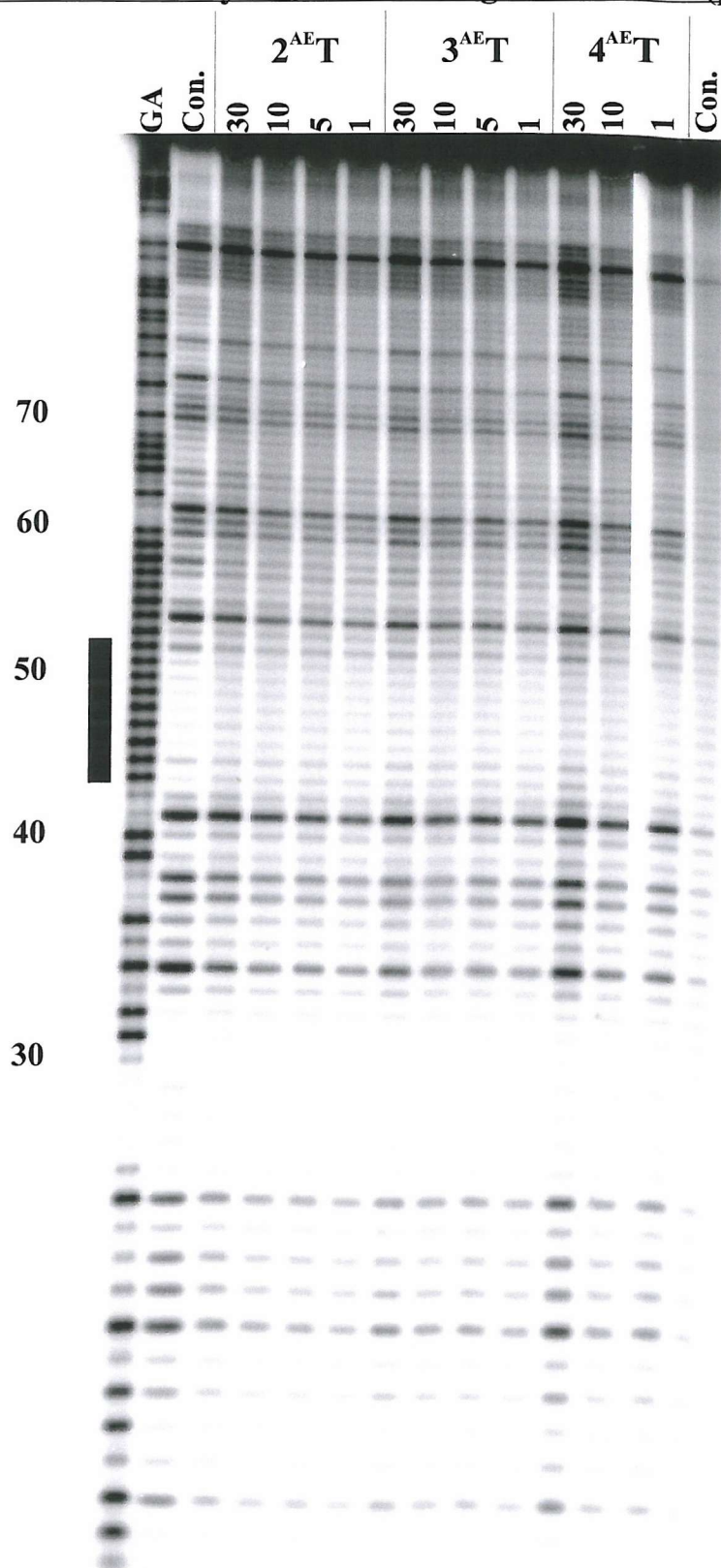
Figure 3.6: DNase I digestion pattern of *Tyr*T(43-59) in the presence of varying concentrations of oligonucleotides 2[AE]T, 3[AE]T, and 4[AE]T at pH 7.5. The "GA" tract represents a Maxam-Gilbert marker specific for purine residues. Lanes labelled Con. show the DNase I digestion of *Tyr*T(43-59) in the absence of oligonucleotide. The solid rectangular box to the left of the gel indicates the 9-base pair triplex target site, and the numbers designate the numbering scheme for the DNA sequence.

1 μM. Quantitative analysis of this band yielded a C_{50} value of 12.2 ± 4.0 μM (Fig. 3.9a and Table 3.1).

The right hand panel of Fig. 3.5 illustrates the DNase I digestion of *Tyr*T(43-59) in the presence of $4^{AE}T$ at pH 5.0. It can be seen that although a complete footprint is not generated within the target site, there is attenuation of bands in this region, particularly at position 53, at high oligonucleotide concentrations (20 -15 μM). The band at position 43 is also enhanced at concentrations of 4 μM and above. Quantitative analysis of these data yielded C_{50} values of 13.5 ± 0.9 μM for the footprint 7.9± 1.2 μM for the enhancement (Fig. 3.9a and Table 3.1).

Fig. 3.6 shows the DNase I digestion pattern of *Tyr*T(43-59) in the presence of each of these 2'-aminoethoxy T containing oligonucleotides, determined in 10 mM Tris-HCl (pH 7.5), containing 50 mM NaCl, and 10 mM $MgCl_2$. It can be seen that none of the oligonucleotides generates a footprint within the expected target site (positions 43 - 51), and there is no enhancement of band 43.

(3.3.4) 2'-aminoethoxy-5-propargylamino U

Quantitative DNase I footprinting investigations with oligonucleotides containing this base analogue were conducted at pH 5.0 to protonate the single cytosine residue, the aminoethoxy, and the propargylamino side chains. The left hand panel of Fig. 3.7 shows the DNase I digestion pattern of *Tyr*T(43-59) in the presence of oligonucleotide $3^{AEP}U$. It can be seen that a distinct footprint is generated between positions 44 - 54 (the expected target site) with the band at position 53 being significantly attenuated at the highest oligonucleotide concentrations. The band at position 43 is also enhanced at oligonucleotide concentrations of 0.5 μM and above. The footprint persists down to an oligonucleotide concentration of about 0.7 μM. Quantitative analysis yielded a C_{50} value of 2.2 ± 0.4 μM for the footprint while the enhancement was not quantified (Fig. 3.9c and Table 3.1).

2'-aminoethoxy-5-propargylamino U Modified Oligonucleotides (pH 5).
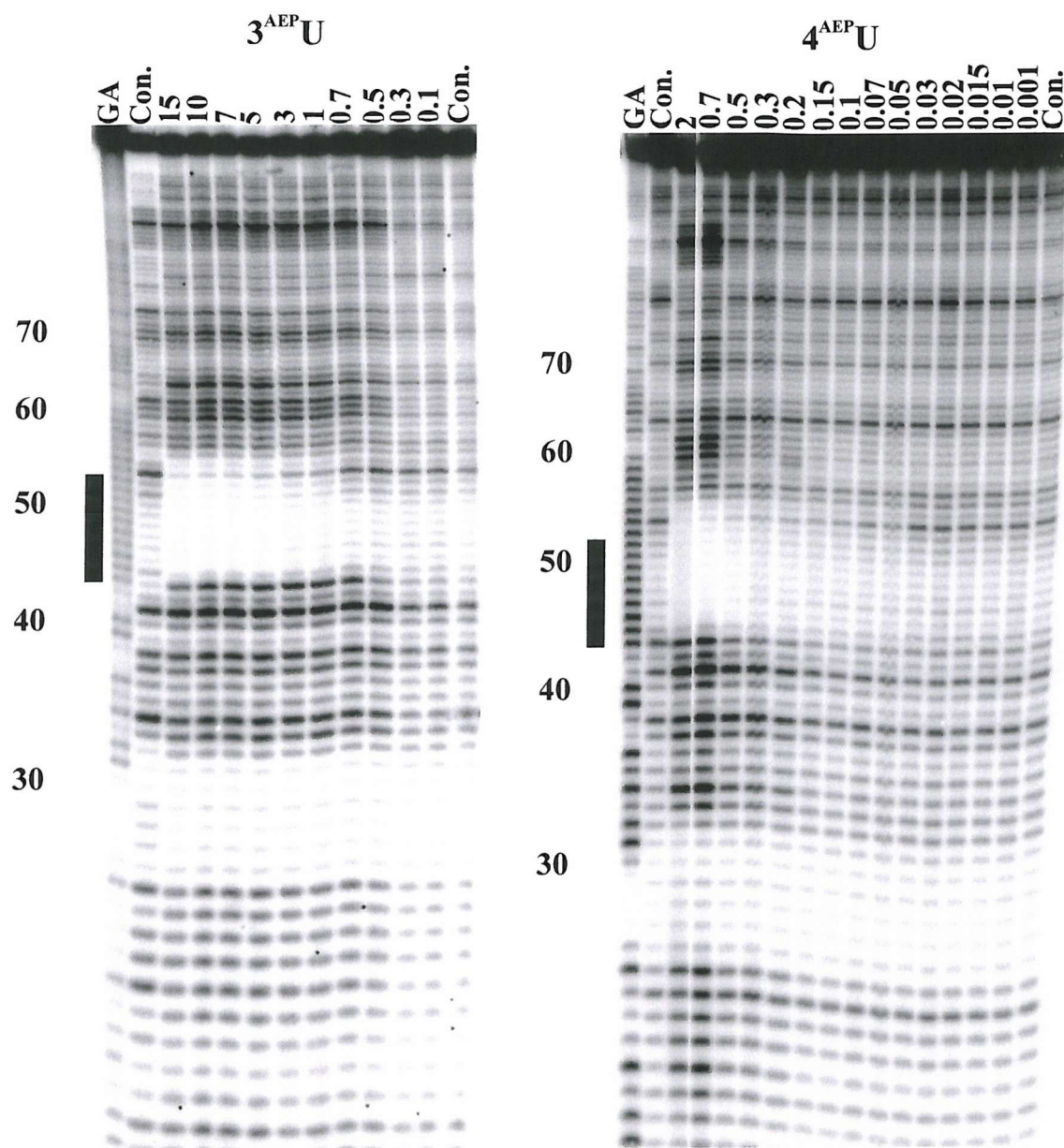
Figure 3.7: DNase I footprints showing the digestion pattern of, *Tyr*T(43-59) in the presence of 3$^{\text{AEP}}$U (left hand panel) and 4$^{\text{AEP}}$U (right hand panel) at pH 5.0. Oligonucleotide concentrations (μM) are indicated at the top of the lanes. "GA" tracts are Maxam-Gilbert markers specific for purine residues. Lanes labelled Con. show the digestion pattern of *Tyr*T(43-59) in the absence of oligonucleotide. The solid rectangular boxes to the left of each gel indicate the 9 base pair target sites, and the numbers designate the numbering scheme of the DNA sequence.

The right hand panel of Fig. 3.7 shows the DNase I digestion of *Tyr*T(43-59) in the presence of oligonucleotide 4 ^{AEP}U at pH 5.0. A distinct footprint can be seen between positions 44 - 54 that persists to an oligonucleotide concentration of approximately 0.03 µM. Furthermore the band at position 43 is enhanced at oligonucleotide concentrations of 0.15 µM and above. Quantitative analysis of these data yielded a C_{50} value of 0.1 ± 0.03 µM for the footprint while the enhancement was not quantified (Fig. 3.9c and Table 3.1).

Since oligonucleotides containing this bis-modified analogue appear to form stable triplexes at pH 5, further experiments with 3 ^{AEP}U and 4 ^{AEP}U were carried out at pH 7.5. The results of DNase I digestion experiments with 3 ^{AEP}U are shown in the left hand panel of Fig 3.8. It can be seen there is faint attenuation between positions 44 - 54, at the highest oligonucleotide concentration (30 µM). This weak footprint can be seen to persist to approximately 20 - 25 µM. The intensity of the band at position 43 is enhanced at the highest oligonucleotide concentration and its intensity decreases in a concentration dependent fashion down to approximately 6 µM. Quantitative analysis yielded a C_{50} value of 25.8 ± 9.5 µM for this footprint which is significantly lower than that determined at pH 5.0 (Fig. 3.9d and Table 3.1). The enhancement was not quantified.

The right hand panel of Fig. 3.8 illustrates DNase I digestion of *Tyr*T(43-59) in the presence of oligonucleotide 4 ^{AEP}U at pH 7.5. A clear footprint can be seen between positions 44 - 54 that persists to an oligonucleotide concentration of about 0.4 µM. The intensity of the band at position 43 is also enhanced at the higher oligonucleotide concentrations and this decreases in a concentration dependent fashion. Quantitative analysis yielded a C_{50} value of 0.5 ± 0.1 µM for the footprint (Fig. 3.9d and Table 3.1).

The quantitative data for all these footprints were used to construct the footprinting plots shown in Fig. 3.9, and analysed to produce the C_{50} values which are summarised in Table 3.1. These demonstrate that 4^{AEP}U stabilised triplex formation to a higher degree than any of the other oligonucleotides. Although 3^{AEP}U stabilised triplex formation to a lesser extent than that of 4^{AEP}U, it was significantly better than any of the 5-propargylamino dU, or 2'-aminoethoxy T containing oligonucleotides.
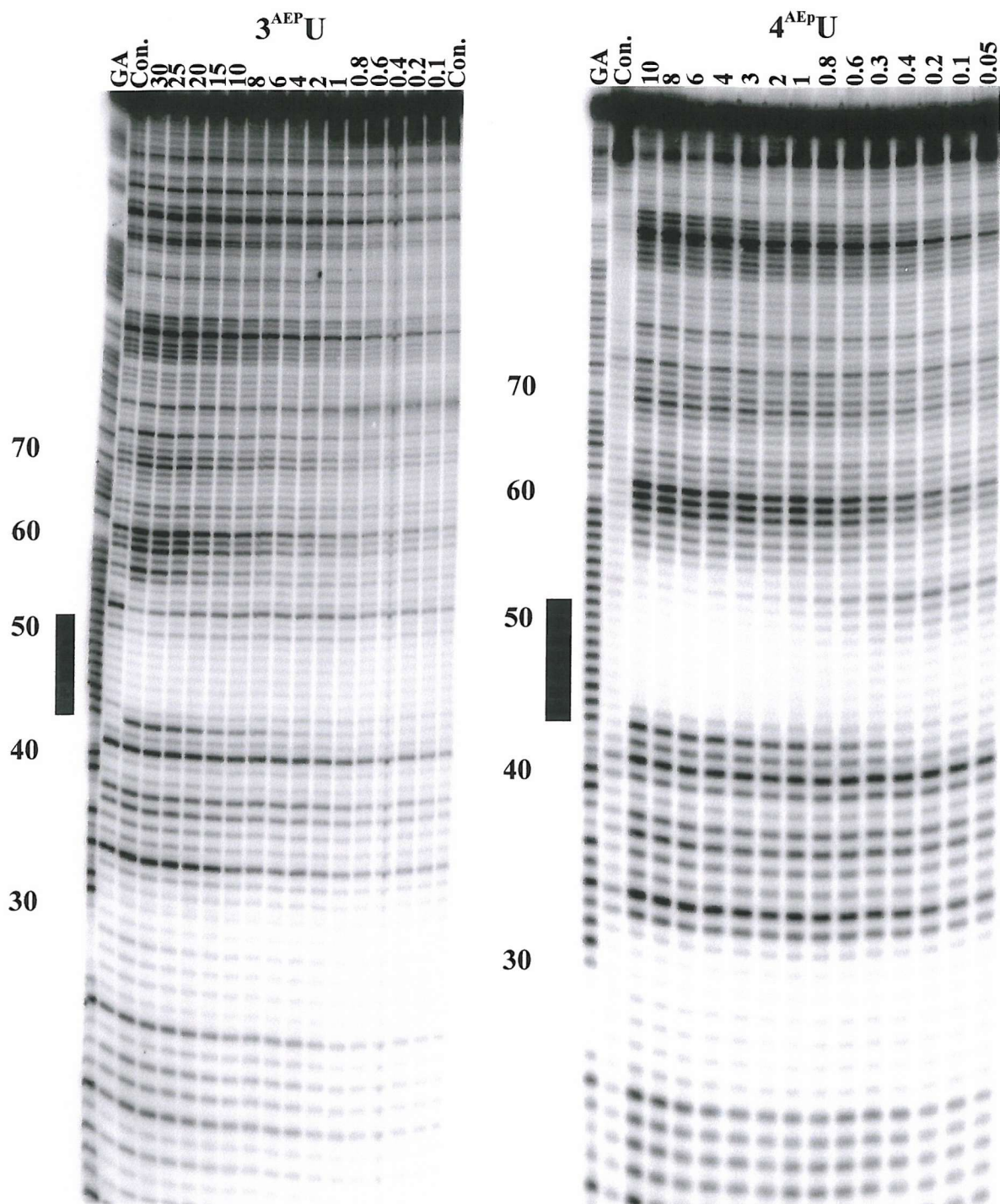
Figure 3.8: DNase I footprinting gels showing the results obtained with *Tyr*T(43-59) and varying concentrations of 5'-TT^{AEP}UT^{AEP}UTC^{AEP}UT-3' (left hand panel), and 5'-^{AEP}UT^{AEP}UT^{AEP}UTC^{AEP}UT-3' (right hand panel), in 50 mM Tris-HCl (pH 7.5), 10 mM MgCl$_2$. Oligonucleotide concentrations (μM) are indicated at the top of the lanes. "GA" tracts are Maxam-Gilbert markers specific for purine residues. Lanes labelled Con. indicate the digestion pattern of *Tyr*T(43-59) in the absence of oligonucleotide. The solid rectangular boxes to the left of each gel indicates the 9-base pair triplex target site, and the numbers designate the numbering scheme of the DNA sequence.
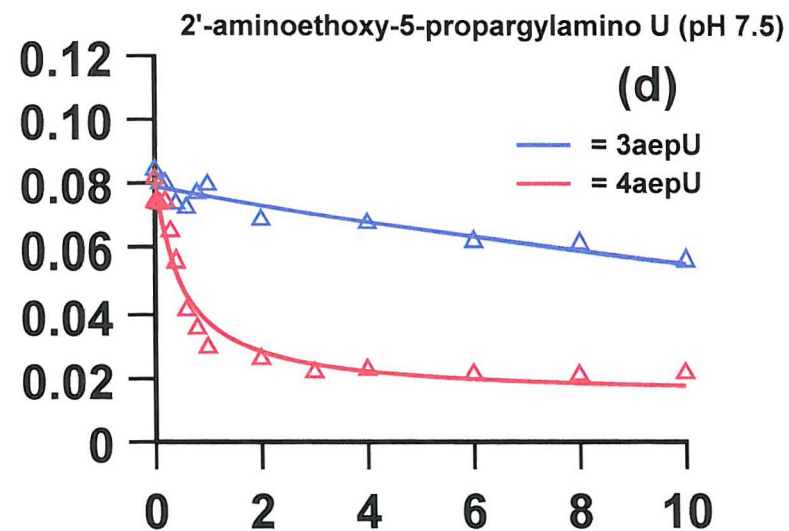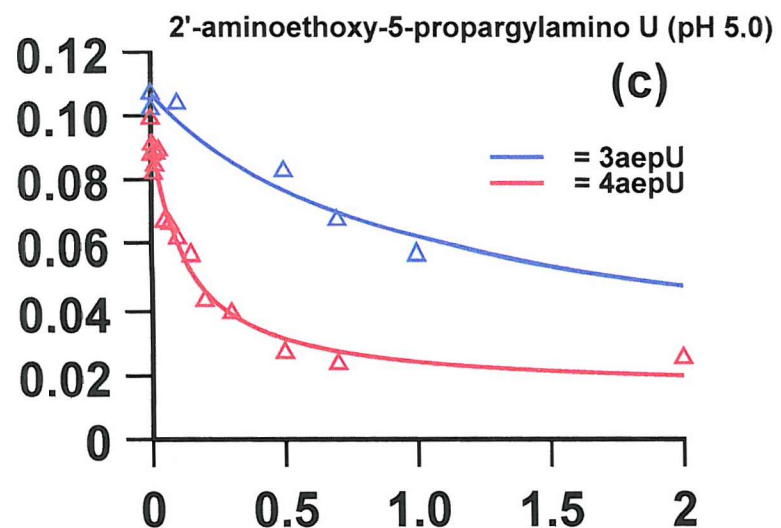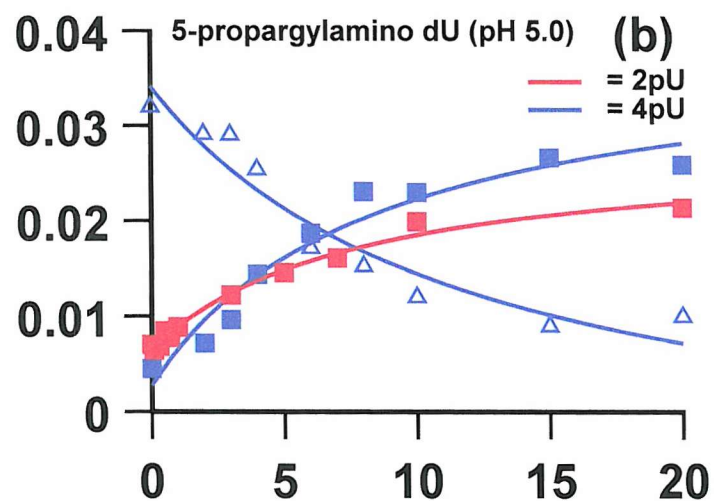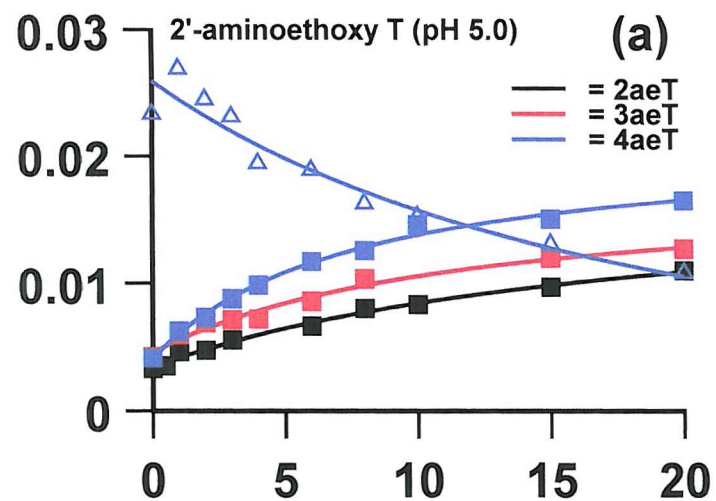
Figure 3.9: Plots showing band enhancement (solid symbols) and footprints (open symbols). The abscissa represents oligonucleotide concentration (μM), and the ordinate represents relative band intensity (arbitary units).

(3.4) Parallel GT triplex formation.

Oligonucleotides 5'-^{P}UGG^{P}U^{P}UG^{P}UGT-3' (9^{P}UGT) and
5'-^{P}UGG^{P}U^{P}UG^{P}UG^{P}U^{P}U^{P}U^{P}U^{P}UG^{P}UT-3' (17G^{P}UT), were designed to investigate whether incorporation of 5-propargylamino dU into oligonucleotides could stabilise triplexes containing parallel G·GC and T·AT triplets. These triplexes are usually much less stable than those containing T·AT and C$^+$·GC triplets. It was postulated that the propargylamino group might enhance the strength of this interaction. 9^{P}UGT should form a triplex containing four G·GC triplets, four ^{P}U·AT triplets, and a single T·AT triplet. Whereas the 17G^{P}UT oligonucleotide should bind to the entire 17 base pair polypurine tract, producing five G·GC triplets, eleven ^{P}U·AT triplets and a single T·AT triplet.

The left hand panel of Fig. 3.10 shows the DNase I digestion pattern of *Tyr*T(43-59) in the presence of 9^{P}UGT; the oligonucleotide should bind between positions 51 - 59. However the gel clearly illustrates that the oligonucleotide does not affect the DNase I cleavage pattern, producing neither attenuation or enhancement, usually associated with triplex formation.

The right hand panel of Fig. 3.10 shows DNase I digestion of *Tyr*T(43-59) in the presence of 17G^{P}UT. It can be observed that there is no evidence for any interaction between this oligonucleotide and the DNA sequence.

These results suggest that 5-propargylamino dU can not be used to stabilise parallel GT triplex formation, producing results similar to unmodified oligonucleotides (Faucon *et al* 1996) and this will be covered in greater detail in section 3.10.

(3.5) Antiparallel triplex formation.

Oligonucleotides 5'-^{P}UG^{P}UG^{P}U^{P}UGGT-3' (9GGT) and
5-^{P}U^{P}UG^{P}U^{P}U^{P}U^{P}U^{P}U^{P}UG^{P}UG^{P}U^{P}UGGT-3' (17GGT), were designed to assess the ability of propargylamino dU to stabilise antiparallel GT triplex formation.

5-propargylamino dU Modified Olionucleotides (pH 5).
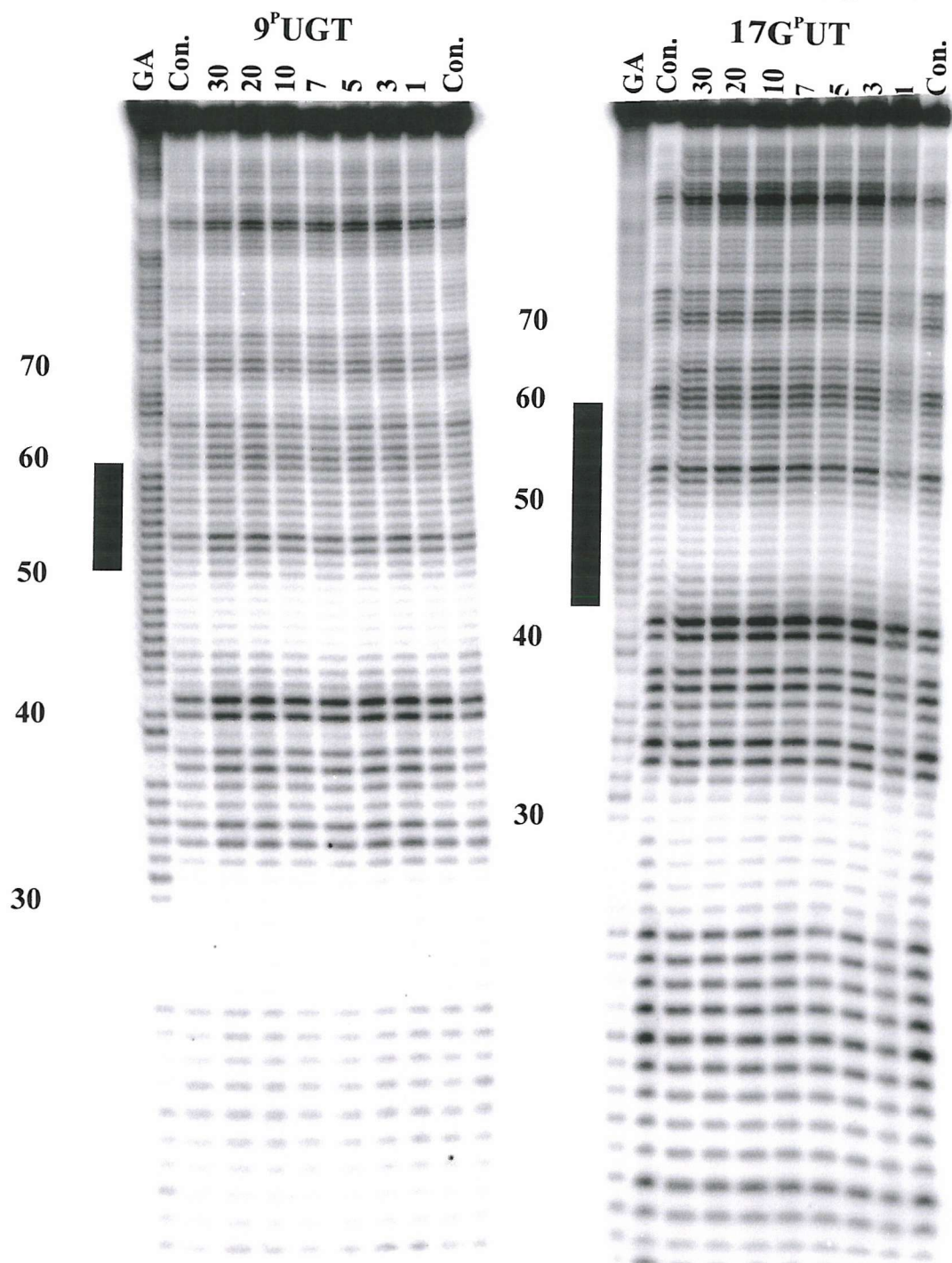
Figure 3.10: DNase I footprinting gels showing the effect of 5'-ᴾUGGᴾUᴾUGᴾUGT-3' (left hand panel), and ᴾUGGᴾUᴾUᴾUGᴾUᴾUGᴾUᴾUᴾUᴾUᴾUᴾUGᴾUT-3' (right hand panel) on the digestion of *Tyr*T(43-59) in 50 mM sodium acetate (pH 5), 10 mM MgCl$_2$. Oligonucleotide concentrations (μM) are indicated at the top of the lanes. "GA" tracts are Maxam-Gilbert markers specific for purine residues. Lanes labelled Con. indicate the digestion pattern of *Tyr*T(43-59) in the absence of oligonucleotide. The solid rectangular boxes to the left of the gels indicate the triplex target sites, and the numbers designate the numbering scheme of the DNA sequence.

The left hand panel of Fig. 3.11 shows the DNase I digestion pattern of *Tyr*T(43-59) in the presence of 9GGT at pH 5.0 in the presence of 10 mM MgCl$_2$. The oligonucleotide was designed to bind between positions 51 - 59. It can be seen that this oligonucleotide has not affected the cleavage pattern and produces neither footprints or enhancements.

The right hand panel of Fig 3.11 shows the digestion of *Tyr*T(43-59) in the presence of 17GGT at pH 5.0 in the presence of 10 mM MgCl$_2$ The oligonucleotide was designed to recognise the full 17 base pair polypurine tract. However the gel indicates no footprint between positions 43 - 59. There is also a lack of band enhancement at position 43 demonstrating that the oligonucleotide does not interact with the DNA.

Since several studies have shown that manganese produces more stable antiparallel triplexes than magnesium, these experiments were repeated in the presence of manganese chloride. The left hand panel of Fig. 3.12 shows the DNase I cleavage of *Tyr*T(43-59) in the presence of 9GGT at pH 5.0 in the presence of 10 mM MnCl$_2$. The right hand panel shows the result of similar experiments with 17GGT. Again no footprint can be seen on either gel at the proposed triplex target sites, and that there is a lack of any enhancement at the 3' terminal regions.

These results demonstrate that 5-propargylamino dU cannot be used to stabilise antiparallel GT triplex formation, with results similar to unmodified oligonucleotides (Faucon *et al* 1996, Keppler *et al* 2001). Furthermore the addition of manganese (which usually enhances antiparallel triplex stability) does not alter this.

(3.6) Aminopropyl deoxyuridine.

This analogue was synthesised with an aminopropyl side chain attached to position 5 of deoxyuridine (Fig. 3.1). It was postulated that this modification would enable the terminal amino group to interact with the DNA backbone and facilitate a partial neutralisation of the backbone charge density, in a fashion similar to that of

5-Propargylamino dU Modified Oligonucleotides (pH 5, 10 mM MgCl₂).
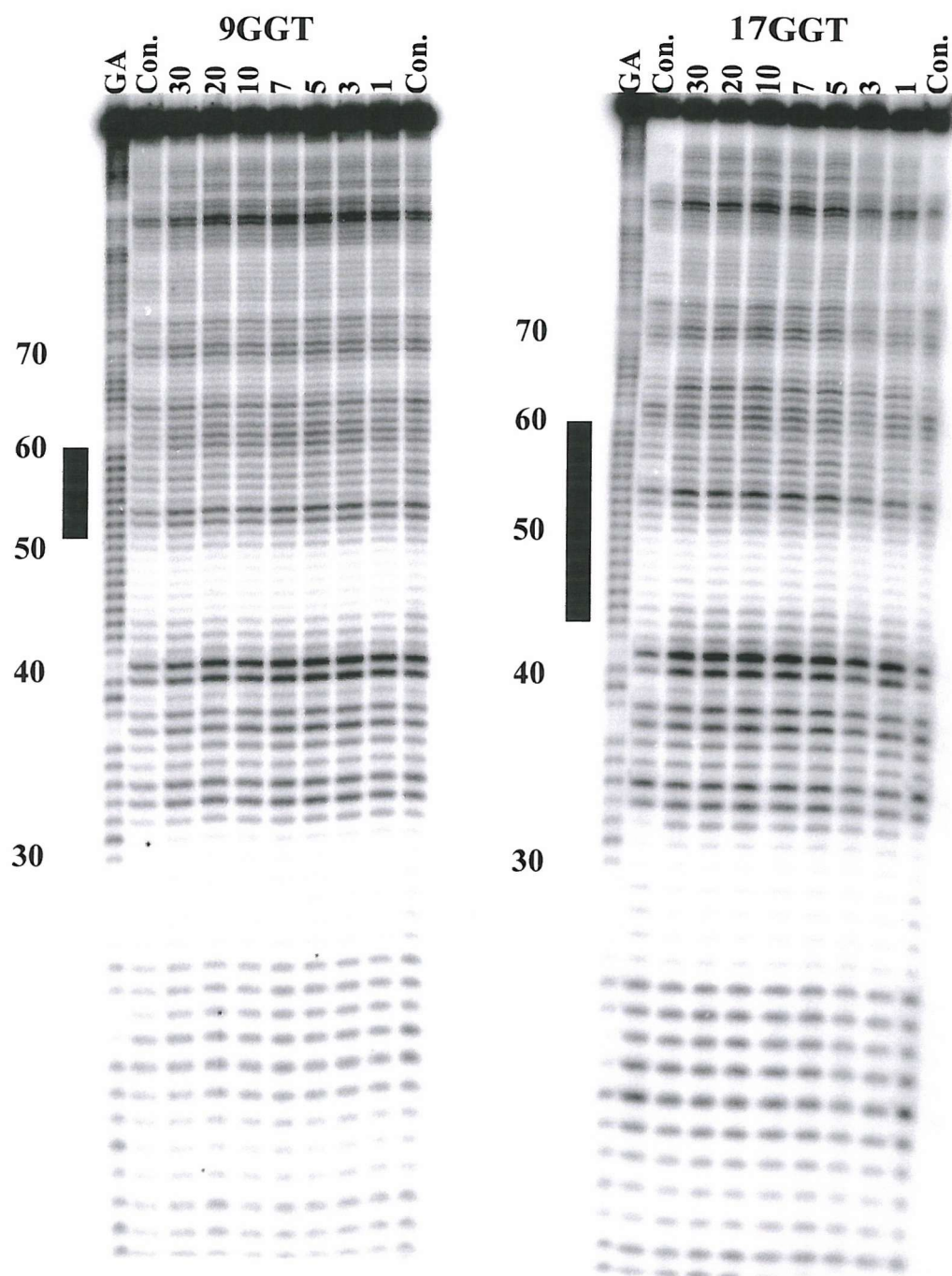
Figure 3.11: The left hand panel shows the DNase I digestion pattern of
*Tyr*T(43-59) in the presence of 9GGT in 50 mM sodium acetate (pH 5.0),
10 mM MgCl₂. The right hand panel shows the digestion in the presence of
17GGT in 50 mM sodium acetate (pH 5.0), 10 mM MgCl₂. Oligonucleotide
concentrations (μM) are indicated at the top of the gels. "GA" tracts are
Maxam-Gilbert markers specific for purine residues. Lanes labelled Con. show
the DNase I digestion pattern of *Tyr*T(43-59) in the absence of oligonucleotide.
The solid rectangular boxes to the left of each gels indicate the triplex target sites,
and the numbers designate the numbering scheme of the DNA sequence.

5-Propargylamino dU Modified Oligonucleotides (pH 5, 10 mM MnCl₂).
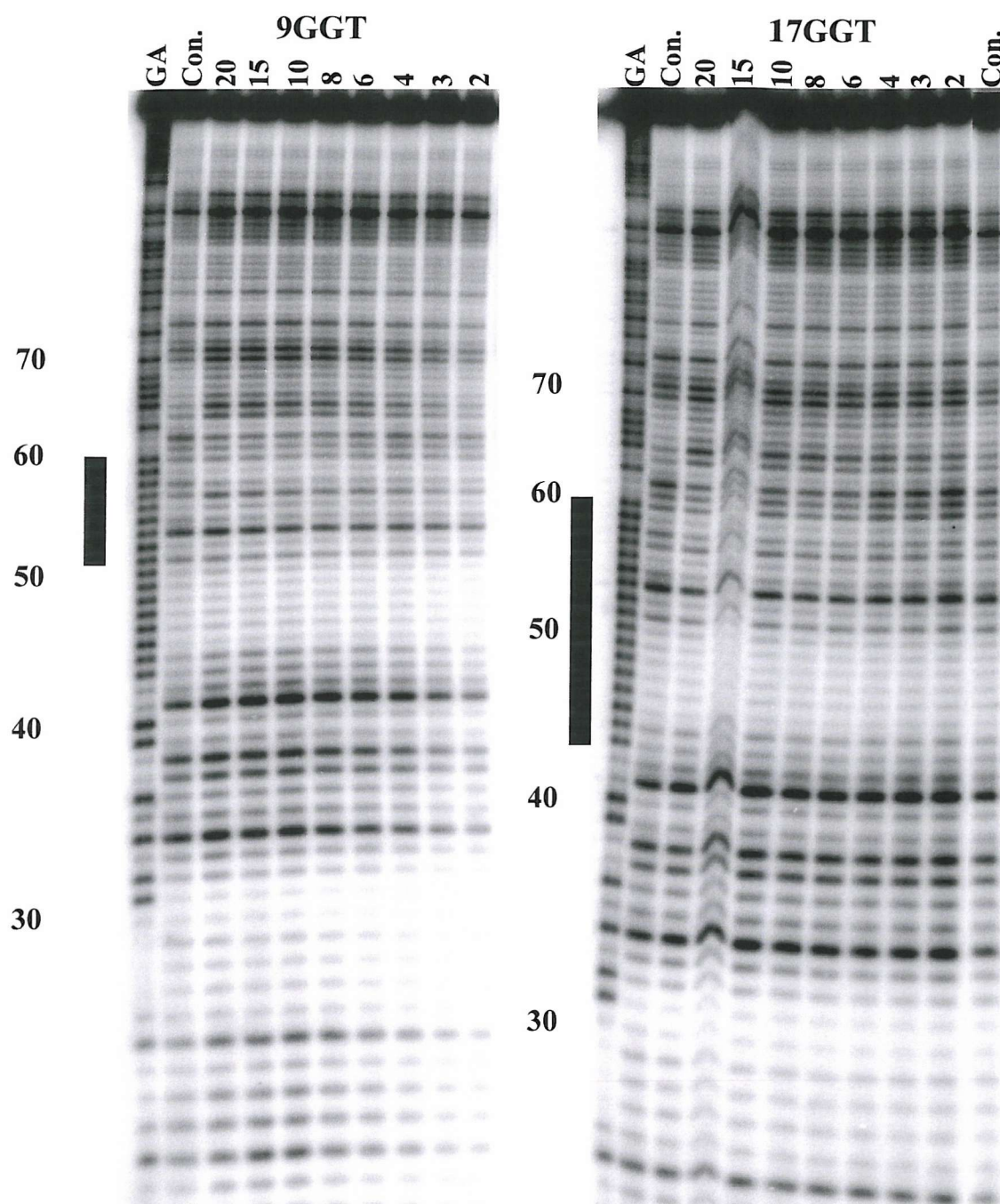
Figure 3.12: The left hand panel shows the DNase I digestion pattern of *Tyr*T(43-59) in the presence of 9GGT at pH 5.0 with 10 mM MnCl₂. The right hand panel shows the digestion pattern in the presence of 17GGT at pH 5.0 with 10 mM MnCl₂. Oligonucleotide concentrations (µM) are indicated at the top of the lanes. "GA" tracts are Maxam-Gilbert markers specific for purine residues. Lanes labelled Con. show the DNase I digestion patern of *Tyr*T(43-59) in the absence of oligonucleotide. The solid rectangular boxes to the left of the gels indicate the triplex target sites, and the numbers designate the numbering scheme of the DNA sequence.

5-propargylamino dU, though it would lack the beneficial stacking interaction of the propynyl group.

The left hand panel of Fig. 3.13 shows the DNase I digestion pattern of *Tyr*T(43-59) in the presence of the 5-aminopropyl dU modified oligonucleotide 5'-TT^{AP}UT^{AP}UTCTT-3' (2^{AP}U), performed in 50 mM sodium acetate (pH 5.0), 10 mM MgCl$_2$. The oligonucleotide was designed to bind between positions 43 - 51. However the gel indicates that there is no footprint between these positions and that there is a lack of band enhancement at the 3' terminal of the expected footprint region. This indicates that the oligonucleotide does not bind to the DNA under these conditions.

The right hand panel of Fig. 3.13 shows the DNase I digestion of *Tyr*T(43-59) in the presence of 2^{AP}U with 10 µM naphthylquinoline (a triplex stabilising ligand) at pH 5.0. We anticipated that addition of this ligand would promote triplex formation, and demonstrate that in principle this oligonucleotide can bind to DNA. Although there is no clear footprint at the target site the band at position 43 is enhanced at all concentrations of the oligonucleotide investigated.

These results indicate a weak interaction between this oligonucleotide and duplex DNA, that is only stabilised in the presence of a triplex stabilising ligand.

(3.7) Propynyl deoxyuridine.

This thymidine analogue has the deoxyuridine base modified at position 5 with a propynyl side chain (Fig. 3.1). This analogue lacks the terminal amino group on the side chain seen in 5-aminopropyl dU and 5-propargylamino dU, but retains the propynyl group of 5-propargylamino dU. Although this analogue is not capable of neutralising the charged phosphodiester backbone, it should have improved stacking interactions relative to the unmodified oligonucleotide. The analogue was incorporated into a 9mer oligonucleotide, 5-TTPTPTCTT-3' (where P indicates the site of substitution), which was designed to form a perfect triplex with *Tyr*T(43-59) between positions 43 - 51.
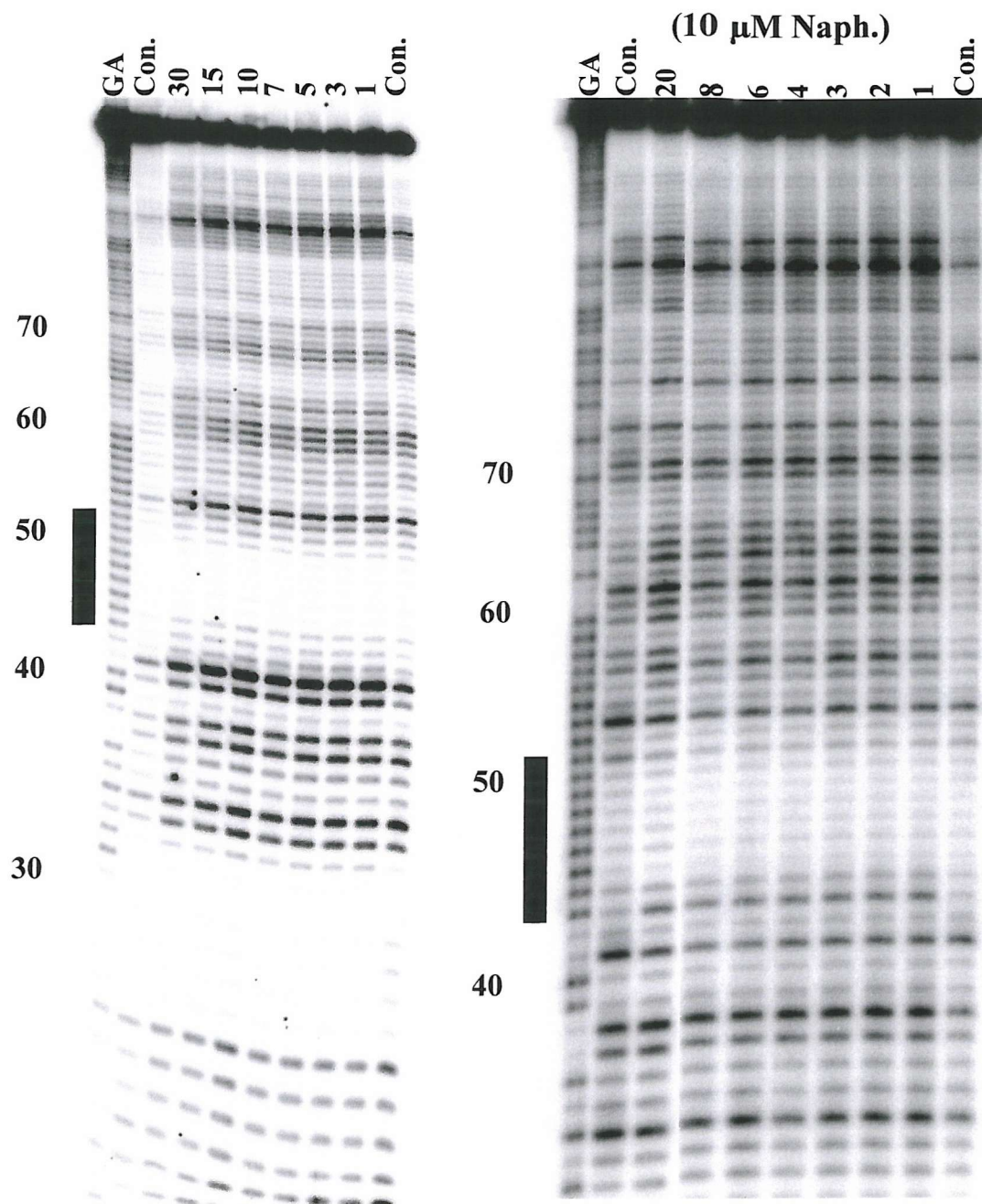
Figure 3.13: DNase I footprinting gels showing the effect of 5-aminopropyl dU modified oligonucleotide 5'-TT^APUT^APUTCTT-3' on the digestion of *Tyr*T(43-59). The left hand panel shows the result in the absence of ligand and the right hand panel shows the result with 10 μM naphthylquinoline, in 50 mM sodium acetate (pH 5), 10 mM MgCl₂. Oligonucleotide concentrations (μM) are shown at the top of the lanes. "GA" tracts are Maxam-Gilbert markers specific for purine residues. Lanes labelled Con. show the digestion pattern of *Tyr*T(43-59) in the absence of oligonucleotide. The solid rectangular boxes to the left of each gel indicate the 9-base pair triplex target site, and the numbers designate the numbering scheme of the DNA sequence.

Figure 3.14: DNase I digestion of *Tyr*T(43-59) in the presence of 5-propynyl dU modified oligonucleotide in the absence of a triplex ligand (left hand panel) and with 10 µM naphthylquinoline (right hand panel). "GA" tracts are Maxam-Gilbert markers specific for purine residues. Lanes labelled Con. show the DNase I digestion of *Tyr*T(43-59) in the absence of oligonucleotide. Oligonucleotide concentrations (µM) are indicated at the top of the lanes. The solid rectangular boxes to the left of the gels indicate the 9-base pair triplex target sites, and the numbers designate the numbering scheme of the DNA sequence.

The left hand panel of Fig. 3.14 shows DNase I digestion of *Tyr*T(43-59) in the presence of 2P performed in 50 mM sodium acetate (pH 5.0), 10 mM $MgCl_2$. It can be seen that no footprint is generated between positions 43 - 51, and that there is no band enhancement at position 43. This indicates that the TFO does not interact with the DNA under these conditions.

The right hand panel of Fig 3.14 shows the DNase I cleavage of *Tyr*T(43-59) in the presence of 2P with 10 μM naphthylquinoline at pH 5. In the presence of this stabilising ligand it can be seen that a footprint is generated between positions 43 - 54 that persists beyond the lowest oligonucleotide concentration (< 0.1 μM). The band at position 43 is also enhanced and again remains so at the lowest oligonucleotide concentration.

The results indicate that the partial substitution of an oligonucleotide with 5-propynyl dU stabilises parallel triplex formation only in the presence of a triplex stabilising ligand.

(3.8) Aminohexyl deoxycytidine.

The 5-aminohexyl dC analogue was designed to increase the pH stability of $C^+ \cdot GC$ triplets, via the incorporation of an aminohexyl side chain at position 5 of the cytosine ring. 5-aminohexyl dC was substituted into the following oligonucleotides; 5'-TTTTTThTT-3', 5'-TThThTTTT-3', and ThhTThThT-3' (where h represents the site of substitution). These were designed to interact with different portions of the polypurine tract in *Tyr*T(43-59) (Fig. 3.1). This analogue was modelled on 5-propargylamino dU, whereby the incorporation of the side chain is postulated to enable the amino group to interact with the DNA backbone and dissipate some of the charge repulsion that arises from the close proximity of three phosphodiester backbones. It is not possible to use 5-propargylamino dC as this would have a very low pKa.
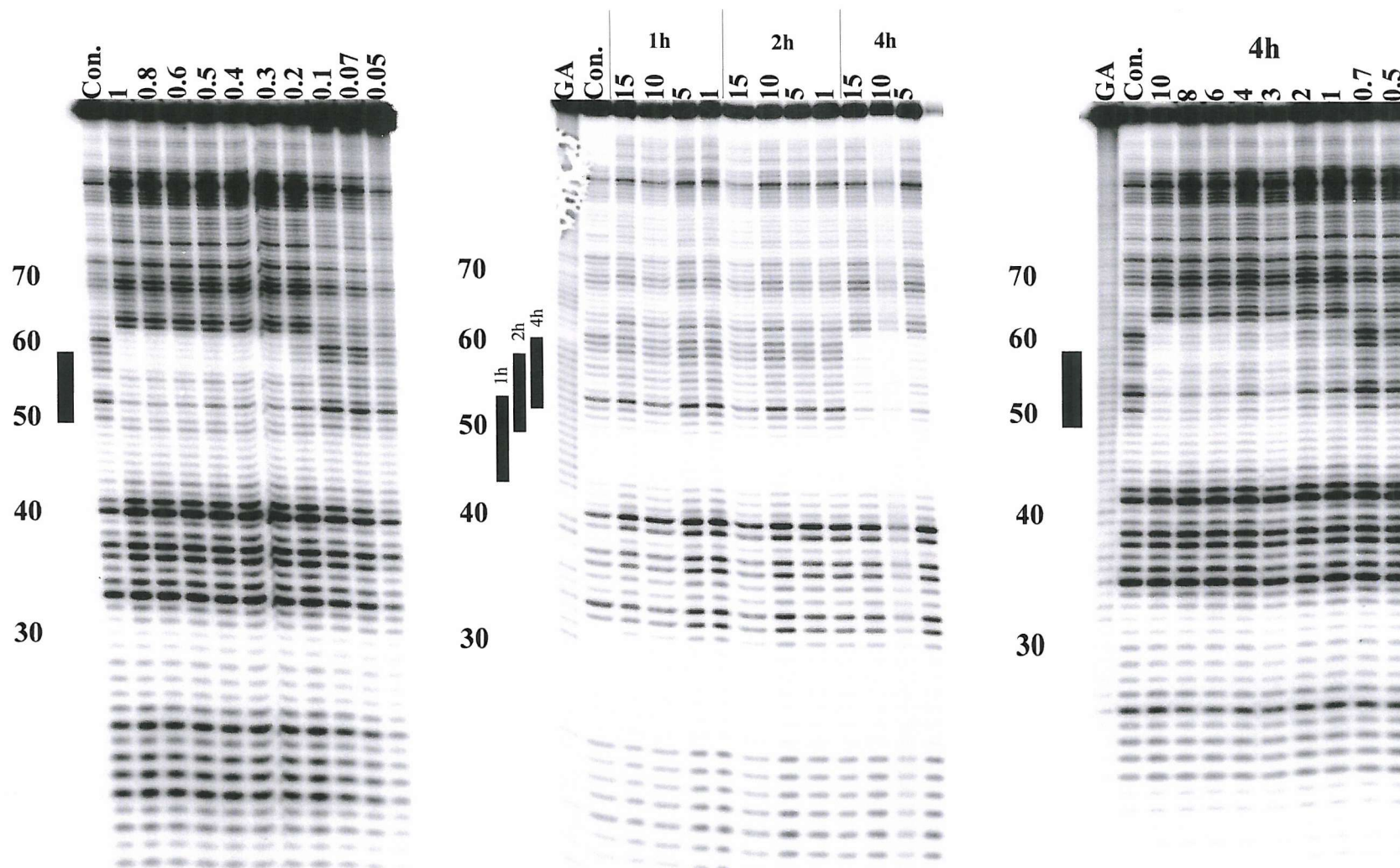
Figure 3.15: DNase I footprinting gels showing the effect of unmodified oligonucletide 5'TCCTTCTCT-3' (left hand panel), and 5-aminohexyl dC modified oligonucleotides (middle and right hand panels) on *Tyr*T(43-59) in 50 mM sodium acetate (pH 5), 10 mM MgCl₂. Oligonucleotide concentrations (μM) are shown at the top of the lanes. "GA" tracts are Maxam-Gilbert markers specific for purine residues. Lanes labelled Con. show the digestion pattern of *Tyr*T(43-59) in the absence of oligonucleotide. The solid rectangular boxes to the left of the gels indicate the 9-base pair triplex target sites, and the numbers designate the numbering scheme for the DNA sequence.
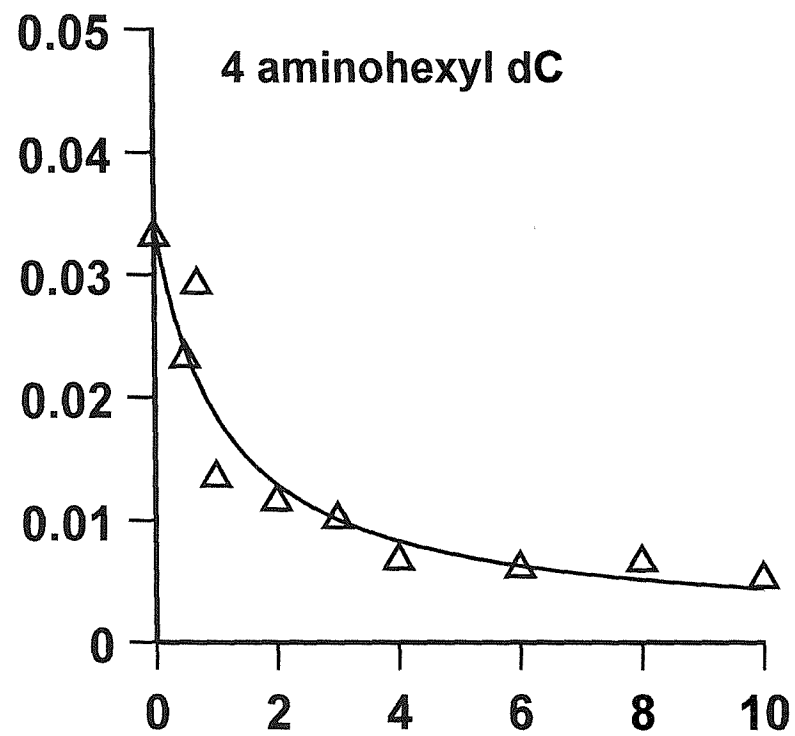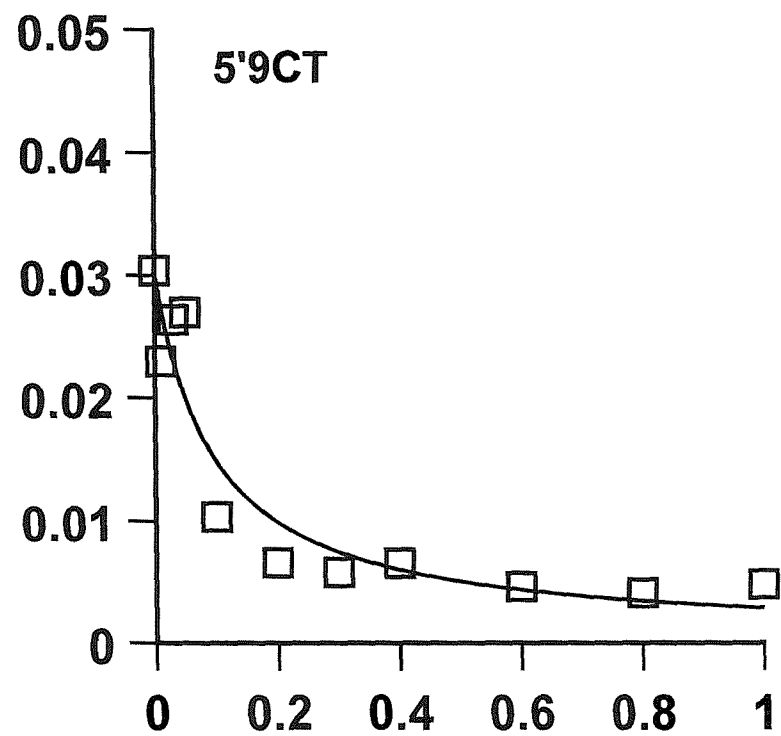
Figure 3.16: Footprinting plots generated with oligonucletides 5'9CT (left hand panel) and 4h (right hand panel) at pH 5. The ordinate represents relative band intensity (arbitary units) and the abscissa represents oligonucleotide concentration (µM). The symbols represent individual data points.

The left hand panel of Fig. 3.15 shows the DNase I digestion of *Tyr*T(43-59) in the presence of the unmodified oligonucleotide 5'-TCCTTCTCT-3' at pH 5. This oligonucleotide was designed to form a parallel triplex between positions 51 - 59. It can be seen that the oligonucleotide produces a footprint at concentrations of 0.08 µM and above between positions 51 - 62. Quantitative analysis of these data yielded a C_{50} value of 0.1 ± 0.03 µM (Fig.3.16).

The central panel of Fig. 3.15 shows the DNase I cleavage of *Tyr*T(43-59) in the presence of each of the aminohexyl dC modified oligonucleotides, performed at pH 5.0. these oligonucleotides were designed to interact with the DNA at different regions of the polypurine tract, as shown in Fig. 3.1. It can be seen that only one of the oligonucleotides, 5'-ThhTThThT-3' (4h) generates a footprint. This footprint can be seen between positions 51 - 61 and persists to an oligonucleotide concentration of less than 5 µM. Oligonucleotides 1h and 2h would have been expected to have bound to the duplex between positions 43 - 51, and 48 - 56 respectively. However there are no footprints in these regions, and no band enhancement at the 3' terminal regions of the postulated triplex sites. This demonstrates that both oligonucleotides do not form stable triplexes under these conditions.

The right hand panel of Fig. 3.15 shows the DNase I digestion of *Tyr*T(43-59) in the presence of oligonucleotide 4h over an expanded concentration range, measured at pH 5. It can be seen that a footprint is generated between positions 51 - 61 at oligonucleotide concentrations of 2 µM and above. Quantitative analysis yielded a C_{50} value of 1.2 ± 0.2 for the footprint (Fig. 3.16).

(3.9) Abasic Residues.

1'-2-H-dideoxyribose (Fig. 3.2) is an abasic nucleotide that has been demonstrated to skip pyrimidine bases within a purine tract, but results in low triplex stability (Horne & Dervan 1991). 1'-β-hexylamino deoxyribose and 1'-methoxy-2'-aminoethoxyribose are novel abasic analogues (Fig. 3.2) which were designed to improve the stability of binding across pyrimidine interruptions by incorporating amino groups
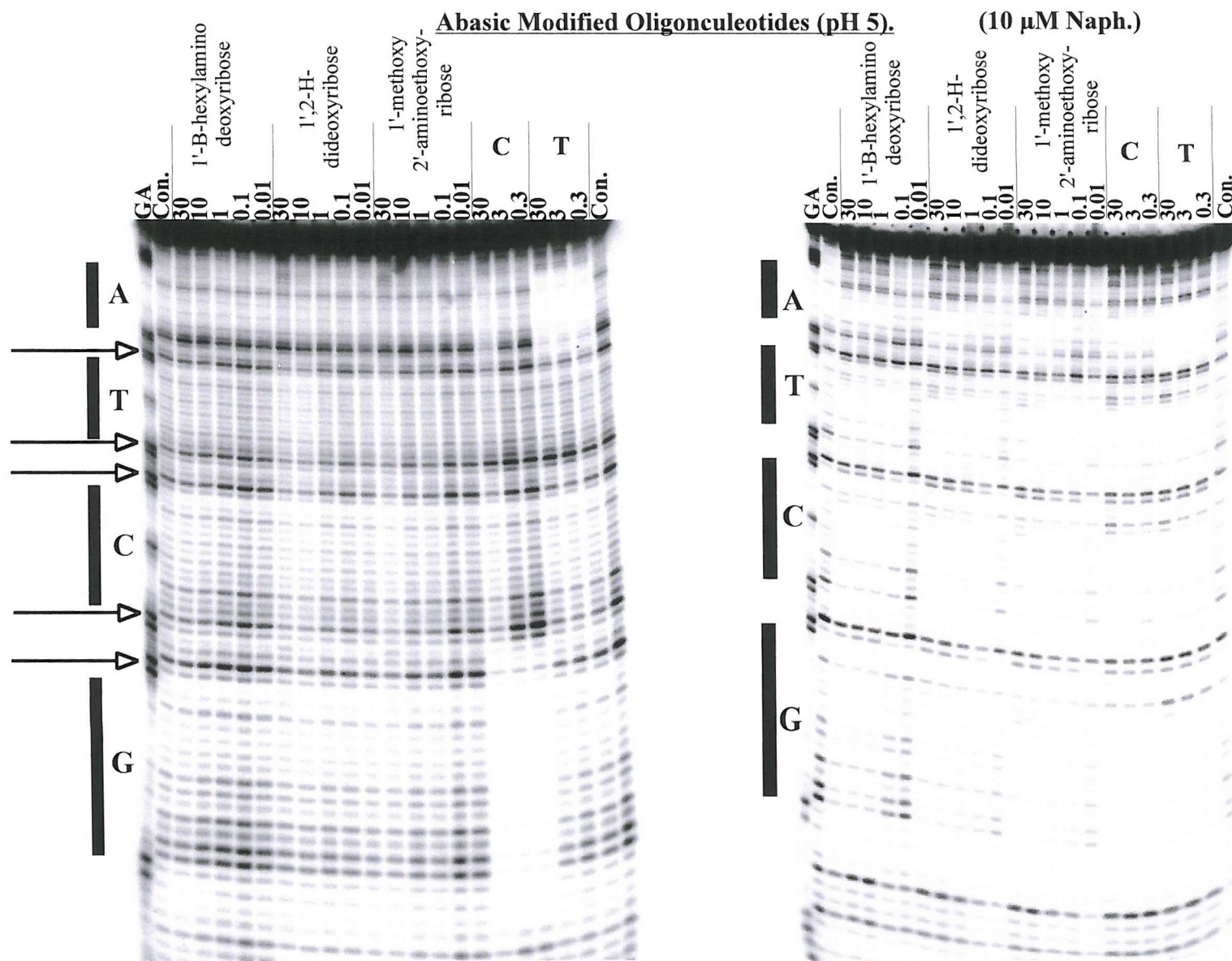
Figure 3.17: DNase I fooprinting gels showing the interactions of abasic modified oligonucleotides with RAD 1 radiolabelled on the pyrimidine strand. The left hand panel shows the results in 50 mM sodium acetate (pH 5.0), 10 mM MgCl₂, the right hand panel shows the results at pH 5.0 in the presence of 10 µM naphthylquinoline. Oligonucleotide concentrations (µM) are indicated at the top of the lanes. "GA" tracts are Maxam-Gilbert markers specific for purine residues. Lanes labelled Con. show the digestion in the absence of oligonucleotide. Lanes labeled C and T show the digestion pattern of perfect triplex formation. The individual letters to the left of each gel indicate the specific triplex target site. The solid rectangular boxes to the left of each gel shows the 4 triplex target sites, and the arrows indicate attenuation.

that can be protonated. Three oligonucleotides were prepared each containing one of these abasic sites at a single position 5'-TCTTCTXTTTCTT-3', where X indicates the position of the abasic site. These oligonucleotides were then targeted to a novel DNA fragment RAD1 which contained four thirteen base triplex target sites, each of which contained a different base at its centre (i.e. A, C, G, T, in turn) to which the abasic site containing oligonucleotides would be directed (Fig. 3.2). The RAD1 fragment was cloned into pUC18 as outlined in the Materials & Methods.

The left hand panel of Fig. 3.17 shows the results of footprinting experiments with the three oligonucleotides containing abasic derivatives and two perfectly matched oligonucleotides, performed at pH 5. The positions of the four target sites are illustrated by the solid rectangular boxes to the left of the gel, and the individual letters represent the central nucleotide to which the abasic residue is targeted. It can be seen that none of the abasic containing oligonucleotides generated a footprint at any of the target sites under these conditions. This should be compared with the clear footprints generated with the oligonucleotides 5'-TCTTCTCTTTCTT-3' and 5'-TCTTCTTTTTCTT-3', which were designed to form perfect triplexes at the target sites containing a central guanine and adenine respectively. These footprints are located only at the perfectly matched sites and persist to the lowest concentration used (0.3 µM), indicating strong site specific parallel triplex formation at the intended target sites. However it can be seen that the bands indicated with arrows are attenuated at oligonucleotide concentrations of 30 and 10 µM, containing 1',2-H-dideoxyribose and 1'-methoxy- 2'-aminoethoxyribose.

The right hand panel of Fig. 3.17 shows the DNase I cleavage of RAD1 in the presence of the abasic containing oligonucleotides together with 10 µM naphthylquinoline. Once again the perfectly matched oligonucleotides produce clear footprints at their expected target sites that persisted to the lowest concentration (0.3 µM). The abasic containing oligonucleotides again show no clear footprints at any of the four target sites. However all the abasic containing oligonucleotides cause some attenuation of DNase I cleavage at every target site, irrespective of the central base. This attenuated cleavage is evident at oligonucleotide concentrations above 0.01 µM.

Number of Base Substitutions	C_{50} Value (µM)	
	Enhancement	Footprint
2 5-propargylamino dU (pH 5)	7.9 ± 1.7	No Footprint
3 5-propargylamino dU (pH 5)	No Enhancement	No Footprint
4 5-propargylamino dU (pH 5)	7.3 ± 1.5	8.6 ± 3.8
2 2'-aminoethoxy T (pH 5)	19.1 ± 4.8	No Footprint
3 2'-aminoethoxy T (pH 5)	12.2 ± 4.0	No Footprint
4 2'-aminoethoxy T (pH 5)	13.5 ± 0.9	7.9 ± 1.2
3 2'-aminoethoxy-5-propargylamino U (pH 5)	/	2.2 ± 0.4
4 2'-aminoethoxy-5-propargylamino U (pH 5)	/	0.13 ± 0.03
3 2'-aminoethoxy-5-propargylamino U (pH 7.5)	/	25.8 ± 9.5
4 2'-aminoethoxy-5-propargylamino U (pH 7.5)	/	0.5 ± 0.1
5'-9CT (pH 5)	/	0.10 ± 0.03
4 aminohexyl dC (pH 5)	/	1.2 ± 0.2

Table 3.1: Presented are the C_{50} values for the partially substituted oligonucleotides used in this chapter. C_{50} values represent the oligonucleotide concentration required to diminish the level of band intensity within the triplex target site to 50% of that observed in the control. / indicates value not determined.

These results demonstrate that 1',2-H-dideoxyribose, 1'-β-hexylamino deoxyribose and 1'-methoxy-2'-aminoethoxyribose do not permit stable triplex formation in the absence of a triplex stabilising ligand. Furthermore the three abasic residues appear to be comparable with one another and demonstrate no sequence specificity.

(3.10) Discussion.

(3.10.1)   5-Propargylamino dU

The results of the footprinting experiments with the 5-propargylamino dU containing oligonucleotides 2^PU, 3^PU, and 4^PU demonstrate a relationship between the number of 5-propargylamino dU substitutions and the stability of triplex formation. Oligonucleotides substituted with two or three analogues failed to produce stable triplexes at pH 5.0, and the results are comparable to those obtained with the native oligonucleotide 5'-TTTTTTCTT-3'. However, both these oligonucleotides generated enhanced cleavage at the triplex-duplex junction, which demonstrates a weak interaction with the duplex target. The chemical integrity of these oligonucleotides was confirmed as both 2^PU, and 3^PU generated footprints in the presence of the triplex binding ligand naphthylquinoline (not shown). Oligonucleotide 4^PU produced a stable triplex at pH 5.0 as evidenced by the formation of a footprint with a C_{50} value of 7.3 ± 1.5 μM. The increase in the stability imparted by 4^PU over the native oligonucleotide, can be accounted for by the four protonated 5-propargylamino dU bases. Protonation is essential as similar experiments conducted at pH 7.5 did not produce a footprint with 4^PU and none of the oligonucleotides enhanced cleavage at position 43 (not shown). However this may also reflect the loss of protonation on the single cytosine residue. Attachment of the propargylamino side chain at position 5 of the base is believed to enhance triplex stability by positioning the positive charge of the amino group so as to interact with one of the phosphodiester strands of the triplex backbone, thereby decreasing charge repulsion. The relatively low stability afforded by the partially substituted oligonucleotides compared with the fully substituted TFOs (Bijapur *et al* 1999) may be due to the 5-propargylamino dU residues being separated from one another. It is postulated that the triplex stability

afforded by this analogue arises not only from the positioning of the amino group, but also from enhanced stacking interactions of the propargyl side chains. Therefore separating the groups, as in the partially substituted oligonucleotides, may limit these stacking interactions and may introduce unfavourable interactions.

Whilst this analogue can be seen to be an improvement over unmodified thymidine, its relatively poor stabilising properties when only partially substituted in an oligonucleotide, may limit its potential applications. Previous work has demonstrated that a fully substituted oligonucleotide, 5'-^{P}U^{P}U^{P}U^{P}U^{P}U^{P}UC^{P}UT-3', enhanced the stability of a triplex 1000-fold compared to 5'-TTTTTTCTT-3' (Bijapur *et al* 1999). These results demonstrate the benefit of using multiple substitutions with this analogue, in contrast to C$^+$·GC triplets. However it is possible that adjacent 5-propargylamino dU residues in a partially substituted oligonucleotide may produce greater triplex stabilisation than seen in the present studies for which modified bases were interspersed.

(3.10.2)   2'-Aminoethoxy T

Partial substitution of thymidine with 2'-aminoethoxy T produces results comparable to those seen with 5-propargylamino dU. Both 2^{AE}T, and 3^{AE}T failed to produce a footprint at the expected target site, but did enhance the 3' terminal band at position 43, as did 2^{P}U, and 3^{P}U. This enhancement demonstrates a weak interaction between the oligonucleotide and duplex DNA. However 4^{AE}T produced a footprint with a C_{50} value of 13.5 ± 0.9 μM, which is approximately 2-fold lower than that observed with 4^{P}U. 2'-aminoethoxy T has been reported to have a higher pKa than 5-propargylamino dU (Bloomers *et al* 1998, Cuenoud *et al* 1998), and therefore 2'-aminoethoxy T substituted oligonucleotides might have been expected to produce comparable results at both pH 5 and pH 7.5 but this is not supported by the DNase I results at pH 7.5 (Fig. 3.6) as no footprint or band enhancement was observed. The pKa of 2'-aminoethoxy T is high enough to permit the protonation of the amino group at pH 7.5, therefore this can not explain the decreased stability, and the lower stability is believed to reflect the loss of protonation of the single cytosine residue. 2'-aminoethoxy T has been reported to stabilise triplex formation when triplets are generated with AT base pairs, to a higher

degree than the natural nucleoside thymidine (Bloomer *et al* 1998, Cuenoud *et al* 1998). The results presented here support these findings, however as with 5-propargylamino dU, triplex formation is only detected when the oligonucleotide is heavily substituted (> 33%), while 2 and 3 substitutions within a 9mer produce only weak interactions. Furthermore incorporation of 4 ^{AE}T residues does not increase triplex stability enough to overcome the destabilising effect of a single un-protonated cytosine residue.

(3.10.3)   2'-Aminoethoxy-5-propargylamino U

The quantitative footprinting investigations with oligonucleotides 3^{AEP}U and 4^{AEP}U at pH 5.0 again shows a positive correlation between the triplex stability and the number of base substitutions within the 9mer oligonucleotide. Comparison of 3^{AEP}U and 4^{AEP}U, which differ by only one additional substitution of ^{AEP}U, show that they have C_{50} values of 2.2 ±0.5 μM and 0.1 ± 0.03 μM respectively (Table 3.1). This 10-fold difference in affinity must be due to the incorporation of the additional 2'-aminoethoxy-5-propargylamino dU base.

A comparison of the triplexes formed with 4^{P}U, 4^{AE}T and 4^{AEP}U, at pH 5.0, reveals significant differences between the analogues. Oligonucleotide 4^{P}U produced a footprint with a C_{50} value of 7.3 ± 1.5 μM, 4^{AE}T a C_{50} value of 13.5 ± 0.9 μM, whereas for 4^{AEP}U the C_{50} value was calculated to be 0.1 μM ± 0.03, which is a 50-fold increase in triplex stability over the 5-propargylamino dU modified oligonucleotide and a 100-fold increase over the 2'-aminoethoxy T modified oligonucleotide. Therefore the incorporation of both the sugar and base modifications within a single nucleotide results in the increased stability observed. This is further supported by the data obtained with 3^{P}U, 3^{AE}T, and 3^{AEP}U for which 3^{P}U and 3^{AE}T did not permit triplex formation but 3^{AEP}U generated a footprint with a C_{50} of 2.2 ± 0.4 μM. The experiments performed at pH 7.5 demonstrate that the sugar modification and propargylamino side chain jointly enable stable triplex formation at near physiological pH when incorporated into a 9mer third strand at three or more positions yielding a C_{50} value of 0.5 ± 0.1 μM for 4^{AEP}U and 25.8 ± 9.5 μM for 3^{AEP}U. The incorporation of the aminoethoxy moiety at the 2' position of ribose significantly improves the stabilising properties of 5-propargylamino dU, which is

thought to be due to the presence of a second amino group that can be protonated. Incorporation of 2'-aminoethoxy-5-propargylamino U enables triplex formation at pH 7.5 even though the oligonucleotide contained a single cytosine residue. This could be because triplex stability is sufficiently increased so that an un-protonated C·GC triplet can be tolerated. However, it is possible that the pKa of this isolated cytosine is raised above 7. The aminoethoxy group has a higher pKa than the propargylamino group, and this may enable stable triplex formation at pHs above 7.0. However the results presented in this chapter show that 2'-aminoethoxy T does not permit stable triplex formation at pH 7.5. The elevated pKa does not therefore fully explain the increased stability of 2'-aminoethoxy-5-propargylamino U. It is possible that the increased stabilising properties of the bis-modified nucleoside do not arise solely from the presence of an additional amino group, but that the two side chains increase favourable stacking and hydrophobic interactions. It has been demonstrated that the substituents are positioned so as to interact with different phosphate groups of the three phosphodiester backbones (unpublished data - Novartis).

It would have been interesting to investigate the effect of using 2'-aminoethoxy-5-propargylamino U at different positions within oligonucleotides, to investigate whether adjacent residues (improving the stacking interactions), and positioning away from cytosine residues, improve the stability of triplex formation. However thermal denaturation experiments presented in Chapter 5 demonstrate that adjacent residues do not increase triplex stability.

(3.10.4)   Antiparallel GT Triplex Formation

The investigations with oligonucleotides 9GGT and 17GGT demonstrate that incorporation of 5-propargylamino dU does not stabilise antiparallel GT triplex formation, as footprints were not observed in 50 mM sodium acetate (pH 5), 10 mM $MgCl_2$. Previous studies have demonstrated antiparallel triplex formation maybe inhibited by magnesium, and that manganese stabilises antiparallel triplex formation (Malkov *et al* 1993). The lack of any footprints within the target region in the presence of 10 mM $MnCl_2$ suggests that 5-propargylamnio dU destabilises antiparallel GT triplex

formation. This suggests that the analogue inhibits the binding of the oligonucleotide to DNA in an antiparallel orientation. These results demonstrate that 5-propargylamino dU can not be used to increase the stability of antiparallel GT triplex formation.

(3.10.5)   Parallel GT Triplex Formation

The investigations with the 9^{P}UGT oligonucleotide also showed that 5-propargylamino dU does not stabilise parallel GT containing triplexes. This result was not unexpected as G·GC constituted 44% of the triplets generated in this complex, and in general parallel GT triplexes are not very stable. However oligonucleotide 17G^{P}UT also failed to generate a stable parallel GT triplex. It was expected that this oligonucleotide should form a triplex containing a stretch of six uninterrupted 5-propargylamino dU bases, which might overcome the destabilising effect of the five G·GC triplets. However the results clearly demonstrate that triplex formation was prevented in all the oligonucleotide concentrations tested. This demonstrates that 5-propargylamino dU does not stabilise parallel GT triplex formation. This failure to stabilise parallel GT triplexes could be because, as noted with unmodified GT oligonucleotides there will be structural distortions at Gp^{P}U and ^{P}UpG steps, as G·GC and ^{P}U·AT triplets are not isostructural.

In general the results presented in this chapter indicate that 5-propargylamino dU can not be used to increase the stability of antiparallel or parallel GT triplexes. The partial substitution of parallel CT containing oligonucleotides with 5-propargylamino dU results in a weak stabilisation, which is related to the number of 5-propargylamino dU substitutions.

(3.10.6)   5-Aminopropyl dU & 5-Propynyl dU

5-Aminopropyl dU did not increase triplex stability when substituted into the oligonucleotide 5'-TT^{AP}UT^{AP}UTCTT-3' compared with that of 5'-TTTTTTCTT-3'. However addition of 10 μM naphthylquinoline produced an enhancement at position 43 which persisted to low oligonucleotide concentrations. A similar effect was seen with

5-propynyl dU

The results suggest that these two analogues do not significantly affect triplex stability. However 5-propargylamino dU is also ineffective when substituted into an oligonucleotide at only 2 positions. It therefore seems likely that a fully substituted oligonucleotide containing 5-aminopropyl dU will produce a stable triplex. Previous studies have shown that a fully substituted 5-propynyl dU oligonucleotide enhances triplex formation (Lacroix *et al* 1999). However it should be noted that both 2^PU, and 2^{AE}T generated band enhancement at the triplex-duplex boundary whereas 2^{AP}U and 2P did not. This demonstrates that 5-propargylamino dU, and 2'-aminoethoxy T are better analogues than 5-aminopropyl dU and 5-propynyl dU.

(3.10.7)   5-Aminohexyl dC

The results obtained for the aminohexyl modification of cytosine demonstrate that when the analogue was substituted into an oligonucleotide in two or three positions, it did not permit stable triplex formation at pH 5.0. However an oligonucleotide substituted at four positions did generate a DNase I footprint, though the stability of the triplex was approximately 10-fold lower than with the unmodified oligonucleotide. Thus it appears that the aminohexyl dC analogue decreases the stability of triplex formation. This may be because the chain length is not optimal for enabling the amino group to interact with the phosphodiester backbone. This distortion may lead to localised structural distortions at the point of substitution, and a decrease in base stacking, not only at the aminohexyl dC position but also adjacent triplets. An alternative explanation for the decreased stability could be that the attachment of the aminohexyl group has lowered the pKa value of the analogue below that of cytosine (pKa 5.5).

(3.10.8)   Abasic Residues

It can be seen that none of the abasic containing oligonucleotides generate a footprint in the absence of a triplex stabilising ligand. However oligonucleotides containing 1',2-H-dideoxyribose, and 1'-methoxy 2'-aminoethoxyribose attenuated several bands within different triplex target sites at a concentration above 10 μM. This attenuation demonstrates that the abasic modifications allow weak triplex formation, and that the specificity of triplex formation has been relaxed. The stronger attenuation observed with all oligonucleotides at every triplex target site in the presence of naphthylquinoline appears to occur to the same degree at every site, regardless of the pyrimidine or purine residue present at its centre. This indicates some interaction between the oligonucleotides and the target site DNA, demonstrating that the oligonucleotides may form unstable triplexes only in the presence of the naphthylquinoline triplex stabilising ligand. However this could result from the oligonucleotide binding to only half of the target site, either 5' or 3' to the abasic site, with the other 7 bases of the oligonucleotide free in solution. Furthermore this weak interaction occurs independently of the central base, with both pyrimidine and purine residues being targeted. Both the 1'-β-hexylamino deoxyribose and the 1'-methoxy-2'-aminoethoxyribose containing oligonucleotides appear to afford no increase in the stability of null site containing triplexes as compared to the 1',2-H-dideoxyribose containing oligonucleotide.

These results demonstrate that 1'-β-hexylamino deoxyribose, and 1'-methoxy-2'-aminoethoxyribose do not increase triplex stability across pyrimidine interruptions. This could be as a result of the modified groups attached to the sugar moiety not increasing the base stacking interactions around the null position above levels demonstrated with the 1',2-H-dideoxyribose. It further indicates that incorporation of the amino groups that have the potential to be protonated do not influence the stability of a null site. However, without detailed modelling studies it is not possible to assess whether the amino side chains are sufficiently long to interact with the phosphodiester backbone. It is possible that analogues with longer alkyl side chains may be better able to stabilise triplex formation across pyrimidine interruptions.

Chapter 4 - Results.

Triple Helical DNA Stabilising Ligands.

(4.1) Foreword

Several different classes of compounds have been shown to specifically interact with triple helical DNA, including benzopyridoindole derivatives (Mergny *et al* 1992), naphthylquinoline (Wilson *et al* 1993), and coralyne (Lee *et al* 1993), discussed in section 1.4.2. A common feature shared by all these compounds is that they are based around aromatic planar systems, which is postulated to enable the ligands to intercalate between base triplets.

This chapter uses quantitative DNase I footprinting to assess the potential of three proflavine derivatives; 4403, 4405, and 4406, and the two isomers of naphthoflavone as triplex stabilising ligands (Fig. 4.1). Four different oligonucleotides; M1, M2, M3, & M4, were used in these investigations and were targeted to different regions of a 25 base pair homopurine·homopyrimidine tract within the DNA sequence *Tyr*T(35-59) (Fig. 4.1). All experiments were conducted in 50 mM sodium acetate (pH 5.0), 10 mM $MgCl_2$, to protonate the cytosine residues within the third strands, and any pH sensitive groups within the ligands.

The *Tyr*T(35-59) sequence was previously made by mutating *Tyr*T(43-59) in nine places, to produce a 25 base pair polypurine tract which is GC rich at one end, and GC/AT mixed at the other (Keppler 1999). This novel fragment was generated to determine the sequence specificity of triplex binding ligands.

Oligonucleotide M1 was designed to form a triplex containing three pairs of adjacent C^+·GC triplets, each separated by T·AT (i.e repeats of CCT), whereas M2 was designed to form a triplex containing two adjacent T·AT triplets between the pairs of C^+·GC triplets. The M3 oligonucleotide should form a triplex with alternating C^+·GC and

(a) _TyrT(35-59)_

5'-CCCCCTCCTCCTTCCTTCTCTCTCT-3
3'-GGGGGAGGAGGAAGGAAGAGAGAGA-5

M1   3'-CCTCCTCCT-5'
M2   3'-CCTTCCTTC-5'
M3   3'-TCTCTCTCT-5
M4   3'-CTCTCTC-5'

(b)

Proflavine
4403

Proflavine
4405

Proflavine
4406

(c)
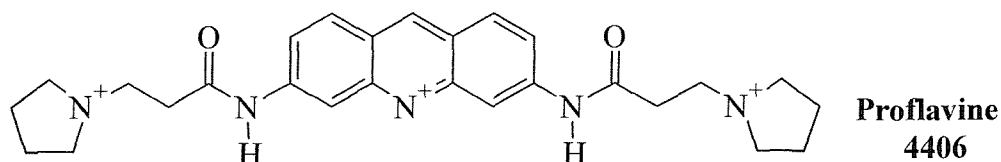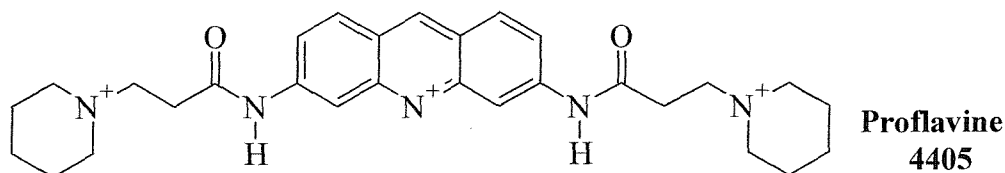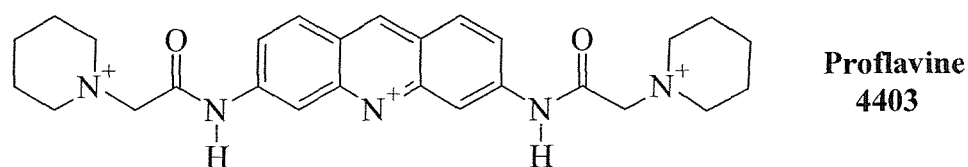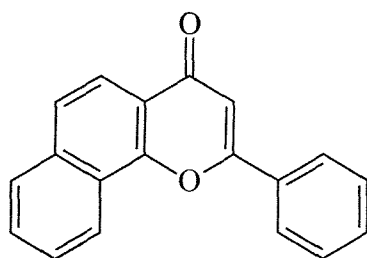
α-Naphthoflavone   β-Naphthoflavone
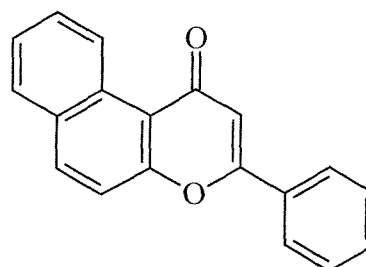
Figure 4.1: Diagram (a) illustrates the homopurine·homopyrimidine tract of _TyrT_(35-59) and the target sites for the M1 - M4 oligonucleotides. Diagrams (b) and (c) show the structures of the three proflavine derivatives and the two isomers of naphthoflavone respectively.

T·AT triplets, a combination which is believed to generate the most stable triplexes (Roberts & Crothers 1996). The oligonucleotide M4 was designed as a truncated version of M3 with the two terminal thymine residues removed, resulting into two terminal cytosine bases. Previous studies have demonstrated that oligonucleotides shorter than 9 bases in length form unstable triplexes (Moser & Dervan 1987), and that terminal C^+·GC triplets stabilise triplex formation (Asensio *et al* 1999). The sequence of the target DNA and the triplex forming oligonucleotides are presented in Fig. 4.1.

It has been suggested that several triplex binding ligands, including naphthylquinoline, coralyne, and BePI bind selectively to T·AT triplets. This selectivity is thought to arise from repulsions between the C^+·GC triplets and the positively charged intercalating ligand. Therefore a ligand demonstrating a specificity towards TpT sequences would be expected to enhance the stability of a triplex generated with the M2 oligonucleotide. While naphthylquinoline is selective for T·AT triplets, anthraquinones show less sequence selectivity, presumably because they possess an uncharged chromophore (Keppler *et al* 1999a). Since the proflavine ring bears positive charges we anticipate that ligands 4403, 4405, and 4406 (Fig. 4.1) will be selective for T·AT triplets, whereas both of the naphthoflavone isomers (Fig. 4.1) are not protonated, and should therefore show less sequence selectivity.

(4.2) Alpha and Beta Naphthoflavone.

The α and β isomers of naphthoflavone (Fig. 4.1) were purchased from Sigma-Aldrich. The triplex stabilising properties of naphthoflavone was reported by Prof. J. B. Chaires at NACON V (unpublished data). α-naphthoflavone has been shown to activate phenacetin O-deethylase by activating cytochrome P-450 (3A4) in human liver microsomes (Nakajima *et al* 1999). This ligand therefore inhibits cytochrome P-450 (1A2) function (Newton *et al* 1995, Daniel *et al* 1999, Nakajima *et al* 1999). β-naphthoflavone has been classified as a potential teratogen, and therefore its potential clinical applications are limited.

Initial footprinting investigations with these oligonucleotides were conducted in the absence of any stabilising ligand, so as to ascertain the triplex stability prior to the addition of ligand.

(4.2.1)   Oligonucleotide M2

The left hand panel of Fig. 4.2 shows the DNase I digestion of oligonucleotide M2 with *Tyr*T(35-59) at pH 5. The oligonucleotide, (5'-CTTCCTTCC-3') was designed to bind to the DNA sequence *Tyr*T(35-59) between positions 44 - 52, and footprint can be seen between positions 45 - 55 persisting to an oligonucleotide concentration of approximately 1 μM. Quantitative analysis of this footprint (Fig. 4.5) yielded a C_{50} value of 1.0 ± 0.3 μM for the interaction of M2 with its target site in the absence of ligand.

The central panel of Fig. 4.2 shows DNase I cleavage of *Tyr*T(35-59) at pH 5 in the presence of varying concentrations of M2 together with 10 μM α-naphthoflavone. A clear footprint can be seen between positions 45 - 55, in which the intensity of the bands returns to the level in the control by 0.1 μM. Furthermore bands at positions 43 and 44 show enhanced cleavage which persists to an oligonucleotide concentration of about 0.3 μM. Quantitative analysis of the footprint revealed that oligonucleotide M2, with 10 μM α-naphthoflavone, generated a triplex with a C_{50} value of 0.6 ± 0.1 μM (Fig. 4.5), a slight increase in affinity relative to that in the absence of ligand.

The right hand panel of Fig. 4.2 shows DNase I cleavage of *Tyr*T(35-59) performed at pH 5 in the presence of varying concentrations of M2 together with 10 μM β-naphthoflavone. A footprint can be seen between positions 45 - 55, but only at relatively high oligonucleotide concentrations (10 μM). At oligonucleotide concentrations between 8 - 2 μM bands within the target site are attenuated returning to that seen in the control by approximately 1 μM. Enhanced cleavage can also be observed at positions 44 and 43, located at the 3' terminal of the footprint site, that remains above the level seen in the control down to an oligonucleotide concentration of about 0.7 μM. Quantitative analysis of the footprint yielded a C_{50} value of 1.7 ± 0.6 μM (Fig. 4.5) for

Figure 4.2: DNase I footprints illustrating the binding of the oligonucleotide 5'-CTTCCTTCC-3' (M2) to *Tyr*T(35-59). The left hand panel shows the result at pH 5 in the absence of ligand. The central panel shows the result with 10 µM alpha naphthoflavone at pH 5. The right hand panel shows the result with 10 µM beta naphthoflavone at pH 5. Oligonucleotide concentrations (µM) are indicated at the top of the lanes. "GA" tracts are Maxam-Gilbert markers specific for purine residues. Lanes labelled Con. show the digestion pattern in the absence of oligonucleotide. The solid rectangular boxes to the left of the gels indicate the triplex target site. The numbers to the left of the gels indicate the sequence numbering scheme.

the interaction of M2 in the presence of 10 μM β-naphthoflavone.

(4.2.2)   Oligonucleotide M3

The left hand panel of Fig. 4.3 shows DNase I cleavage of *Tyr*T(35-59) in the presence of varying concentrations of oligonucleotide M3, performed at pH 5. Oligonucleotide 5'-TCTCTCTCT-3' (M3) was designed to bind to this sequence between positions 50 - 59. A clear footprint can be seen between positions 51 - 61, that persists to an oligonucleotide concentration of about 0.2 μM. The band at position 50, located at the 3' terminal of the footprint is enhanced above the level seen in the control. This enhancement persists to an oligonucleotide concentration of about 0.1 μM. Quantitative analysis of the footprint yielded a C_{50} value of 0.1 $\pm$ 0.04 μM (Fig. 4.5).

The central panel of Fig. 4.3 shows DNase I digestion of *Tyr*T(35-59) in the presence of a varying concentration of M3 with 10 μM α-naphthoflavone, performed at pH 5. A footprint can be seen between positions 51 - 61, which persists to an oligonucleotide concentration of approximately 0.05 μM. Furthermore the band at position 50 shows enhanced cleavage that remains above the level in the control even at the lowest oligonucleotide concentration. Quantitative analysis of the intensity of the bands in the footprint revealed that M3 produced a triplex with a C_{50} value of 0.06 $\pm$ 0.01 μM in the presence of 10 μM α-naphthoflavone (Fig. 4.5).

The right hand panel of Fig. 4.3 shows DNase I cleavage of *Tyr*T(35-59) in the presence of varying concentrations of oligonucleotide M3 with 10 μM β-naphthoflavone, performed at pH 5. It can be seen that oligonucleotide concentrations above 0.6 μM produced attenuated cleavage of the bands between positions 51 - 61. The band at position 50 is also enhanced above the level in the control at oligonucleotide concentrations above 0.6 μM. Quantitative analysis of the intensity of the bands within the footprint revealed that M3 generated a triplex with a C_{50} value of 0.6 $\pm$ 0.3 μM in the presence of 10 μM β-naphthoflavone (Fig. 4.5).

Figure 4.3: DNase I footprints showing the interaction of oligonucleotide 5'-TCTCTCTCT-3' (M3) with *Tyr*T(35-59). The left hand panel shows the result at pH 5 in the absence of ligand. The central panel shows the result with 10 μM alpha naphthoflavone at pH 5. The right hand panel shows the result with 10 μM beta naphthoflavone at pH 5. Oligonucleotide concentrations (μM) are indicated at the top of the lanes. "GA" tracts are Maxam-Gilbert markers specific for purine residues. Lanes labelled Con. show the digestion pattern in the absence of oligonucleotide. The solid rectangular boxes to the left of the gels indicate the triplex target sites, and the numbers designate the sequence numbering scheme.

(4.2.3)   Oligonucleotide M4

The left hand panel of Fig. 4.4 shows DNase I cleavage of *Tyr*T(35-59) in the presence of varying concentrations of M4, performed at pH 5.0. The 7-mer oligonucleotide, 5'-CTCTCTC-3' (M4), was designed to bind between positions 52 - 58. A footprint can be seen between positions 53 - 61, in which the bands are attenuated, persisting to an oligonucleotide concentration of about 2 µM. The intensity of the band at position 52, located at the base of the footprint, is also enhanced above the level in the control, and remains so to an oligonucleotide concentration of about 0.8 µM. Quantitative analysis of the bands within the footprint revealed that M4 generated a triplex with a C_{50} value of 1.8 ± 0.8 µM (Fig. 4.5).

The central panel of Fig. 4.4 shows DNase I digestion of *Tyr*T(35-59) in the presence of varying concentrations of M4 with 10 µM α-naphthoflavone, performed at pH 5. A footprint can be seen between positions 53 - 61 in which bands are attenuated to an oligonucleotide concentration of about 1.0 µM. The band at position 52 is also enhanced at oligonucleotide concentrations of 1 µM and above. Quantitative analysis of the bands within the footprint yielded a C_{50} value of 0.7 ± 0.1 µM for M4 in the presence of 10 µM α-naphthoflavone (Fig. 4.5).

The right hand panel of Fig. 4.4 shows DNase I cleavage of *Tyr*T(35-59) in the presence of varying concentrations of M4 with 10 µM β-naphthoflavone, performed at pH 5. A footprint can be seen between position 53 - 61 that persists to an oligonucleotide concentration of approximately 2 µM. (The lane corresponding to an oligonucleotide concentration of 6 µM does not show any band attenuation; this is believed to be an error and has been excluded from the analysis). Quantitative analysis of the footprint revealed that oligonucleotide M4 generates a triplex with a C_{50} value of 2.9 ± 0.7 µM in the presence of 10 µM β-naphthoflavone (Fig. 4.5).
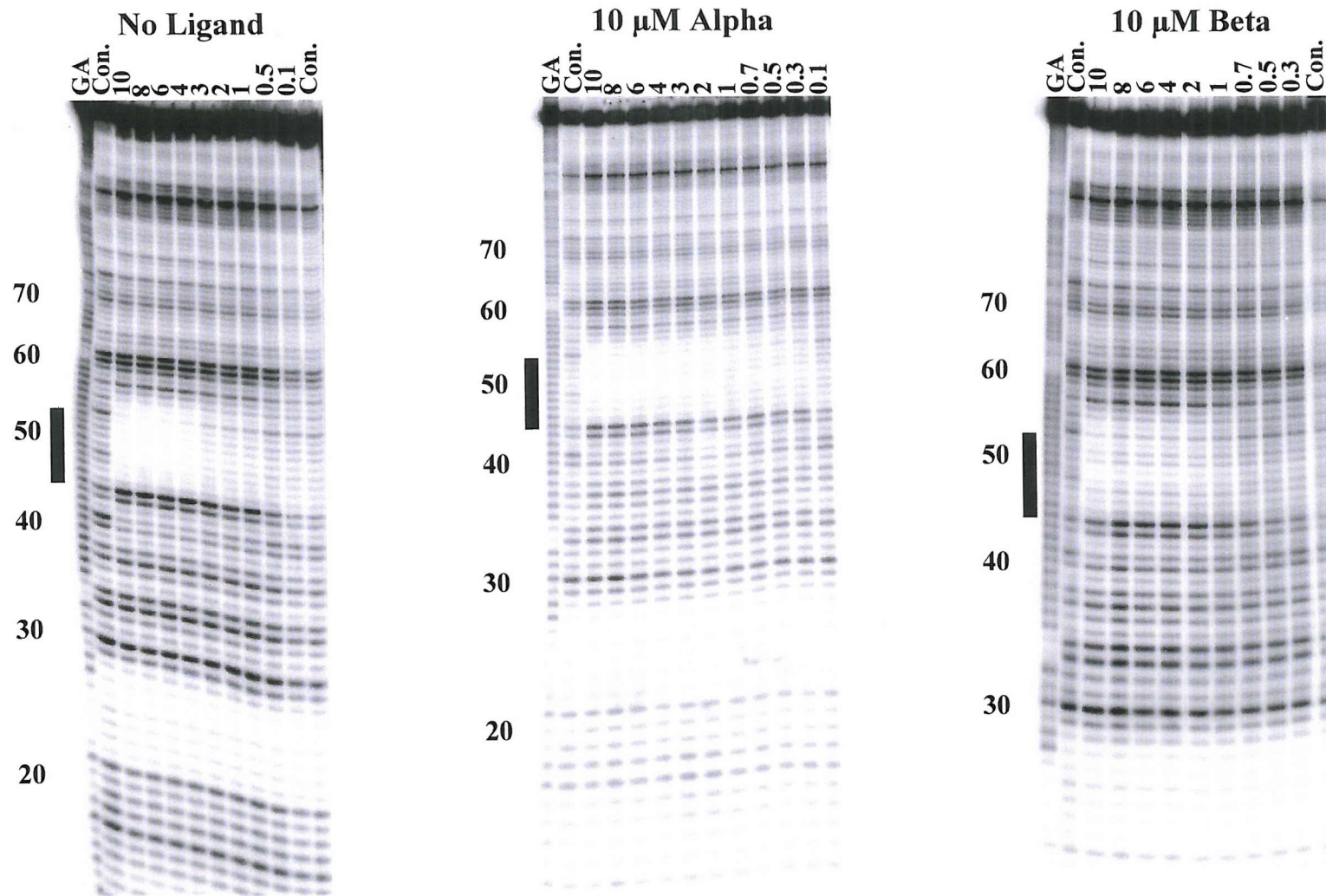
Figure 4.4: DNase I footprints showing the interaction of oligonucleotide 5'-CTCTCTC-3' (M4) with *Tyr*T(35-59). The left hand panel shows the result at pH 5 in the absence of ligand. The central panel shows the result with 10 µM alpha naphthoflavone at pH 5. The right hand panel shows the result with 10 µM beta naphthoflavone at pH 5. Oligonucleotide concentrations (µM) are indicated at the top of the lanes. "GA" tracts are Maxam-Gilbert markers specific for purine residues. Lanes labelled Con. show the digestion pattern in the absence of oligonucleotide. The solid rectangular boxes to the left of the gels indicate the triplex target sites, and the numbers designate the sequence numbering scheme.

Figure 4.5: Footprinting plots for the interaction of oligonucleotides M2, M3, and M4 with their target sites in TyrT(35-59) The black line corresponds to the absence of ligand while the red and blue lines are in the presence of 10 μM alpha and beta naphthoflavone respectively. The abscissa represents oligonucleotide concentration (μM), and the ordinate relative band intensity (arbitary units).

In summary the results presented above demonstrate that α-naphthoflavone stabilises M2, M3, and M4, but β-naphthoflavone has no stabilising effect, and may destabilise the triplexes.

(4.3)   Proflavine Derivatives 4403, 4405, & 4406.

The proflavine derivatives 4403, 4405, and 4406 (Fig 4.1) were provided by Prof. T. Jenkins. Compound 4403 and 4405 possess piperazine groups at positions 3 and 6 of the proflavine ring system, attached with different length linkers. Compound 4406 is similar to 4405 but possess pyrrolidine groups attached to positions 3 and 6 via linkers.

(4.3.1)   Oligonucleotide M1.

The left hand panel of Fig. 4.6 shows DNase I digestion of *Tyr*T(35-59) in the presence of varying concentrations of M1, performed at pH 5. This oligonucleotide was designed to bind to the *Tyr*T(35-59) sequence between positions 38 - 46. A clear footprint can be seen between positions 39 - 48 that persists to an oligonucleotide concentration of approximately 1 μM. In addition two bands at positions 37 & 38 showed enhanced cleavage in the presence of the oligonucleotide. Quantitative analysis of the footprint revealed that the oligonucleotide generated a triplex with a C_{50} value of 1.9 ± 0.5 μM (Fig. 4.7).

The right hand panel of Fig. 4.6 shows DNase I digestion of *Tyr*T(35-59) in the presence of varying concentrations of M1 with 10 μM 4403, performed at pH 5. A footprint can be seen between positions 39 - 49 that persists to an oligonucleotide concentration of about 1 μM. Quantitative analysis of this footprint revealed that oligonucleotide M1 generated a triplex with a C_{50} value of 1.8 ± 0.2 μM in the presence of 10 μM 4403 (Fig. 4.7).
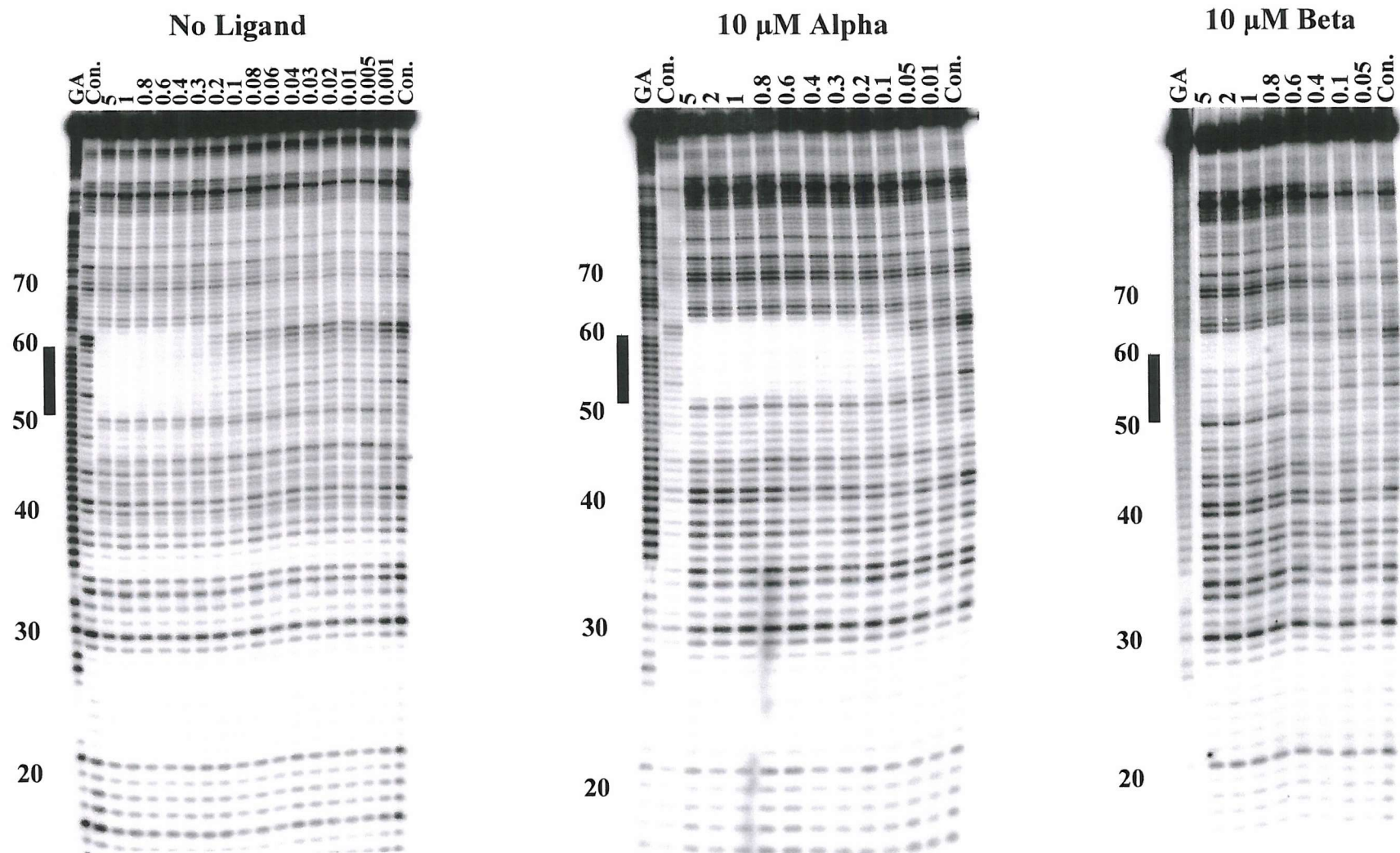
Figure 4.6: DNase I footprints showing the interaction of oligonucleotide 5'-CCTCCTCCT-3' (M1) with *Tyr*T(35-59). The left hand panel shows the result at pH 5 in the absence of ligand. The right hand panel shows the result with 10 µM proflavine derivative 4403 at pH 5. Oligonucleotide concentrations (µM) are indicated at the top of the lanes. "GA" tracts are Maxam-Gilbert markers specific for purine residues. Lanes labelled Con. show the digestion pattern in the absence of oligonucleotide. The solid rectangular boxes to the left of the gels indicate the triplex target sites, and the numbers designate the sequence numbering scheme.
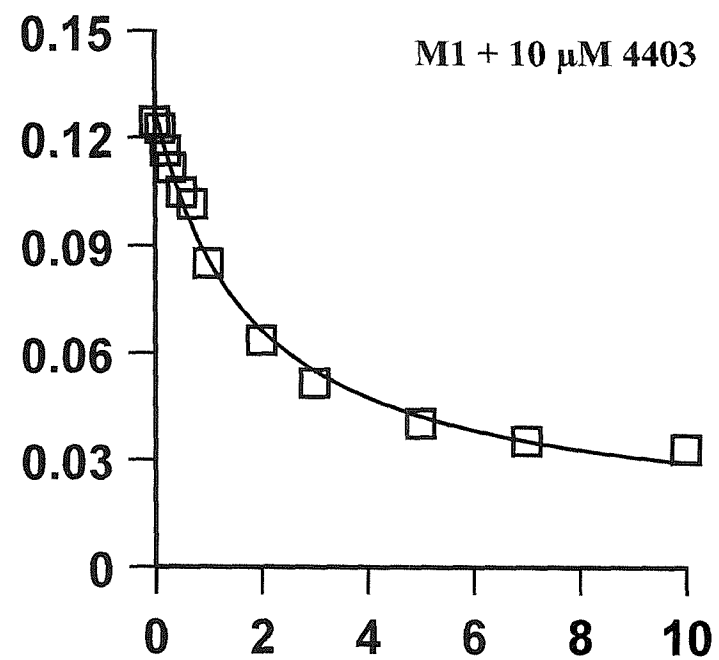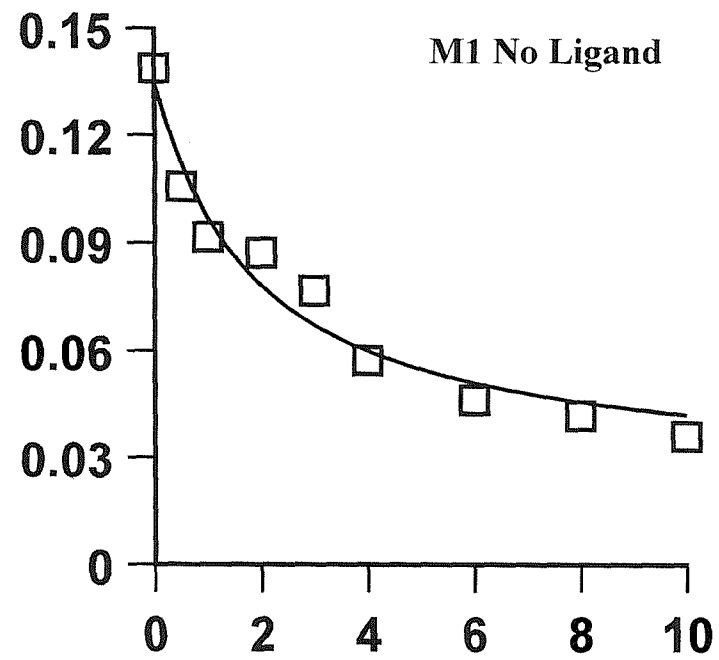
Figure 4.7: Footprinting plots for the interaction of oligonucleotide M1 with its target site. The left hand panel corresponds to oligonucleotide alone, while the right hand panel is in the presence of 10 μM 4403. The abscissa represents oligonucleotide concentration (μM) and the ordinate represents relative band intensity (arbitary units).

(4.3.2)   Oligonucleotide M2.

The left hand panel of Fig. 4.8 shows DNase I digestion of *Tyr*T(35-59) in the presence of M2 with 10 μM proflavine 4403, performed at pH 5. A footprint can be seen between positions 45 - 55, that persists to an oligonucleotide concentration of about 0.2 μM. The intensity of the band at position 44 is enhanced above the level in the control, and this enhancement persists to an oligonucleotide concentration of about 0.05 μM. Quantitative analysis of the bands within the footprint revealed that oligonucleotide M2 generates a triplex with a C_{50} value of 0.2 ± 0.07 μM in the presence of 10 μM 4403 (Fig. 4.9).

The central panel of Fig. 4.8 shows DNase I digestion of *Tyr*T(35-59) in the presence of varying concentrations of M2 with 10 μM proflavine 4405, performed at pH 5. A footprint can be distinguished between positions 45 - 55, that persists to an oligonucleotide concentration of about 0.8 μM. Quantitative analysis of this footprint demonstrated that oligonucleotide M2 generates a triplex with a C_{50} value of 0.7 ± 0.2 μM in the presence of 10 μM 4405 (Fig. 4.9).

The right hand panel of Fig. 4.8 shows DNase I digestion of *Tyr*T(35-59) in the presence of varying concentrations of M2 with 10 μM proflavine 4406, performed at pH 5. A footprint can be seen between positions 45 - 55, that persists to an oligonucleotide concentration of about 1 μM. The intensity of the band at position 44 is also enhanced above the level in the control, down to an oligonucleotide concentration of about 0.6 μM. Quantitative analysis of the bands within the footprint revealed that oligonucleotide M2 generates a triplex with a C_{50} value of 1.2 ± 0.3 μM in the presence of 10 μM 4406 (Fig. 4.9).
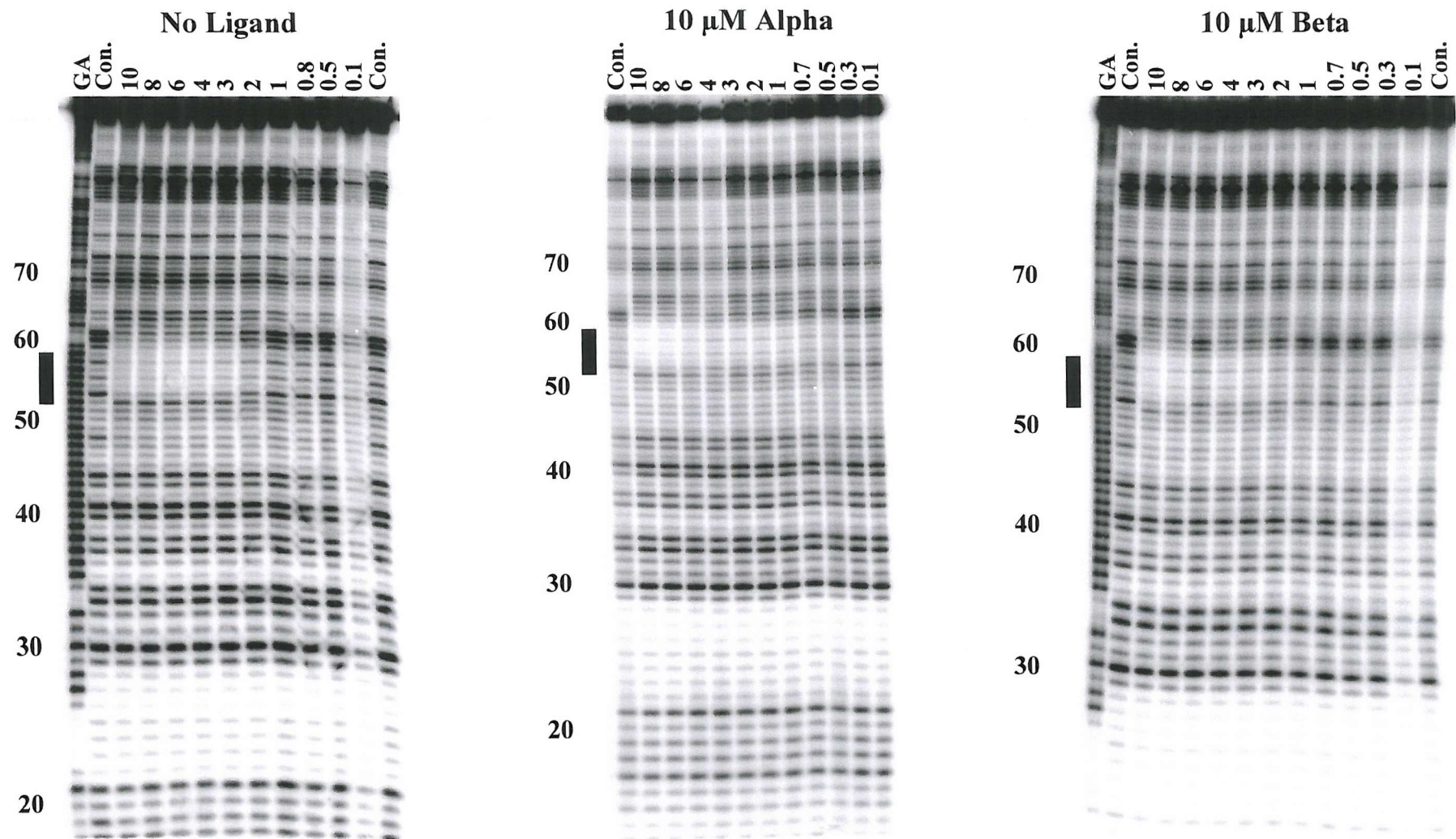
Figure 4.8: DNase I footprints showing the interaction of oligonucleotide 5'-CTTCCTTCC-3' (M2) with *Tyr*T(35-59). The left hand panel shows the result with 10 µM proflavine derivative 4403 at pH 5. The central panel shows the result with 10 µM proflavine derivative 4405 at pH 5. The right hand panel shows the result with 10 µM proflavine derivative 4406 at pH 5. Oligonucleotide concentrations (µM) are indicated at the top of the lanes. "GA" tracts are Maxam-Gilbert markers specific for purine residues. Lanes labelled Con. show the digestion pattern in the absence of oligonucleotide. The solid rectangular boxes to the left of each gel indicate the triplex target site, and the numbers designate the sequence numbering scheme.

Figure 4.9: Footprinting plots showing the interaction of oligonucleotide M2 with its target site in the presence and absence of proflavine derivatives 4403, 4405, and 4406. The abscissa represents oligonucleotide concentration (μM) and the ordinate represents relative band intensity (arbitary units).

(4.3.3)   Oligonucleotide M3

The left hand panel of Fig 4.10 shows DNase I cleavage of *Tyr*T(35-59) in the presence of varying concentrations of M3 with 10 μM proflavine 4403, performed at pH 5. A footprint can be seen between positions 51 - 61 that persists to an oligonucleotide concentration of about 0.03 μM. The band at position 50 is also enhanced above the level in the control; this enhancement persists to an oligonucleotide concentration of about 0.08 μM. Quantitative analysis of the footprint yielded a C_{50} value of 0.08 ± 0.01 μM for oligonucleotide M3 in the presence of 10 μM 4403 (Fig. 4.11).

The central panel of Fig 4.10 shows DNase I cleavage of *Tyr*T(35-59) in the presence of M3 with 10 μM proflavine 4405, performed at pH 5. A footprint can be seen between positions 51 - 61 that persists to an oligonucleotide concentration of about 0.5 μM. The band at position 50 is enhanced above the level in the control at oligonucleotide concentrations above 0.5 μM. Quantitative analysis of the bands within the footprint reveals that oligonucleotide M3 generates a triplex with a C_{50} value of 0.4 ± 0.1 μM in the presence of 10 μM 4405 (Fig. 4.11).

The right hand panel of Fig 4.10 shows DNase I cleavage of *Tyr*T(35-59) in the presence of varying concentrations of M3 with 10 μM proflavine 4406, performed at pH 5. A footprint can be seen between positions 51 - 61 that persists to an oligonucleotide concentration of about 0.5 μM. The band at position 50 is enhanced above the level in the control at oligonucleotide concentrations above 0.5 μM. Quantitative analysis of the bands within the footprint reveals that oligonucleotide M3 generates a triplex with a C_{50} value of 0.7 ± 0.1 μM in the presence of 10 μM 4406 (Fig. 4.11).
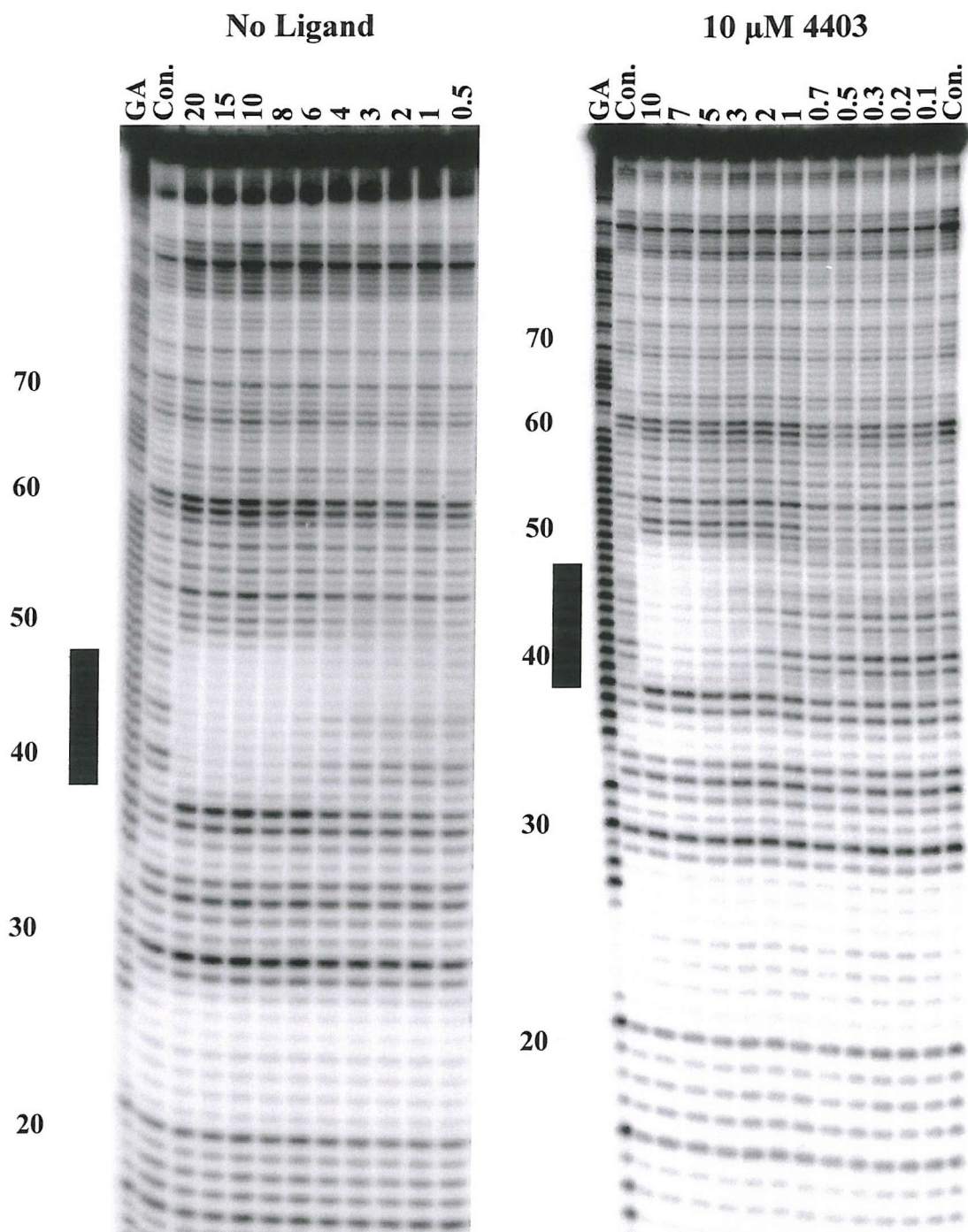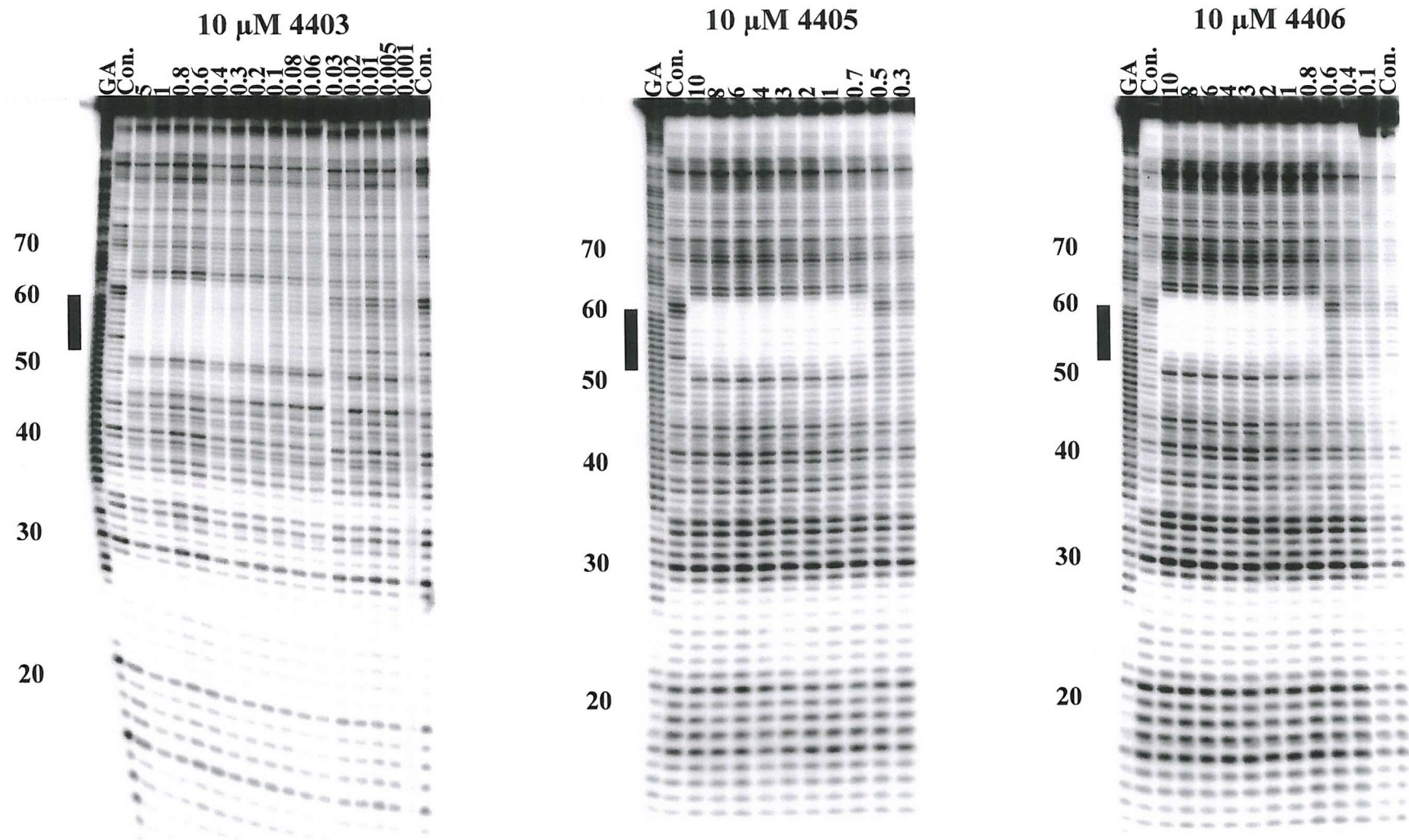
Figure 4.10: DNase I footprints showing the interaction of oligonucleotide 5'-TCTCTCTCT-3' (M3) with *Tyr*T(35-59). The left hand panel shows the result with 10 μM proflavine derivative 4403 at pH 5. The central panel shows the result with proflavine derivative 4405 at pH 5. The right hand panel shows the result with 10 μM proflavine derivative 4406 at pH 5. Oligonucleotide concentrations (μM) are indicated at the top of the lanes. "GA" tracts are Maxam-Gilbert markers specific for purine residues. Lanes labelled Con. show the digestion pattern in the absence of oligonucleotide. The solid rectangular boxes to the left of the gels indicate the triplex target sites, and the numbers designate the sequence numbering scheme.
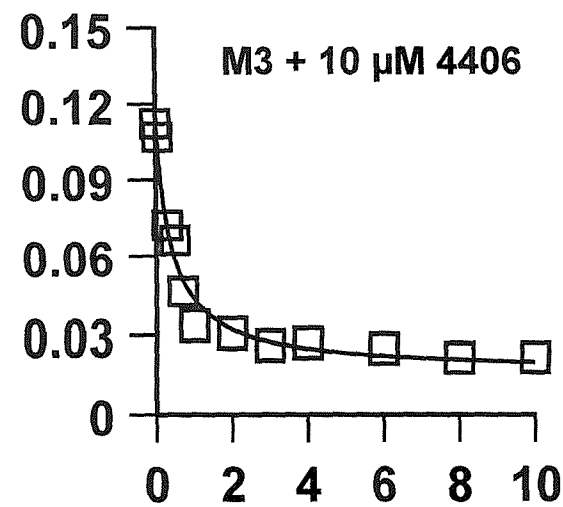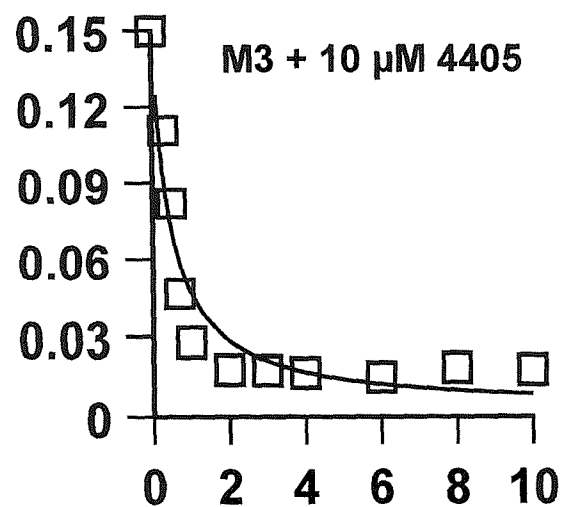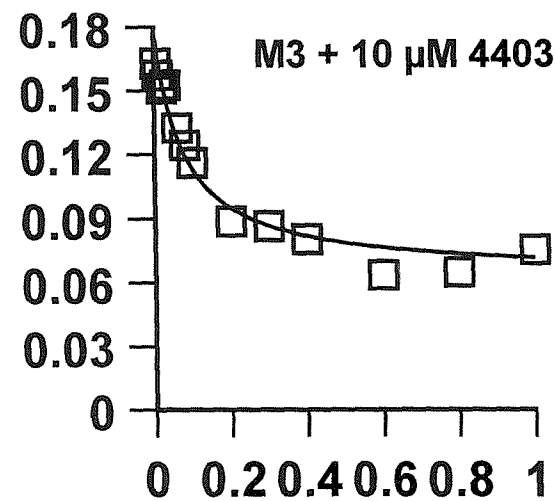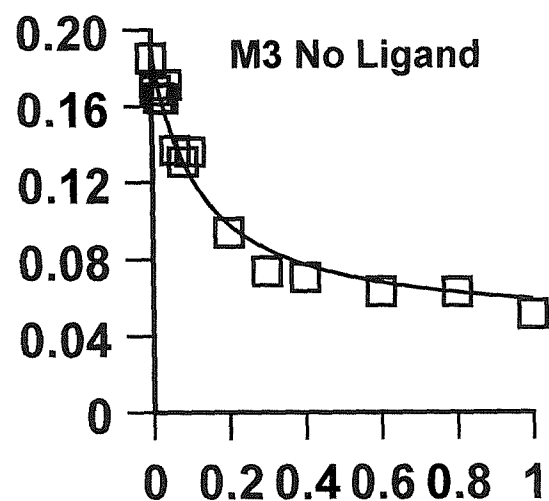
Figure 4.11: Footprinting plots showing the interaction of oligonucleotide M3 with its target site in the absence and presence of 10 μM proflavine derivatives 4403, 4405, and 4406. The abscissa represents oligonucleotide concentration (μM), and the ordinate represents relative band intensity (arbitary units).

(4.3.4) **Oligonucleotide M4**

The left hand panel of Fig 4.12 shows DNase I digestion of *Tyr*T(35-59) in the presence of varying concentrations of M4 with 10 μM proflavine 4403, performed at pH 5. A footprint can be seen between positions 53 - 61, that persists to an oligonucleotide concentration of about 0.6 μM. The band at the 3' terminal of the footprint (position 52) is enhanced, and remains so down to an oligonucleotide concentration of about 0.6 μM. Quantitative analysis of the bands within the footprint reveals that oligonucleotide M4 generates a triplex in the presence of 10 μM 4403 with a C_{50} value of 1.6 ± 0.4 μM (Fig. 4.13).

The central panel of Fig 4.12 shows DNase I digestion of *Tyr*T(35-59) in the presence of varying concentrations of M4 with 10 μM proflavine 4405, performed at pH 5. A footprint can be seen between positions 53 - 61, that persists to an oligonucleotide concentration of about 1 μM. The band at the 3' terminal of the footprint (position 52) is enhanced, and remains so down to an oligonucleotide concentration of about 2 μM. Quantitative analysis of the footprint yielded a C_{50} value of 1.4 ± 0.4 μM for M4 in the presence of 10 μM 4405 (Fig. 4.13).

The right hand panel of Fig 4.12 shows DNase I digestion of *Tyr*T(35-59) in the presence of M4 with 10 μM proflavine 4406, performed at pH 5. A footprint can be seen between positions 53 - 61, that persists to an oligonucleotide concentration of about 2 μM. Quantitative data analysis of the bands within the footprint reveals that oligonucleotide M4 generates a C_{50} value of 4.9 ± 0.8 μM in the presence of 10 μM 4406 (Fig. 4.13).

All the C_{50} values derived from the footprinting experiments in this chapter are presented in Table 4.1.
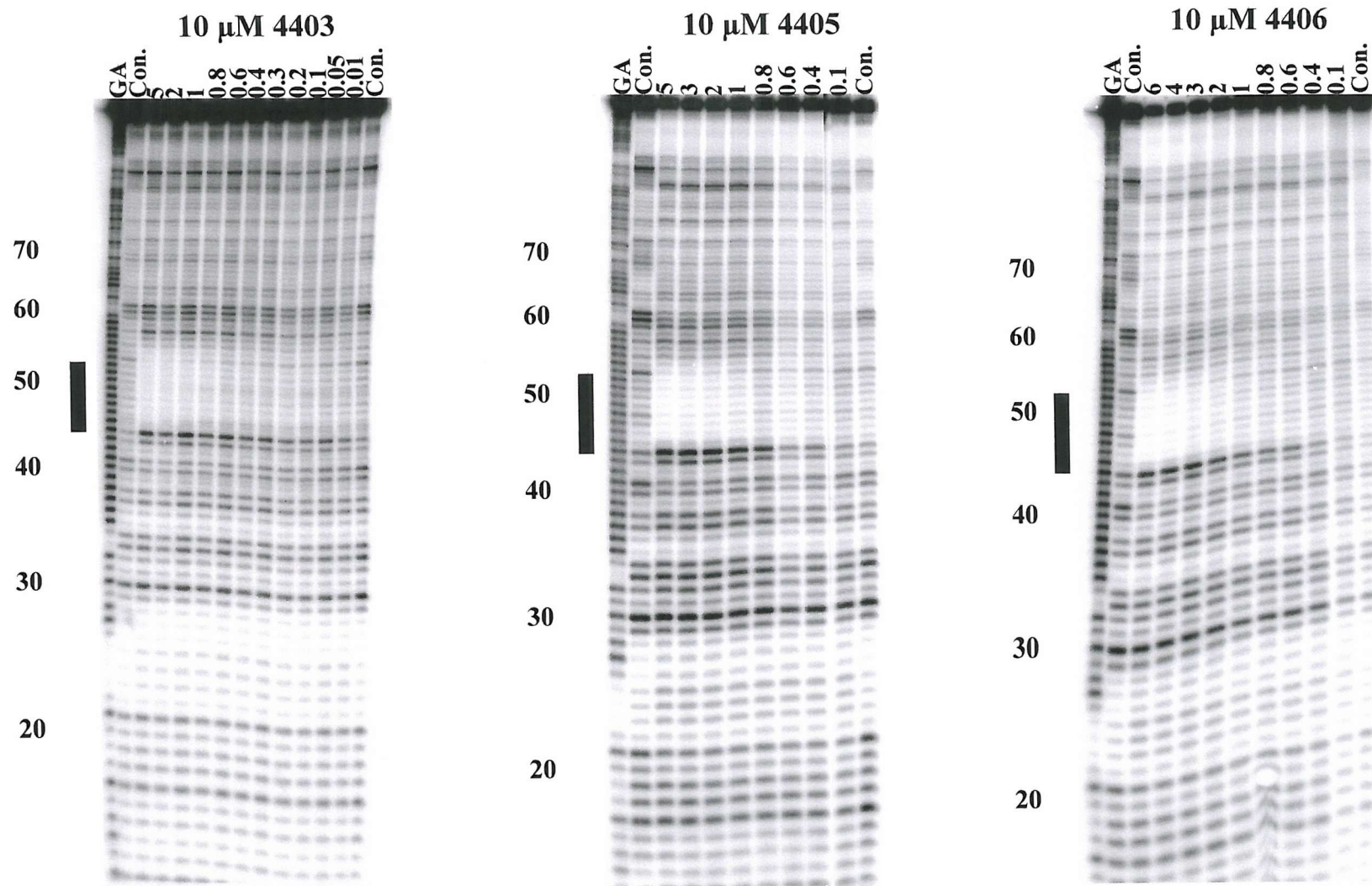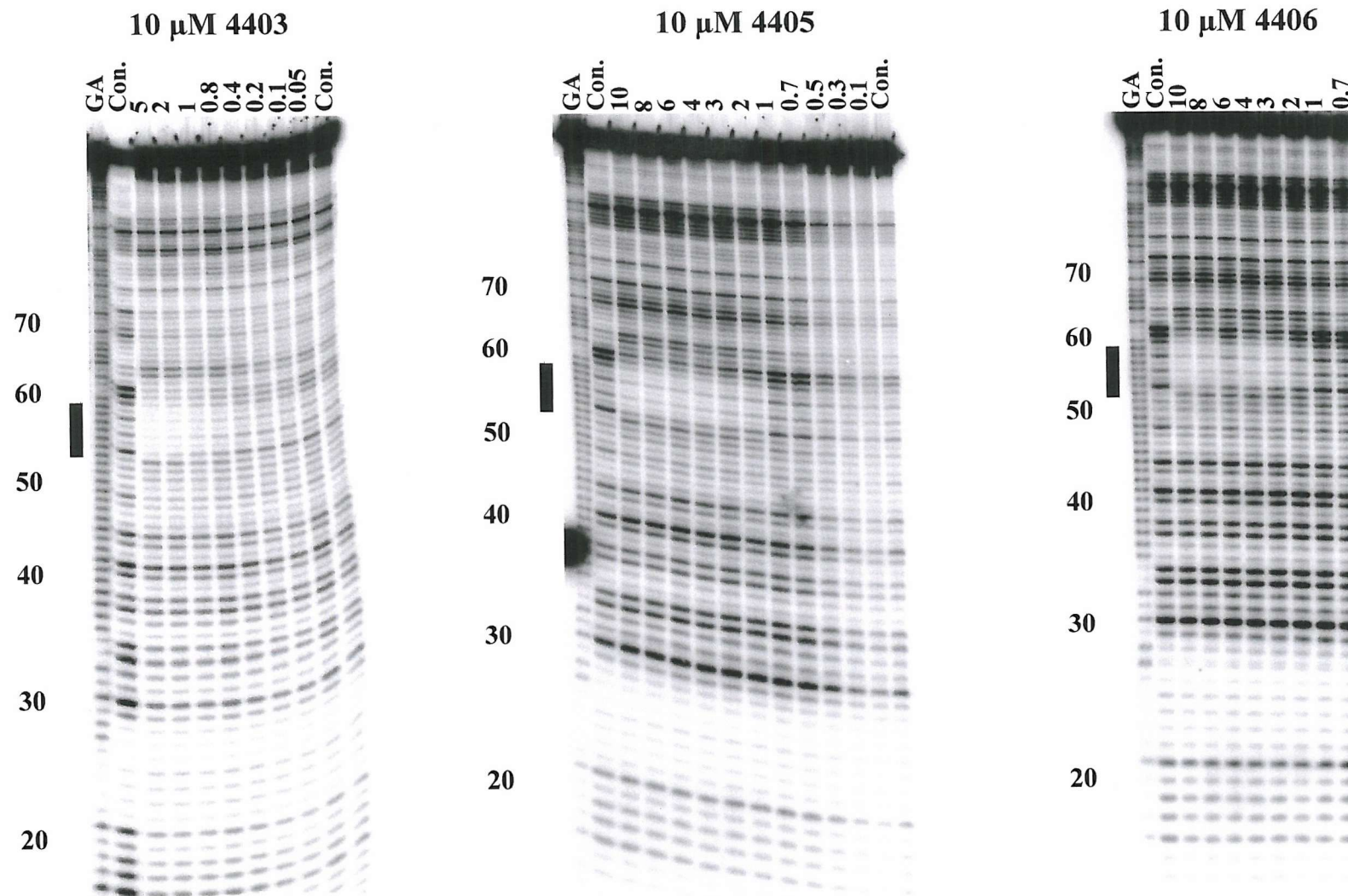
Figure 4.12: DNase I footprints showing the interaction of oligonucleotide 5'-CTCTCTC-3' (M4) with *Tyr*T(35-59). The left hand panel shows the result with 10 μM proflavine derivative 4403 at pH 5. The central panel shows the result with 10 μM proflavine derivative 4405 at pH 5. The right hand panel shows the result with 10 μM proflavine derivative 4406 at pH 5. Oligonucleotide concentrations (μM) are indicated at the top of the lanes. "GA" tracts are Maxam-Gilbert markers specific for purine residues. Lanes labelled Con. show the digestion pattern in the absence of oligonucleotide. The solid rectangular boxes to the left of the gels indicate the triplex target sites, and the numbers designate the sequence numbering scheme.
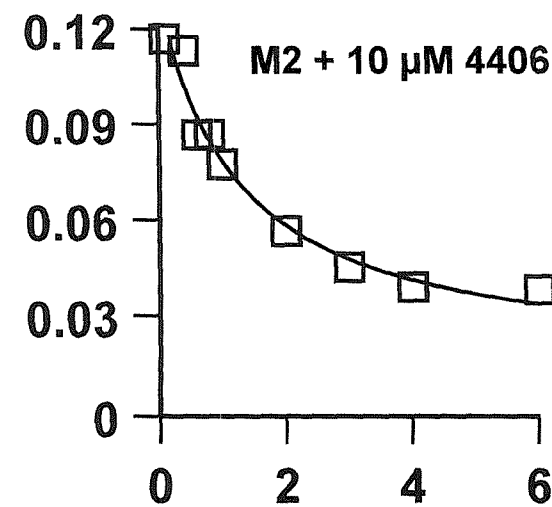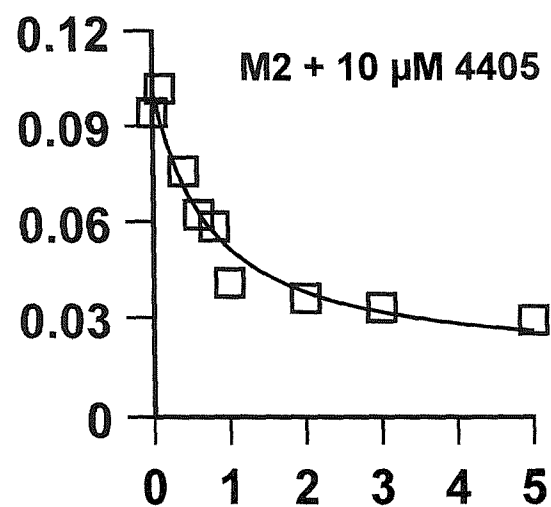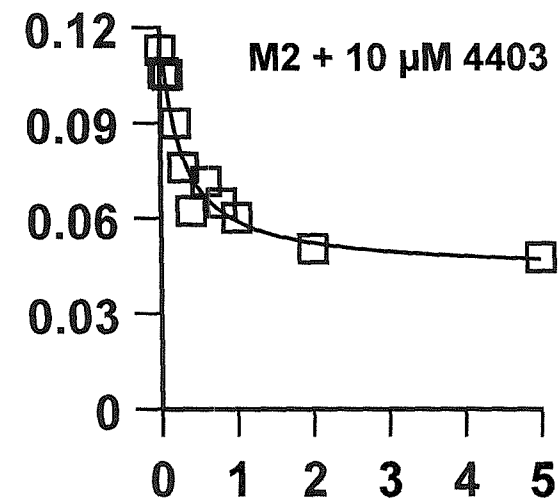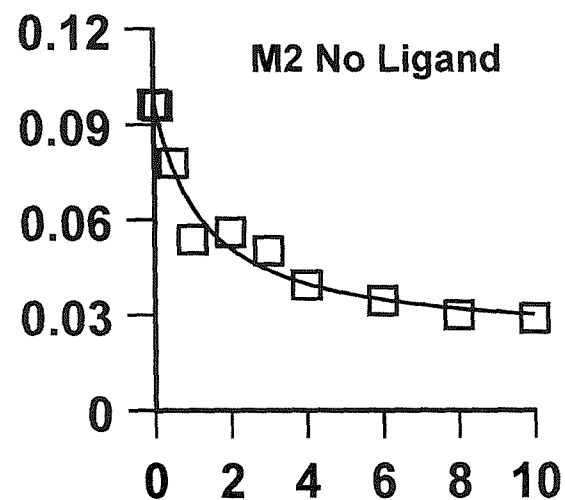
Figure 4.13: Footprinting plots showing the interaction of oligonucleotide M4 with its target site in the presence and absence of 10 μM proflavine derivatives 4403, 4405 and 4406. The abscissa represents oligonucleotide concentration (μM), and the ordinate represents relative band intensity (arbitary units).

(4.4) Discussion.

The results presented in this chapter have examined the ability of proflavine derivatives 4403, 4405, 4406 and the alpha and beta isomers of naphthoflavone to stabilise parallel triplexes of different base composition.

The results presented indicate that proflavine derivatives 4405 and 4406 did not stabilise triplexes formed with any oligonucleotide. However 4403 enhances the stability of the triplex generated with M2 and M3 (Table 4.1). The footprinting studies conducted with the α and β isomers of naphthoflavone demonstrate a marked difference in the stabilising properties of the two compounds. Whilst α-naphthoflavone stabilised every triplex, β-naphthoflavone has either no effect or de-stabilised every triplex.

Before considering the effect of the ligands on triplex stability it is worth noting that the triplexes formed with the 9-mer oligonucleotides have decreased affinity in the order M3>M2>M1. M3 consists of alternating C^+·GC and T·AT triplets, and would be expected to have the greatest affinity as predicted by Roberts & Crothers (1996). M2 and M1 have an increasing number of C^+·GC triplets which will reduce stability on account of repulsion between the adjacent positively charged cytosine residues. M4 is only a 7-mer oligonucleotide and binds with a lower affinity than M3, though its affinity is still higher than might be expected for such a short third strand.

(4.4.1)   Proflavine derivatives.

The lack of triplex stabilisation observed with M1 and proflavine 4403 was not surprising as this triplex does not contain any T·AT triplets that are not adjacent to protonated cytosine residues. It seems reasonable to suggest that this positively charged chromophore cannot intercalate adjacent to C^+·GC triplets as a result of repulsion between the positive charges on the cytosine residues and on the proflavine ring.

	No Ligand	Alpha Naphthoflavone	Beta Naphthoflavone	Proflavine Derivative 4403	Proflavine Derivative 4405	Proflavine Derivative 4406
M1	1.9 ± 0.8	/	/	1.8 ± 0.2	/	/
M2	1.0 ± 0.3	0.6 ± 0.1	1.7 ± 0.6	0.2 ± 0.07	0.7 ± 0.2	1.2 ± 0.3
M3	0.13 ± 0.04	0.06 ± 0.01	0.6 ± 0.3	0.08 ± 0.01	0.4 ± 0.1	0.7 ± 0.1
M4	1.8 ± 0.8	0.7 ± 0.1	2.9 ± 0.7	1.6 ± 0.4	1.4 ± 0.4	4.9 ± 0.8

Table 4.1: C_{50} values derived from the DNase I footprinting gels shown in this chapter. The footprinting data were fitted to the equation $I/I_0 = C_{50}/(L + C_{50})$, where I and I_0 represent relative band intensity in the presence and absence of oligonucleotide. L represents oligonucleotide concentration, and C_{50} represents the oligonucleotide concentration required to reduce the band intensity by 50 %. / indicates non-determined value.

The stability of the triplex generated with M2 is enhanced by the addition of 10 μM proflavine 4403 (Table 4.1). An increase in the stability was expected as this oligonucleotide provides two potential sites of intercalation between adjacent T·AT triplets which are removed from the protonated cytosine residues. However the increase in stability is relatively low, with ligand 4403 enhancing the stability 4-fold, while the change for ligand 4405 is negligible. This weak stabilising effect may reflect the limited number of potential intercalation sites for the ligand (only 2 per triplex). It is also possible that the position of the intercalation sites determines the degree of stabilisation. Oligonucleotide M2 contains TpT sites towards the centre of the triplex and the ligand might have a greater effect if these were positioned at the terminal regions, where the third strand will be more likely to fray from the target. Previous studies have suggested that increasing favourable interactions at the terminal regions of a triplex may contribute to increasing triplex affinity (Colocci *et al* 1993).

The results presented clearly demonstrate that the oligonucleotide M3 generates a very stable triplex in the absence of a stabilising ligand, with a C_{50} value of 0.13 μM ± 0.04. The high triplex stability is directly related to the oligonucleotide sequence, 5'-TCTCTCTCT-3', as every protonated cytosine residue is separated by a neutral thymine residue, thereby preventing charge repulsion from de-stabilising the triplex. The general lack of stability afforded by all the proflavine derivatives (except possibly 4403) to the M3 triplex is presumably because it does not contain any intercalation sites away from a protonated cytosine residues. Therefore the ligand can only intercalate at either CpT or TpC steps. In addition it is possible that this triplex, with alternating positively charged and neutral triplets, already has optimal stability. The intercalation of any ligand into this structure will therefore disrupt the regular alternation of positively charged and neutral triplets and would decrease triplex stability.

The results with the oligonucleotide M4 demonstrate that in the absence of a stabilising ligand it can generate a stable triplex with the *Tyr*T(35-59) sequence, even though it is only 7 base long, lower than the minimum length reported by Moser & Dervan (1987). The affinity of this triplex is however less than that with oligonucleotide M3, due to its shorter length resulting in decreased Hoogsteen hydrogen bonding, and

stacking interactions. The terminal C$^+$·GC triplets will also enhance triplex stability as previously suggested (Asensio *et al* 1999), and these attributes would contribute to the strong C$_{50}$ value observed (1.79 µM ± 0.96). Furthermore the lack of stabilisation by all the proflavine derivatives is similar to that for M3.

The results presented here indicate that the positively charged ligand 4403 may only be able to stabilise a triplex that presents intercalation sites that are not adjacent to charged bases. These results confirm a similar study conducted with the charged ligand naphthylquinoline (Keppler 1999), which also only stabilised the triplex with M2.

The difference in the stabilisation afforded by ligands 4403 and 4405 must be due to the length of the linkers at positions 3 and 6 of the proflavine ring, connecting the terminal piperazine groups to the proflavine ring. Derivative 4403 has 1 less carbon atom than 4405, and as such positions the piperazine groups in a different position to that of 4405. However without detailed molecular modelling studies the optimal chain length can not be accurately determined. The overall lack of triplex stability afforded by ligand 4406 is surprising since several anthraquinone derivatives possessing this side group have been shown to be effective triplex binding ligands. These groups were attached to the proflavine ring via the same linkers used with 4405, and this compound is shown to stabilise triplex DNA to a lower degree than derivative 4403. Therefore stability may be improved by reducing the length of the linkers to mirror those of derivative 4403.

(4.4.2) Naphthoflavone.

It can be seen that the alpha isomer of naphthoflavone stabilises triplexes formed with M2, M3, and M4, whereas the beta isomer appears to de-stabilise all three triplexes. The degree of stability afforded by α-naphthoflavone appears to be independent of the triplex as in each case stability was enhanced by approximately 2-fold. The stabilisation of triplex DNA irrespective of the potential intercalation site was predicted as the ligand does not bear a positive charge, and as such is not prevented from intercalating adjacent to protonated cytosine residues. Whilst a 2-fold stabilisation of triplex DNA by α-

naphthoflavone is not as great as the stabilisation afforded by some previously reported compounds (naphthylquinoline, and BePI) it should be noted that these compounds bear a positive charge which restricts the sequences that can be stabilised. However the anthraquinones do not bear a positive charge and stabilise the M2 - M4 triplexes to a higher degree than that achieved with α-naphthoflavone (Keppler 1999).

The fact that α-naphthoflavone stabilises the formation of both the M3 and the M4 triplexes demonstrates that intercalation of this uncharged ligand does not de-stabilise alternating CT triplex DNA as previously postulated. Intercalation of this ligand would interrupt the pattern of alternating $C^+ \cdot GC$ and $T \cdot AT$ triplets, which has previously been postulated to decrease alternating CT triplex stability (Roberts & Crothers 1996). These results would tend to suggest that triplex stability can be further enhanced by an un-charged ligand presumably due to increased stacking interactions.

The lack of triplex stabilisation afforded by β-naphthoflavone can only be attributed to the isomer distorting the triple helix. It can be seen from Table 4.1 that β-naphthoflavone actually de-stabilises triplex formation by as much as 4.6-fold suggesting that it either binds to single-stranded DNA preventing its association with the duplex, or that it binds to duplex DNA.

In general the results present in this chapter are consistent with the suggestion that positively charged compounds preferentially stabilise the M2 triplex, as it contains adjacent $T \cdot AT$ triplets. In contrast the neutral compound alpha naphthoflavone stabilises triplexes irrespective of their sequence.

Chapter 5.

Triplex and Duplex DNA Thermal Denaturation Profiles Measured using Fluorescently Labelled Oligonucleotides.

(5.1) Foreword

One technique that is often used to support DNase I footprinting studies is that of UV thermal denaturation. When intermolecular triplexes are studied by UV melting a biphasic profile is obtained (Plum *et al* 1990). The first transition corresponds to the triplex to duplex melt, with the second melt relating to the duplex to single strand transition. UV melting studies require the DNA sample to be gradually heated in a controlled manner with the simultaneous measurement of the absorbance at 260 nm. Since duplex DNA has a lower absorbance at 260 nm than single stranded DNA, on account of the stacked bases, the denaturation is accompanied by an increase in absorbance (typically 25%). The mid-point of the transition (Tm, melting temperature) is characteristic of the particular DNA and its physical environment. Ligands that bind to duplex or triplex DNA stabilise the structure and so shift the melting profile to higher temperatures. Similarly the use of base analogues will alter the melting temperatures. However it has been reported that UV melting studies with antiparallel triplexes and some modified parallel triplexes are not possible since there is no change in absorbance (Faucon *et al* 1996, Arimondo *et al* 1998, 2000, Jetter & Hobbs 1993). To date no substantiated explanation has been offered as to why these triplexes form without hypochromicity. In addition the triplex-duplex and duplex-single strand transitions often overlap and do not permit unambiguous identification of the individual components. Therefore it can be seen that this technique has its limitations, and in an attempt to overcome these shortcomings, we have designed a novel technique to measure DNA thermal denaturation profiles using fluorescently labelled oligonucleotides.

Fluorescence occurs when a fluorescent molecule absorbs light at a given wavelength and subsequently emits it at a longer wavelength. We have designed oligonucleotides that form intramolecular triplexes in which methyl red is attached to the

third strand and fluorescein is attached opposite this on one of the duplex strands. The close proximity of these groups causes collisional quenching of fluorescein fluorescence when the triplex is generated. On denaturing the complex the fluorophore and quencher are separated by a large distance and there is a corresponding increase in the fluorescence signal (Fig. 5.1). The location of the fluorophore and quencher is such that only the melting of the third strand is detected Oligonucleotides were also designed in which the fluorophore and quencher were attached to the duplex strands of the triplex, enabling the duplex to single strand transition to be measured (Fig.5.2). The fluorescence was monitored in a Roche RT-PCR LightCycler, which allows gradual heating of up to 32 samples (0.1 °C sec^{-1}) with rapid acquisition of data (experimental details can be found in section 2.10)

The results presented in this chapter show the thermal denaturation profiles of intramolecular parallel triplexes and duplexes in the presence of various ligands, and intramolecular parallel triplexes incorporating base analogues. All of the oligonucleotides presented in this chapter were synthesised by Dr. Catherine McKeen, Oswell DNA services.

(5.2) Fluorescence melting profiles of intramolecular triplexes and duplexes.

Oligonucleotide TB1818 was designed to generate an intramolecular parallel triplex (Fig. 5.2). This had the quencher (methyl red) attached to the third strand and the fluorophore (fluorescein) attached to the duplex target strand, positioned so as to measure the triplex-duplex transition (Fig. 5.2). TB1819 was designed to form an intramolecular antiparallel duplex and had the quencher and fluorophore attached to opposite strands of the intramolecular duplex and measures the duplex-single strand transition (Fig. 5.2). Experiments were carried out in 50 mM sodium acetate (pH 5), 0.1 M NaCl, 1 mM EDTA, 50 mM sodium phosphate (pH 7), 0.1 M NaCl, 1 mM EDTA, and 50 mM HEPES (pH 7), 10 mM $MgCl_2$, 1 mM EDTA.
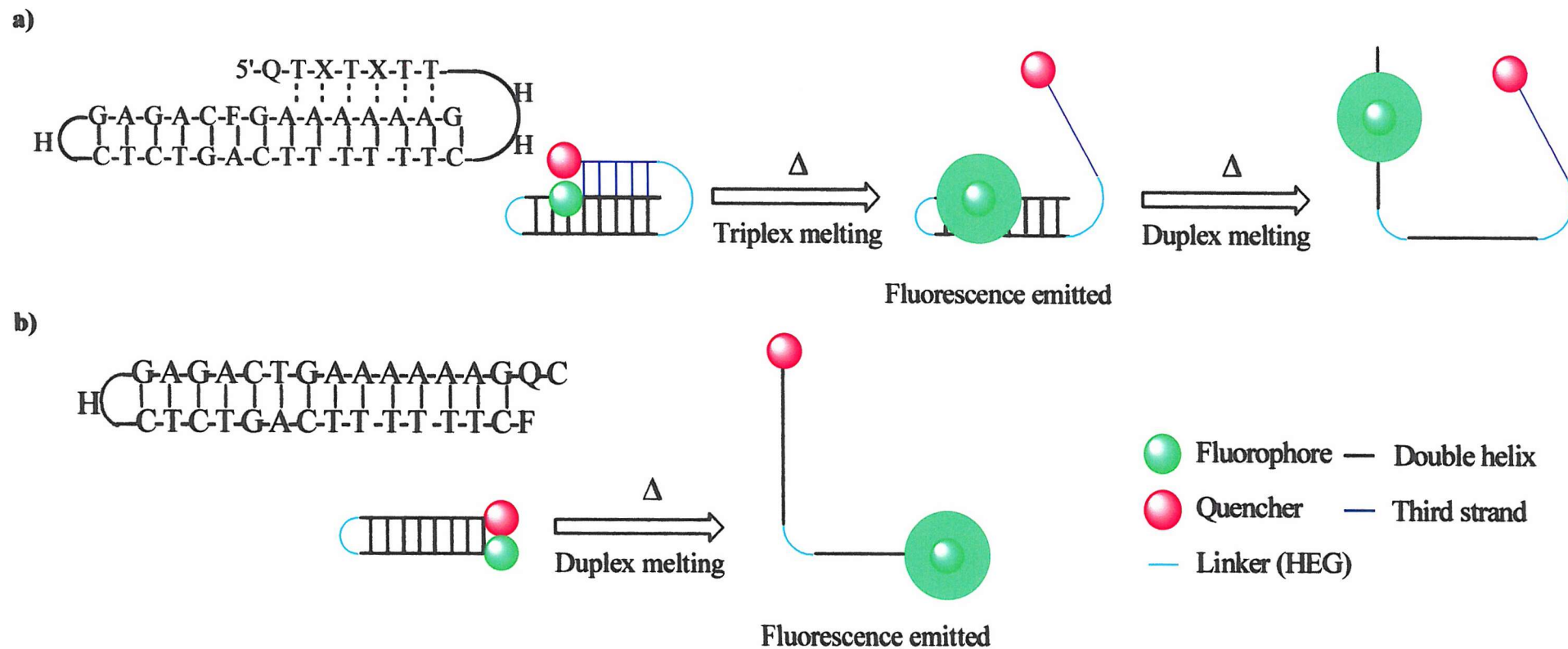
Figure 5.1: Diagram a) illustrates the fluorescent thermal denaturation of an oligonucleotide designed to generate an intramolecular triplex. Diagram b) illustrates the fluorescent thermal denaturation of an oligonucleotide designed to generate an intramolecular duplex. Both transitions result in an increase in the fluorescent signal.

(a)

```
                        5'-QTTTTTT——H
                          ╱GAGACFGAAAAAA-3'|
TB1818          H┤
                          ╲CTCTGACTTTTTTC—H
```

```
TB1819              ╱GAGACTGAAAAAAGQ-
                 H┤
                    ╲CTCTGACTTTTTTCF-
```

```
              5'-QT*T*TT——O           TB1794
                ╱GAGACFGAAAAAA-3'|      TB1795
           O┤                           F67449
                ╲CTCTGACTTTTTTC—O
```

```
                          5'-QTT**TT——O
F67450              ╱GAGACFGAAAAAA-3'|
                 O┤
                    ╲CTCTGACTTTTTTC—O
```

(b)

5-Propargylamino dU
TB1794

2'-Aminoethoxy T
TB1795

2'-Aminoethoxy-5-propargylamino U
F67449 & F67450
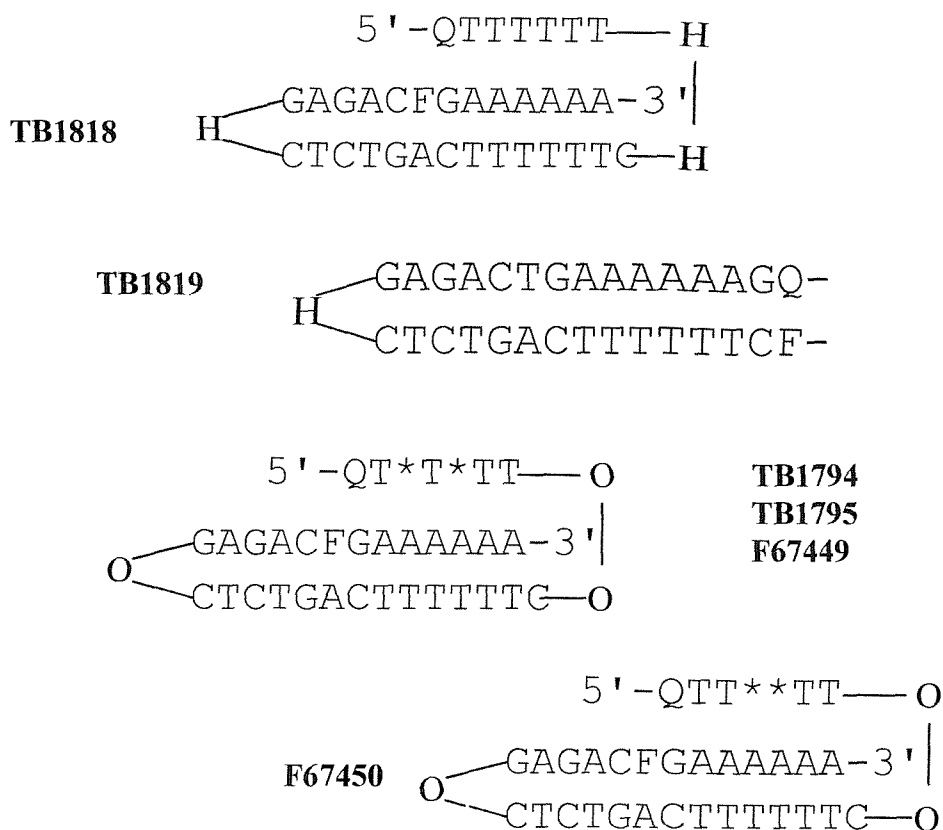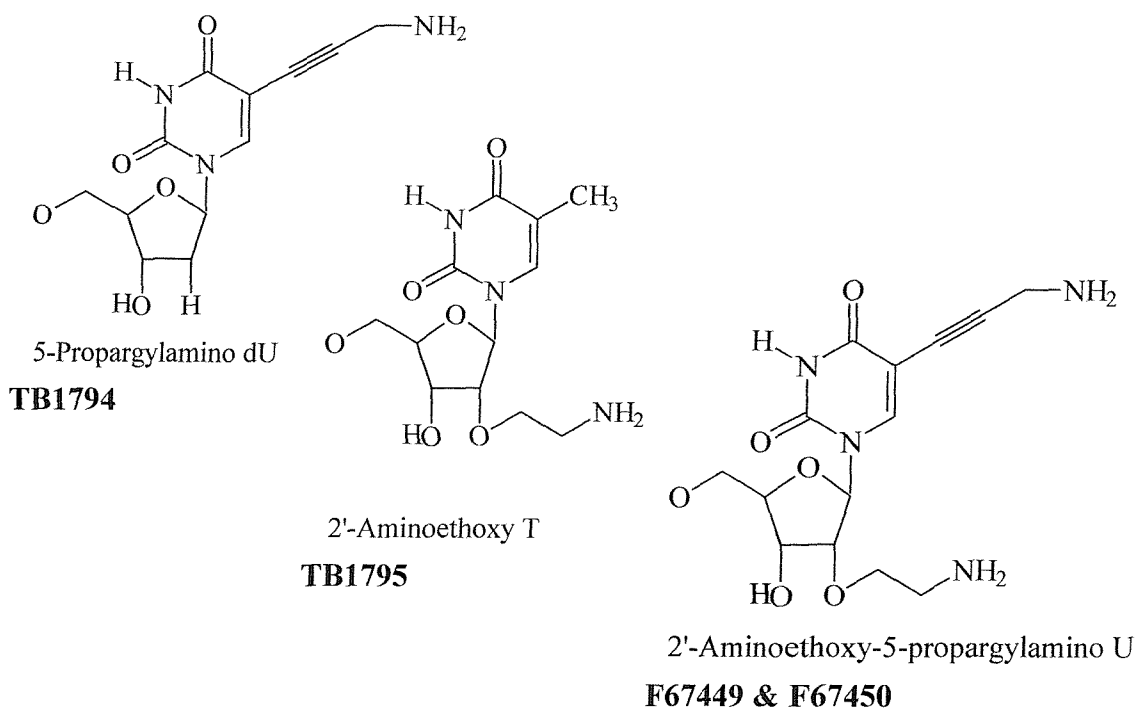
Figure 5.2: (a) illustrates the fluorescently labelled oligonucleotides used. F represents fluorescein, Q represents methyl red, H represents HEG linker, O represents octandiol linker, and * indicates base modification. (b) illustrates the base modification used in oligonucleotides TB1794, TB1795, F67449, and F67450.

Before considering the effect of ligands and base modifications on the fluorescence profile it is first necessary to consider the fluorescence changes on melting the oligonucleotides alone, under various conditions. In each case the oligonucleotide concentration was 250 nM.

The left hand panel of Fig. 5.3 shows fluorescence melting profiles for the intramolecular triplex formed by TB1818; these are compared with the underlying duplex (TB1819) which are presented in the right hand panel. It can be seen that in each case the fluorescence increases with temperature as the complex dissociates. Looking first at the results for the triplex at pH 5.0 (black line), it can be seen that the starting fluorescence is low, consistent with the formation of a structure in which the fluorophore and quencher are in close proximity. On increasing the temperature the fluorescence increases approximately five-fold, reaching a maximum at about 55°C. The derivative plot (see insert) reveals that the mid-point for this transition (Tm) occurs at 37.3°C. The fluorescence then decreases slightly at temperature above 55°C. Although this may be due to the effect of temperature on the quantum yield of the fluorophore, it most probably corresponds to melting of the duplex at a higher temperature. The derivative plot reveals that this transition has a end-point of 72.7°C. The presence of this second fluorescence transition was unexpected, but it presumably represents melting of the underlying duplex, which is retained as an intermediate structure after dissociation of the third strand. Since the duplex is a relatively rigid structure the fluorophore and quencher will be kept apart, giving a large increase in fluorescence. When the duplex melts at higher temperatures the oligonucleotide will be fully single-stranded, and the average distance between these two species will decrease, resulting in a small decrease in fluorescence.

Since these conditions are used in most of the other studies in this chapter we examined the nature of these transitions in greater detail. The heating rate of 0.1°C sec^{-1} is somewhat faster than that normally employed for UV-melting studies with intermolecular DNA complexes. Since the kinetics of triplex formation are known to be slow we were concerned these LightCycler experiments might not be at thermodynamic equilibrium. Note that this is the slowest heating rate for the Roche LightCycler. Two variations were used to examine this possibility. Firstly we examined the cooling
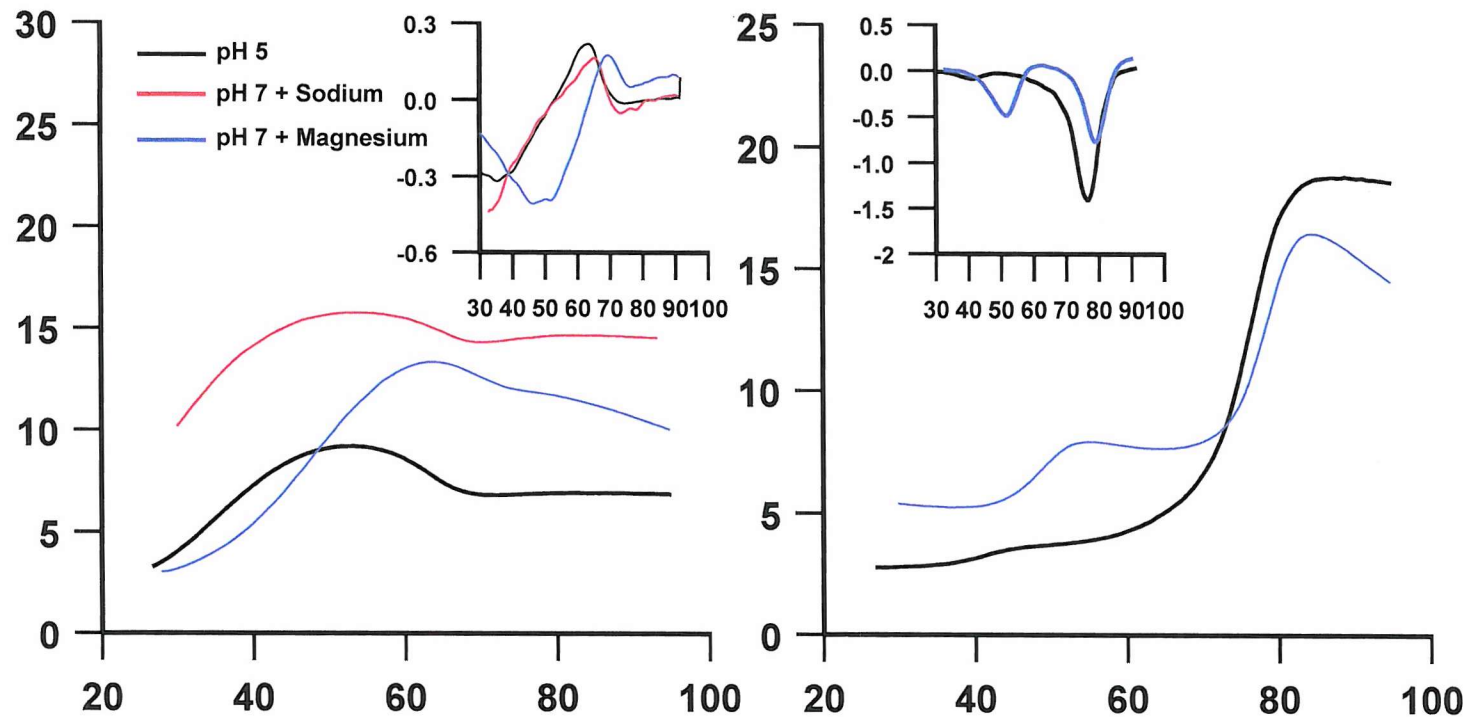
Figure 5.3: Shown are the fluorescence melting profiles of TB1818 (left hand panel), and TB1819 (right hand panel) at pH 5 and pH 7. The inserted figures show the corresponding derivative fluorescence plots from which the Tm values were calculated. The abscissa represents temperature (Celsius), and the ordinate represents fluorescence or the fluorescence derivative (arbitary units).

Oligonucleotide / Buffer	TB1818		TB1819	
	Triplex-duplex Transition Tm (°C)	Duplex-single strand Transition Tm (°C)	Transition 1 Tm (°C)	Duplex-single strand Transition Tm (°C)
50 mM sodium acetate (pH 5) + 0.1 M NaCl	37.3	72.7	/	76.4
50 mM HEPES (pH 7) + 10 mM MgCl$_2$	45.2	76.9	48.4	79.7

Table 5.1: Shows the Tm values for the oligonucleotides TB1818 and TB1819 in 50 mM sodium acetate (pH 5), 0.1 M NaCl, 1 mM EDTA, or 50 mM HEPES (pH 7), 10 mM MgCl$_2$, 1 mM EDTA.

(annealing) and melting profiles under the same conditions. This produced the same temperature-fluorescence profiles (Fig. 5.4) suggesting that this intramolecular reaction is sufficiently fast to be at equilibrium during the heating and cooling profiles. Secondly we measured the melting curves at even higher rates of heating. The results (Fig. 5.4) show that the apparent melting temperature does not change up to a rate of 0.2 °C sec^{-1} but beyond this, at rates of 0.5 °C sec^{-1} and above there is a difference in heating and cooling profiles.

The other curves in the left hand panel of Fig. 5.3 show the melting profile at pH 7.0, in the presence and absence of magnesium. At this pH the total fluorescence signal is greater than that at pH 5 as the pK of fluorescein is 6.4, and the protonated species does not fluoresce. In the presence of magnesium the triplex-duplex transition is more stable (7.9°C) than that at pH 5.0 in the presence of only sodium. At pH 7.0 in the absence of magnesium the triplex-duplex transition occurs at lower temperatures, and it is not possible to accurately determine the Tm from these data. Both of these triplex-duplex transitions are followed by a decrease in fluorescence, which is presumed to correspond to the duplex-single strand transition.

The right hand panel of Fig. 5.3 shows the results of similar experiments with the intramolecular duplex (TB1819). This shows a clear increase in fluorescence with Tm values of 76.4 and 79.7°C at pH 5.0 and 7.0 respectively. A second much smaller transition is also evident at lower temperatures which can not be accurately determined at pH 5. However at pH 7 in the presence of magnesium a larger transition is observed with a Tm value of 48.4°C which is thought to be due to a small quantity of intermolecular duplex which can be formed by annealing two molecules of this sequence (covered in greater detail in the discussion). All of the Tm values can be seen summarised in Table 5.1.
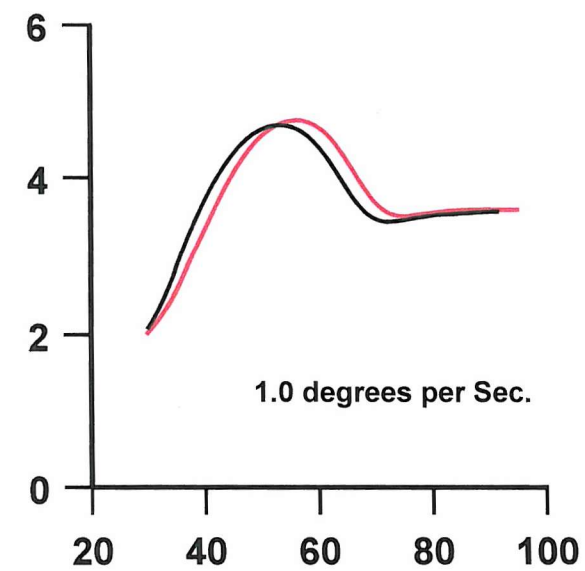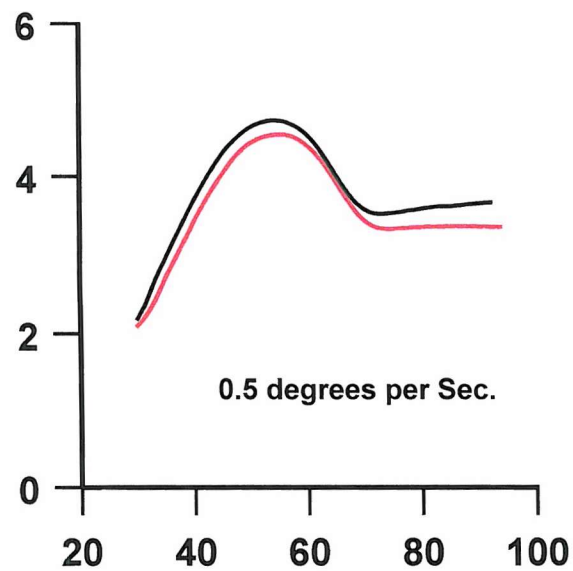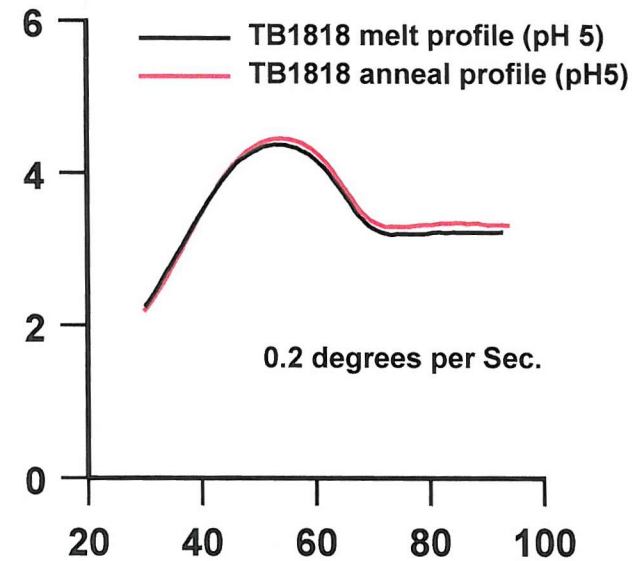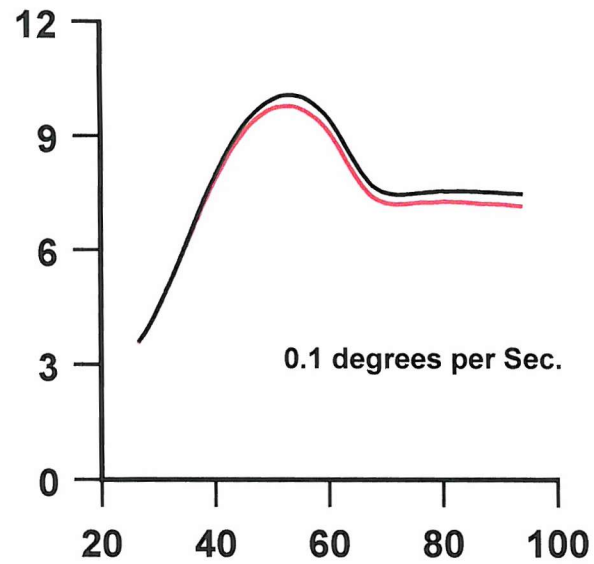
Figure 5.4: Shown are the melting (black line) and annealling (red line) profiles of TB1818 at pH 5. Different rates of heating and cooling are shown on each axis. The abscissa represents temperature (Celsius), and the ordinate represents fluorescence (arbitary units).

(5.3) Intramolecular triplexes containing modified bases.

Several derivatives of oligonucleotide TB1818 which forms an intramolecular parallel triplex were prepared, containing modified bases in the third strand. TB1794, contained two 5-propargylamino dU bases (PU) (Fig. 5.2), oligonucleotide TB1795 contained two 2'-aminoethoxy T bases (EA-T) (Fig. 5.2), and F67449 contained 2'-aminoethoxy-5-propargylamino U residues (EA-PU) in the third strand (Fig. 5.2). In each of these oligonucleotides the modified bases were separated by one thymidine residue. In contrast oligonucleotide F67450 contained 2 adjacent 2'-aminoethoxy-5-propargylamino U bases in the third strand (Fig. 5.2). All of the oligonucleotides were designed to form intramolecular parallel triplexes with a methyl red moiety (quencher) attached to the Hoogsteen strand, and a fluorophore (dFAM) attached to one of the duplex strands so as to measure the triplex-duplex transition in the same way as in the previous section.

(5.3.1)   Thermal Denaturation Studies at pH 5.

The left hand panel of Fig. 5.5 shows the triplex-duplex fluorescence profiles of the modified and un-modified oligonucleotides measured at pH 5. The profile for the unmodified oligonucleotide has already been described and produces a triplex-duplex transition of 36°C, which is followed by a decrease in fluorescence which is presumed to correspond to the melting of the duplex. It can be seen that TB1794 which contains two 5-propargylamino dU bases in the third strand induces melts with a single transition at a much higher temperature than the control oligonucleotide. Furthermore it can be observed that following this transition the fluorescence remains constant and there is no decrease as seen in the control. This curve is characterised by a Tm of 66.6°C, an increase of 30.1°C over the unmodified triplex. The profile for TB1795 demonstrates that incorporating two 2'-aminoethoxy T bases within the Hoogsteen strand also significantly stabilises the triplex-duplex transition. It can be seen that the transition has shifted to a much higher temperature with a Tm of 64.6°C, which is 2.0°C lower than with propargylamino dU and 28.1°C higher than the control. The profiles for F67449 and

F67450 are not significantly different from one another, and are characterised by Tm values of 73.6°C and 73.8°C respectively. It appears that incorporation of 2'-aminoethoxy-5-propargylamino U generates the most stable triplex which melts 37.0°C and 37.2°C higher than the control. All of these Tm values are summarised in Table 5.2 and Fig. 5.6. It appears that each of these modifications has significantly stabilised the intramolecular triplex so that the triplex-duplex transition and duplex-single strand transition occur at the same temperature. The values for these transitions are presented in Table 5.2 and Fig. 5.6. The order of stability is $T < {}^{EA}T < {}^{P}U < {}^{EAP}U$

(5.3.2)   Thermal Denaturation Studies at pH 7.

The right hand panel of Fig. 5.5 shows the triplex-duplex transitions of the base modified oligonucleotides measured at pH 7.0 as previously described. The unmodified oligonucleotide (TB1818) melts with a triplex-duplex transition of 31.8°C. This transition is followed by a decrease in fluorescence, which is not as big as that observed at pH 5.0. The profile of the propargylamino dU modified oligonucleotide (TB1794) is very different from the control and shows a single transition which occurs at a significantly higher temperature with a Tm of 66.8°C, an increase in stability of 35.0°C compared to the control. The melting profile for the 2'-aminoethoxy T modified oligonucleotide is very similar to that produced by the propargylamino dU modified oligonucleotide, with the triplex-duplex transition of 65.2°C, which is 1.6°C lower than with propargylamino dU but 33.4°C higher than the unmodified oligonucleotide. Both of the 2'-aminoethoxy-5-propargylamino oligonucleotides form more stable complexes than the other oligonucleotides with triplex-duplex transitions of 72.8°C for F67449 and a Tm of 72.4°C for F67450, an increase of 41°C and 40.6°C over the control respectively. The values for these transitions are presented in Table 5.2 and Fig. 5.6

These fluorescence results are in agreement with the footprinting studies presented in chapter 3, suggesting that the bis-amino substituted analogue produces a larger increase in stability than that observed with either of the mono-substituted analogues at both pH 5 and pH 7. Furthermore the results also indicate that
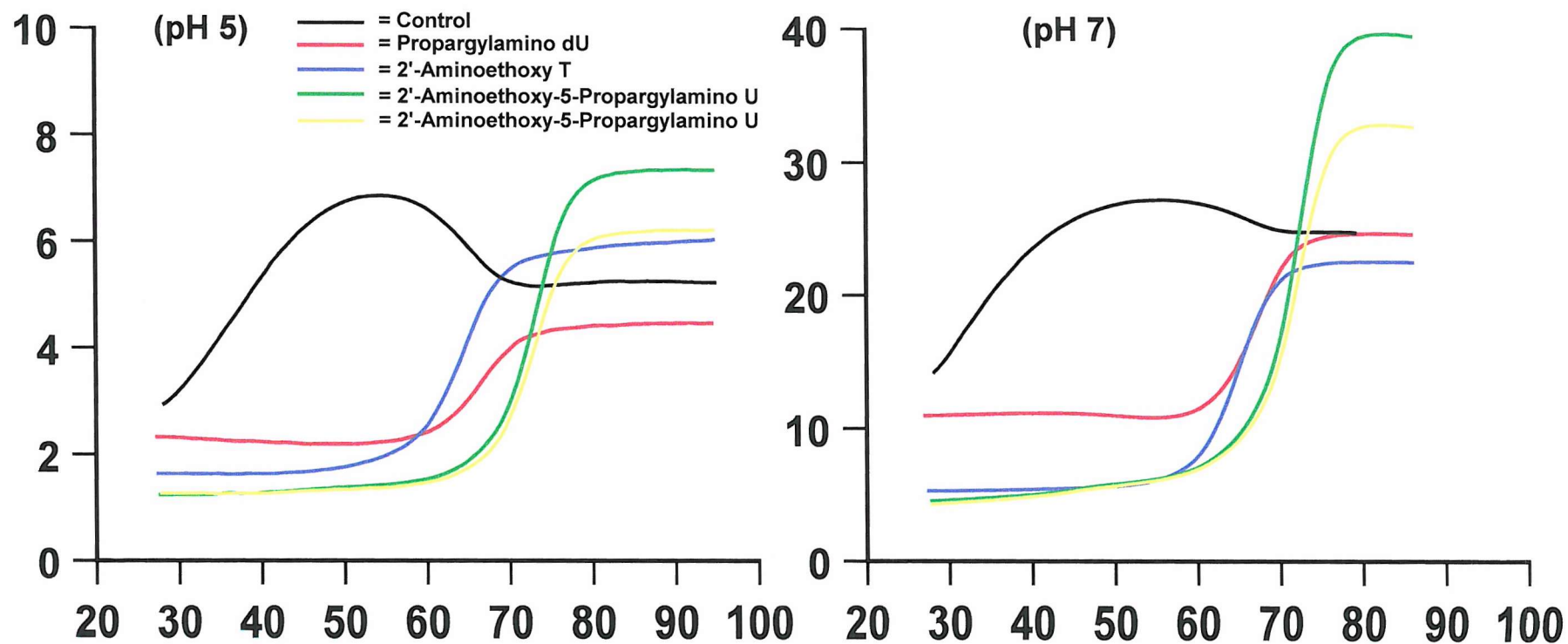
Figure 5.5: Fluorescent DNA thermal denaturation profiles generated by base modified oligonucleotides at pH 5 (left) and pH 7 (right). The ordinate represents fluorescence (arbitary units) and the abscissa represents temperature (Celsius).

Base Analogues	pH 5 Triplex-single Strand Transition		pH 7 Triplex-single Strand Transition	
Oligonucleotide	Tm (°C)	ΔTm (°C)	Tm (°C)	ΔTm (°C)
TB1818 (Control)	36.5	0	31.8	0
TB1794 (Propargylamino dU)	66.6	30.1	66.8	35.0
TB1795 (Aminoethoxy T)	64.6	28.1	65.2	33.4
F67449 (Bis-amino)	73.6	37.1	72.8	41.0
F67450 (Bis-amino)	73.8	37.3	72.4	40.6
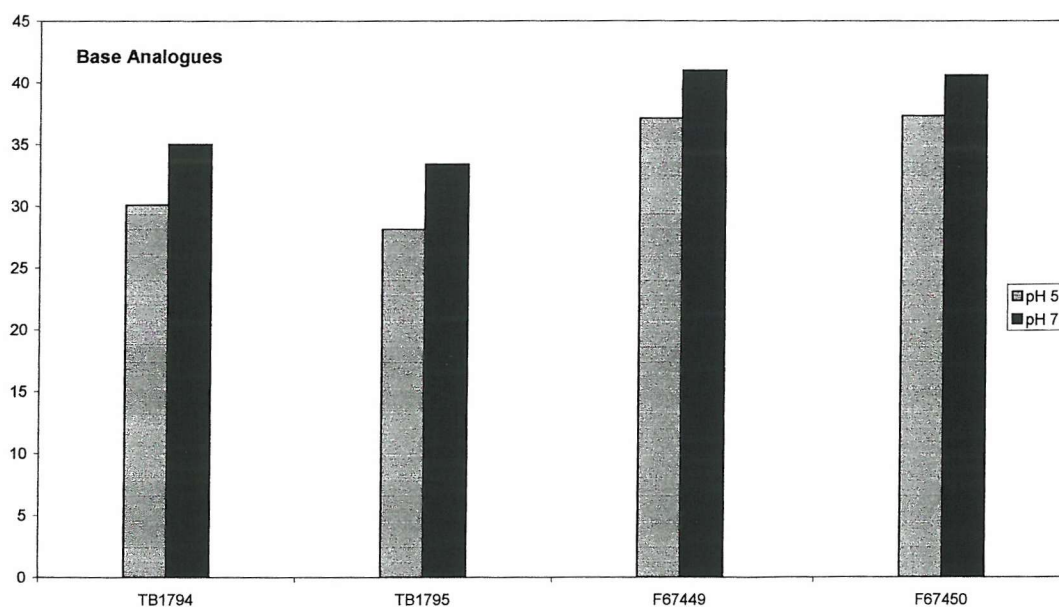
Table 5.2 & Figure 5.6: Table 5.2 shows the Tm and ΔTm values for the based modified oligonucleotides TB1818 (unmodified), TB1794 (5-propargylamino dU), TB1795 (2'-aminoethoxy T), F67449 (2'aminoethoxy-5-propargylamino U), and F67450 (2'aminoethoxy-5-propargylamino U) at pH 5 and pH 7. Figure 5.6 illustrates the difference in triplex stability afforded at pH 5 and pH 7. The abscissa represents the base modified oligonucleotide and the ordinate represents ΔTm (Celsius).

5-propargylamino dU and 2'-aminoethoxy T produce very similar changes in the stability.

(5.4) Intramolecular triplexes & duplexes with various ligands at pH 5.0.

All experiments described below were carried out in 50 mM sodium acetate (pH 5.0), 0.1 M NaCl, 1 mM EDTA with varying concentrations of intercalating ligands, minor groove binding ligands and antibiotics. Each ligand was tested against both the intramolecular triplex (TB1818) and duplex (TB1819) to assess the relative effect on triplex and duplex DNA. The oligonucleotide concentration was 250 nM in all experiments.

(5.4.1)   Naphthylquinoline.

Naphthylquinoline has an unfused positively charged aromatic system (Wilson *et al* 1995) that has been shown to selectively stabilise T·AT triplets (Cassidy *et al* 1996), see section 1.4.2.4. This compound has been shown to stabilise triplex DNA by as much as 100-fold at low pH (Chandler *et al* 1995, Cassidy *et al* 1996).

The left hand panel of Fig. 5.7 shows the melting curves for oligonucleotide TB1818 with increasing concentrations of naphthylquinoline. The profile in the absence of ligand has already been described, producing a melting curve with a Tm for the triplex-duplex transition of 34.6°C followed by a decrease in fluorescence (explained in section 5.2). This characteristic profile is repeated in the presence of naphthylquinoline, though the triplex-duplex transition is shifted to successively higher temperatures indicative of triplex stabilisation. It can be seen that increasing concentrations of naphthylquinoline causes a small decrease in the maximum fluorescence, which is presumably due to overlap between the duplex and triplex melts. Analysis of these curves reveals that 10 µM naphthylquinoline increases the triplex-duplex transition by 26.2°C. The Tm values corresponding to the triplex-duplex transitions are summarised in Table 5.3 and Fig. 5.8.

Figure 5.7: Fluorescent DNA thermal denaturation profiles generated with oligonucleotides TB1818 (left) and TB1819 (right) in the presence of an increasing concentration of naphthylquinoline in a pH 5 buffer. The ordinate represents fluorescence (arbitary units) and the abscissa represents temperature (Celsius).

Naphthylquinoline	Triplex-duplex Transition (TB1818)		Duplex-single strand Transition (TB1819)	
Concentration (µM)	Tm (°C)	ΔTm (°C)	Tm (°C)	ΔTm (°C)
0	34.6	/	76.5	/
0.1	36.5	1.9	75.9	-0.6
0.5	47.6	13.0	75.9	-0.6
1	50.5	15.9	76.0	-0.5
2	54.5	19.9	77.6	0.9
5	59.4	24.8	78.2	1.7
10	60.8	26.2	79.3	2.8

Table 5.3 & Figure 5.8: Table 5.3 shows the Tm and ΔTm values for the oligonucleotides TB1818 and TB1819 in the presence of naphthylquinoline at pH 5. Figure 5.8 illustrates the stability afforded to both the triplex-duplex transition (TB1818) and the duplex-single strand transition (TB1819). The abscissa represents ligand concentration (µM), and the ordinate represents ΔTm (Celsius).

The right hand panel of Fig. 5.7 shows the fluorescence melting curves for the intramolecular duplex TB1819 with increasing concentrations of naphthylquinoline. The curve for the control has already been described (see section 5.2). The Tm of the intramolecular duplex-single strand transition in the absence of any ligand is 76.5°C. It can be seen that increasing the ligand concentration from 0 to 2 μM does not significantly alter the melting profile. However on increasing the concentration of naphthylquinoline to 5 μM and 10 μM the duplex-single strand transition appears to shift to higher temperatures, and 10 μM naphthylquinoline stabilised the duplex DNA by 2.8°C. The Tm values for the duplex-single strand transitions are summarised in Table 5.3 and Fig. 5.8.

These results confirm that naphthylquinoline produces significant stabilisation of the triplex-duplex transition, whereas the duplex-single strand transition is relatively unaffected, as expected for a triplex specific ligand.

(5.4.2)   1,4 Bis-Amidoanthraquinone

Anthraquinones have a tricyclic ring system (Fig. 5.9), with the bis-substituted analogues shown to stabilise triplex DNA in a manner dependent upon the position of substitution (Fox *et al* 1995), see section 1.4.2.3.

The left hand panel of Fig. 5.10 illustrates the thermal denaturation profiles of oligonucleotide TB1818 with increasing concentrations of 1,4 bis-amidoanthraquinone. The melting curve in the absence of ligand has already been described. It can be seen that increasing the ligand concentration induces significant changes to the shape of the melting profile. At a ligand concentration of 0.1 μM two transitions are produced; the first transition is very shallow, occurring over the temperature range 35 - 65°C, whereas the second transition is much steeper occurring between 65 - 70°C. At ligand concentrations of 0.5 μM and above the first transition is abolished, and the second transition is shifted to a higher temperature (approximately 67 - 77°C). Increasing the ligand concentration to 1 μM and 2 μM results in an increase in the fluorescence at low
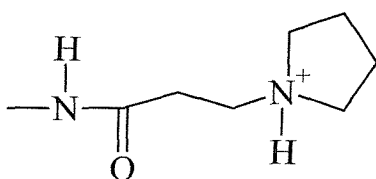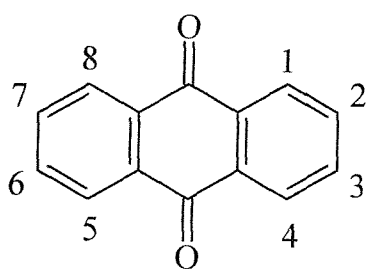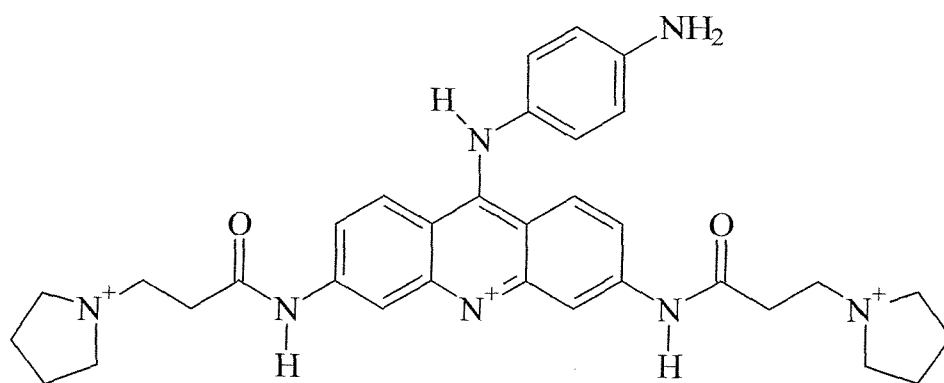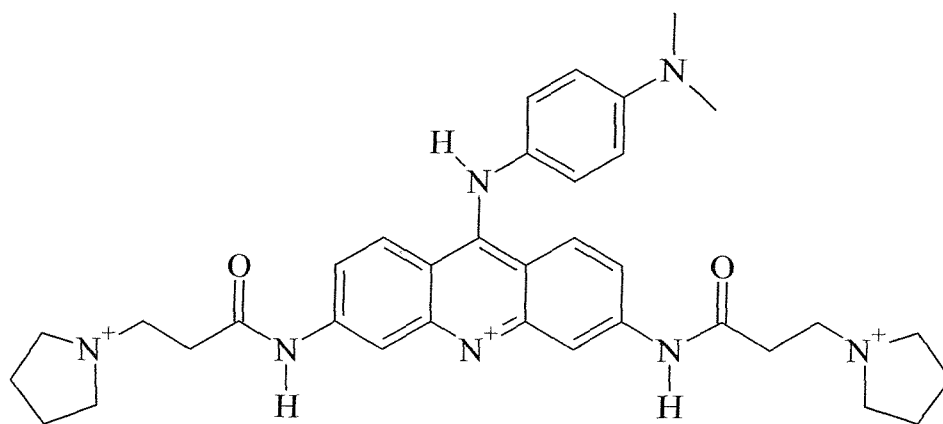
Figure 5.9: Diagram a) shows the structure of anthraquinone, where the numbers indicate the position of substitution with the amido side chain shown. Diagram b) shows the structures of acridine derivatives BR19 (top), and BR20 (bottom).

Figure 5.10: Fluorescent DNA thermal denaturation profiles generated with oligonucleotides TB1818 (left) and TB1819 (right) in the presence of an increasing concentration of 1,4 bis-amidoanthraquinone at pH 5. The ordinate represents fluoresence (arbitary units) and the abscissa represents temperature (Celsius).

1,4	Triplex-duplex Transition (TB1818)		Duplex-single strand Transition (TB1819)	
Concentration (μM)	Tm (°C)	ΔTm (°C)	Tm (°C)	ΔTm (°C)
0	38.5	/	76.5	/
0.1	69.7	31.2	78.1	1.6
0.5	75.5	37.0	82.9	6.4
1	78.4	39.9	85.5	9.0
2	83.6	45.1	89.7	13.2
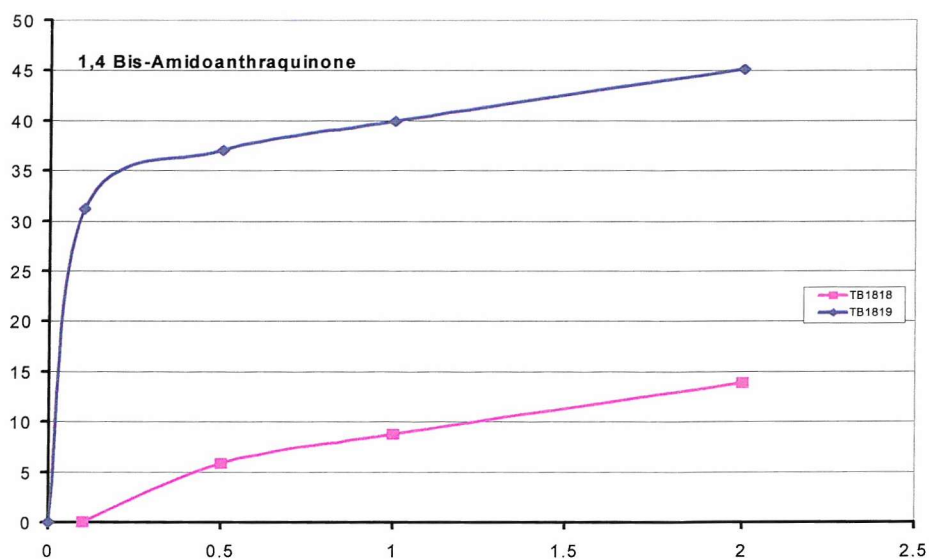
Table 5.4 & Figure 5.11: Table 5.4 shows the Tm and ΔTm values for the oligonucleotides TB1818 and TB1819 in the presence of 1,4 bis-amidoanthraquinone at pH 5. Figure 5.11 illustrates the stability afforded to the duplex-single strand transition of TB1819 and the transition of TB1818. The abscissa represents ligand concentration (μM), and the ordinate represents ΔTm (Celsius).

temperatures prior to the triplex-duplex transition; this could be attributed to the ligand destabilising the triplex and due to the fluorescence of the ligand itself (see discussion for greater detail). Increasing the concentration of 1,4 bis-amidoanthraquinone above 2 μM resulted in the basal fluorescence from the ligand being too large to measure the DNA melting profile. The Tm values for the triplex-duplex transition in the presence of 1,4 bis-amidoanthraquinone are summarised in Table 5.4 and Fig 5.11.

The right hand panel of Fig. 5.10 illustrates the melting profiles of the intramolecular duplex TB1819 with increasing concentrations of 1,4 bis-amidoanthraquinone. The profile in the absence of ligand has already been described. On adding the ligand (0.1 - 0.5 μM) the curves are shifted to higher temperatures, with an increase in the duplex-single strand transition of 6.4 °C with 0.5 μM ligand. Increasing the concentration of the ligand to 1 - 2 μM results in an increase in fluorescence, which is presumably due to the fluorescence of the ligand itself. However it is clear that at these concentrations the curves are shifted to higher temperatures. 2 μM ligand increases the duplex-single strand transition by 12.2 °C. Increasing the ligand concentration to 5 μM and 10 μM resulted in significantly higher levels of fluorescence that obscured the duplex-single strand transition and are therefore not shown. The Tm values for the duplex-single strand transitions are summarised in Table 5.4 and Fig. 5.11.

The results indicate that 1,4 bis-amidoanthraquinone induces significant stabilisation of both the triplex-duplex and the duplex-single strand transitions, demonstrating low selectivity. However its effect on the triplex DNA is unusual and very different from that of naphthylquinoline. These results will be considered in greater detail in the discussion.

(5.4.3)   1,5 Bis-Amidoanthraquinone.

The graph presented in the left hand panel of Fig. 5.12 shows the thermal denaturation profiles of the intramolecular triplex TB1818 in the presence of an increasing concentration of 1,5 bis-amidoanthraquinone. The profile in the absence of
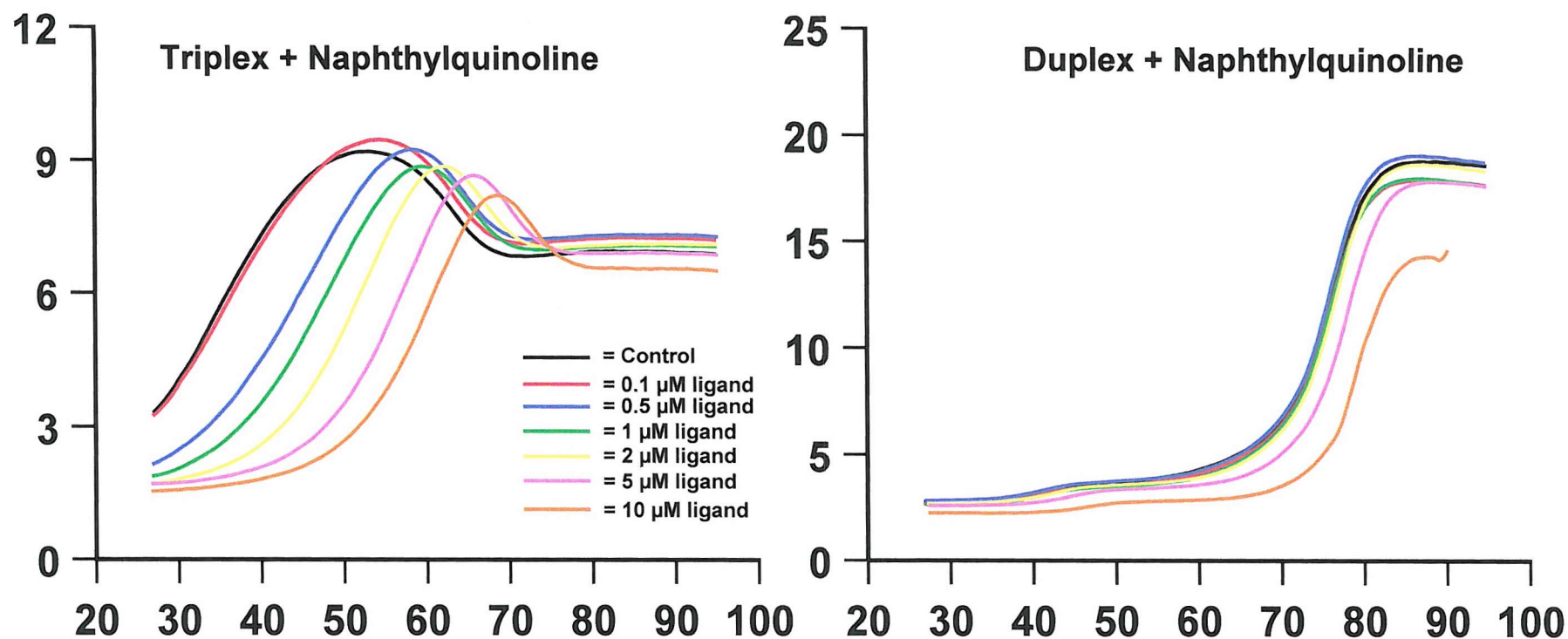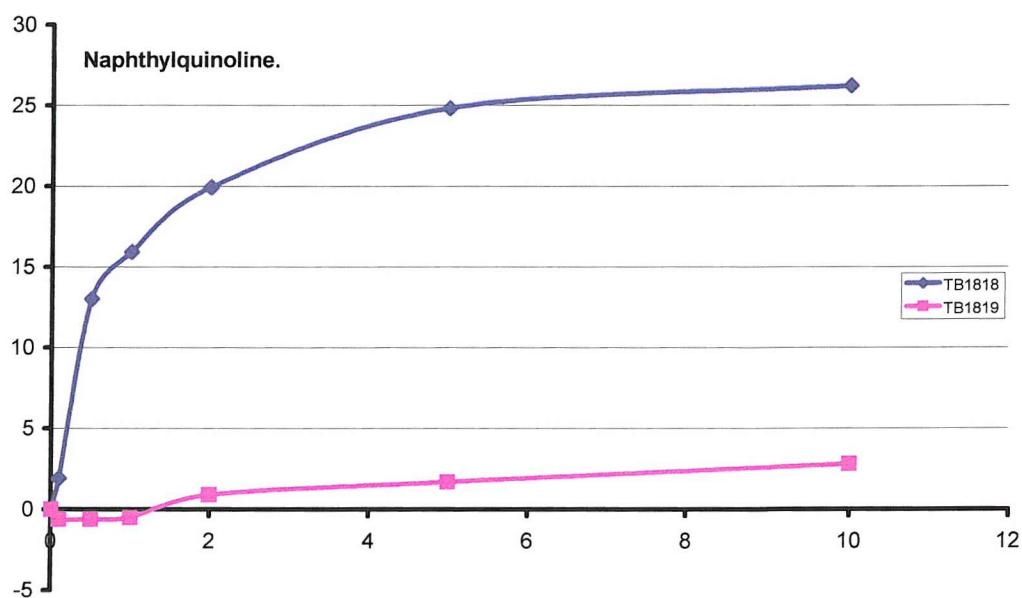
Figure 5.12: Fluorescent DNA thermal denaturation profiles generated with oligonucleotides TB1818 (left) and TB1819 (right) in the presence of an increasing concentration of 1,5 bis-amidoanthraquinone at pH 5. The ordinate represents fluorescence (arbitary units) and the abscissa represents temperature (Celsius).

1,5	TB1818 Transition 1		TB1818 Transition 2	
Concentration (µM)	Tm (°C)	ΔTm (°C)	Tm (°C)	ΔTm (°C)
0	36.2	/	/	/
0.1	41.3	5.1	/	/
0.5	43.1	6.9	74.2	38
1	43.4	7.2	76.0	39.8
2	/	/	80.5	44.3
	Duplex-single strand Transition (TB1819)			
	Tm (°C)		ΔTm (°C)	
0	76.6		/	
0.1	77.5		0.9	
0.5	80.3		3.7	
1	83.3		6.7	
2	86.6		10	

Table 5.5 & Figure 5.13: Table 5.5 shows the Tm and ΔTm values for the oligonucleotides TB1818 and TB1819 in the presence of 1,5 bis-amidoanthraquinone at pH 5. / indicates non-determined value. Figure 5.13 illustrates the stability afforded to the first transition of TB1818, and the duplex-single strand transition (TB1819). The abscissa represents ligand concentration (µM), and the ordinate represents ΔTm (Celsius).

ligand has already been described . Adding the ligand at a concentration of 0.1 µM results in a decrease in the maximum fluorescence (around 60 °C) and shifts the triplex-duplex transition to a higher temperature with a ΔTm of 5.1 °C. However it can be seen that the shape of the profile is also altered with the appearance of a small second transition between 70 - 80 °C. Increasing the ligand concentration to 0.5 - 1 µM accentuates the second transition, whilst the intensity of the original triplex-duplex transition is diminished. The addition of 1 µM stabilised the triplex-duplex transition by 7.2 °C. Increasing the concentration of 1,5 bis-amidoanthraquinone to 2 µM increases the initial fluorescence, and abolishes transition 1 whilst, the second transition has shifted to a higher temperature, with a Tm of 80.5 °C, which is 6.3 °C higher than that seen with 0.5 µM ligand. The Tm values for these transitions are summarised in Table 5.5 and Fig. 5.13.

The right hand panel of Fig. 5.12 illustrates the melting profiles of TB1819 in the presence of increasing concentrations of 1,5 bis-amidoanthraquinone. Adding the ligand at a concentration of 0.1 µM does not significantly alter the melting profile with a small increase in Tm of 0.9 °C. Further increasing the ligand concentration shifts the transitions to higher temperatures. At a concentration of 2 µM the initial level of fluorescence is increased as a result of the intrinsic fluorescence of the ligand itself. 2 µM ligand increased the duplex-single strand transition by 10 °C. All of these Tm values are summarised in Table 5.5 and Fig. 5.13. This ligand appears to bind to triplex DNA better than duplex DNA.

(5.4.4)   1,8 Bis-Amidoanthraquinone.

The left hand panel of Fig. 5.14 shows the thermal denaturation profiles of TB1818 with increasing concentrations of 1,8 bis-amidoanthraquinone. It can be seen that adding the ligand at a concentration of 0.1 µM does not alter the profile, however with 0.5 µM the maximum fluorescence (55 °C) is decreased. The addition of both 0.5 µM and 1 µM ligand clearly increases the stability of the triplex-duplex transition. At concentrations of 1 µM and above the triplex-duplex transition is shifted to successively
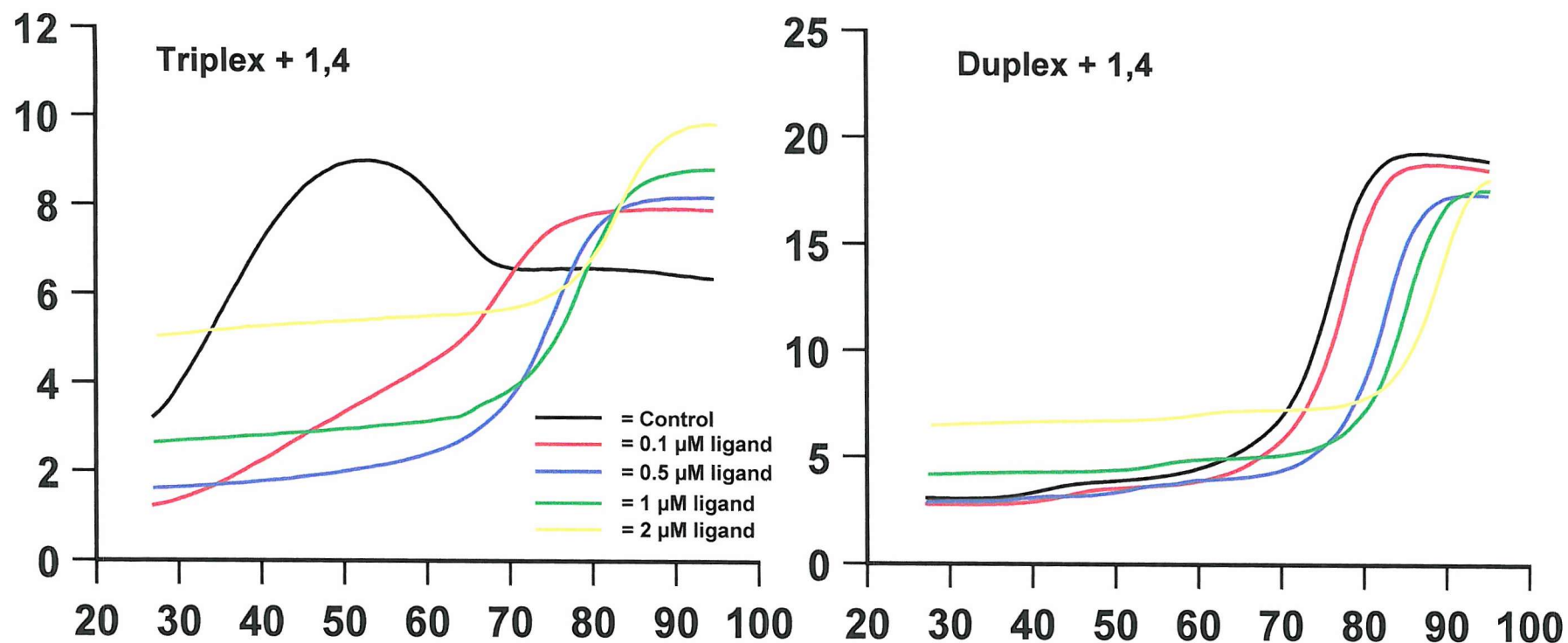
Figure 5.14: Fluorescent DNA thermal denaturation profiles generated with oligonucleotides TB1818 (left) and TB1819 (right) in the presence of an increasing concentration of 1,8 bis-amidoanthraquinone at pH 5. The ordinate represents fluorescence (arbitary units) and the abscissa represents temperature (Celsius).

1,8 Concentration (μM)	(TB1818) Transition 1		(TB1818) Transition 2	
	Tm (°C)	Δ Tm (°C)	Tm (°C)	Δ Tm (°C)
0	36.9	/	/	/
0.1	36.0	-0.9	/	/
0.5	43.7	6.8	/	/
1	49.1	12.2	/	/
2	50.2	13.3	70.3	33.4
5	57.4	20.5	69.0	33.1
10	/	/	73.2	36.3

	(TB1819) Duplex-single strand Transition	
	Tm (°C)	Δ Tm (°C)
0	77.2	/
0.1	76.9	-0.3
0.5	77.2	0
1	77.4	0.2
2	77.6	0.4
5	78.4	1.2
10	80.8	3.7

Table 5.6 & Figure 5.15: Table 5.6 shows the Tm and Δ Tm values for the oligonucleotides TB1818 and TB1819 in the presence of 1,8 bis-amidoanthraquinone at pH 5. / indicates non-determinable value. Figure 5.15 illustrates the stability afforded to the first transition of TB1818 and the duplex-single strand transition (TB1819). The abscissa represents ligand concentration (μM), and the ordinate represents ΔTm (Celsius).

higher temperatures and a small second transition is evident between 70 - 80°C. 5 µM ligand increases the triplex-duplex transition by 20.5°C. However at a ligand concentration of 10 µM both transitions overlap and prevent unambiguous determination of the Tm values. The Tm values can be seen summarised in Table 5.6 and Fig. 5.15.

The right hand panel of Fig. 5.14 shows the thermal denaturation profiles of TB1819 with increasing concentrations of 1,8 bis-amidoanthraquinone. It can be seen that there is very little difference in the profiles of the control and ligand concentrations of 0.1 - 2 µM, with Tm values similar to that of the control, 77.2°C. Increasing the concentration of the ligand to 5 µM shifts the duplex-single strand transition to a higher temperature, an increase of 1.2°C. At 10 µM ligand the initial fluorescence is higher than in any other curve and is presumably due to the fluorescence of the ligand. The transition is shifted to a higher temperature, with an increase in the Tm of 3.6°C. The Tm values for these transitions are summarised in Table 5.6 and Fig. 5.15. It can be seen that this ligand has a much greater effect on triplex than duplex DNA.

(5.4.5)   2,6 Bis-Amidoanthraquinone.

The left hand panel of Fig. 5.16 shows the melting profiles of oligonucleotide TB1818 with increasing concentrations of 2,6 bis-amidoanthraquinone. It can be seen that the profiles generated with ligand concentrations of 0 - 1 µM are very similar, with Tm values of 36.2°C in the absence of ligand, 40.4°C at a concentration of 1 µM, an increase of 4.2°C. Increasing the concentration of ligand to 2 µM decreases the maximum fluorescence and shifts the triplex-duplex transition to a higher temperature. At ligand concentrations of 5 - 10 µM there is a significant change in the shape of the curve and two transitions are evident. In the presence of 10 µM ligand the triplex-duplex transition was increased by 20.2°C. The triplex-duplex transitions are summarised in Table 5.7 and Fig. 5.17.
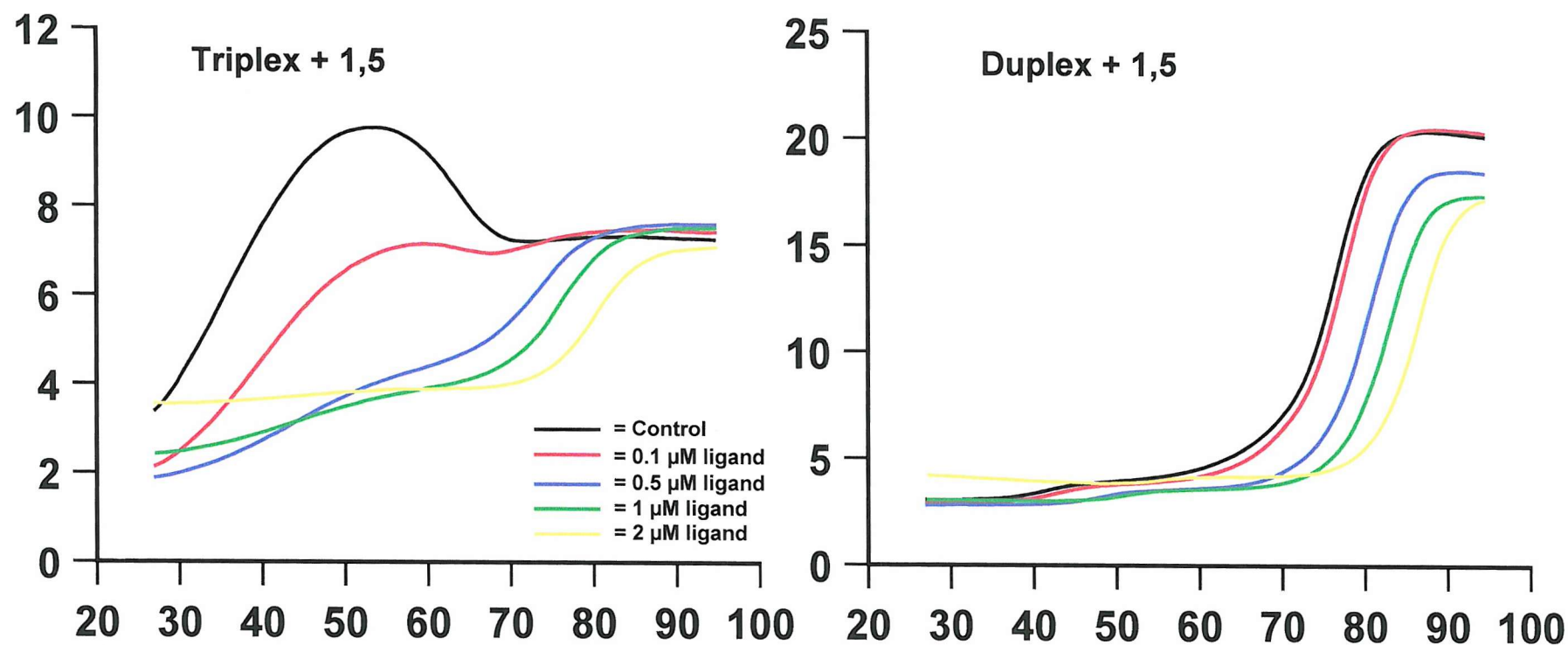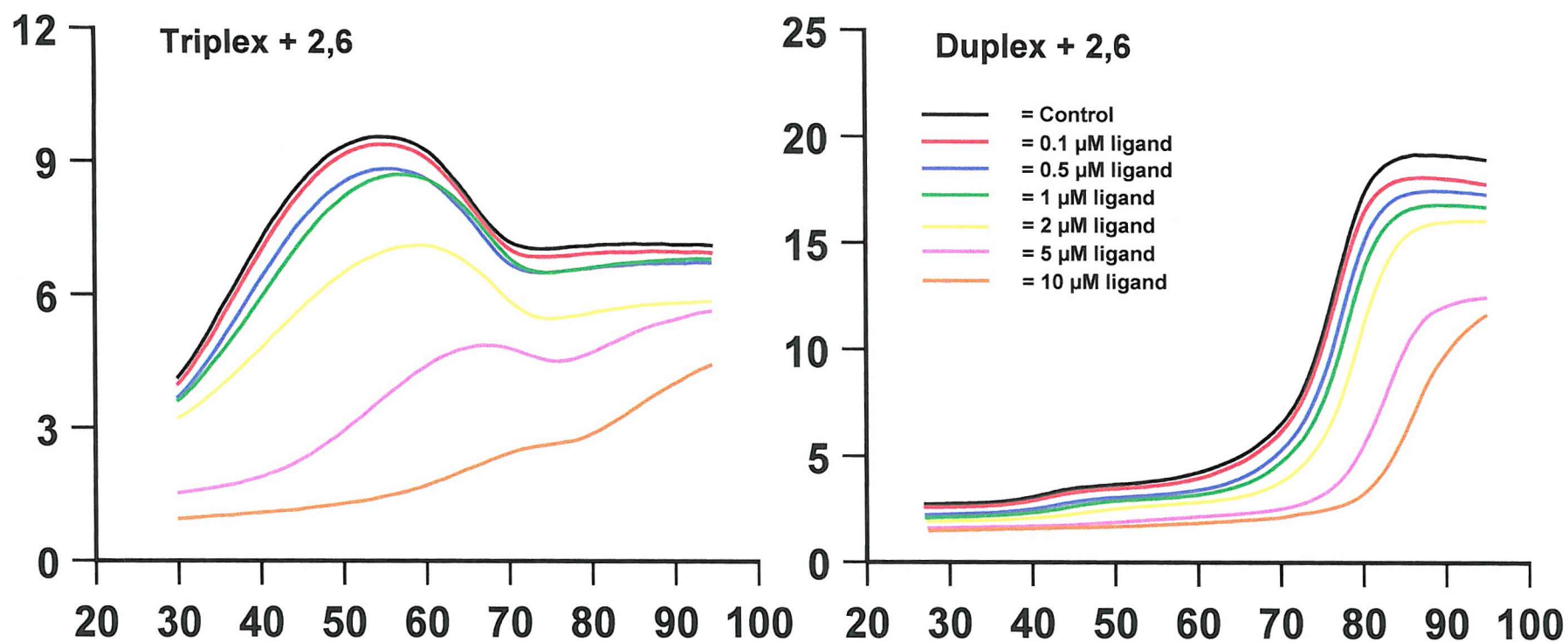
Figure 5.16: Fluorescent DNA thermal denaturation profiles generated with oligonucleotides TB1818 (left) and TB1819 in the presence of an increasing concentration of 2,6 bis-amidoanthraquinone at pH 5. The ordinate represents fluorescence (arbitary units) and the abscissa represents temperature (Celsius).

2,6	TB1818 Transition 1		TB1818 Transition 2	
Concentration (μM)	Tm (°C)	ΔTm (°C)	Tm (°C)	ΔTm (°C)
0	36.2	/	/	/
0.1	36.5	0.3	/	/
0.5	38.1	1.9	/	/
1	40.4	4.2	/	/
2	41.1	4.9	/	/
5	45.7	9.5	83.3	47.1
10	56.4	20.2	84.5	48.3
	Duplex-single strand Transition (TB1819)			
	Tm (°C)		ΔTm (°C)	
0	76.6		/	
0.1	77.0		0.4	
0.5	77.6		1.0	
1	78.3		1.7	
2	79.4		2.8	
5	83.1		6.5	
10	86.3		6.7	

Table 5.7 & Figure 5.17: Table 5.7 shows the Tm and ΔTm values for the oligonucleotides TB1818 and TB1819 in the presence of 2,6 bis-amidoanthraquinone at pH 5. / indicates non-determined value. Figure 5.17 illustrates the stability afforded to the first transition of TB1818, and the duplex-single strand transition (TB1819). The abscissa represents ligand concentration (μM), and the ordinate represents ΔTm (Celsius).

The right hand panel of Fig. 5.16 illustrates the thermal denaturation profiles of TB1819 with increasing concentrations of 2,6 bis-amidoanthraquinone. It can be seen that adding the ligand at concentrations up to 2 µM induces a small shift in the duplex-single strand transition to higher temperatures, with 2 µM 2,6 bis-amidoanthraquinone increasing the duplex-single strand transition by 2.8 °C. Increasing the concentration of 2,6 bis-amidoanthraquinone to 5 µM and 10 µM shifts the duplex-single strand transition to higher temperatures, with an increase of 9.7 °C with 10 µM ligand. The Tm values for these duplex-single strand transitions are summarised in Table 5.7 and Fig. 5.17. It appears that at low concentrations this ligand has a small preference for triplex over duplex DNA.

(5.4.6)   2,7 Bis-Amidoanthraquinone.

The left hand panel of Fig. 5.18 illustrates the thermal denaturation profiles generated with increasing concentration of 2,7 bis-amidoanthraquinone. Increasing the concentration of ligand from 0 - 2 µM appears to stabilise the triplex-duplex transition in a concentration dependent manner, however at concentrations above 1 µM a second transition is evident at 75 °C. Increasing the ligand concentration further decreases the maximum in the fluorescence profile, this effect will be considered in the discussion. Increasing the concentration of 2,7 bis-amidoanthraquinone to 5 µM and 10 µM generates significantly different melting profiles, in which the triplex-duplex transition is obscured by the formation of the second transition. Analysis of the melt curves reveals that 5 µM ligand stabilises the triplex-duplex transition by 20.8 °C. The second transition may to be an artifact due to the ligand stabilising both triplex and duplex DNA and is covered in greater detail in the discussion. These triplex-duplex transition Tm values are summarised in Table 5.8 and Fig. 5.19.

The right hand panel of Fig. 5.18 shows the thermal denaturation profiles of oligonucleotide TB1819 with increasing concentrations of 2,7 bis-amidoanthraquinone. Increasing the ligand concentration from 0 µM to 2 µM stabilises the transition by as much as 7.5 °C. Ligand concentrations of 5 µM and above also produce large decreases
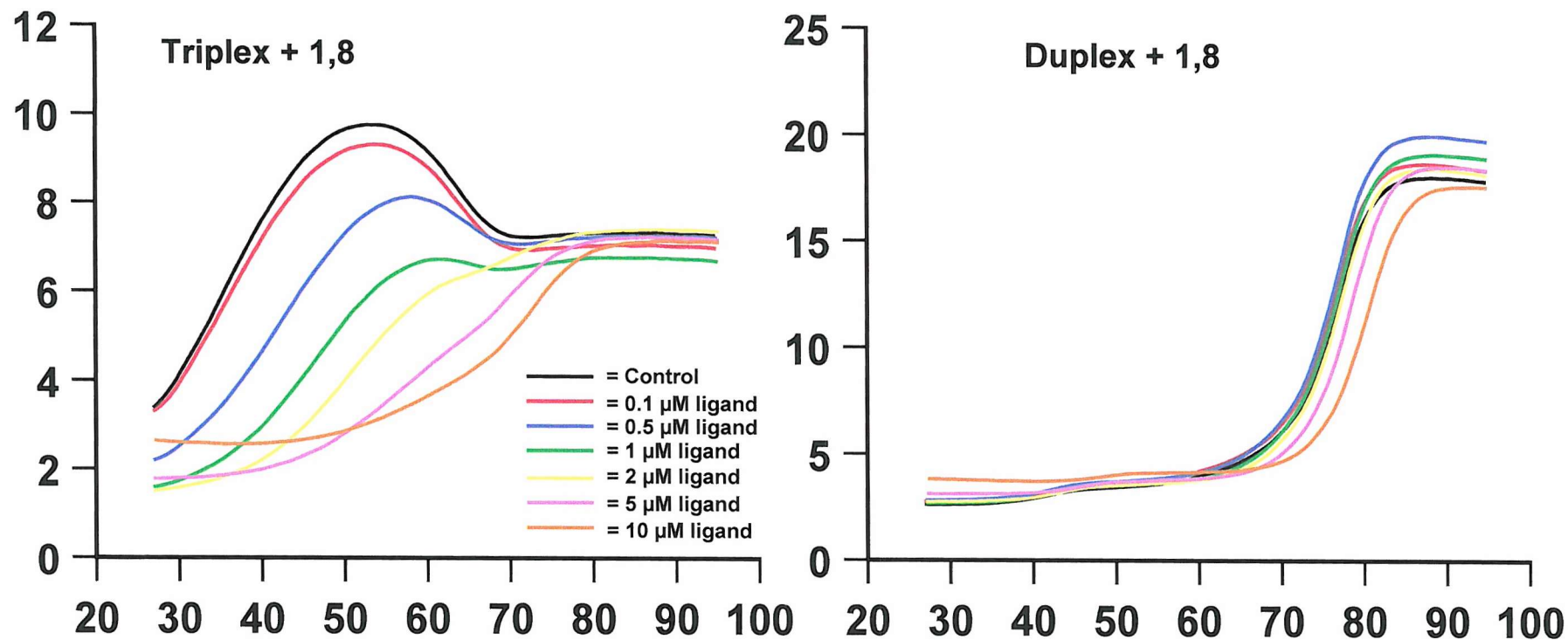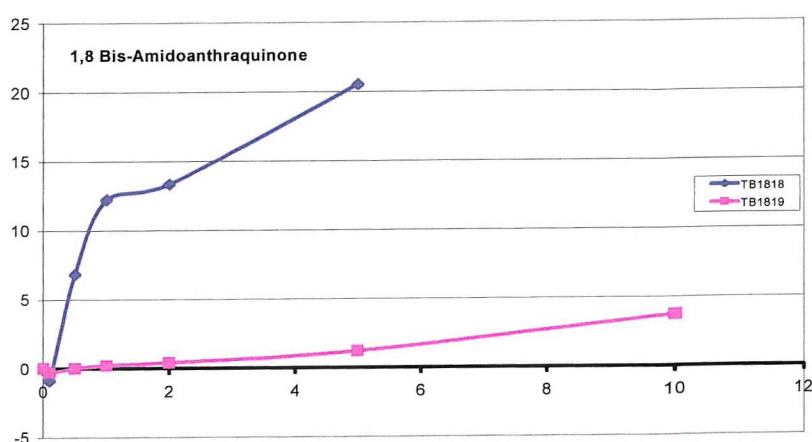
Figure 5.18: Fluorescent DNA thermal denaturation profiles generated with oligonucleotides TB1818 (left) and TB1819 (right) in the presence of an increasing concentration of 2,7 bis-amidoanthraquinone at pH 5. The ordinate represents fluorescence (arbitary units) and the abscissa represents temperature (Celsius).

2,7	TB1818 Transition 1		TB1818 Transition 2	
Concentration (µM)	Tm (°C)	ΔTm (°C)	Tm (°C)	ΔTm (°C)
0	38.0	/	/	/
0.1	45.0	7.0	/	/
0.5	51.7	13.7	/	/
1	53.9	15.9	/	/
2	56.4	18.4	/	/
5	58.5	20.5	83.4	45.4
10	55.4	17.4	86.8	48.8
	Duplex-single strand Transition (TB1819)			
	Tm (°C)		ΔTm (°C)	
0	75.7		/	
0.1	76.9		1.2	
0.5	78.1		2.4	
1	78.3		2.6	
2	80.2		7.5	
5	84.7		9.0	
10	86.8		11.1	

Table 5.8 & Figure 5.19: Table 5.8 shows the Tm and ΔTm values for the oligonucleotides TB1818 and TB1819 in the presence of 2,7 bis-amidoanthraquinone at pH 5. / indicates non-determined value. Figure 5.19 illustrates the stability afforded to the first transition of TB1818 and the duplex-single strand transition (TB1819). The abscissa represents ligand concentration (µM), and the ordinate represents ΔTm (Celsius).

in the maximum fluorescence. The results suggest that 2,7 bis-amidoanthraquinone stabilises the duplex-single strand transition at concentrations above 0.5 μM, and this will be discussed in greater detail in the discussion. The Tm values for the duplex-single strand transition are summarised in Table 5.8 and Fig. 5.19.

(5.4.7)   Alpha and Beta Naphthoflavone.

The triplex stabilising properties of naphthoflavone (Fig. 5.20) were reported by Prof. J.B. Chaires at NACON V, un-published data, and investigated by DNase I footprinting in Chapter 4 of this thesis.

The left hand panel of Fig. 5.21 illustrates the melting profiles of TB1818 with increasing concentrations of alpha naphthoflavone. Addition of 0.1 - 0.5 μM alpha naphthoflavone shifts the triplex-duplex transition to higher temperatures, and reduces the maximum in the fluorescence profile. Increasing the concentration of alpha naphthoflavone to 1 - 5 μM shifts the triplex-duplex transition to higher temperatures, with the transition stabilised by as much as 12.9°C. However 10 μM ligand shifts the triplex-duplex transition to a slightly lower temperature than with both 2 μM and 5 μM alpha naphthoflavone. The Tm values for these triplex-duplex transitions are summarised in Table 5.9 and Fig. 5.22.

The right hand panel of Fig. 5.21 shows the thermal denaturation profiles of TB1819 with increasing concentrations of alpha naphthoflavone. It can be seen that the profiles generated are relatively unaffected by the addition of alpha naphthoflavone. There is a small decrease in the fluorescence between 0 - 5 μM and no shift of the duplex-single strand transition. Increasing the concentration of ligand to 10 μM results in a significant decrease in the maximum fluorescence, but does not shift the duplex-single strand transition. The Tm values for these duplex-single strand transitions are summarised in Table 5.9 and Fig. 5.22.

Alpha Naphthoflavone
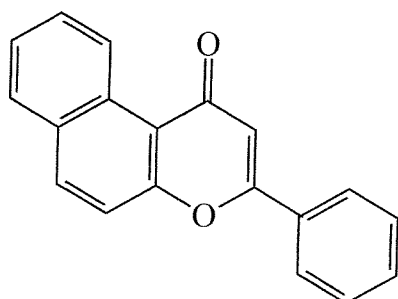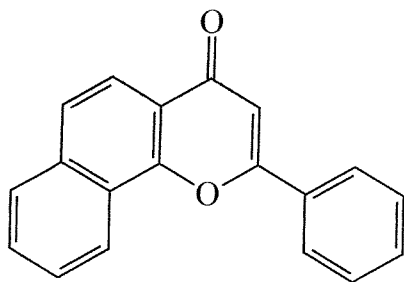
Beta Naphthoflavone

Distamycin A

pKa = 8.6

pKa = 5.7

pKa = 7.6

pKa = 8.1

pKa = 8.8

pKa = 7.6
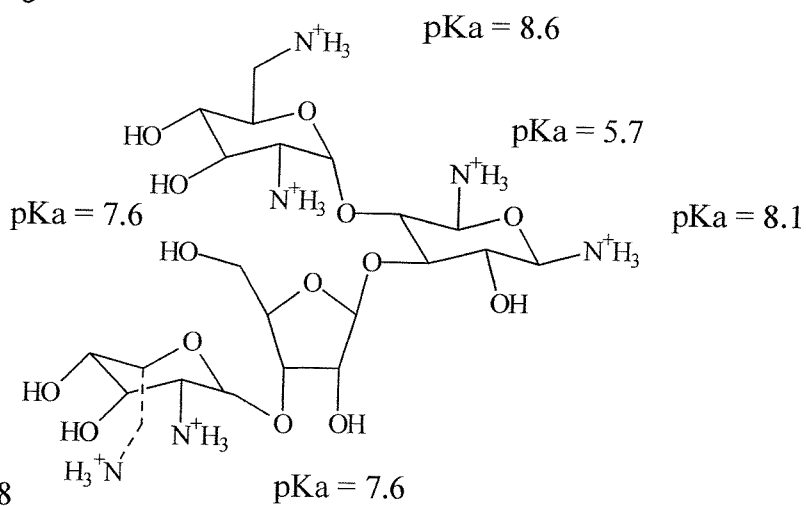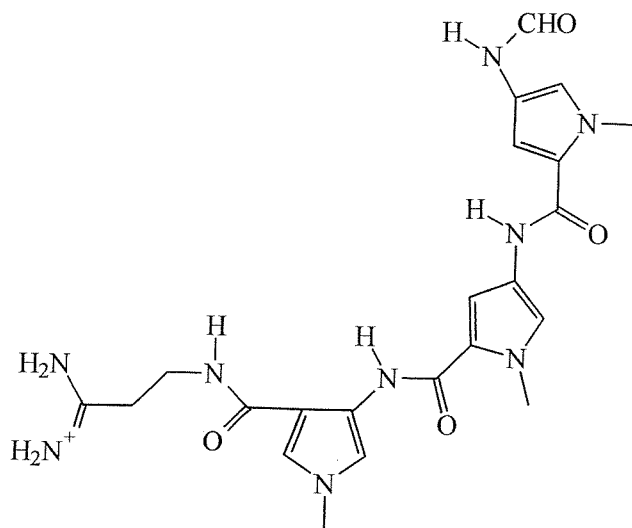
Neomycin

Hoechst 33258

Figure 5.20: Presented above are the structures of some of the triplex and duplex stabilising ligands used in this chapter. The pKa values of the neomycin amino groups are also shown.
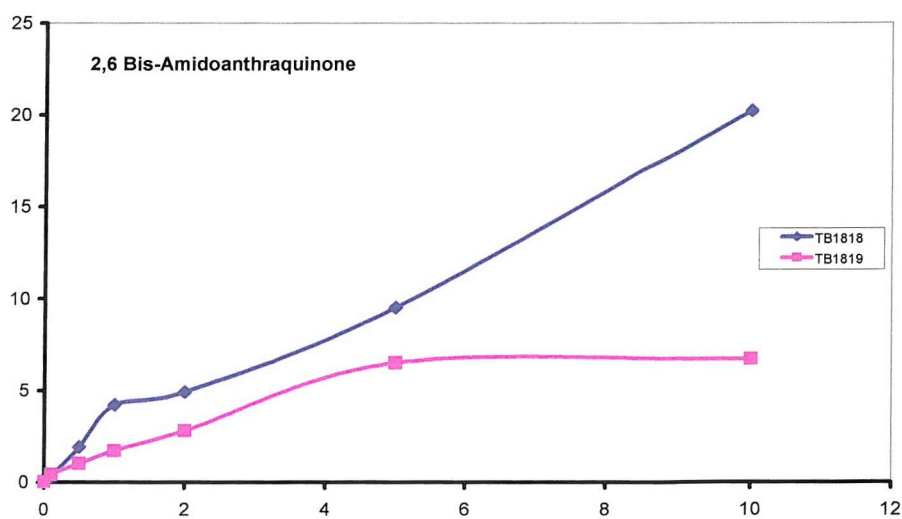
Figure 5.21: Fluorescent DNA thermal denaturation profiles generated with oligonucleotides TB1818 (left) and TB1819 (right) in the presence of an increasing concentration of alpha-naphthoflavone in a pH 5 buffer. The ordinate represents fluorescence (arbitary units) and the abscissa represents temperature (Celsius).

Alpha Naphthoflavone	Triplex-duplex Transition (TB1818)		Duplex-single strand transition (TB1819)	
Concentration (μM)	Tm (°C)	Δ Tm (°C)	Tm (°C)	Δ Tm (°C)
0	37.3	/	76.4	/
0.1	38.1	0.8	76.0	-0.4
0.5	43.4	6.1	76.0	-0.4
1	47.5	10.2	76.5	0.1
2	48.7	11.4	77.1	0.7
5	50.3	12.9	77.0	0.6
10	47.2	9.8	76.7	0.3
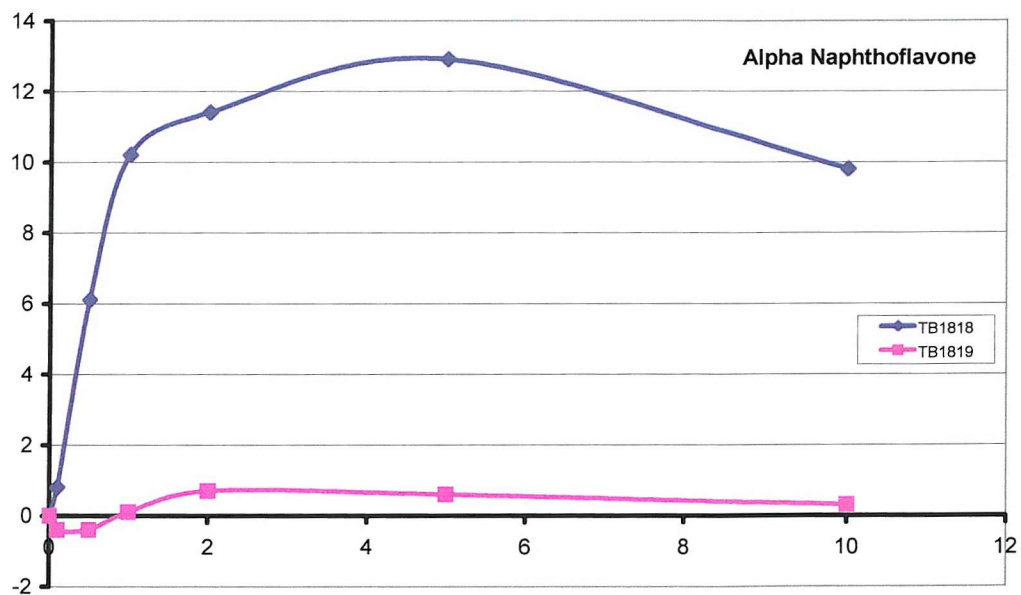
Table 5.9 & Figure 5.22: Table 5.9 shows the Tm and Δ Tm values for the oligonucleotides TB1818 and TB1819 in the presence of alpha-naphthoflavone at pH 5. Figure 5.22 illustrates the stability afforded to the triplex-duplex trabsition (TB1818) and the duplex-single strand transition (TB1819). The abscissa represents ligand concentration (μM), and the ordinate axis represents ΔTm (Celsius).
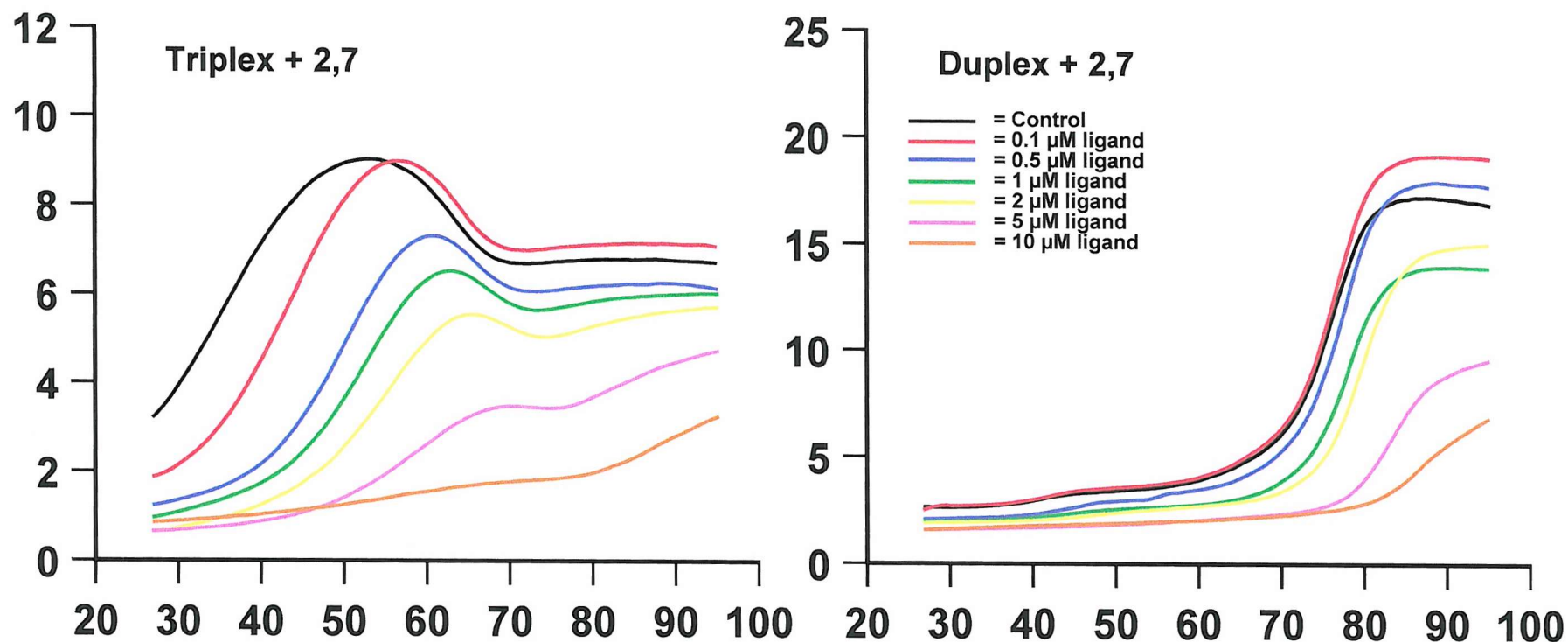
Figure 5.23: Fluorescent DNA thermal denaturation profiles generated with oligonucleotides TB1818 (left) and TB1819 (right) in the presence of an increasing concentration of beta-naphthoflavone in a pH 5 buffer. The ordinate represents fluorescence (arbitary units) and the abscissa represents temperature (Celsius).

Beta-Naphthoflavone	Triplex-duplex Transition (TB1818)		Duplex-single strand Transition (TB1819)	
Concentration (µM)	Tm (°C)	ΔTm (°C)	Tm (°C)	ΔTm (°C)
0	37.7	/	76.6	/
0.1	37.2	-0.5	76.5	-.01
0.5	40.9	3.2	76.3	-0.3
1	44.3	6.6	76.7	0.1
2	44.6	6.9	76.7	0.1
5	43.7	6.0	76.6	0
10	44.4	6.7	76.6	0
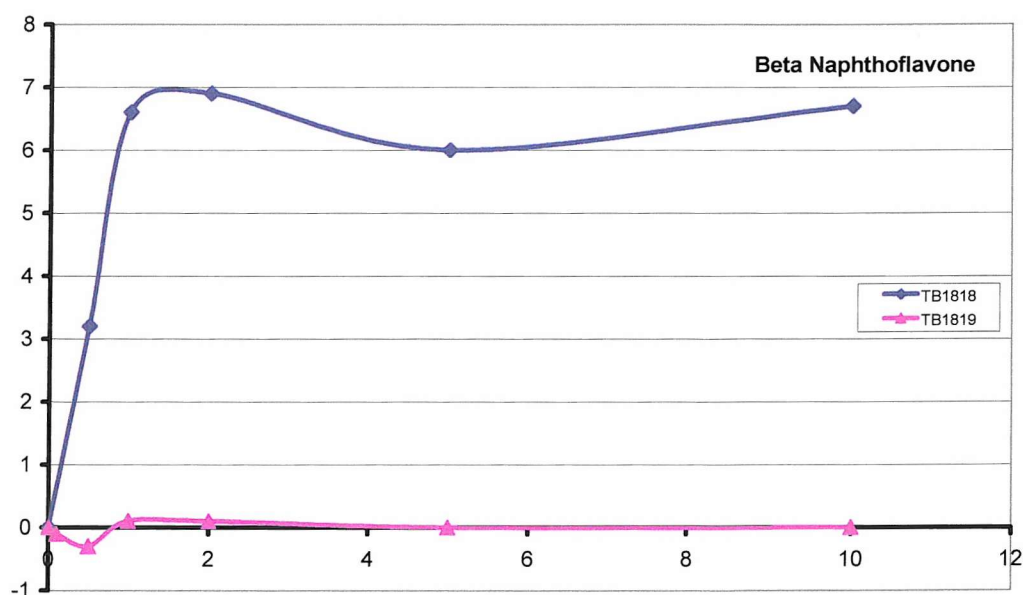
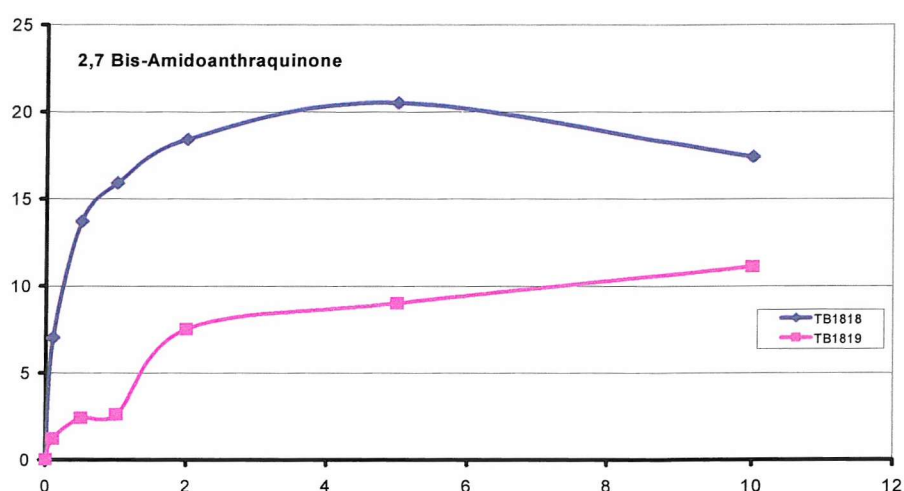**Table 5.10 & Figure 5.24:** Table 5.10 shows the Tm and ΔTm values for the oligonucleotides TB1818 and TB1819 in the presence of beta-naphthoflavone at pH 5. Figure 5.24 illustrates the stability afforded to both the triplex-duplex transition (TB1818), and the duplex-single strand transition (TB1819). The abscissa represents the ligand concentration (µM), and the ordinate represents ΔTm (Celsius).

These results suggest that alpha-naphthoflavone selectively stabilises the triplex-duplex transition at low concentrations.

The left hand panel of Fig. 5.23 illustrates the thermal denaturation profiles of oligonucleotide TB1818 with increasing concentrations of beta naphthoflavone. It can be seen that the ligand shifts the triplex-duplex transition to higher temperatures, and that this is accompanied by a concentration dependent decrease in the maximum fluorescence. The Tm increases up to a ligand concentration of 2 μM; higher ligand concentrations do not produce any further stabilisation. The Tm values for these triplex-duplex transitions are summarised in Table 5.10 and Fig. 5.24.

The right hand panel of Fig. 5.23 shows the melting curves for TB1819 with increasing concentrations of beta naphthoflavone. It can be seen that increasing the ligand concentration to 10 μM does not affect the thermal denaturation profile and that there is no shift in the duplex-single strand transition. The Tm values for these transitions are summarised in Table 5.10 and Fig. 5.24.

These results show that beta-naphthoflavone stabilises the triplex-duplex transition by 6.9°C, but does not significantly affect the duplex-single strand transition.

(5.4.8)   Acridine Derivatives.

The acridine derivatives BR19 and BR20 (Fig. 5.9) were a gift from Prof. S. Neidle, and were designed to stabilise quadruplex DNA.

The left hand panel of Fig. 5.25 shows the thermal denaturation profiles of TB1818 with increasing concentration of the acridine derivative BR19. Addition of 0.1 μM BR19 does not significantly affect the profile. However increasing the ligand concentration to 0.5 - 10 μM induces significant changes to the thermal denaturation profile. Between 0.5 - 2 μM ligand two transitions are generated, in which the first (triplex-duplex) transition occurs at approximately the same temperature as that of

Figure 5.25: Fluorescent DNA thermal denaturation profiles generated with oligonucleotides TB1818 (left) and TB1819 (right) in the presence of an increasing concentration of the acridine derivative BR19 in a pH 5 buffer. The ordinate represents fluorescence (arbitary units) and the abscissa represents temperature (Celsius).

BR19	TB1818 Transition 1		TB1818 Transition 2	
Concentration (µM)	Tm (°C)	ΔTm (°C)	Tm (°C)	ΔTm (°C)
0	36.5	/	/	/
0.1	36.0	- 0.5	/	/
0.5	36.9	0.4	72.4	35.9
1	42.5	6.0	72.6	36.1
2	43.2	6.7	73.9	36.4
5	/	/	77.9	41.4

	Duplex-single strand transition (TB1819)	
	Tm (°C)	ΔTm (°C)
0	76.6	/
0.1	76.6	0
0.5	79.1	2.5
1	80.0	3.4
2	83.9	7.3
5	86.4	9.8
10	90.6	14.0
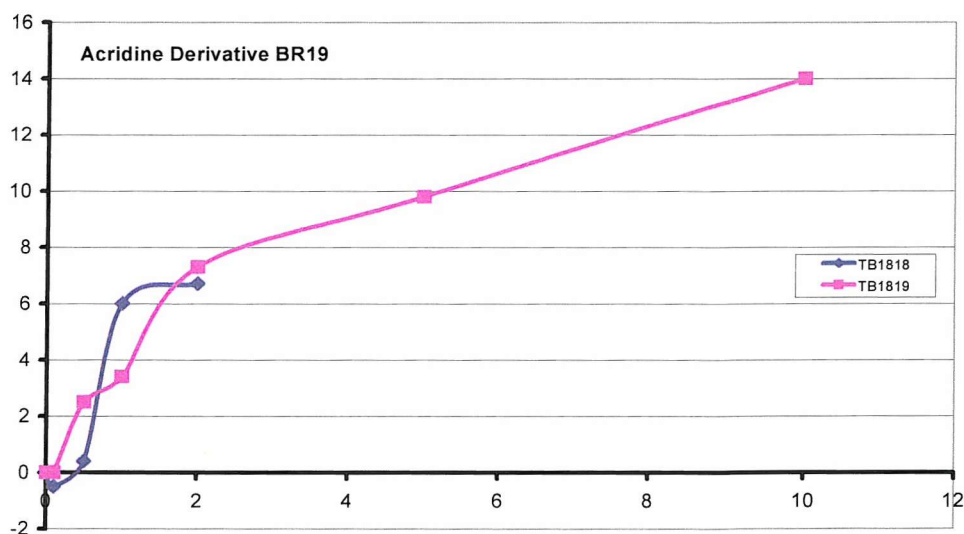
Table 5.11 & Figure 5.26: Table 5.11 shows the Tm and ΔTm values for the oligonucleotides TB1818 and TB1819 in the presence of the acridine derivative BR19 at pH 5. / indicates non-determined value. Figure 5.26 illustrates the stability afforded to the first transition of TB1818, and the duplex-single strand transition (TB1819). The abscissa represents ligand concentration (µM), and the ordinate represents ΔTm (Celsius).

control, though the transition is shallower and the maximum in the fluorescence profile is significantly decreased. The second transition occurs at higher temperatures and appears to correspond to the duplex melt. At BR19 concentrations of 5 μM and above the triplex-duplex transition is abolished, whilst the second transition can be seen to be shifted to higher temperatures. The Tm values for these triplex-duplex transitions are summarised in Table 5.11 and Fig. 5.26.

The right hand panel of Fig. 5.25 shows the thermal denaturation profiles of TB1819 with increasing concentrations of the acridine derivative BR19. Addition of 0.1 μM ligand has a negligible effect on the stability of the DNA duplex. However increasing the concentration of BR19 above 0.1 μM shifts the duplex-single strand transition to higher temperatures in a concentration dependent manner, as well as decreasing the maximum fluorescence. The transition was stabilised by 14.0 °C with 10 μM ligand. The Tm values for the duplex-single strand transitions are summarised in Table 5.11 and Fig. 5.26.

The left hand panel of Fig. 5.27 shows the thermal denaturation profiles of oligonucleotide TB1818 with increasing concentrations of acridine derivative BR20. Addition of 0.1 - 5 μM BR20 generates a second transition at temperatures close to the predicted duplex melt that appears to be stabilised in a concentration dependent manner (covered in greater detail in the discussion). The fluorescence signal of the transition occurring at a lower temperature decreases with an increasing concentration of ligand and the stability increased by 8.0 °C in the presence of 5 μM ligand. The melting profile in the presence of 10 μM BR20 does not show a transition at the lower temperature, whilst the higher temperature transition is stabilised further. In addition the maximum fluorescence is significantly decreased in a ligand dependent fashion. These triplex-duplex transition Tm values are summarised in Table 5.12 and Fig. 5.28.

The right hand panel of Fig. 5.27 shows the thermal denaturation profiles of TB1819 with increasing concentrations of the acridine derivative BR20. It can be seen that the profile moves to progressively higher temperatures with increasing ligand concentrations. This is accompanied by a ligand dependent decrease in the final
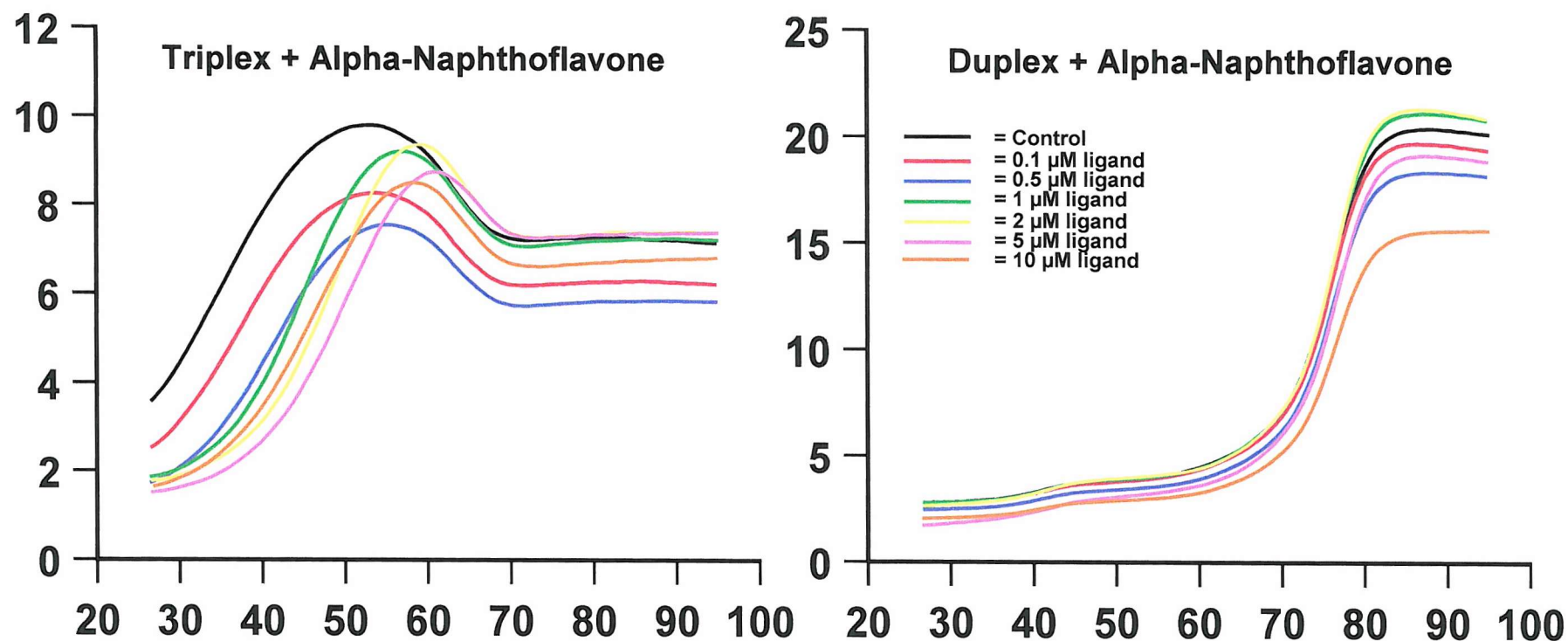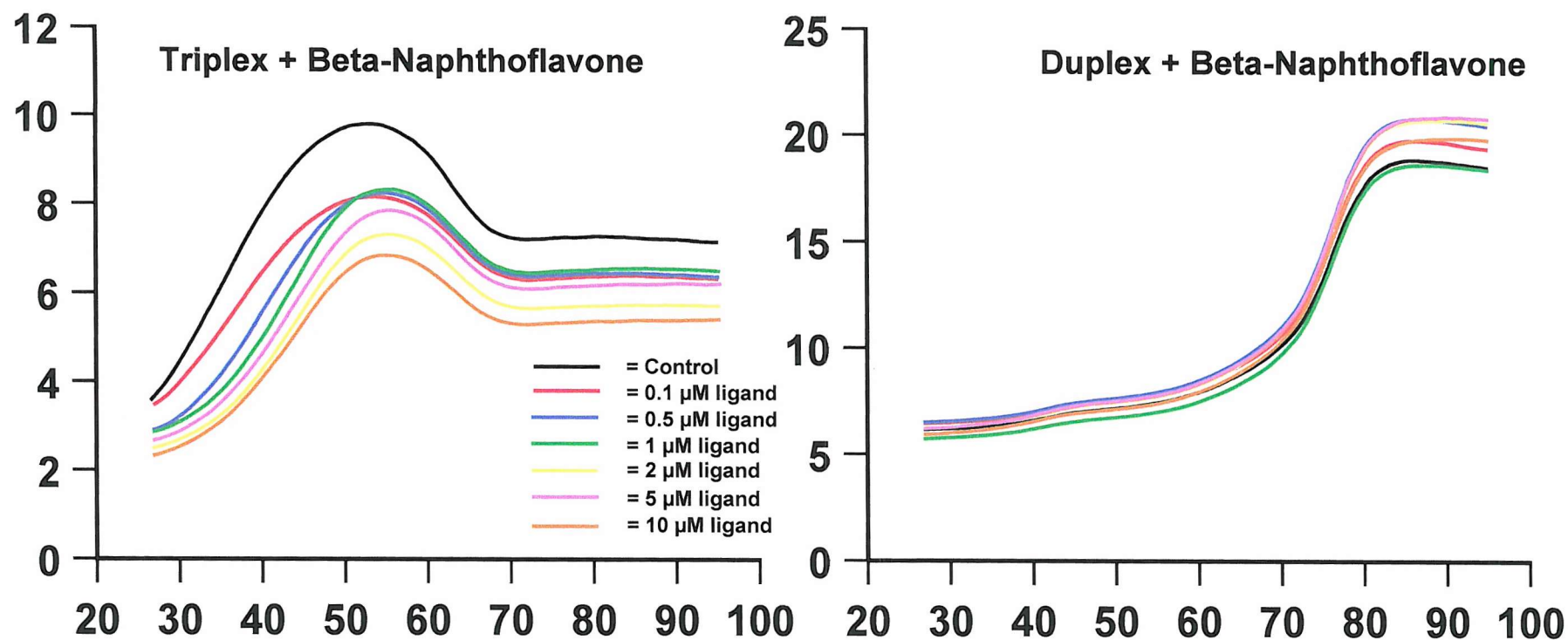
Figure 5.27: Fluorescent DNA thermal denaturation profiles generated with oligonucleotides TB1818 (left) and TB1819 (right) in the presence of an increasing concentration of the acridine derivative BR20 at pH 5. The ordinate represents fluorescence (arbitary units) and the abscissa represents temperature (Celsius).

BR20	TB1818 Transition 1		TB1818 Transition 2	
Concentration (µM)	Tm (°C)	ΔTm (°C)	Tm (°C)	ΔTm (°C)
0	37.8	/	/	/
0.1	36.3	- 1.5	/	/
0.5	37.5	- 0.3	/	/
1	43.3	5.5	75.6	37.8
2	43.3	5.5	75.6	37.8
5	45.8	8.0	78.0	40.2
10	/	/	84	46.2
	Duplex-single strand Transition (TB1819)			
	Tm (°C)		ΔTm (°C)	
0	77.0		/	
0.1	76.9		- 0.1	
0.5	78.2		1.2	
1	84.0		7.0	
2	84.0		7.0	
5	86.7		9.7	
10	88.5		11.5	

Table 5.12 & Figure 5.28: Table 5.12 shows the Tm and ΔTm values for the oligonucleotides TB1818 and TB1819 in the presence of the acridine derivative BR20 at pH 5.0. / indicates non-determined value. Figure 5.28 illustrates the stability afforded to the first transition of TB1818, and the duplex-single strand transition (TB1819). The abscissa represents the ligand concentration (µM), and the ordinate represents ΔTm (Celsius).

fluorescence. These duplex-single strand transition Tm values are summarised in Table 5.12 and Fig. 5.28.

These results suggest that both acridine derivatives BR19 and BR20 stabilise the triplex-duplex transition and the duplex-single strand transition. This will be considered in greater detail in the discussion.

(5.4.9)   Neomycin Sulphate.

The aminoglycoside neomycin sulphate (Fig. 5.20) has been reported to selectively stabilise T·AT triplex DNA (Arya & Coffee Jr. 2000, Ayra *et al* 2001). Its structure prevents intercalation, and it has therefore been suggested that it binds to one of the triplex grooves.

The left hand panel of Fig. 5.29 illustrates the melting profiles of oligonucleotide TB1818 in the presence of increasing concentrations of the aminoglycoside neomycin. It can be seen that addition of neomycin causes a shift of the triplex-duplex transition to higher temperatures, as well as a concentration dependent decrease in the maximum fluorescence. The triplex-duplex transition was stabilised by 23.5 °C at a ligand concentration of 10 µM. The Tm values for these triplex-duplex transitions are summarised in Table 5.13 and Fig. 5.30.

The right hand panel of Fig. 5.29 shows the DNA melting profiles of the oligonucleotide TB1819 with increasing concentrations of neomycin. Addition of the ligand decreases the maximum fluorescence in a concentration dependent manner, but has little effect on the Tm of the duplex-single strand transition, stabilising the duplex by only 1.6 °C in the presence of 10 µM ligand. The Tm values are summarised in Table 5.13 and Fig. 5.30.

These results suggest that neomycin stabilises the triplex-duplex transition, but has little effect on the duplex-single strand transition. This is covered in greater detail in
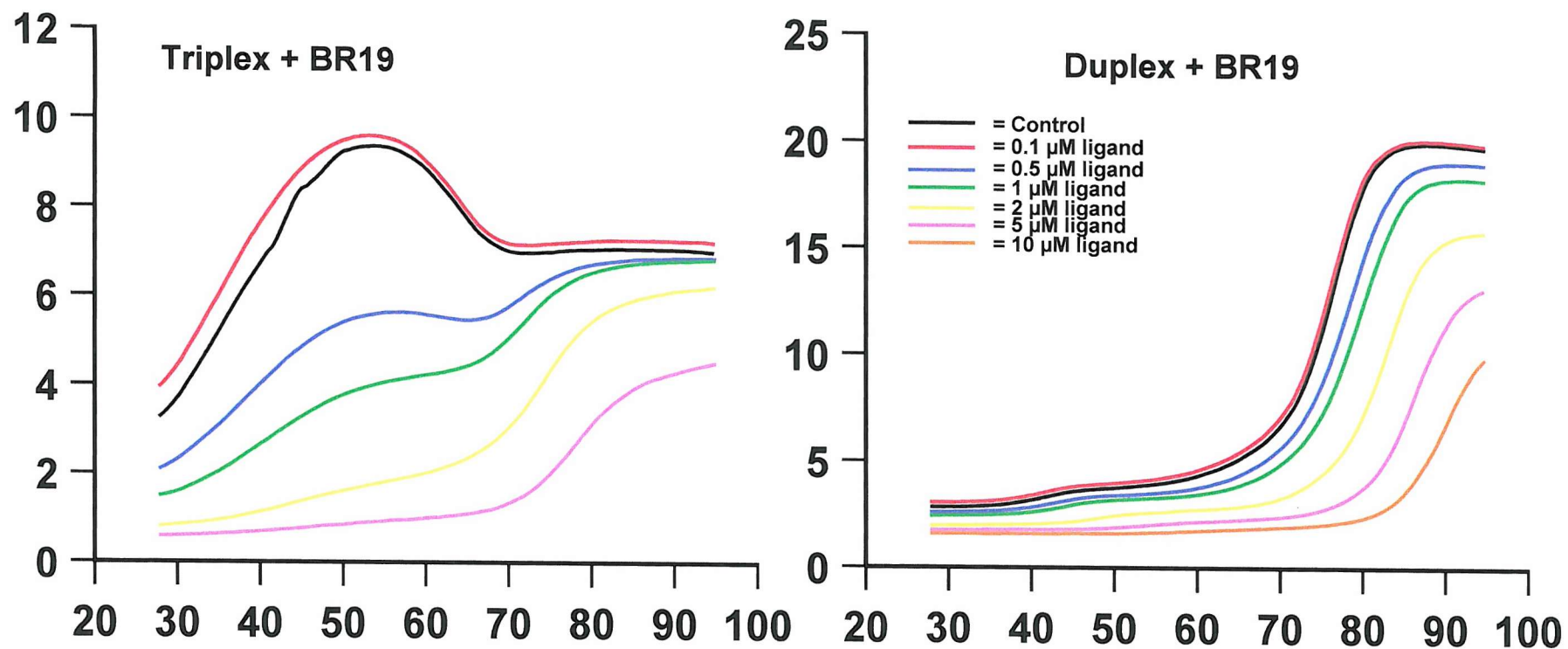
Figure 5.29: Fluorescent DNA thermal denaturation profiles generated with oligonucelotides TB1818 (left) and TB1819 (right) in the presence of an increasing concentration of neomycin sulphate in a pH 5 buffer. The ordinate represents fluorescence (arbitary units) and the abscissa represents temperature (Celsius).

Neomycin Sulphate	Triplex-duplex Transition (TB1818)		Duplex-single strand Transition (TB1819)	
Concentration (μM)	Tm (°C)	ΔTm (°C)	Tm (°C)	ΔTm (°C)
0	35.9	/	78.3	/
0.1	40.0	4.1	78.3	0
0.5	47.8	11.9	78.6	0.3
1	50.2	14.3	78.6	0.3
2	53.3	17.1	79.1	0.8
5	57.5	21.3	79.5	1.2
10	59.7	23.5	79.9	1.6

Table 5.13 & Figure 5.30: Table 5.13 shows the Tm and ΔTm values for the oligonucleotides TB1818 and TB1819 in the presence of neomycin sulphate at pH 5. Figure 5.30 illustrates the stability afforded to the triplex-duplex transition (TB1818), and the duplex-single strand transition (TB1819). The abscissa represents ligand concentration (μM), and the ordinate represents ΔTm (Celsius).

the discussion.

(5.4.10)   Ethidium Bromide.

Ethidium bromide is a well known duplex DNA intercalating ligand (Waring *et al* 1965, 1966). However it has also been shown to stabilise poly(A)·2poly(T) DNA to a higher degree than poly(A)·poly(T) DNA (Scaria & Shfer 1991).

The left hand panel of Fig. 5.3.1 shows the melting profiles of oligonucleotide TB1818 in the presence of increasing concentrations of ethidium bromide. It can be seen that the ligand induces a significant shift of the triplex-duplex transition to higher temperatures in a concentration dependent manner, stabilising by 33.1 °C in the presence of 10 μM ligand. These Tm values are summarised in Table 5.14 and Fig. 5.32.

The right hand panel of Fig. 5.31 illustrates the thermal denaturation profile of oligonucleotide TB1819 in the presence of increasing concentrations of ethidium bromide. It can be seen that the addition of ethidium bromide at concentrations up to 5 μM does not affect the stability of the duplex-single strand transition. Even increasing the concentration to 10 μM only produces a ΔTm of 0.8 °C. The Tm values for these duplex-single strand transitions are summarised in Table 5.14 and Fig. 5.32.

The results suggest that under these conditions ethidium bromide stabilises the triplex-duplex transition in a concentration dependent fashion, but that it has little effect on the duplex-single strand transition. At first sight the results with the duplex DNA are surprising since ethidium is a well known duplex DNA binding agent, that causes changes in UV melting profiles. We suggest that this is because this sequence contains a block of $A_n \cdot T_n$, which is known to be a poor intercalation site, and this will be discussed in greater detail in the discussion.
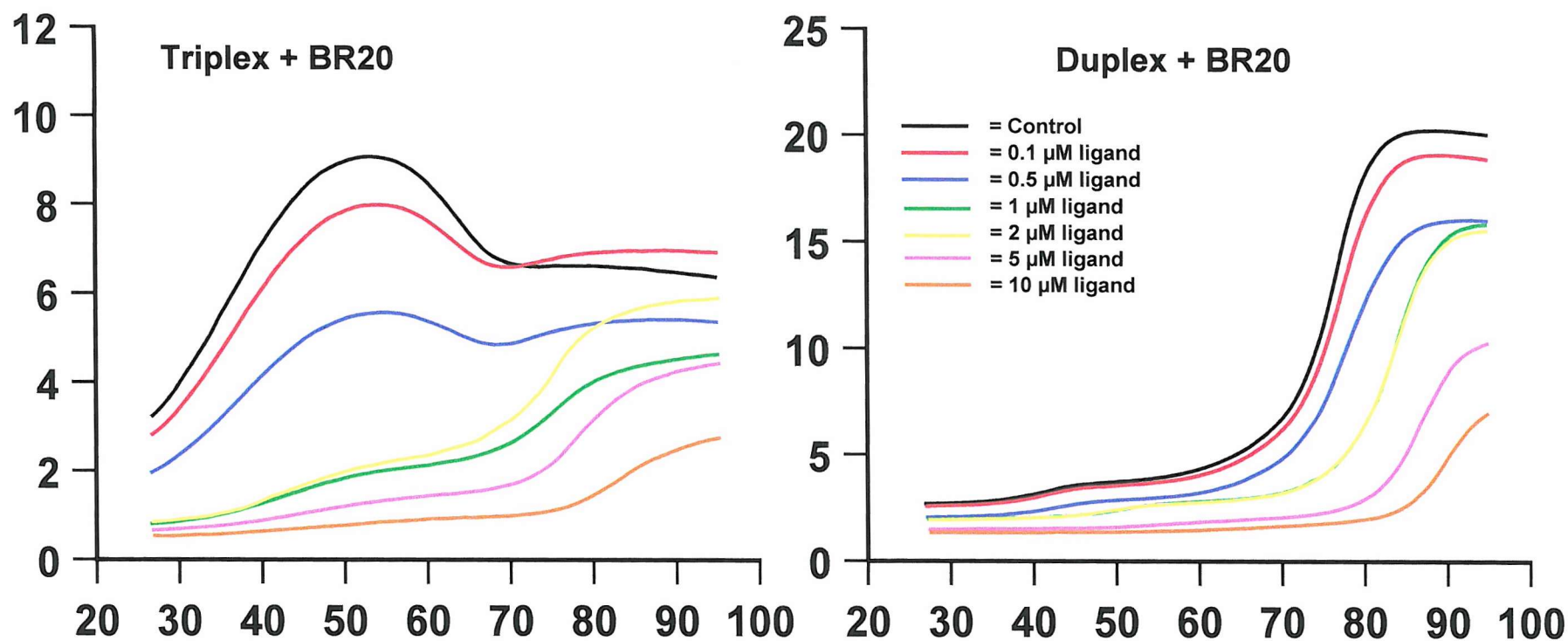
Figure 5.31: Fluorescent DNA thermal denaturation profiles generated with oligonucleotides TB1818 (left) and TB1819 in the presence of an increasing concentration of ethidium bromide in a pH 5 buffer. The ordinate represents fluorescence (arbitary units) and the abscissa represents temperature (Celsius).

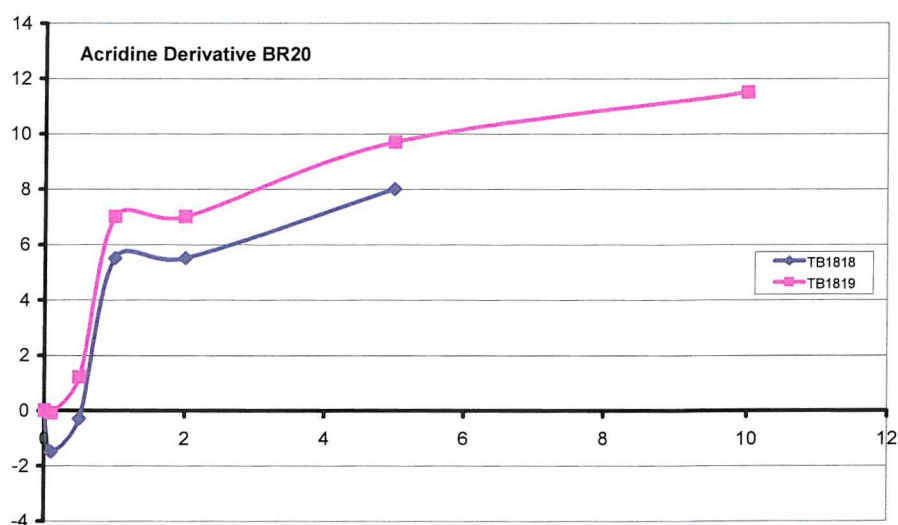| Ethidium Bromide	Triplex-duplex Transition (TB1818)		Duplex-single strand transition (TB1819)	
Concentration (μM)	Tm (°C)	ΔTm (°C)	Tm (°C)	ΔTm (°C)
0	36.5	/	77.3	/
0.1	36.4	- 0.1	77.1	-0.2
0.5	37.7	1.2	77.4	0.1
1	38.7	2.2	77.4	0.1
2	42.7	6.2	77.6	0.3
5	67.5	31	77.8	0.5
10	69.6	33.1	78.1	0.8

Table 5.14 & Figure 5.32: Table 5.14 shows the Tm and ΔTm values for oligonucleotides TB1818 and TB1819 in the presence of ethidium bromide at pH 5. Figure 5.32 illustrates the stability afforded to the triplex-duplex transition (TB1818), and the duplex-single strand transition (TB1819). The abscissa represents ligand concentration (μM), and the ordinate represents ΔTm (Celsius).

(5.4.11)   Hoechst 33258

Hoechst 33258 is a synthetic minor groove binding ligand (Fig. 5.20). Previous studies have concluded that Hoechst 33258 binds to A:T but not G:C base pairs, with a preference for 4 consecutive A:T base pairs (Harshman & Dervan 1985, Drobyshev *et al* 1999).

The left hand panel of Fig. 5.33 illustrates the thermal denaturation profiles of oligonucleotide TB1818 with increasing concentrations of the minor groove binding ligand Hoechst 33258. It can be seen that adding ligand at concentrations up to 1 μM shifts the triplex-duplex transition to lower temperatures, whereas the second (duplex) melt is stabilised in a concentration dependent manner. The triplex-duplex transition was destabilised by as much as 6.6°C with 0.5 μM ligand. However increasing the concentration of the ligand above 1 μM resulted in stabilisation of the triplex-duplex transition (results not shown), suggesting a second mode of binding for Hoechst 33258. These triplex-duplex transition Tm values are summarised in Table 5.15 and Fig. 5.34.

The right hand panel of Fig. 5.33 shows the DNA melting profile of oligonucleotide TB1819 with increasing concentrations of Hoechst 33258. It can be seen that increasing concentrations of Hoechst 33258 induces a concentration dependent shift of the duplex-single strand transition to higher temperatures, with a ΔTm of 13.5°C in the presence of 10 μM ligand. These duplex-single strand transition Tm values are summarised in Table 5.15 and Fig. 5.34.

These results indicate that Hoechst 33258 stabilises the duplex-single strand transition by as much as 13.5°C in a concentration dependent fashion. In contrast Hoechst 33258 appears to destabilise the triplex-duplex transition below a concentration of 1 μM.
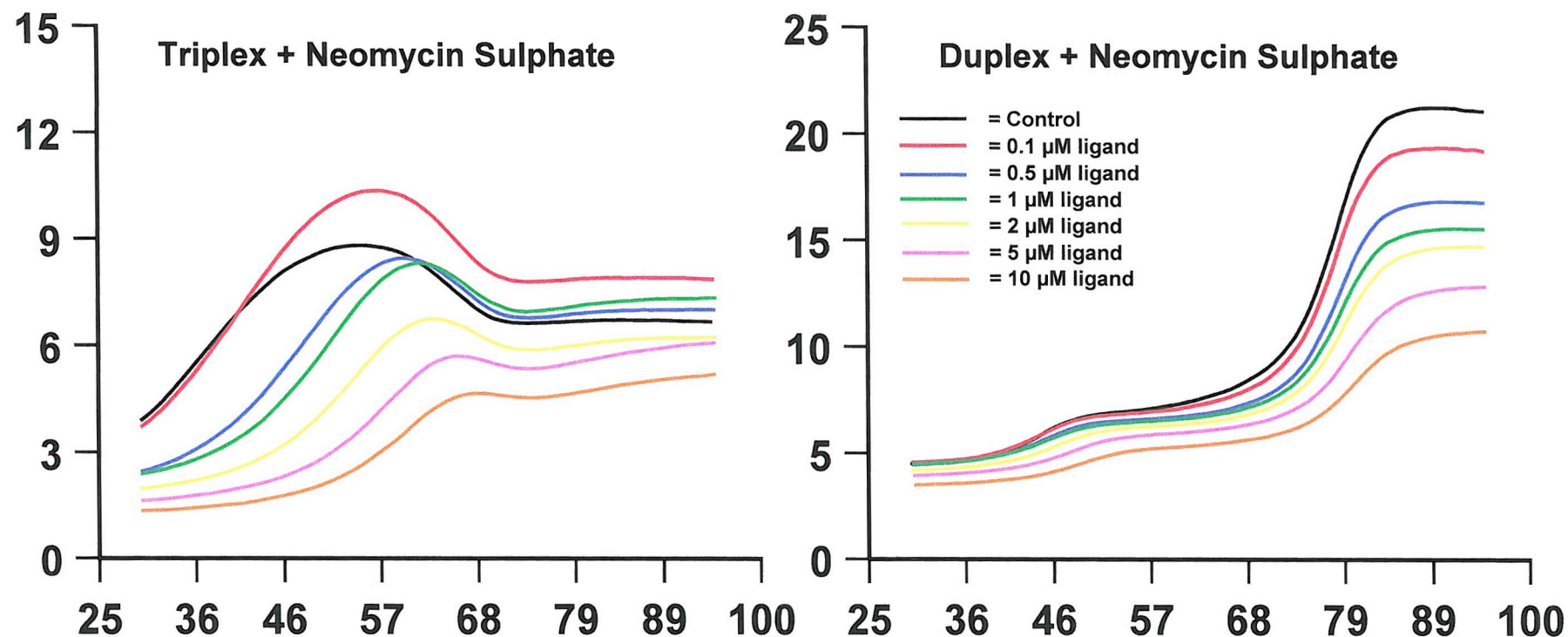
Figure 5.33: Fluorescent DNA thermal denaturation profiles generated with oligonucleotides TB1818 (left) and TB1819 (right) in the presence of an increasing concentration of Hoechst 33258 in a pH 5 buffer. The ordinate represents fluorescence (arbitary units) and the abscissa represents temperature (Celsius).

Hoechst 33258	Triplex-duplex Transition (TB1818)		Duplex-single strand Transition (TB1819)	
Concentration (µM)	Tm (°C)	ΔTm (°C)	Tm (°C)	ΔTm (°C)
0	36.4	/	76.4	/
0.1	37.3	0.9	76.7	0.3
0.5	29.8	-6.6	82.7	6.3
1	30.2	-6.2	83.7	7.3
2	/	/	85.8	9.4
5	/	/	87.7	11.3
10	/	/	89.9	13.5

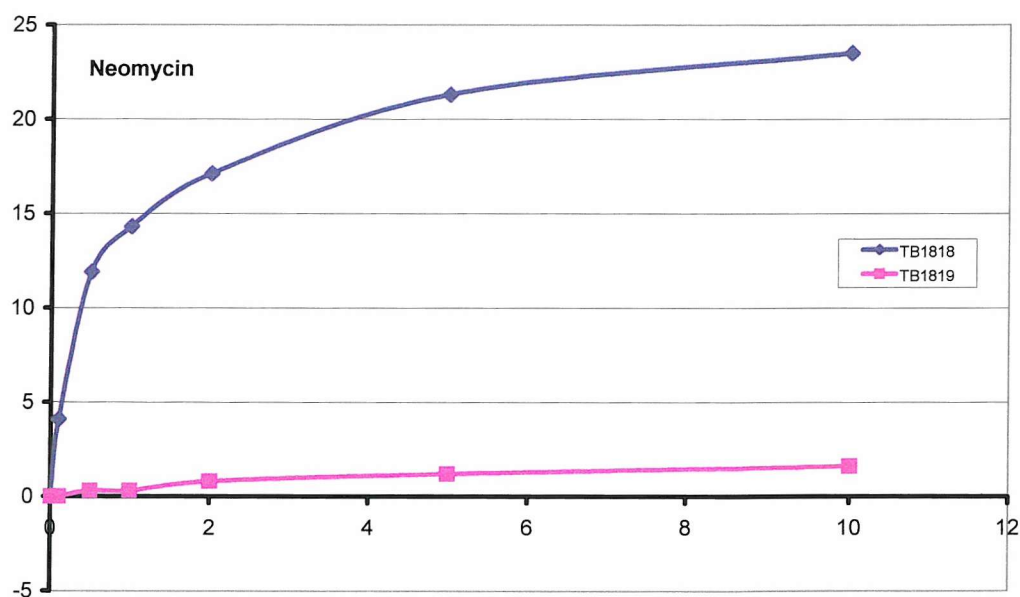**Table 5.15 & Figure 5.34:** Table 5.15 shows the Tm and ΔTm values for the oligonucleotides TB1818 and TB1819 in the presence of Hoechst 33258 at pH 5. / indicates non-determined value. Figure 5.34 illustrates the stability afforded to the duplex-single strand transition (TB1819), and destabilisation of the triplex-duplex transition (TB1818). The abscissa represents ligand concentration (µM), and the ordinate represents ΔTm (Celsius).

(5.4.12)   Distamycin.

The antibiotic distamycin A is an oligopeptide containing three N-methylpyrrole rings (Fig. 5.20), that has been reported to bind to the minor groove of duplex DNA, with a preference for $A_n \cdot T_n$ (Zimmer 1975, Zimmer *et al* 1979, Klevit *et al* 1986, Pelton & Wemmer 1990, Capobianco *et al* 1991), however it has also been reported to mildly stabilise G·C base pairs (Lee *et al* 1988, Capobianco *et al* 1991). It has also been reported that distamycin A destabilises triplex DNA (Durand & Maurizot 1996).

The left hand panel of Fig. 5.35 shows the thermal denaturation profiles of TB1818 in the presence of increasing concentrations of the minor groove binding antibiotic distamycin. It can be seen that addition of distamycin shifts the triplex-duplex transition to lower temperatures in a concentration dependent fashion. 0.5 μM ligand destabilised triplex DNA by 3.1 °C, whereas higher concentrations destabilised the transition beyond the lower limits of the experiment. It can also be seen that distamycin appears to stabilise the second transition (duplex melt). The Tm values for these triplex-duplex transitions are summarised in Table 5.16 and Fig. 5.36.

The right hand panel of Fig. 5.35 shows the melt profiles of oligonucleotide TB1819 in the presence of increasing concentrations of distamycin. It can be seen that increasing the concentration of ligand shifts the duplex-single strand transition to higher temperatures in a concentration dependent manner, and that 10 μM distamycin stabilises the duplex-single strand transition by 6.0 °C. The Tm values for these duplex-single strand transitions are summarised in Table 5.16 and Fig. 5.36.

These results suggest that distamycin destabilises DNA triplexes in a concentration dependent manner. In contrast this ligand stabilises DNA duplexes as expected.
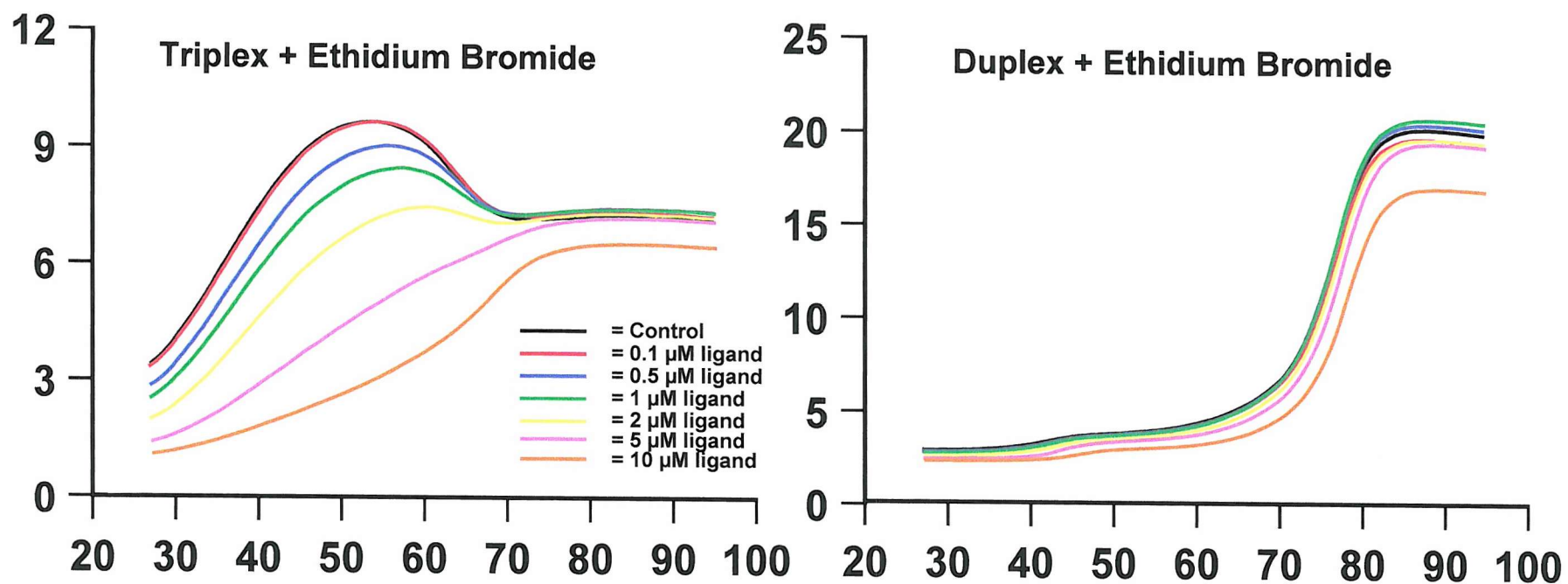
Figure 5.35: Fluorescent DNA thermal denaturation profiles generated with oligonucleotides TB1818 (left) and TB1819 (right) in the presence of an increasing concentration of distamycin in a pH 5 buffer. The ordinate represents fluorescence (arbitary units) and the abscissa represents temperature (Celsius).

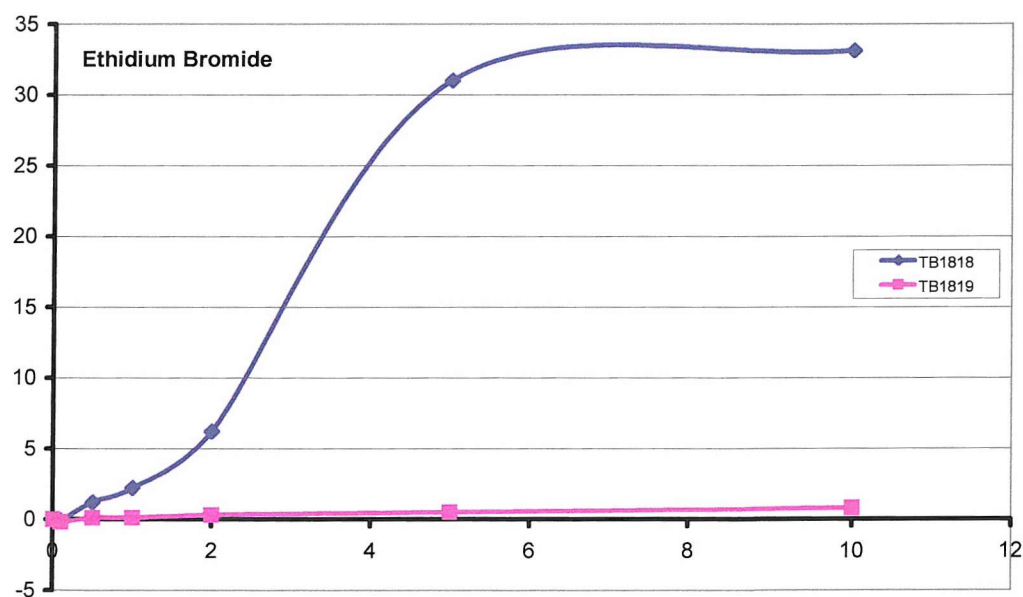| Distamycin	Triplex-duplex Transition (TB1818)		Duplex-single strand Transition (TB1819)	
Concentration (μM)	Tm (°C)	ΔTm (°C)	Tm (°C)	ΔTm (°C)
0	37.4	/	77.1	/
0.1	37.9	0.5	77.1	0
0.5	34.3	- 3.1	77.9	0.8
1	/	/	78.4	1.3
2	/	/	80.0	2.9
5	/	/	81.6	4.5
10	/	/	83.1	6.0
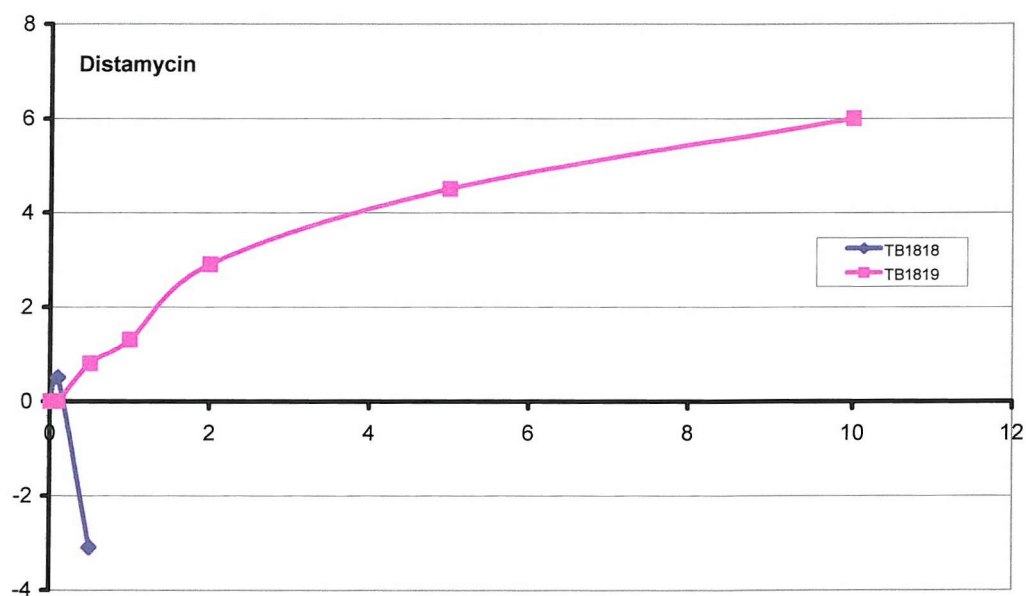
Table 5.16 & Figure 5.36: Table 5.16 shows the Tm and ΔTm values for the oligonucleotides TB1818 and TB1819 in the presence of distamycin at pH 5. / indicates non-determined value. Figure 5.36 illustrates the stability afforded to the duplex-single strand transition (TB1819), and destabilisation of the triplex-duplex transition (TB1818). The abscissa represents ligand concentration (μM), and the ordinate represents ΔTm (Celsius).

(5.5) Intramolecular triplexes & duplexes with various ligands at pH 7.0.

Similar experiments with the oligonucleotides TB1818 and TB1819 were also carried out at pH 7 in the presence of 10 mM magnesium to investigate the effect of these ligands under more physiological conditions. The melting profile in the absence of ligand has been considered in section 5.2.

(5.5.1)   Naphthylquinoline.

The left hand panel of Fig. 5.37 shows the melt profiles of oligonucleotide TB1818 in the presence of increasing concentrations of naphthylquinoline measured at pH 7 in the presence of 10 mM magnesium. As described in section 5.2 the control profile shows a triplex-duplex transition (Tm of 48.8 °C) followed by a steady decrease in fluorescence at higher temperatures. Although low ligand concentrations do not produce any significant changes, concentrations above 1 µM shifts the triplex-duplex transition to higher temperatures in a concentration dependent fashion, with a ΔTm of 12.0 °C with 10 µM ligand. It should be noted that the change in melting temperature is less than that observed at pH 5 (section 5.4.1). The Tm values for the triplex-duplex transitions are summarised in Table 5.17 and Fig. 5.38.

The right hand panel of Fig. 5.37 shows the thermal denaturation profiles of TB1819 in the presence of increasing concentrations of naphthylquinoline at pH 7. As for the experiments at pH 5 the naphthylquinoline decreases the fluorescence signal in a concentration dependent fashion. However the Tm value for the transition is not affected by the addition of the ligand. The results demonstrate that naphthylquinoline does not stabilise the duplex-single strand transition at pH 7, as previously noted at pH 5. These results are summarised in Table 5.17 and Fig. 5.38.
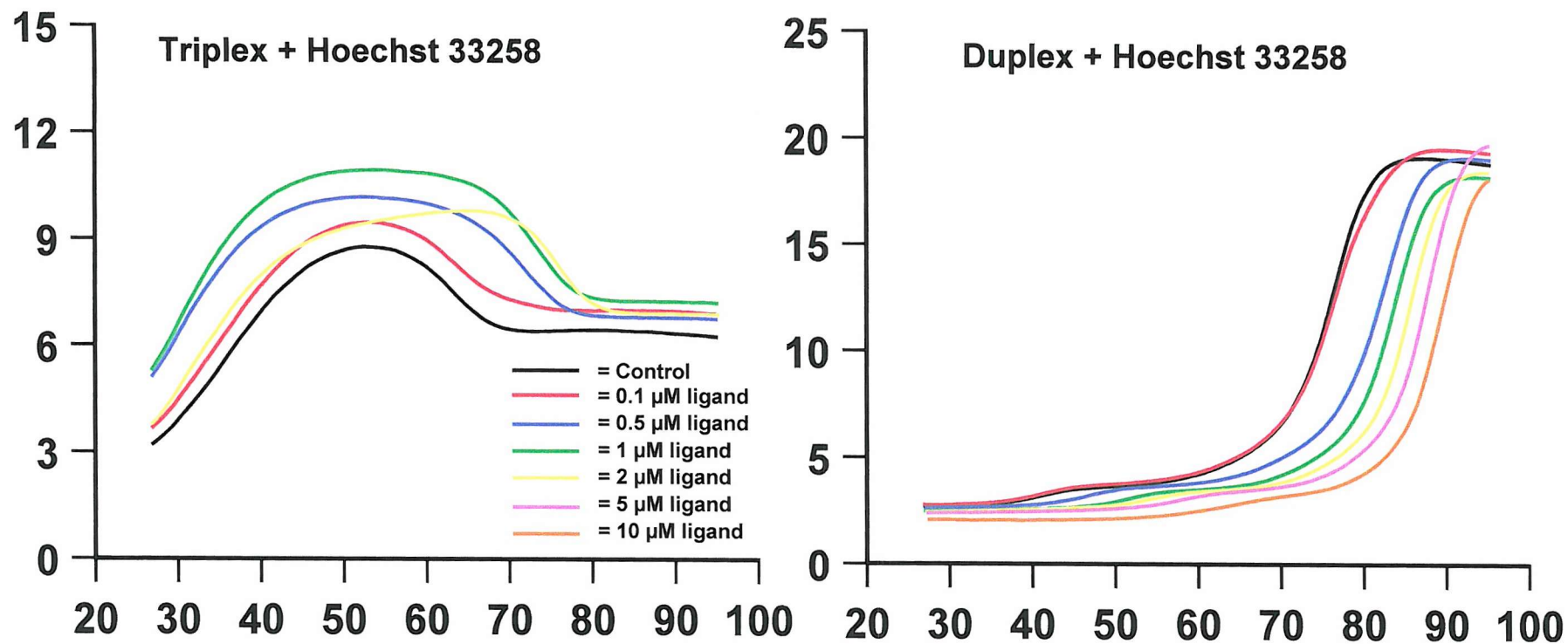
Figure 5.37: Fluorescent DNA thermal denaturation profiles generated with oligonucleotides TB1818 (left) and TB1819 (right) in the presence of an increasing concentration of naphthylquinoline at pH 7. The ordinate represents fluorescence (arbitary units) and the abscissa represents temperature (Celsius).

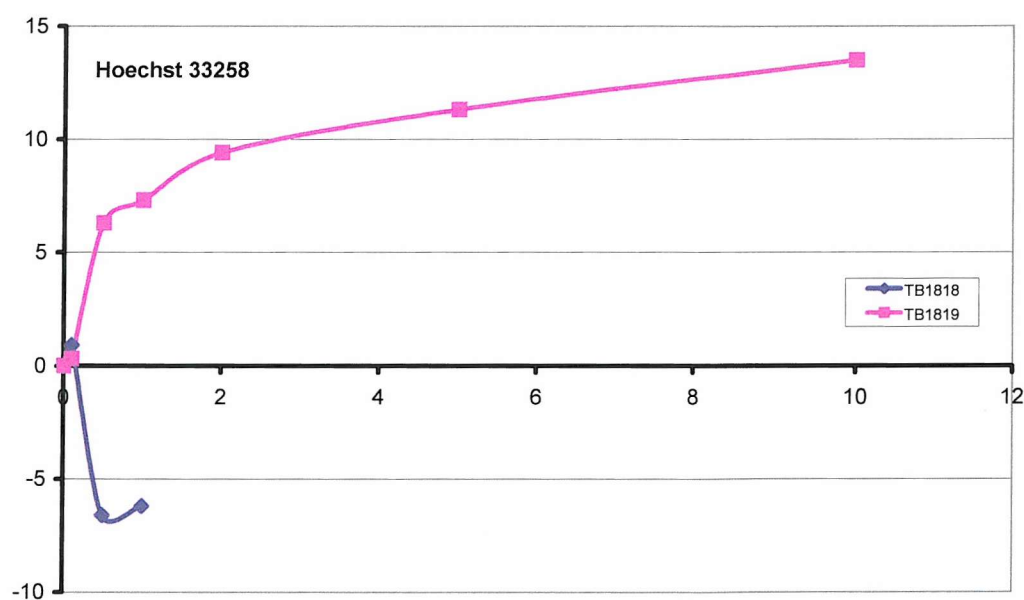| Naphthylquinoline	Triplex-duplex Transition (TB1818)		Duplex-single strand Transition (TB1819)	
Concentration (μM)	Tm (°C)	ΔTm (°C)	Tm (°C)	ΔTm (°C)
0	48.8	/	79.6	/
0.1	49.0	0.2	79.6	0
0.5	49.6	0.8	79.3	-0.3
1	51.0	3.2	79.4	-0.2
2	53.0	5.2	79.4	-0.2
5	57.3	9.5	79.5	-0.1
10	60.8	12.0	79.8	0.2
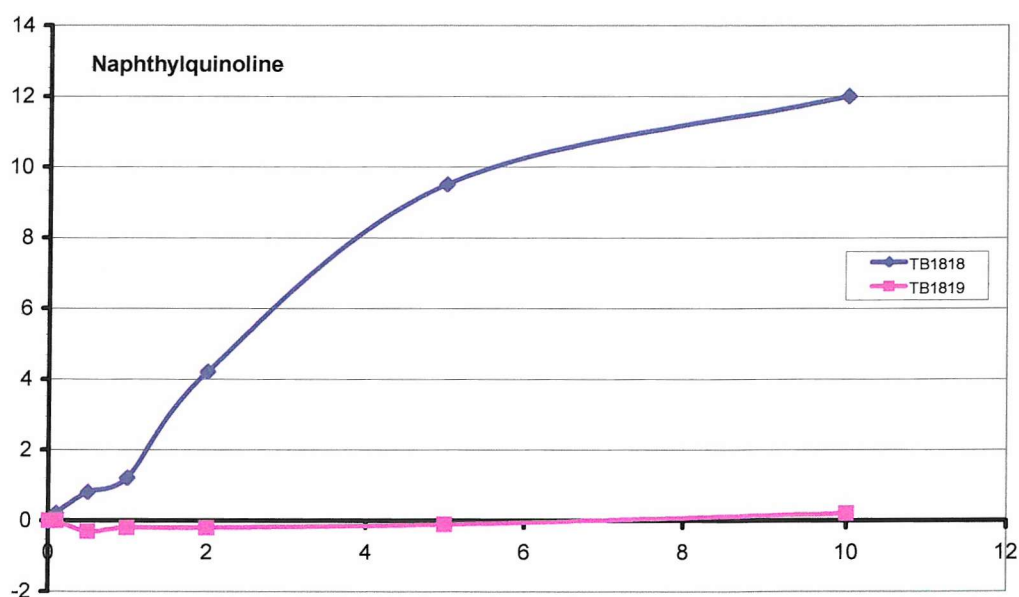
Table 5.17 & Figure 5.38: Table 5.17 shows the Tm and ΔTm values for the oligonucleotides TB1818 and TB1819 in the presence of naphthylquinoline at pH 7. Figure 5.38 illustrates the stability afforded to the triplex-duplex transition (TB1818), and the duplex-single strand transition (TB1819). The abscissa represents ligand concentration (μM), and the ordinate represents ΔTm (Celsius).

(5.5.2)   1,4 Bis-Amidoanthraquinone.

The left hand panel of Fig. 5.39 shows the thermal denaturation profiles of oligonucleotide TB1818 in the presence of increasing concentrations of 1,4 bis-amidoanthraquinone. On addition of 0.1 μM ligand the triplex-duplex transition shifts to a higher temperature and this is accompanied by a second transition at around 70°C that may correspond to the duplex melt. Analysis of the melt profile revealed that the stability of the triplex-duplex transition had increased by 6.8°C. Increasing the concentration of 1,4 bis-amidoanthraquinone to 0.5 - 2 μM produces curves which show a single transition that appears to correspond to the original second transition (duplex melt). Ligand concentrations above 2 μM increases the total fluorescence and obscured accurate determination of Tm values (data not shown). The Tm values for these triplex-duplex transitions are summarised in Table 5.18 and Fig. 5.40.

The right hand panel of Fig. 5.39 shows the melting profile of oligonucleotide TB1819 in the presence of increasing concentrations of 1,4 bis-amidoanthraquinone. Addition of the ligand results in a concentration dependent decrease in the maximum fluorescence and shifts the duplex-single strand transition to higher temperatures. It can be seen that 5 - 10 μM ligand results in an increase in the initial fluorescence and is postulated to be due to fluorescence of the ligand. The Tm values for the duplex-single strand transitions are summarised in Table 5.18 and Fig. 5.40, and suggest that this ligand stabilises the duplex-single strand transition, but to a lower degree than at pH 5.

(5.5.3)   1,5 Bis-Amidoanthraquinone.

The left hand panel of Fig. 5.41 shows the thermal denaturation profiles of oligonucleotide TB1818 with increasing concentrations of 1,5 bis-amidoanthraquinone. Addition of the ligand at concentrations above 0.5 μM results in a significant decrease in the fluorescence maximum, and shifts the transition to higher temperatures. The triplex-duplex transition is stabilised by 8.2°C in the presence of 10 μM ligand. Furthermore it can be seen that 5 - 10 μM ligand induces the formation of a second
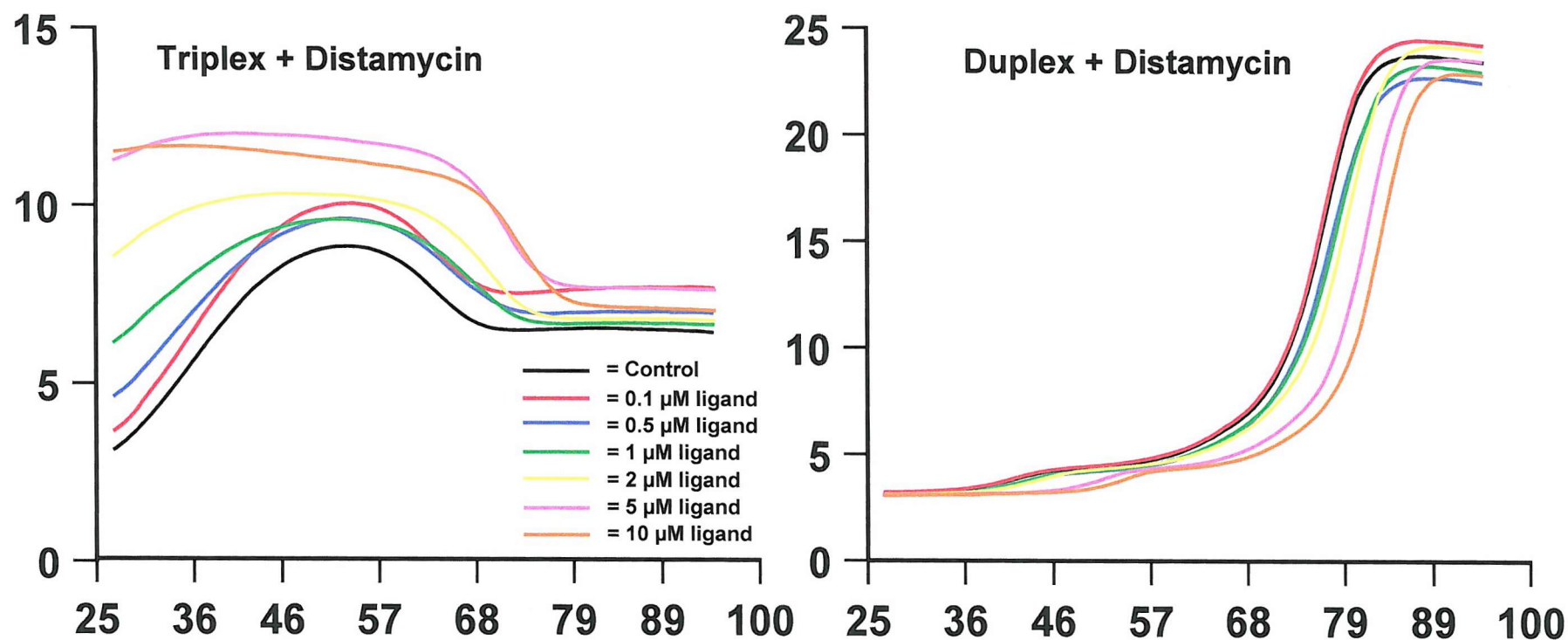
Figure 5.39: Fluorescent DNA thermal denaturation profiles generated with oligonucleotides TB1818 (left) and TB1819 (right) in the presence of an increasing concentration of 1,4 bis-amidoanthraquinone at pH 7. The ordinate represents fluorescence (arbitary units) and the abscissa represents temperature (Celsius).

1,4	Triplex-duplex Transition (TB1818)		Duplex-single strand Transition (TB1819)	
Concentration (μM)	Tm (°C)	ΔTm (°C)	Tm (°C)	ΔTm (°C)
0	44.4	/	78.3	/
0.1	51.2	6.8	78.5	0.2
0.5	72.1	27.7	79.5	1.2
1	74.0	29.6	80.6	2.3
2	76.5	32.1	82.8	4.5
5	/	/	85.5	7.2
10	/	/	89.1	10.8

Table 5.18 & Figure 5.40: Table 5.18 shows the Tm and ΔTm values for the oligonucleotides TB1818 and TB1819 in the presence of 1,4 bis-amidoanthraquinone at pH 7. / indicates non-determined value. Figure 5.40 illustrates the stability afforded to the duplex-single strand transition of TB1819, and the transition of TB1818. The abscissa represents ligand concentration (μM), and the ordinate represents ΔTm (Celsius).

Figure 5.41: Fluorescent DNA thermal denaturation profiles generated with oligonucleotides TB1818 (left) and TB1819 (right) in the presence of an increasing concentration of 1,5 bis-amidoanthraquinone at pH 7. The ordinate represents fluorescence (arbitary units) and the abscissa represents temperature (Celsius).

1,5	TB1818 Transition 1		TB1818 Transition 2	
Concentration (μM)	Tm (°C)	ΔTm (°C)	Tm (°C)	ΔTm (°C)
0	45.8	/	/	/
0.1	45.5	- 0.3	/	/
0.5	45.5	- 0.3	/	/
1	46.6	0.8	/	/
2	46.8	0.8	/	/
5	51.0	5.2	71.2	25.4
10	54.0	8.2	71.7	25.9

	Duplex-single strand Transition (TB1819)	
	Tm (°C)	ΔTm (°C)
0	48.3	/
0.1	48.8	0.5
0.5	49.3	1.0
1	49.3	1.0
2	50.4	2.1
5	52.2	3.9
10	53.5	5.2

Table 5.19 & Figure 5.42: Table 5.19 shows the Tm and ΔTm values for the oligonucleotides TB1818 and TB1819 in the presence of 1,5 bis-amidoanthraquinone at pH 7. / indicates non-determined value. Figure 5.42 illustrates the stability afforded to the first transition of TB1818, and the duplex-single strand transition (TB1819). The abscissa represents ligand concentration (μM), and the ordinate represents ΔTm (Celsius).

transition between 65 - 75°C, which may correspond to the stabilisation of the duplex-single strand transition. These results suggest that 1,5 bis-amidoanthraquinone stabilises the triplex-duplex transition at pH 7 but to a lower extent than that observed at pH 5. Furthermore the formation of two transitions at concentrations above 5 μM may indicate the formation of a heterogenous population. This is considered in greater detail in the discussion. The Tm values for these transitions are summarised in Table 5.19 and Fig. 5.42

The right hand panel of Fig. 5.41 shows the thermal denaturation profiles of oligonucleotide TB1819 with increasing concentrations of 1,5 bis-amidoanthraquinone. It can be seen that the ligand causes a small shift in the duplex-single strand transition to higher temperatures in a concentration dependent manner, with a Tm of 5.2°C at the highest ligand concentration. The results indicate that 1,5 bis-amidoanthraquinone stabilises the duplex-single strand transition in a concentration dependent manner, but to a lower extent than that seen at pH 5 (section 5.4.3). The Tm values for these duplex-single strand transitions are summarised in Table 5.19 and Fig. 5.42

(5.5.4)   1,8-Bis-Amidoanthraquinone.

The left hand panel of Fig. 5.43 shows the thermal denaturation profiles of oligonucleotide TB1818 with increasing concentrations of 1,8 bis-amidoanthraquinone. It can be seen that ligand concentrations above 0.5 μM shifts the triplex-duplex transition to higher temperatures in a concentration dependent manner. Ligand concentrations of 5 - 10 μM induces a second transition at about 60°C, which converges with the triplex-duplex transition at 10 μM, preventing accurate determination of the Tm value. The results indicate that 1,8 bis-amidoanthraquinone stabilises the triplex-duplex transition at pH 7, but to a lower extent than at pH 5 (this is considered in greater detail in the discussion). The Tm values for these transitions are summarised in Table 5.20 and Fig. 5.44.
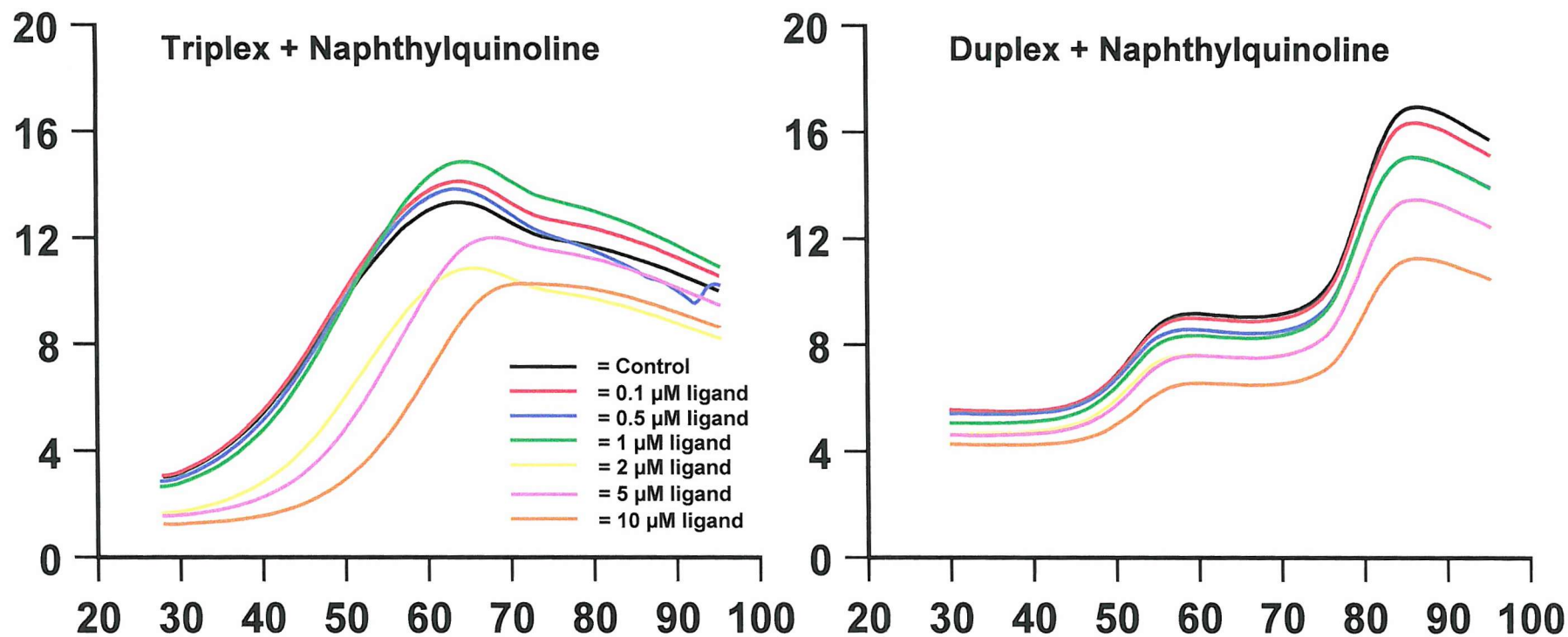
Figure 5.43: Fluorescent DNA thermal denaturation profiles generated by oligonucleotides TB1818 (left) and TB1819 (right) in the presence of an increasing concentration of 1,8 bis-amidoanthraquinone at pH 7. The ordinate represents fluorescence (arbitary units) and the abscissa represents temperature (Celsius).

1,8	Triplex-Duplex Transition (TB1818)		Duplex-single strand Transition (TB1819)	
Concentration (µM)	Tm (°C)	ΔTm (°C)	Tm (°C)	ΔTm (°C)
0	45.1	/	78.1	/
0.1	44.8	-0.3	78.1	0
0.5	45.6	0.5	78.1	0
1	45.9	0.8	78.1	0
2	48.5	3.4	78.1	0
5	52.6	7.5	78.6	0.5
10	/	/	79.0	0.9

Table 5.20 & Figure 5.44: Table 5.20 shows the Tm and ΔTm values for the oligonucleotides TB1818 and TB1819 in the presence of 1,8 bis-amidoanthraquinone at pH 7. / indicates non-determined value. Figure 5.44 illustrates the stability afforded to the triplex-duplex transition (TB1818), and the duplex-single strand transition (TB1819). The abscissa represents ligand concentration (µM), and the ordinate represents ΔTm (Celsius).

The right hand panel of Fig. 5.43 shows the melt profiles for TB1819 in the presence of increasing concentrations of 1,8 bis-amidoanthraquinone. It can be seen that the ligand has very little effect at concentrations up to 2 μM. Increasing the concentration to 5 - 10 μM shifts the duplex-single strand transition to slightly higher temperatures, though the Tm only increases by 0.5 °C and 0.9 °C respectively. The results indicate that 1,8 bis-amidoanthraquinone does not significantly stabilise duplex DNA which is comparable to the results obtained at pH 5 (section 5.4.4). The Tm values for these duplex-single strand transitions are summarised in Table 5.20 and Fig. 5.44.

(5.5.5) 2,6 Bis-Amidoanthraquinone.

The left hand panel of Fig. 5.45 shows the thermal denaturation profiles for oligonucleotide TB1818 in the presence of increasing concentrations of 2,6 bis-amidoanthraquinone. It can be observed that the ligand has very little effect at concentrations up to 1 μM. Increasing the ligand concentration above 1 μM decreases the maximum fluorescence signal and shifts the triplex-duplex transition to higher temperatures in a concentration dependent manner. At ligand concentrations of 5 - 10 μM there is a significant change in the shape of the curve and two transitions are evident. The apparent Tm of the triplex-duplex transition was increased by 3.8 °C with the addition of 10 μM 2,6 bis-amidoanthraquinone. The Tm values for these transitions are summarised in Table 5.21 and Fig. 5.46. These results suggest that 2,6 bis-amidoanthraquinone stabilises the triplex-duplex transition but to a lower extent than that observed at pH 5.

The right hand panel of Fig. 5.45 illustrates the thermal denaturation profiles for TB1819 with increasing concentrations of 2,6 bis-amidoanthraquinone. It can be seen that ligand concentrations up to 2 μM do not significantly alter the melting profile. Higher ligand concentrations shifts the duplex-single strand transition to slightly higher temperatures and reduces the fluorescence signal. The Tm values for these duplex-single strand transitions are summarised in Table 5.21 and Fig. 5.46. These results suggest that 2,6 bis-amidoanthraquinone has similar effects on both the duplex-single strand and
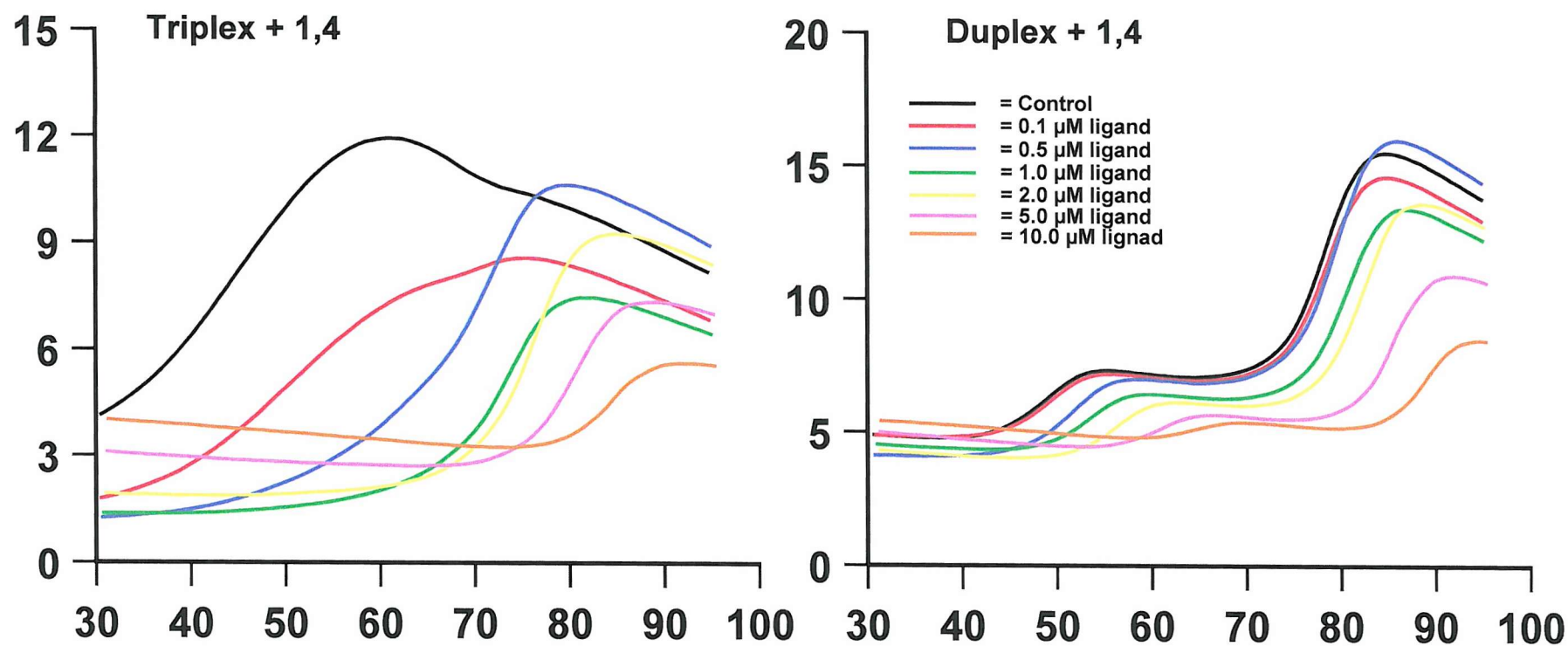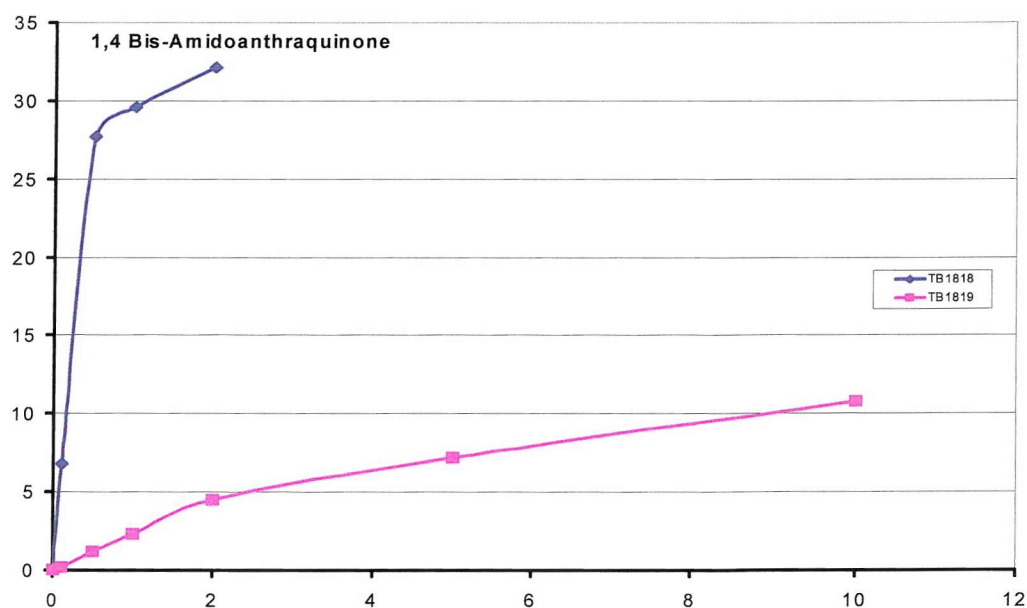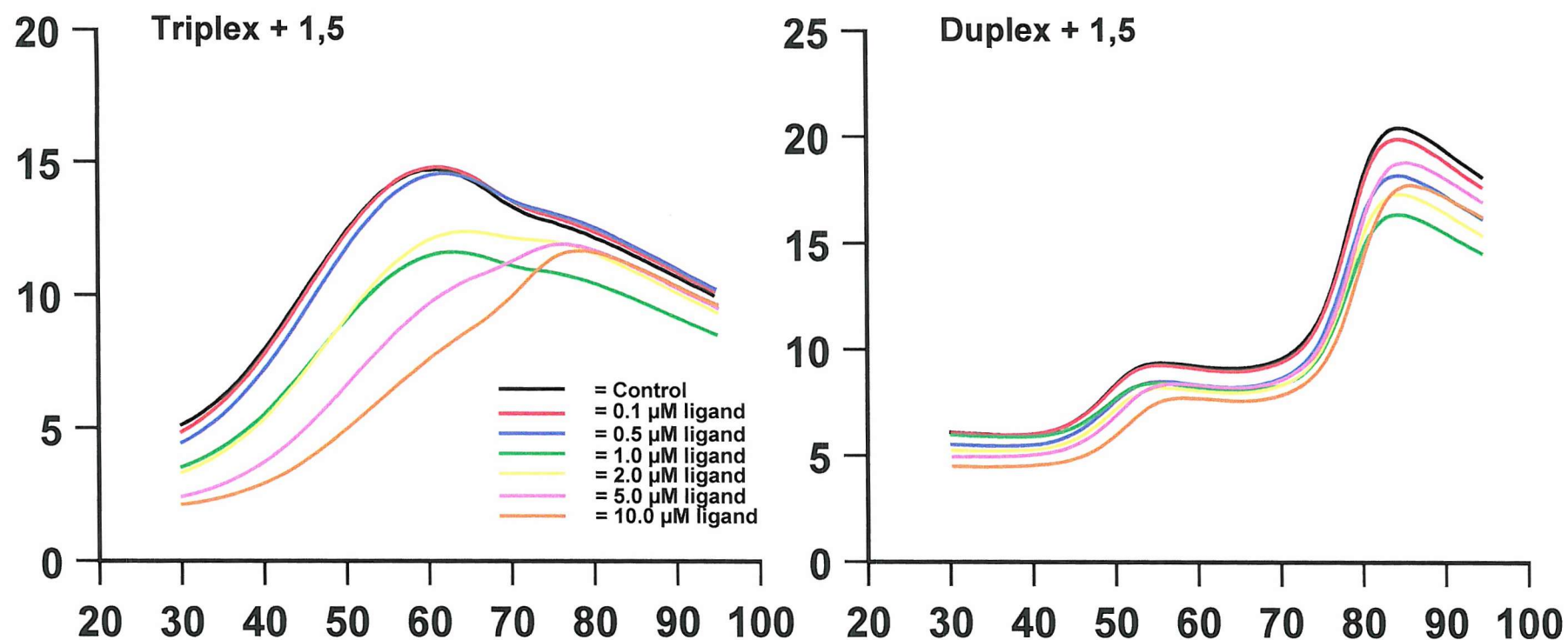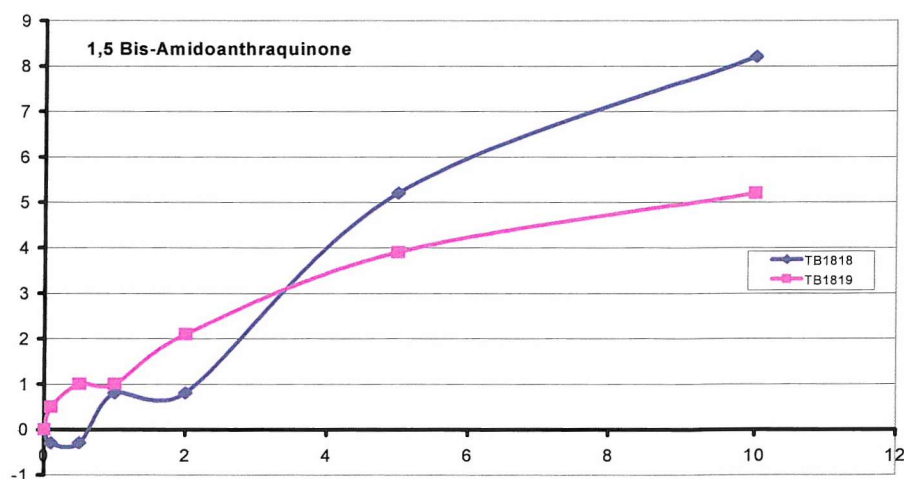
-119-

Figure 5.45: Fluorescent DNA thermal denaturation profiles generated with oligonucleotides TB1818 (left) and TB1819 (right) in the presence of an increasing concentration of 2,6 bis-amidoanthraquinone at pH 7. The ordinate represents fluorescence (arbitary units) and the abscissa represents temperature (Celsius).

2,6	TB1818 Transition 1		TB1818 Transition 2	
Concentration (μM)	Tm (°C)	ΔTm (°C)	Tm (°C)	ΔTm (°C)
0	45.2	/	/	/
0.1	45.0	- 0.2	/	/
0.5	45.8	0.5	/	/
1	46.3	1.1	/	/
2	47.5	2.3	/	/
5	48.2	3.0	/	/
10	49.0	3.8	76.0	30.8

	Duplex single-strand Transition (TB1819)	
	Tm (°C)	ΔTm (°C)
0	78.1	/
0.1	77.9	- 0.2
0.5	78.3	0.2
1	78.3	0.2
2	78.8	0.7
5	80.3	2.2
10	81.4	3.3

Table 5.21 & Figure 5.46: Table 5.21 shows the Tm and ΔTm values for the oligonucleotides TB1818 and TB1819 in the presence of 2,6 bis-amidoanthraquinone at pH 7. / indicates non-determined value. Figure 5.46 illustrates the stability afforded to the first transition of TB1818, and the duplex-single strand transition (TB1819). The abscissa represents ligand concentration (μM), and the ordinate represents ΔTm (Celsius).

triplex-duplex transitions at pH 7, this is significantly lower than pH 5.

(5.5.6)   2,7 Bis-Amidoanthraquinone.

The left hand panel of Fig. 5.47 demonstrates the thermal denaturation profiles for oligonucleotide TB1818 with increasing concentrations of 2,7 bis-amidoanthraquinone. It can be seen that 2,7 bis-amidoanthraquinone concentrations of 0.5 - 1 µM shifts the triplex-duplex transition to higher temperatures and decreases the maximum fluorescence signal. Increasing the concentration of 2,7 bis-amidoanthraquinone to 2 - 10 µM significantly reduces the fluorescence signal and shifts the triplex-duplex transition to higher temperatures, generating a second transition above 70°C. 10 µM ligand produces a ΔTm of 15.3°C. The Tm values for these triplex-duplex transitions are summarised in Table 5.22 and Fig. 5.48. These results suggest that 2,7 bis-amidoanthraquinone stabilises the triplex-duplex transition in a concentration dependent manner, but this effect is less than that observed at pH 5 (section 5.4.6).

The right hand panel of Fig. 5.47 shows the thermal denaturation profiles of oligonucleotide TB1819 in the presence of increasing concentrations of 2,7 bis-amidoanthraquinone. It can be seen that ligand concentrations of 2 µM and above decreases the maximum fluorescence signal, and shifts the duplex-single strand transition to higher temperatures in a concentration dependent manner. However the transition is only stabilised by 1.3°C on addition of 5 µM 2,7 bis-amidoanthraquinone. Increasing the ligand concentration to 10 µM significantly reduces the fluorescence signal, preventing accurate determination of the Tm (result not shown). The Tm values for these transitions are summarised in Table 5.22 and Fig. 5.48. The results indicate that at pH 7 2,7 bis-amidoanthraquinone does not significantly stabilise the duplex-single strand transition. This contrasts the results obtained at pH 5, see section 5.4.6.
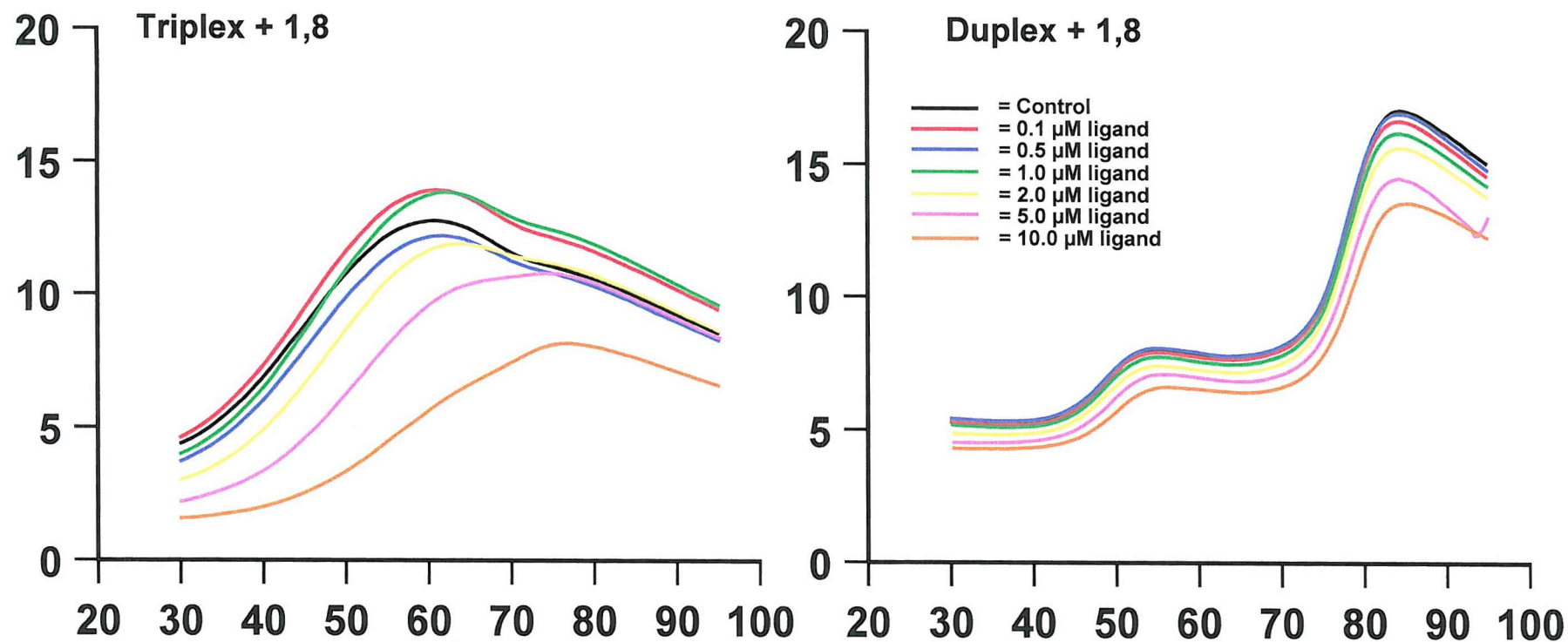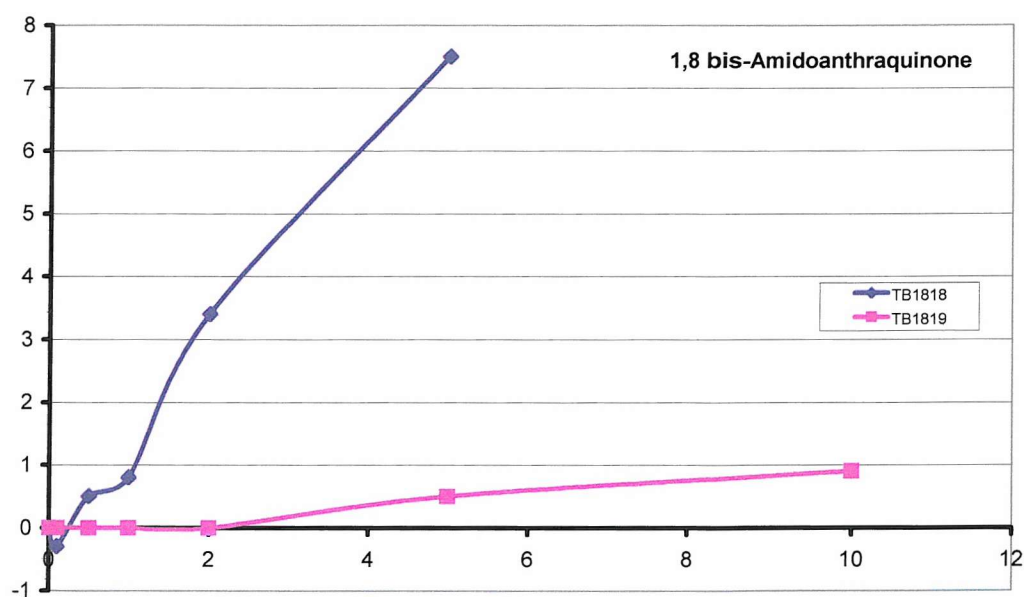
Figure 5.47: Fluorescent DNA thermal denaturation profiles generated with oligonucelotides TB1818 (left) and TB1819 (right) in the presence of an increasing concentration of 2,7 bis-amidoanthraquinone at pH 7. The ordinate represents fluorescence (arbitary units) and the abscissa represents temperature (Celsius).

2,7	TB1818 Transition 1		TB1818 Transition 2	
Concentration (µM)	Tm (°C)	ΔTm (°C)	Tm (°C)	ΔTm (°C)
0	44.7	/	/	/
0.1	46.1	1.4	/	/
0.5	49.8	5.1	/	/
1	51.5	6.8	/	/
2	53.7	9.0	/	/
5	59.4	14.7	/	/
10	60.0	15.3	76.1	31.4
	Duplex-single strand Transition (TB1819)			
	Tm (°C)		ΔTm (°C)	
0	78.6		/	
0.1	78.6		0	
0.5	78.6		0	
1	78.8		0.2	
2	79.1		0.5	
5	79.9		1.3	

Table 5.22 & Figure 5.48: Table 5.22 shows the Tm and ΔTm values for the oligonucleotides TB1818 and TB1819 in the presence of 2,7 bis-amidoanthraquinone at pH 7. / indicates non-determined value. Figure 5.48 illustrates the stability afforded to the first transition of TB1818, and the duplex-single strand transition (TB1819). The abscissa represents ligand concentration (µM) and the ordinate represents ΔTm (Celsius).

(5.5.7)   Acridine Derivatives.

The left hand panel of Fig. 5.49 shows the thermal denaturation profiles for oligonucleotide TB1818 in the presence of increasing concentrations of the acridine derivative BR19. It can be seen that the ligand has little effect at concentrations up to 1 µM. Increasing the concentration of BR19 to 2 - 10 µM induces a significant reduction in the maximum fluorescence signal but does not appear to shift the triplex-duplex transition. Analysis of the melt curve indicated that the triplex-duplex transition was stabilised by 3.4 °C at a ligand concentration of 10 µM. The Tm values for these triplex-duplex transitions are summarised in Table 5.23 and Fig. 5.50. These results suggest that BR19 does not significantly stabilise triplex DNA at pH 7. These results will be covered in greater detail in the discussion.

The right hand panel of Fig. 5.49 shows the melt profiles for oligonucleotide TB1819 in the presence of increasing concentrations of the acridine derivative BR19. It can be seen that increasing the concentration of BR19 decreases the maximum fluorescence, but it does not appear to shift the duplex-single strand transition. The ligand has very little effect up to 2 µM, but produces a ΔTm of 6.2 °C at 10 µM BR19. The Tm values for these duplex-single strand transitions are summarised in Table 5.23 and Fig. 5.50. These results suggest that acridine derivative BR19 stabilises the duplex-single strand transition at concentrations above 5 µM, though the results may be influenced by the ligand quenching the fluorescence signal (covered in detail in the discussion). These results are in contrast to the significant stabilisation observed at pH 5 (section 5.4.8).

The left hand panel of Fig. 5.51 shows the melting profiles of oligonucleotide TB1818 in the presence of increasing concentrations of the acridine derivative BR20. It can be seen that BR20 decreases the maximum fluorescence signal in a concentration dependent manner, but does not appear to significantly affect the triplex-duplex transition. Whilst increasing the concentration of BR20 to 2 - 10 µM appears to affect the triplex-duplex transition, it induces the formation of a second transition. Analysis of the
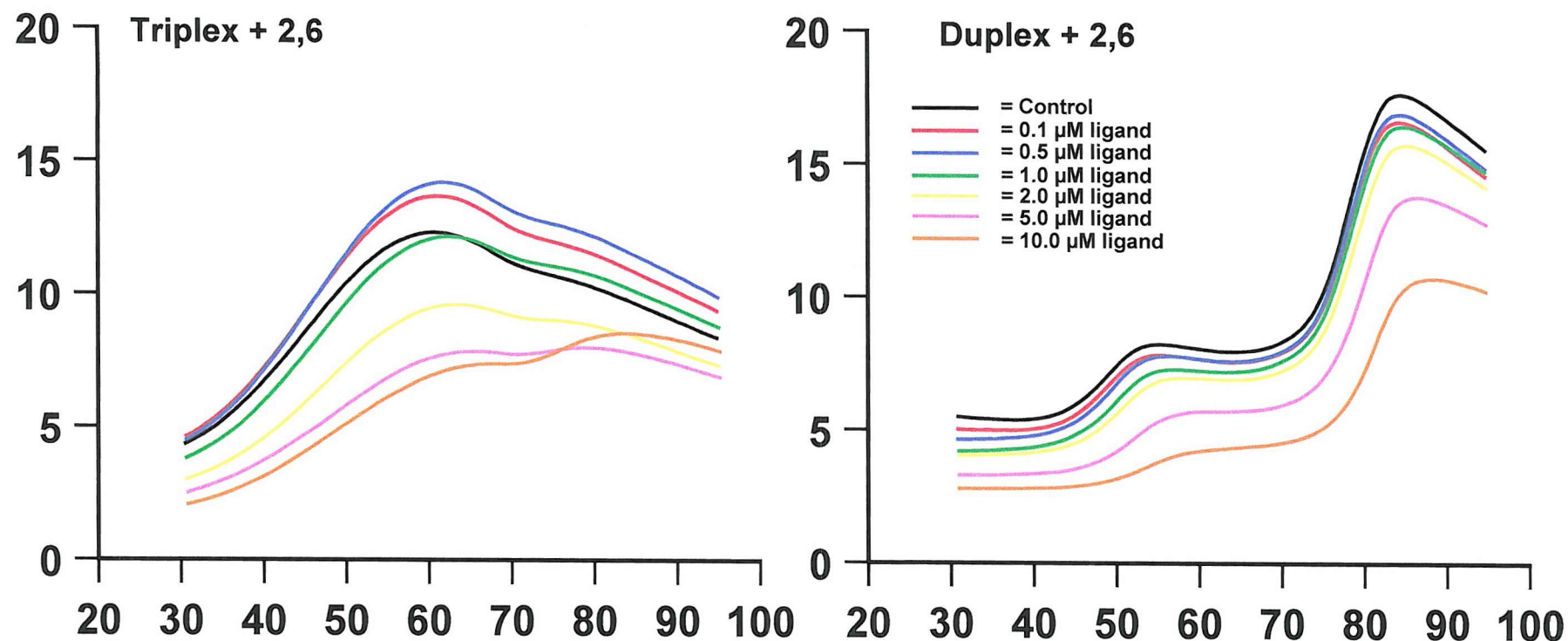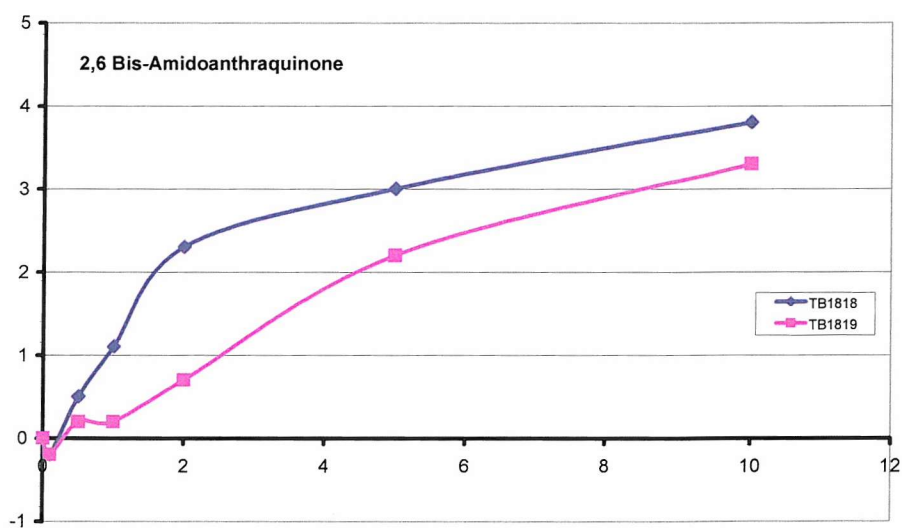
Figure 5.49: Fluorescent DNA thermal denaturation profiles generated with oligonucleotides TB1818 (left) and TB1819 (right) in the presence of an increasing concentration of the acridine derivative BR19 at pH 7. The ordinate represents fluorescence (arbitary units) and the abscissa represents temperature (Celsius).

BR19	Triplex-duplex Transition (TB1818)		Duplex-single strand Transition (TB1819)	
Concentration (µM)	Tm (°C)	ΔTm (°C)	Tm (°C)	ΔTm (°C)
0	49.2	/	80.7	/
0.1	49.0	- 0.2	80.7	0
0.5	49.6	0.4	80.8	0.1
1	49.6	0.4	81.1	0.4
2	48.8	- 0.4	81.5	0.8
5	49.9	0.7	84.0	3.3
10	52.6	3.4	86.9	6.2

Table 5.23 & Figure 5.50: Table 5.23 shows the Tm and ΔTm values for the oligonucleotides TB1818 and TB1819 in the presence of the acridine derivative BR19 at pH 7. Figure 5.50 illustrates the stability afforded to the triplex-duplex transition (TB1818), and the duplex-single strand transition (TB1819). The abscissa represents ligand concentration (µM), and the ordinate represents ΔTm (Celsius).
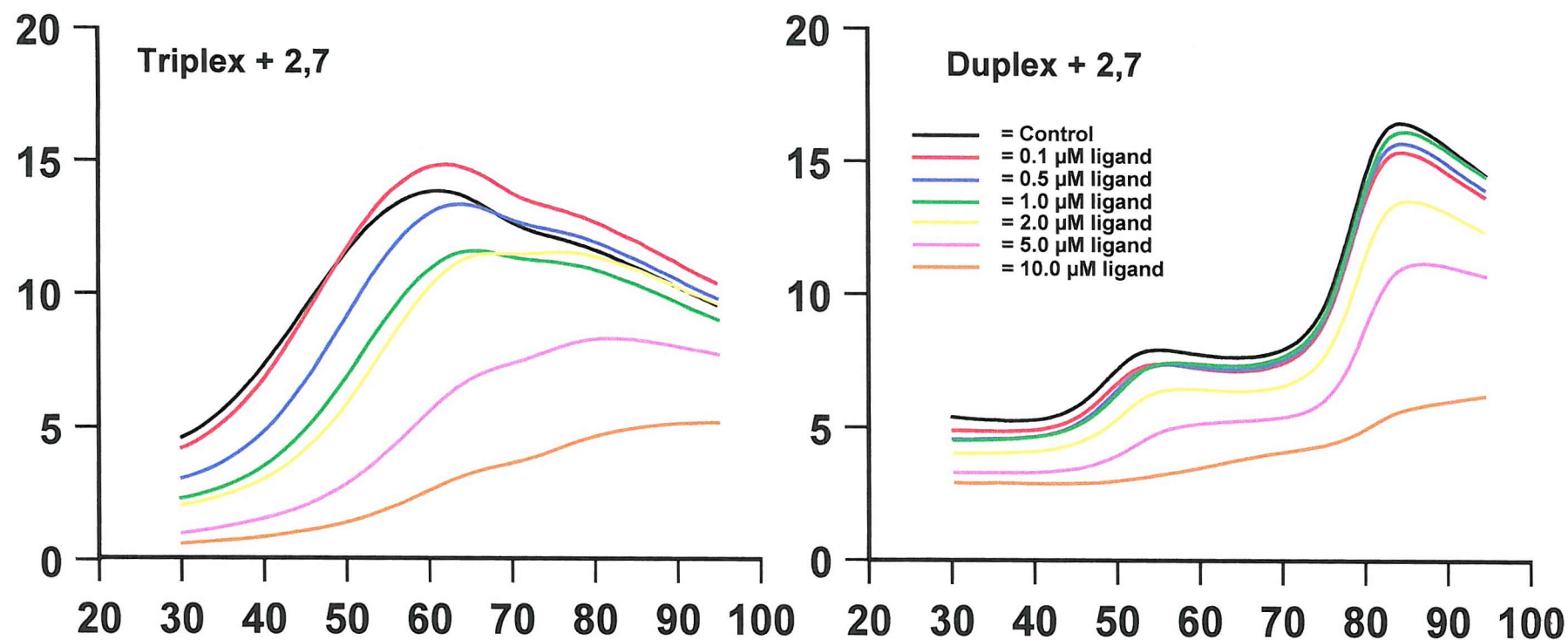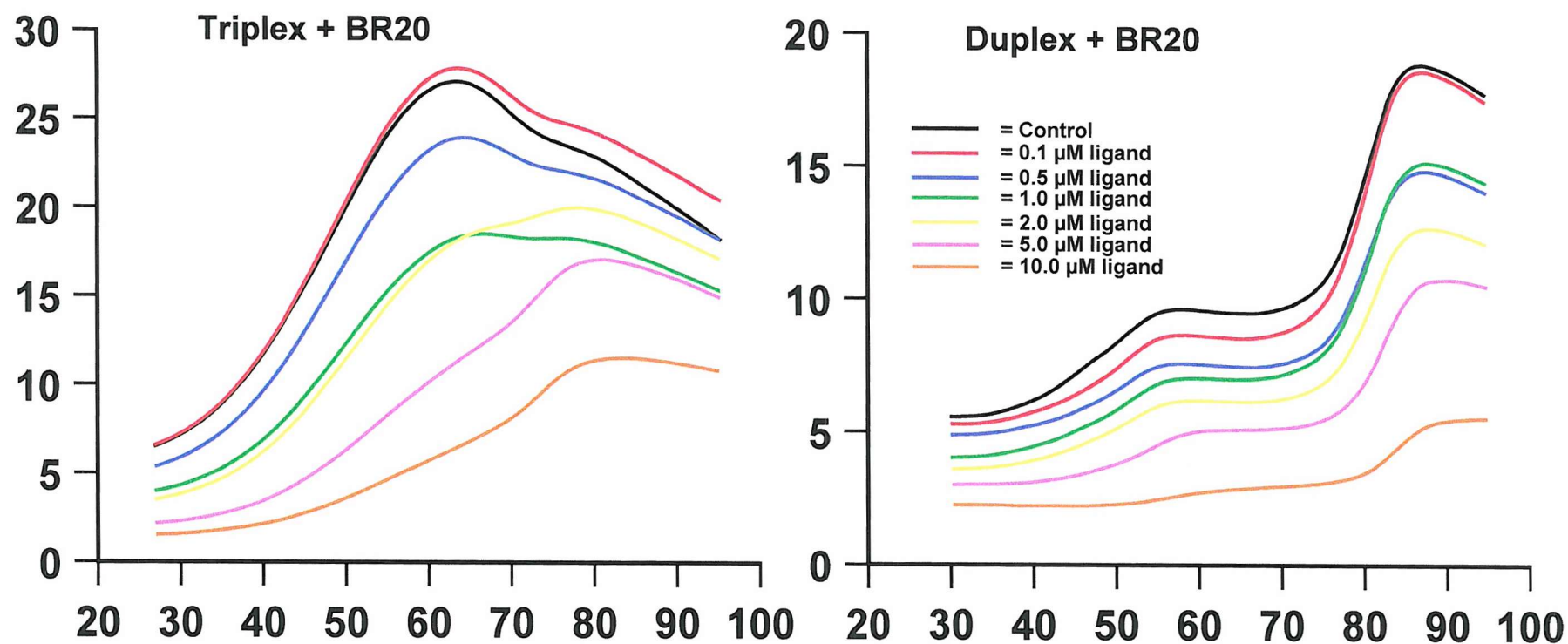
Figure 5.51: Fluorescent DNA thermal denaturation profiles generated with oligonucleotides TB1818 (left) and TB1819 (right) in the presence of an increasing concentration of the acridine derivative BR20 at pH 7. The ordinate represents fluorescence (arbitary units) and the abscissa represents temperature (Celsius).

BR20	TB1818 Transition 1		TB1818 Transition 2	
Concentration (μM)	Tm (°C)	ΔTm (°C)	Tm (°C)	ΔTm (°C)
0	47.6	/	/	/
0.1	47.4	- 0.2	/	/
0.5	48.6	1.0	/	/
1	50.0	2.4	/	/
2	50.9	3.3	73.2	25.6
5	51.3	3.7	73.0	25.4
10	/	/	73.7	26.1

	Duplex-single strand Transition (TB1819)	
	Tm (°C)	ΔTm (°C)
0	80.5	/
0.1	80.7	0.2
0.5	80.7	0.2
1	80.9	0.4
2	81.3	0.8
5	82.3	1.8
10	84.1	3.6

Table 5.24 & Figure 5.52: Table 5.24 shows the Tm and ΔTm values for the oligonucleotides TB1818 and TB1819 in the presence of the acridine derivative BR20 at pH 7. / indicates non-determined value. Figure 5.52 illustrates the stability afforded to the first transition of TB1818, and the duplex-single strand transition (TB1819). The abscissa represents ligand concentration (μM), and the ordinate represents ΔTm (Celsius).

thermal denaturation profiles reveals that at 10 μM ligand the triplex-duplex transition has merged with the second transition preventing unambiguous determination. In contrast 5 μM BR20 stabilises the triplex-duplex transition by only 3.7°C. The results indicate that BR20 does not significantly stabilise the triplex-duplex transition at pH 7. The Tm values for these triplex-duplex transitions are summarised in Table 5.24 and Fig. 5.52.

The right hand panel of Fig. 5.51 shows the thermal denaturation profiles for oligonucleotide TB1819 in the presence of increasing concentrations of acridine derivative BR20. Concentrations of BR20 above 0.1 μM significantly decreases the maximum fluorescence signal, but does not appear to stabilise the duplex-single strand transition, with a ΔTm of only 3.6°C with 10 μM ligand. The Tm values for these duplex-single strand transitions are summarised in Table 5.24 and Fig. 5.52. These results indicate that BR20 does not significantly stabilise the duplex-single strand transition at pH 7, in contrast to the stabilisation afforded at pH 5 (section 5.4.8).

(5.5.8) Alpha and Beta Naphthoflavone.

The left hand panel of Fig. 5.53 shows the thermal denaturation profiles for oligonucleotide TB1818 in the presence of increasing concentrations of alpha naphthoflavone. It can be seen that increasing the ligand concentration to 0.5 μM has little effect on the melt profile, but that above a concentration of 0.5 μM the maximum fluorescence is reduced in a concentration dependent manner. 5 μM alpha naphthoflavone stabilises the triplex-duplex transition by 12.7°C, though increasing the concentration to 10 μM lowers the Tm value below that observed in the presence of either 2 μM or 5 μM ligand. These results are similar to those obtained at pH 5 (section 5.4.7). The Tm values for these triplex-duplex transitions are summarised in Table 5.25 and Fig. 5.54.

The right hand panel of Fig. 5.53 shows the melt profiles for oligonucleotide TB1819 in the presence of increasing concentrations of alpha naphthoflavone. It can be seen that the ligand does not significantly alter the DNA melt profile even at

Figure 5.53: Fluorescent DNA thermal denaturation profiles generated with oligonucleotides TB1818 (left) and TB1819 (right) in the presence of an increasing concentration of alpha-naphthoflavone at pH 7. The ordinate represents fluorescence (arbitary units) and the abscissa represents temperature (Celsius).

Alpha Naphthoflavone	Triplex-duplex Transition (TB1818)		Duplex-single strand Transition (TB1819)	
Concentration (µM)	Tm (°C)	ΔTm (°C)	Tm (°C)	ΔTm (°C)
0	48.1	/	80.4	/
0.1	47.6	- 0.5	80.4	0
0.5	48.7	0.6	80.4	0
1	52.1	3.0	80.5	0.1
2	56.6	8.5	80.6	0.2
5	60.8	12.7	80.5	0.1
10	53.7	5.6	80.2	-0.2

Table 5.25 & Figure 5.54: Table 5.25 shows the Tm and ΔTm values for the oligonucleotides TB1818 and TB1819 in the presence of alpha-naphthoflavone at pH 7. Figure 5.54 illustrates the stability afforded to both the triplex-duplex transition (TB1818), and the duplex-single strand transition (TB1819). The abscissa represents ligand concentration (µM), and the ordinate represents ΔTm (Celsius).
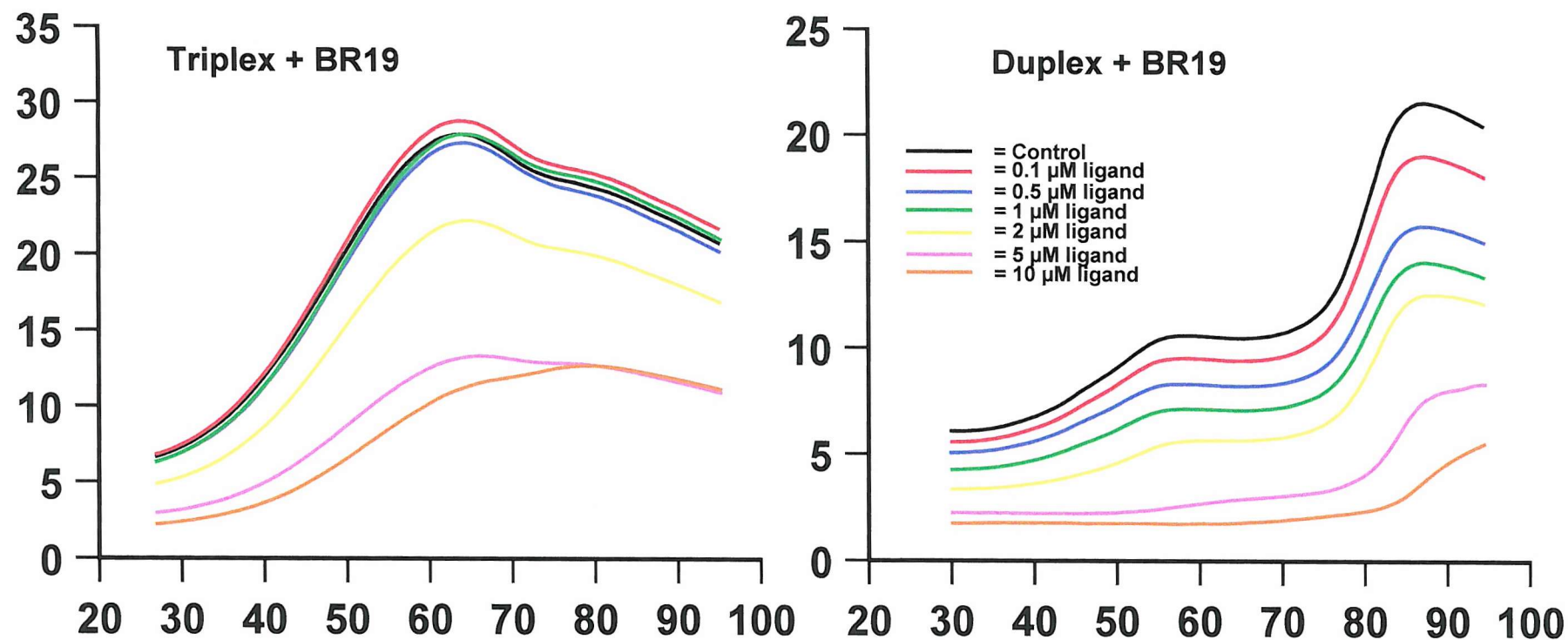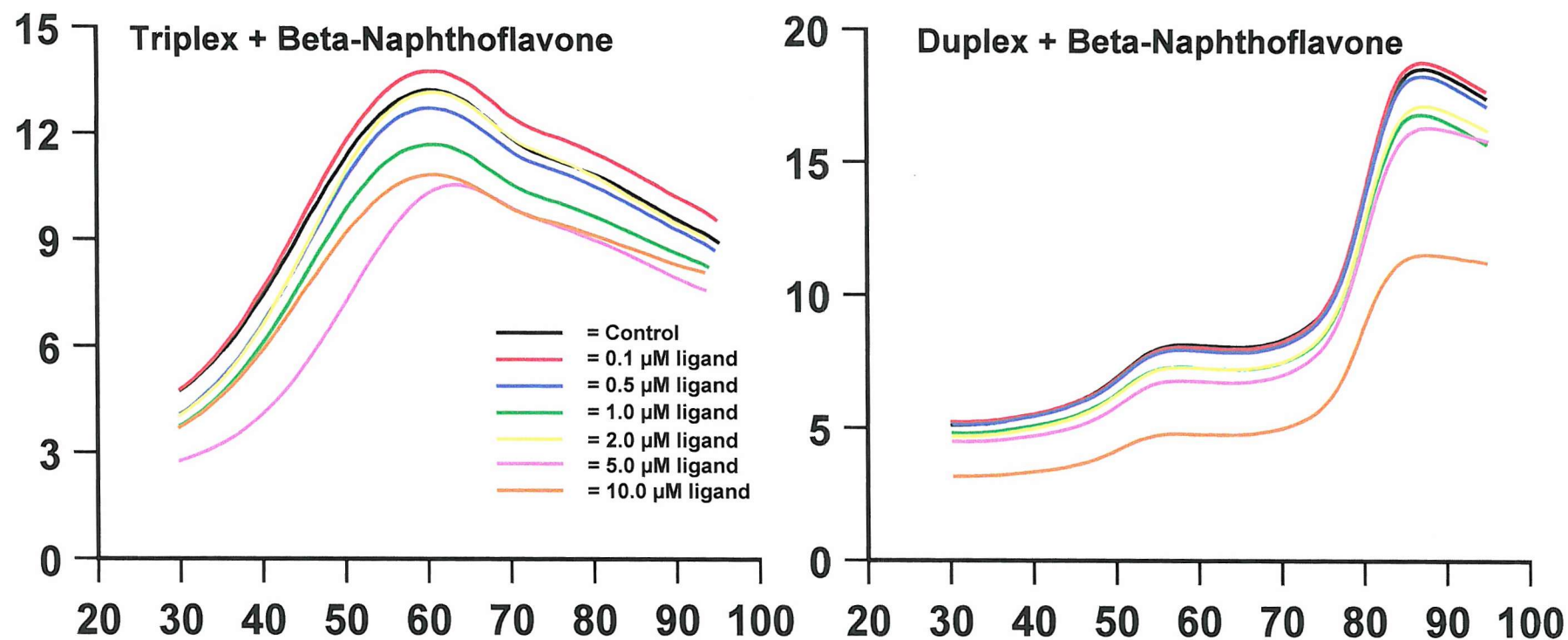
Figure 5.55: Fluorescent DNA thermal denaturation profiles generated with oligonucleotides TB1818 (left) and TB1819 (right) in the presence of an increasing concentration of beta-naphthoflavone at pH 7. The ordinate represents fluorescence (arbitary units) and the abscissa represents temperature (Celsius).

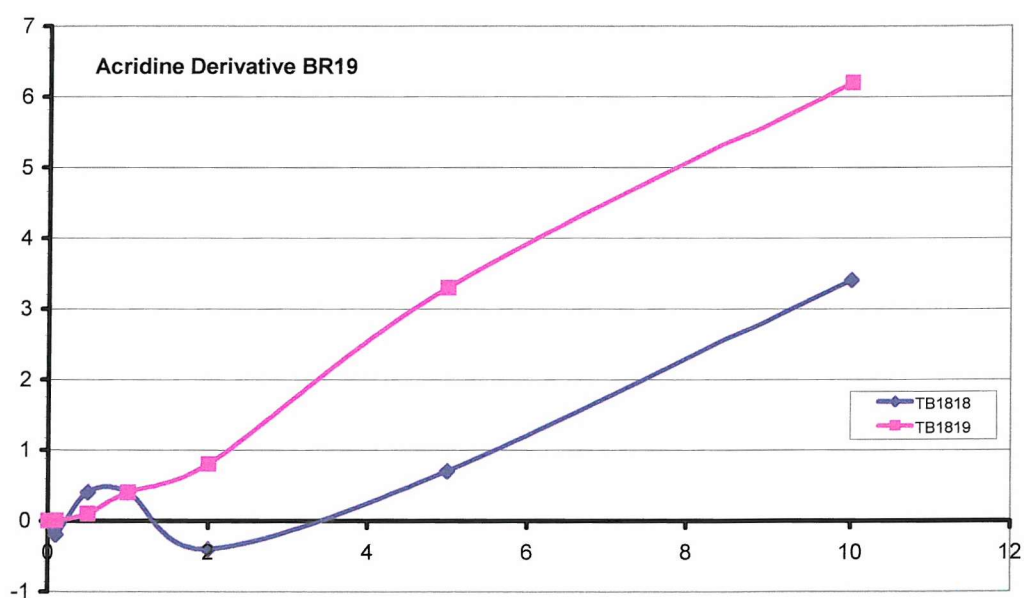| Beta-Naphthoflavone	Triplex-duplex Transition (TB1818)		Duplex-single strand Transition (TB1819)	
Concentration (µM)	Tm (°C)	ΔTm (°C)	Tm (°C)	ΔTm (°C)
0	44.1	/	80.3	/
0.1	44.2	0.1	80.2	-0.1
0.5	44.9	0.8	80.2	-0.1
1	45.0	0.9	80.3	0
2	46.0	1.9	80.3	0
5	50.7	6.6	80.3	0
10	45.7	1.6	79.5	-0.8

Table 5.26 & Figure 5.56: Table 5.26 shows the Tm and ΔTm values for the oligonucleotides TB1818 and TB1819 in the presence of beta-naphthoflavone at pH 7. Figure 5.56 illustrates the stability afforded to the triplex-duplex transition (TB1818), and the duplex-single strand transition (TB1819). The abscissa represents ligand concentration (µM), and the ordinate represents ΔTm (Celsius).
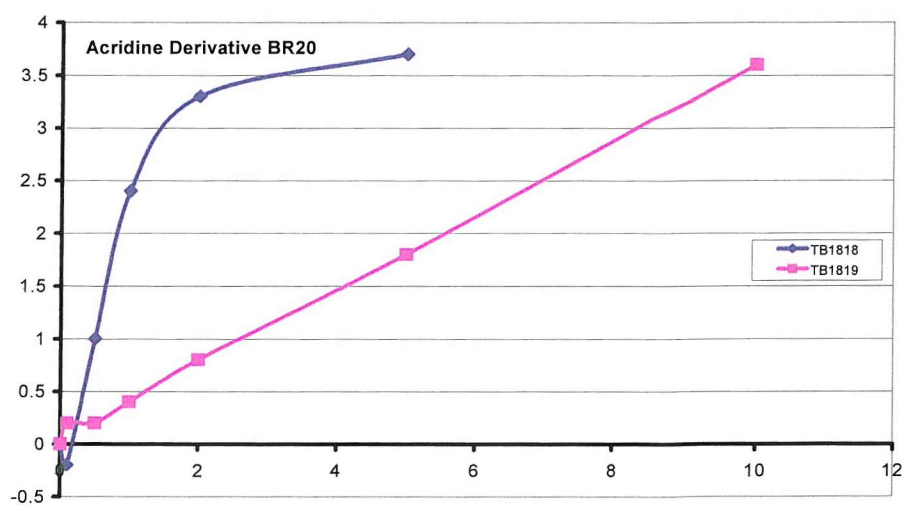
concentrations as high as 10 μM. These results indicate that alpha naphthoflavone does not significantly stabilise the duplex-single strand transition at pH 7, which is comparable to the results at pH 5 (section 5.4.7). The Tm values for these duplex-single strand transition Tm values can be seen summarised in Table 5.25 and Fig. 5.54.

The left hand panel of Fig. 5.55 shows the thermal denaturation profiles for oligonucleotide TB1818 in the presence of increasing concentrations of beta naphthoflavone. It can be seen that the ligand has very little effect at concentrations up to 1 μM. However increasing the concentration to between 1 - 5 μM shifts the triplex-duplex transition to higher temperatures in a concentration dependent manner. However with 10 μM ligand the transition shifts to a lower temperature than in the presence of 5 μM beta naphthoflavone, and is only 1.6°C higher than the control. The Tm values for these triplex-duplex transitions are summarised in Table 5.26 and Fig. 5.56. These results indicate that beta naphthoflavone stabilises the triplex-duplex transition at pH 7, and that stabilisation is comparable to that observed at pH 5 (section 5.4.7)

The right hand panel of Fig. 5.55 shows the melting profiles for oligonucleotide TB1819 in the presence of increasing concentrations of beta naphthoflavone. It can be seen that ligand concentrations up to 5 μM do not significantly alter the thermal denaturation profile. At 10 μM ligand there is a significant reduction in the level of fluorescence, however the transition appears to occur with the same Tm as previously observed. The Tm values for these duplex-single strand transitions are summarised in Table 5.26 and Fig. 5.56. These results indicate that beta naphthoflavone does not stabilise the duplex-single strand transition at pH 7, comparable to the results at pH 5 (section 5.4.7).

(5.5.9)   Neomycin Sulphate.

The left hand panel of Fig. 5.57 shows the melting profiles of oligonucleotide TB1818 in the presence of increasing concentrations of neomycin sulphate. Increasing the ligand concentration decreases the maximum fluorescence signal and shifts the
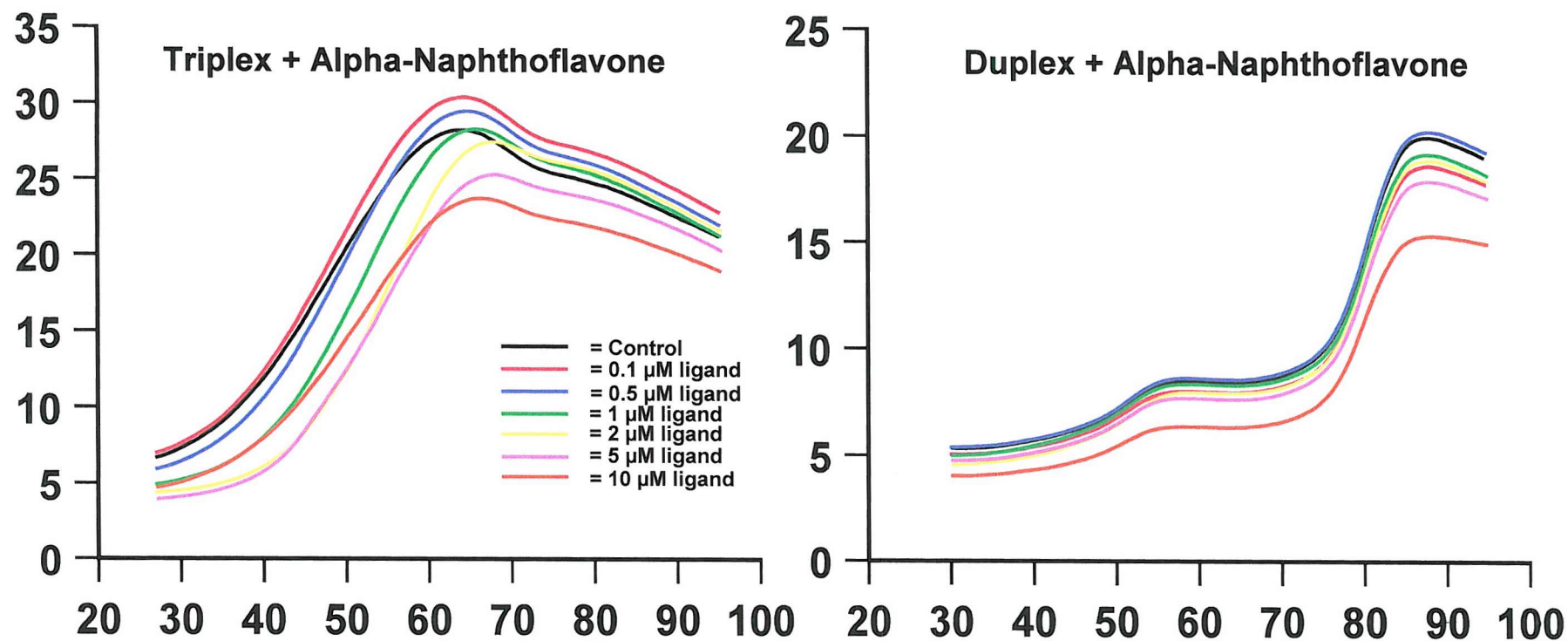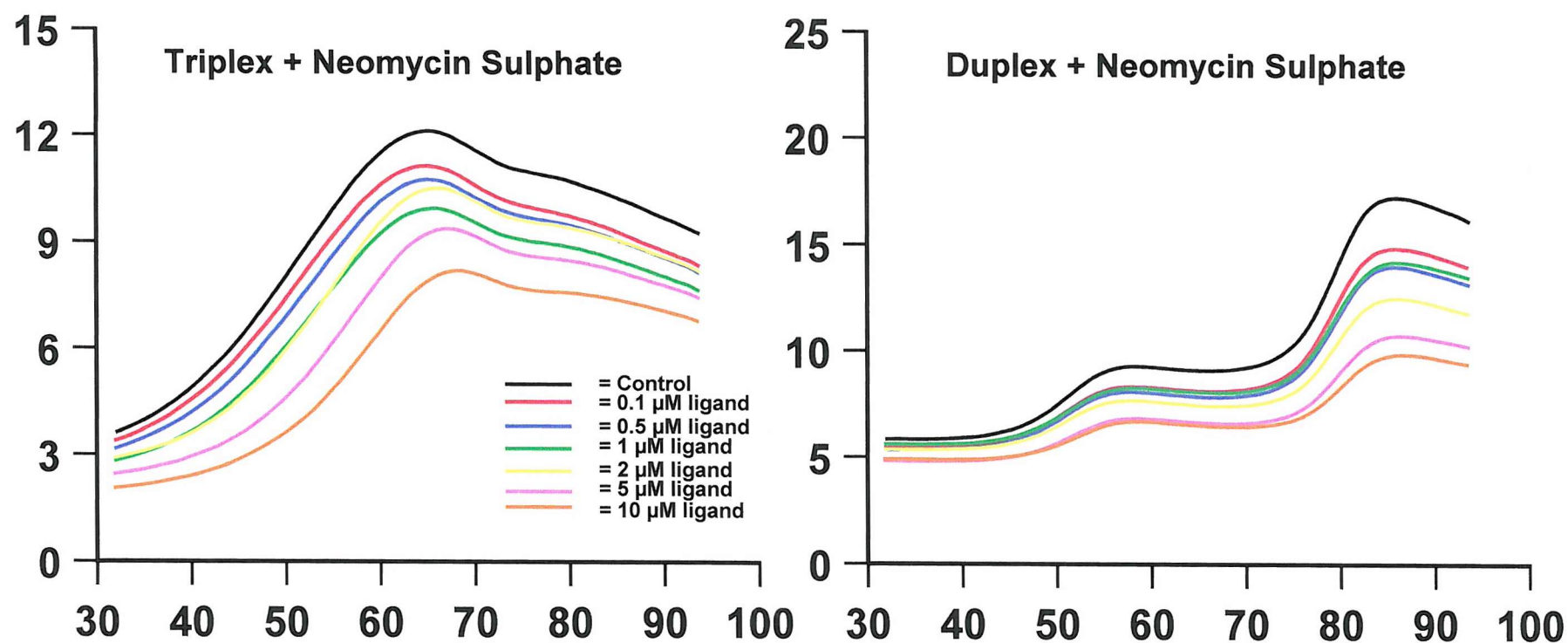
Figure 5.57: Fluorescent DNA thermal denaturation profiles generated with oligonucleotides TB1818 (left) and TB1819 (right) in the presence of an increasing concentration of neomycin sulphate at pH 7. The ordinate represents fluorescence (arbitary units) and the abscissa represents temperature (Celsius).

Neomycin Sulphate	Triplex-duplex Transition (TB1818)		Duplex-single strand Transition (TB1819)	
Concentration (μM)	Tm (°C)	ΔTm (°C)	Tm (°C)	ΔTm (°C)
0	50.6	/	79.7	/
0.1	51.9	1.3	79.5	-0.2
0.5	52.7	2.1	79.5	-0.2
1	54.1	3.5	79.5	-0.2
2	55.3	4.7	79.5	-0.2
5	57.5	6.9	79.6	-0.1
10	59.9	9.6	80.2	0.5
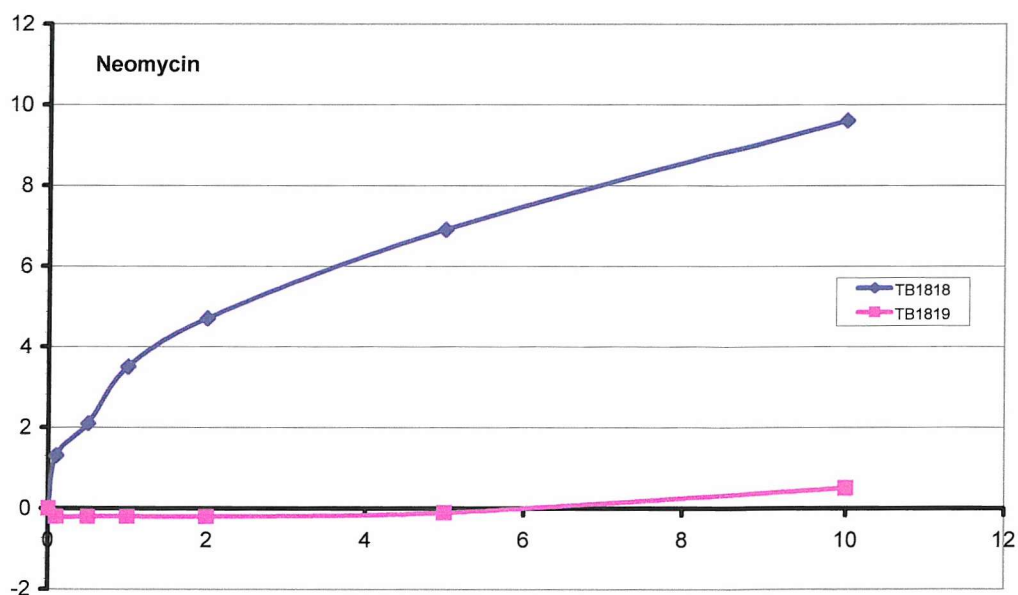
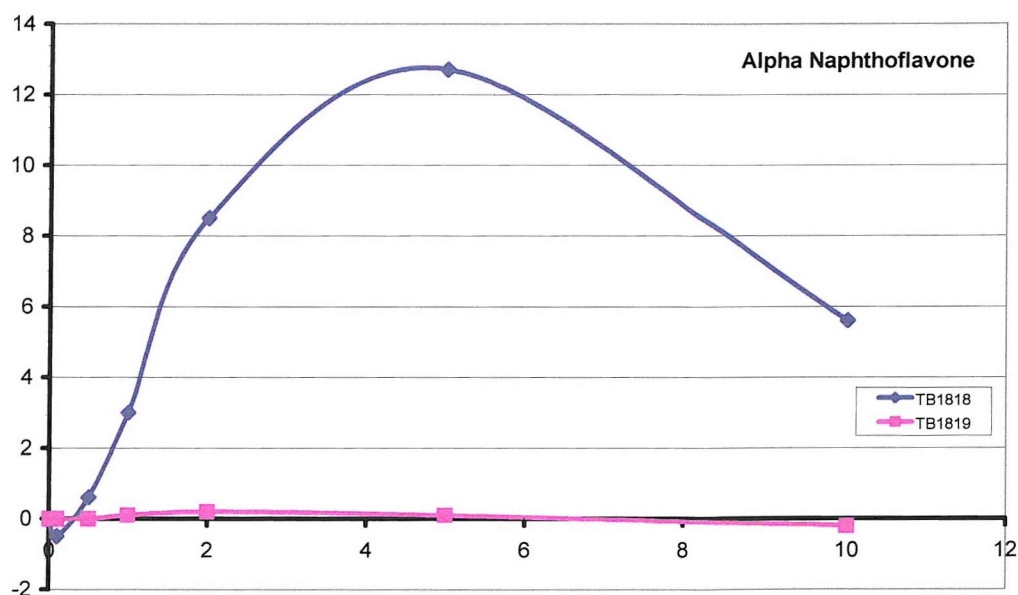**Table 5.27 & Figure 5.58:** Table 5.27 shows the Tm and ΔTm values for the oligonucleotides TB1818 and TB1819 in the presence of neomycin sulphate at pH 7. Figure 5.58 illustrates the stability afforded to the triplex-duplex transition (TB1818), and the duplex-single strand transition (TB1819). The abscissa represents ligand concentration (μM), and the ordinate represents ΔTm (Celsius).
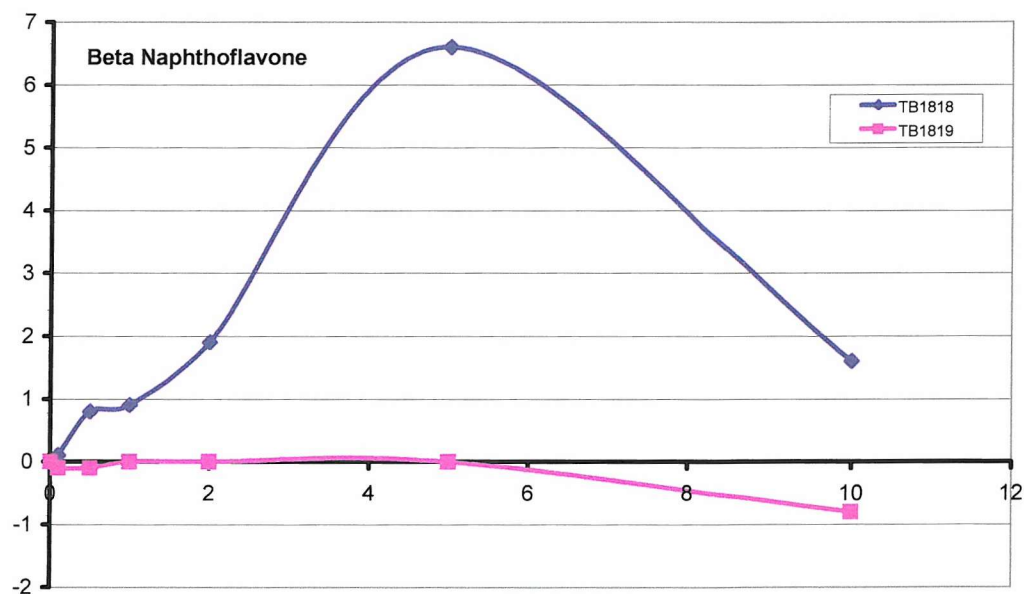
triplex-duplex transition to higher temperatures in a concentration dependent manner, with a ΔTm of 9.6°C in the presence of 10 µM ligand. The Tm values for these triplex-duplex transitions are summarised in Table 5.27 and Fig. 5.58. These results indicate that neomycin sulphate stabilises the triplex-duplex transition in a concentration dependent manner, though the stabilisation afforded is lower than observed at pH 5 (section 5.4.9).

The right hand panel of Fig. 5.57 shows the thermal denaturation profiles for oligonucleotide TB1819 in the presence of increasing concentrations of neomycin sulphate. It can be seen that ligand concentrations up to 1 µM do not significantly alter the melting profile, except there is a decrease in fluorescence intensity. The Tm values for these duplex-single strand transitions are summarised in Table 5.27 and Fig. 5.58. These results indicate that neomycin sulphate does not significantly stabilise the duplex-single strand transition at pH 7, which is comparable to the results obtained at pH 5 (section 5.4.9).

(5.6) Discussion

The results presented in this chapter demonstrate that the Roche LightCycler can be used to obtain DNA melting profiles for fluorescently labelled oligonucleotides. This technique has several advantages over conventional UV-melting experiments, which has been widely used for determining DNA stability and the effects of binding ligands. Firstly this is a high throughput method which requires small sample volumes. Conventional UV-melting curves typically require 1 ml samples, with an OD_{260} of about 0.5 (*i.e.* 75 μM in bases), whereas the LightCycler uses 20 μl volumes of 0.25 μM oligonucleotide (*i.e.* 7.5 μM base concentration for a 30mer oligonucleotide). The LightCycler therefore uses about 50-times less oligonucleotide. Secondly the relative signal is much greater. For UV-melting curves there is typically only a 25% increase in absorbance on melting the DNA, whereas for these fluorescence studies there is often a 5-fold change. In addition the formation of some triplexes is not accompanied by changes in absorbance. Thirdly this technique can have a very high throughput, running 32 samples in parallel, with a heating rate of $0.1°sec^{-1}$ (*i.e.* recording from 30-90°C takes

only 15 minutes). We originally expected that this technique could be used for measuring the melting of the third strand alone, without any interference from melting of the underlying duplex. This aspect has proved less successful than anticipated, since the triplex melt is often followed by a decrease in fluorescence, which is probably related to melting of the duplex (see below).

The relatively fast rate of heating was a potential problem, since the kinetics of intermolecular triplex formation are known to be very slow. Proper interpretation of melting profiles requires that the system is in thermodynamic equilibrium throughout the process - *i.e.* the rate of heating must be slower than the rate at which the system relaxes to its new equilibrium. We checked this by comparing the annealing and dissociation curves which showed no evidence for hysteresis and were superimposable in every case. In addition we examined the effect of even faster heating rates on the melting and annealing curves. We find that rates of $0.5\,^\circ$C sec^{-1} and faster result in hysteresis with the annealing profile generating higher Tm values than the melting profile. These results suggest that heating at a rate of $0.1\,^\circ$sec^{-1} is not a problem for these intramolecular triplexes. Nonetheless it might be a problem for studying intermolecular triplexes and duplexes which will have much slower rates of association.

(5.6.1) Unmodified oligonucleotides alone

Before discussing the effects of base analogues on the stability of DNA triplexes and duplexes it is worth considering some general features of the melting profiles, and the ways in which they may affect the interpretation.

(5.6.1.1) Intramolecular duplexes

The melting curves for oligonucleotide TB1819 show a sharp change in fluorescence signal at about 77°C, which must correspond to the duplex→single strand transition. In addition these traces all show a second smaller melting transition around 45°C, which is more pronounced at pH 7.0. The most likely explanation for this

a)

```
3'-FGAAAAAAGTCAGAG-H-CTCTGACTTTTTTCQ
5'-QCTTTTTTCAGTCTC-H-GAGACTGAAAAAAGF
```

b)

```
5'-QCTTTTTTCAGTCTC-H-GAGACTGAAAAAAGF-3

3'-FGAAAAAAGTCAGAG
                    H
5'-QCTTTTTTCAGTCTC
```

c)

```
                          GAGACTGAAAAAAGF-3'
                        H
5'-QCTTTTTTCAGTCTC
3'-FGAAAAAAGTCAGAG-H-CTCTGACTTTTTTCQ-5'
5'-QCTTTTTTCAGTCTC-H-GAGACTGAAAAAAGF-3'
```

Figure 5.59: Illustrated above are the postulated intermolecular structures; diagram a) demonstrates the possible intermolecular antiparallel duplex generated with 2 TB1819 oligonucleotides. Diagrams b) and c) illustrates the potential of TB1819 to form unstable intermolecular antiparallel triplex structures.

transition is that it corresponds to a small amount of the intermolecular duplex formed by the association of two DNA molecules as shown in Fig. 5.59 (a). This is consistent with the observation that this transition becomes more pronounced at higher oligonucleotide concentrations, as expected for a bimolecular reaction. We also considered the possibility that the oligonucleotide might also adopt the triple helical structures shown in Fig. 5.59 (b) and (c). However these can be discounted as minor groove binding ligands shift this transition to higher temperatures, whereas the results discussed below show that these ligands destabilise triplex DNA.

(5.6.1.2) Intramolecular triplexes

The melting curves for TB1818, the oligonucleotide designed to form an intramolecular triplex, shows a melting transition of 37.3°C at pH 5.0 and 45.2 °C at pH 7.0 in the presence of magnesium. We presume that this corresponds to the triplex→duplex transition. However, this transition is followed by a decrease in the fluorescence signal at higher temperatures. The presence of this second transition was unexpected. The best explanation for this second transition is that it is caused by denaturing the underlying duplex which remains after dissociating the Hoogsteen (third) strand. Since duplex DNA is relatively rigid (less flexible than single stranded DNA) the length of the intermediate species (duplex with a single strand overhang) will separate the fluorophore and quencher, however the final single stranded species will be less ordered and enable the fluorophore and quencher to come into close proximity. The closer approach of the fluorophore and quencher will result in a lower fluorescence signal. This explanation is consistent with the observation that this transition is missing with the more stable triplexes generated using base analogues, for which there is a single transition corresponding to triplex →single strands. In addition this second transition is missing with ligands which are known to selectively stabilise triplex DNA, for which there is again a single transition corresponding to triplex→single strands. However, the mid point of this transition is lower than that measured for the intramolecular duplex TB1819. We can offer several explanations for this difference. Firstly the overhanging single strand may destabilise the remaining duplex. Secondly in TB1818 the methyl red

is attached to the 5 position of one of the duplex T residues, which may cause a slight destabilisation of the duplex. Thirdly, the duplex portion of TB1818 is one base longer than TB1819. The combination of these effects may explain the different melting temperatures, but it is also possible that they are measuring two different molecular events.

(5.6.2) Triplexes containing nucleotide analogues.

The results presented in this chapter show that 5-propargylamino dU, 2'-aminoethoxy T, and 2'-aminoethoxy-5-propargylamino U significantly stabilised DNA triplexes relative to structures containing unmodified thymidine. This effect can be seen at both pH 5 and pH 7. Oligonucleotides containing 5-propargylamino dU or 2'-aminoethoxy T display very similar Tm values at both pHs, whereas the oligonucleotides containing the bis-amino modified analogue produce significantly higher stabilisation than either of the mon-substituted bases. Although adjacent $C^+ \cdot GC$ triplets are known to destabilise triplexes the adjacent incorporation of 2'-aminoethoxy-5-propargylamino U within an oligonucleotide (F67450) produces similar melting temperatures to the oligonucleotide in which these are separated by thymidine.

These results confirm the results of the footprinting studies presented in chapter 3. Incorporation of the bis-amino modified base analogue produces significant stabilisation of the triplex, with a larger increase in stability than that observed with either of the mono-substituted analogues. Although the triplex footprinting experiments showed that oligonucleotides containing 2'-aminoethoxy-5-propargylamino U formed less stable intermolecular triplexes at pH 7 than at pH 5, this effect is not evident in the fluorescent thermal denaturation studies. This difference can be explained as the melting experiments concern intramolecular triplexes, while the footprinting studies are with intermolecular triplexes and that the intramolecular triplexes do not contain any cytosine residues in the third strand in contrast to the footprinting studies which contain one $C^+ \cdot GC$ triplet.

(5.6.3) Effects of triplex binding ligands

Before discussing the effects of individual ligands on the stability of DNA triplexes and duplexes it is worth considering some general features of these interactions, and the ways in which they may affect the interpretation.

Firstly, although the effects on duplex DNA are generally clear cut, the results for triplex DNA are complicated by the unexpected second transition. In some instances (such as with naphthylquinoline) the shape of the triplex melting profile is not affected by addition of the ligand, but is merely shifted to higher temperatures. In other cases (such as with the anthraquinones) the first transition coalesces with the second and it is not always possible to distinguish between the two.

Secondly, the situation is often further complicated by a direct effect of the ligand on the fluorescence yield. In some cases the ligand itself fluoresces thereby masking any changes in DNA fluorescence. In other instances the ligand may only fluoresce when bound to DNA, so that the measured changes reflect not only DNA melting, but dissociation of the ligand at higher temperatures. More commonly the ligand directly quenches the fluorescence signal, presumably by some interaction with fluorescein itself. As a result the shape of the melting profile remains constant, but the overall is signal is reduced. Examples of this effect include the 2,6-disubstituted anthraquinone, BR-19 and BR-20. Each of these effects must be considered when interpreting the melting profiles.

Thirdly, it is also worth noting that the oligonucleotide concentration used in these studies was 0.25 μM. In some instances ligand concentrations lower than this (*i.e.* 0.1 μM) appear to increase the melting temperature. This can only result from a combination of strong binding and rapid kinetics of exchange. Under these conditions if the ligand bound tightly (*i.e.* irreversibly) then the DNA molecules to which it is bound will exhibit a shift in melting temperature, while the remainder will not be affected, thereby producing a biphasic melting curve. If however, the ligand is in relatively rapid exchange, then its distribution will be time-averaged. A further related complication is

that ligand molecules which dissociate first may rebind to remaining structured regions, thereby further increasing their stability.

Lastly, it should be remembered that the stoichiometry of interaction of these ligands with DNA has not been determined. At low concentrations it is likely that only one ligand binds to each triplex, and that progressive change in the melting temperature corresponds to the increased occupancy of this (single) site. However, at higher concentrations it is reasonable to presume that each of these intramolecular complexes can bind more than one ligand molecule..

(5.6.3.1) Naphthylquinoline.

The results presented in sections 5.4.1 and 5.5.1 clearly demonstrate that naphthylquinoline stabilises the triplex-duplex transition at both pH 5 and pH 7. The stabilising effect is significantly higher at pH 5 (ΔTm 26.2°C), than at pH 7 (ΔTm 12°C). This difference can be attributed to the requirement for protonation of naphthylquinoline (Cassidy *et al* 1996). The ring nitrogen has a pKa of 7.1, whilst the terminal nitrogen on the aminoalkyl side chain is fully charged at all pHs. The results suggest that although protonation of the ring nitrogen enhances the triplex stabilising properties of naphthylquinoline, it is not essential to enable intercalation between T·AT triplets. The results confirm that naphthylquinoline has little effect on duplex DNA, and indicate that naphthylquinoline stabilises triplex DNA preferentially over duplex DNA as initially reported by Wilson *et al* (1993). This is thought to be because the naphthylquinoline ring system is too large to optimally stack within a duplex.

(5.6.3.2) Bis-Amidoanthraquinones.

Triplex stabilisation has been previously reported with bis-amidoanthraquinones (Fox *et al* 1995, & Keppler *et al* 1999). Both molecular modelling and footprinting studies concluded that 2,7 functionalised compounds displayed the greatest triplex affinity, whereas 1,4 isomers were shown to selectively stabilise duplex DNA. The

results presented in sections 5.4.2 and 5.5.2 suggest that 1,4 bis-amidoanthraquinone stabilises the triplex-duplex transition. The apparent stabilisation of triplex DNA by the 1,4 isomer was unexpected as previous studies (Fox *et al* 1995) have suggested that this isomer only binds to duplex DNA, since both amido groups are located on the same side of the chromophore. It may be that the apparent stabilisation of the triplex DNA by 1,4 bis-amidoanthraquinone is an artifact. Increasing the concentration of this ligand increases the basal level of fluorescence and this may be due to the fluorescence of the ligand. The lower stabilisation of the duplex-single strand transition for TB1818 compared with TB1819 may result from competition between the 1,4 isomer and the third strand for access to the major groove of the DNA duplex.

The 1,5 bis-amidoanthraquinone generates similar thermal denaturation profiles to those seen with the 1,4 isomer. It has been previously reported that the 1,5 di-substituted isomer binds to duplex as well as triplex DNA; (Keppler *et al* 1999), this is confirmed by the effect of this ligand on TB1819.

The 1,8 bis-amidoanthraquinone has been shown to intercalate into DNA triplexes positioning both side chains within the same triplex groove. This unique ability may explain the high triplex specificity observed since it does not appear to stabilise duplex DNA. In the presence of this ligand oligonucleotide TB1818 displays a single melting transition unlike the 1,4 and 1,5 isomers. This is consistent with the suggestion that the 1,4 and 1,5 isomers bind to both duplex and triplex DNA, while the 1,8 isomer is selective for triplex DNA.

The 2,6 di-substituted isomer was the subject of the initial study into this serries of ligands (Fox *et al* 1995) which showed that it had a higher affinity for triplex DNA than the 1,4 isomer, though later studies concluded that both the 1,8 and the 1,5 di-substituted isomers had a higher triplex affinity (Keppler *et al* 1999). The results presented in sections 5.4.5 and 5.5.5 are again complicated by the presence of two transitions in the triplex melt. Although this may reflect the lack of distinction between triplex and duplex DNA the second of these transitions is associated with an increase in fluorescence in contrast to the decrease seen in the absence of drug. At low

LIGAND (1 µM)	TB1818 pH 5 Δ Tm (°C)	TB1818 pH 7 Δ Tm (°C)
Naphthylquinoline	15.9	3.2
α-Naphthoflavone	10.2	3.0
β-Naphthoflavone	6.6	0.9
1,5	7.2	0.8
1,8	12.2	0.8
2,6	4.2	1.1
2,7	15.9	6.8
BR19	6.0	0.4
BR20	5.5	2.4
Neomycin	14.3	3.5
Ethidium Bromide	2.2	/

LIGAND (1 µM)	TB1819 pH 5 Δ Tm (°C)	TB1819 pH 7 Δ Tm (°C)
Naphthylquinoline	-0.5	-0.2
α-Naphthoflavone	0.1	0.1
β-Naphthoflavone	0.1	0
1,4	9.0	1.0
1,5	6.7	1.0
1,8	0.2	0
2,6	1.7	0.2
2,7	2.6	0.2
BR19	3.4	0.4
BR20	7.0	0.4
Neomycin	0.3	-0.2
Ethidium Bromide	0.1	/
Hoechst 33258	7.3	/
Distamycin	0.8	/

Tables 5.28 & 5.29: Table 5.28 (top) shows the Δ Tm values of TB1818 in the presence of various 1 µM ligands, at both pH 5 and pH 7. Table 5.29 (bottom) shows the Δ Tm values of TB1819 in the presence of various 1 µM ligands, at both pH 5 and pH 7.

concentrations this ligand appears to preferentially stabilise triplex DNA supporting the previous suggestion that this is a selective triplex binding ligand (Keppler *et al* 1999). At higher concentrations it appears to stabilise both duplex and triplex DNA.

The results presented in sections 5.4.6 and 5.5.6 show that 2,7 bis-amidoanthraquinone selectively stabilises triplex DNA at concentrations below 1 μM. However concentrations above 1 μM (pH 5) generate a second melting transition indicative of stabilisation of the duplex-single strand transition.

These results suggest that the order of triplex affinity for these di-substituted amidoanthraquinones at pH 5 is; 2,7 > 1,8 $\geq$ 1,5 > 2,6 (Table 5.28). This order of stability is in agreement with previously published work (Keppler *et al* 1999). However at pH 7 the order of triplex affinity is 2,7 > 2,6 > 1,8 $\geq$ 1,5 (Table 5.28).

(5.6.3.3)   Naphthoflavone.

The triplex stabilising properties of naphthoflavone were reported by Prof. J. Chaires at the international meeting NACON V (unpublished data), and was discovered by competition dialysis assay (Ren & Chaires 1999). The results presented in sections 5.4.7 and 5.5.8 show that both the alpha and beta anomers of naphthoflavone stabilise the triplex-duplex transition of TB1818 at both pH 5 and pH 7, though α-naphthoflavone has the greatest effect. An unusual feature of both these compounds is that ligand concentrations above 5 μM show a decrease in triplex stability, and would indicate a second mode of binding. The results show that both alpha and beta naphthoflavone do not stabilise duplex DNA. The potential of this uncharged triplex specific ligand is that it may be able to interact with any sequence, unlike positively charged ligands such as naphthylquinoline and acridine which can not intercalate adjacent to $C^{+}\cdot GC$ triplets due to charge repulsion.

(5.6.3.4)   Acridine Derivatives.

The acridine derivatives BR19 and BR20 were designed to stabilise quadruplex DNA (Read *et al* 2001). However the results presented in this chapter demonstrate that both compounds can also bind to triplex DNA, and that BR19 stabilises the triplex-duplex transition by 6.7°C at a ligand concentration of 2 μM. However both these compounds have a much greater effect on duplex DNA. In addition the stabilisation of triplex DNA is greater at low pH, suggesting that the charged form of the ligand intercalates between T·AT triplets.

(5.6.3.5)   Neomycin Sulphate.

The results presented in sections 5.4.9 and 5.5.9 demonstrate that neomycin stabilises the triplex DNA in a concentration dependent manner and shows that its effect is greater at pH 5 (ΔTm 23.5°C) than at pH 7 (ΔTm 9.6°C). This antibiotic contains 6 amino groups that could potentially be protonated; one of these amino groups has a pKa value of 5.7 (Ayra *et al* 2001), therefore it is possible to envisage that at pH 7 protonation of this group does not occur. The results show that neomycin does not stabilise duplex DNA, and confirms its reported triplex specific selectivity (Arya & Coffee Jr 2000, Arya *et al* 2001). Since the structure of neomycin precludes intercalation it has been suggested that it must be binding to one of the triplex grooves (Ayra & Coffee Jr 2000).

(5.6.3.6)   Ethidium Bromide.

The studies with ethidium bromide demonstrate it stabilises the triplex-duplex transition in a concentration dependent manner, whereas the duplex-single strand transition is hardly affected even at 10 μM. This result was unexpected as it is generally accepted that ethidium bromide stabilises duplex DNA via intercalation, and has limited triplex stabilising properties (Mergny *et al* 1991). However it has been reported that ethidium bromide stabilises poly(dA)·2poly(dT) triplexes to a significantly higher degree than the underlying duplex poly(dA)·poly(dT) (Scaria & Shafer 1991). The lack of an

effect on TB1819 may be explained since it contains a tract of six consecutive AT base pairs.

(5.6.3.7)   Hoechst 33258.

Hoechst 33258 is a synthetic minor groove binding ligand. Previous studies have concluded that Hoechst 33258 binds to A:T but not G:C base pairs, with a preference for 4 consecutive A:T base pairs (Harshman & Dervan 1985, Drobyshev *et al* 1999). Since triplex forming oligonucleotides bind in the DNA major groove, there will be no steric interaction with Hoechst 33258, and this might therefore be expected to bind to triple helical DNA. The results presented in section 5.4.11 demonstrate that Hoechst 33258 stabilises the duplex-single strand transition in a concentration dependent manner. In contrast Hoechst 33258 destabilises triplex DNA at concentrations below 1 µM. Increasing the concentration of Hoechst 33258 above 1 µM yielded some triplex stabilisation (results not shown) but accurate determination of the Tm value was not possible. This increase in stability may be due a second mode of binding of the ligand (Bailly *et al* 1993) whereby it intercalates within the DNA helix as opposed to binding in the minor groove. The results at low concentrations suggest that the DNA structure formed when Hoechst binds in the DNA minor groove is not compatible with triplex formation. This supports the previous study of Durand *et al* (1994) where Hoechst 33258 was shown to destabilise triplex DNA. It has been shown however that tethering Hoechst 33258 to an oligonucleotide enhances triplex stability (Robles *et al* 1996), believed to be due to a single molecule of Hoechst 33258 occupying the minor groove. However, in these studies it is not clear whether Hoechst 33258 is binding within the triplex or to the duplex immediately adjacent to the triplex. The results presented in this chapter suggest that Hoechst 33258 cannot bind to triple helical DNA, and therefore when tethered to triplex forming oligonucleotides it may be targeted to adjacent duplex regions.

(5.6.3.8) **Distamycin A.**

The antibiotic distamycin A is an oligopeptide containing three N-methylpyrrole rings, that has been reported to bind to the minor groove of duplex DNA, with a preference for $A_n{\cdot}T_n$ (Zimmer 1975, Zimmer *et al* 1979, Klevit *et al* 1986, Capobianco *et al* 1991), and that distamycin A destabilises triplex DNA (Durand & Maurizot 1996). The results presented in section 5.4.12 show that at pH 5 distamycin A stabilises the duplex-single strand transition, in a concentration dependent manner. In contrast triplex DNA is destabilised by this ligand and the triplex-duplex transition occurs below 25 °C at distamycin A concentrations above 0.5 µM. The destabilisation of triplex DNA probably results from distamycin A altering the dimensions of the minor groove thereby preventing the third strand binding to the major groove.

Chapter 6.

Conclusions.

Triple helical nucleic acids offer the possibility of sequence specific gene regulation, and may be used to treat bacterial/viral infections as well as cancer. However there are several limitations currently associated with the antigene strategy, two of which have been addressed in this thesis; 1) is the lower intrinsic stability of triplex DNA compared with that of duplex DNA, and 2) the requirement for the recognition of an un-interrupted polypurine tract. The decreased stability is believed to rise from the close proximity of the three negatively charged phosphodiester backbones, that is only partially overcome under physiological conditions, while pyrimidine residues can not be recognised due to the formation of single hydrogen bonds. In an attempt to overcome these issues base analogues have been designed to enhance triplex stability and expand the triplex recognition sequences. Furthermore triplex specific ligands which are presumed to bind via intercalation between base triplets have been used to increase the stability of triple helical nucleic acids.

In general the footprinting results presented in Chapter 3 indicate that partial substitution of 9-mer parallel TFO's with 5-propargylamino dU or 2'-aminoethoxy T at less than 4 positions does not afford an increase in triplex stability, and the results are comparable to those obtained with an unmodified oligonucleotide. Both these thymidine analogues produce significant enhancements in triplex stability when incorporated at 4 positions within these oligonucleotides, and they are of roughly equal potency. Previous studies with 5-propargylamino dU and 2'-aminoethoxy T have demonstrated increased triplex stability (Bijapur *et al*, 1999, Gowers *et al*, 1999, Bloomers *et al* 1998, Cuenoud *et al* 1998). However the oligonucleotides used in these studies were fully substituted with these base analogues and were used in conjunction with protonated cytosine residues. The stabilising properties of these analogues are thought to be due to the position of the amino groups which are positioned so as to interact with the phosphate atoms in the DNA backbone, thereby reducing some of the charge repulsion. Therefore it is possible that the increased triplex stability reported by Bijapur *et al* (1999), Gowers *et*

-135-

al (1999), Bloomers *et al* (1998) and Cuenoud *et al* (1998) is due to the regular alternation of the positively charged amino group between the negatively charged phosphate atoms, and that partial substitution of an oligonucleotide with 5-propargylamino dU or 2'-aminoethoxy T at interspersed positions generates a non-uniform backbone geometry. Furthermore the results demonstrate that 5-propargylamino dU can not be used to increase the stability of antiparallel triplexes, nor can it be used to stabilise parallel GT triplex formation. However combining the amino substituents of 5-propargylamino dU and 2'-aminoethoxy T within the same analogue, generating the bis-amino thymidine analogue 2'-aminoethoxy-5-propargylamino U, increases triplex stability more than either of the two individual analogues, and promotes triplex stability at both pH 5 and pH 7.5 with an oligonucleotide substituted at 3 or 4 positions.

The results presented for the abasic residues demonstrate that 1'-β-hexylamino deoxyribose, and 1'-methoxy-2'-aminoethoxyribose do not increase triplex stability across a single pyrimidine interruption any more than 1',2-H-dideoxyribose. This is thought to be due to a loss of base stacking about the null site, and indicates that incorporation of these protonated groups does not influence the stability across a null site.

Chapter 4 investigated the sequence specificity of naphthoflavone and proflavine derivative triplex specific ligands. The results demonstrate that the positively charged proflavine derivative 4403 stabilised triplex DNA which contained TpT steps, and may indicate that this ligand only intercalates at adjacent T·AT triplets and not next to protonated cytosine. This is presumably due to the protonated proflavine chromophore. Derivative 4403 stabilised triplex DNA to a higher degree than derivative 4405; this is postulated to be due to the difference in the length of the linker attaching the chromophore to the piperazine. The stabilising properties of naphthoflavone were first reported by Prof. J.B. Chaires at NACON V (un-published data), and I have shown that α-naphthoflavone stabilises triplex formation irrespective of the oligonucleotide sequence. This universal triplex stabilisation is believed to be due to the un-charged nature of the ligand increasing the number of potential intercalation sites. However β-naphthoflavone appears to destabilise triplex formation, either because it causes

structural distortions at the site of intercalation, or because it binds preferably to duplex, rather than triplex DNA.

The results presented in Chapter 5 demonstrate the use of fluorescently labelled oligonucleotides to determine DNA stability using a novel technique that we have developed. Using this technique I have determined accurate melting curves for both intramolecular triplex-duplex and duplex-single strand transitions using both the melting and annealing profiles generated with a Roche PCR-LightCycler, heating the samples at a rate of 0.1 °C sec^{-1}. The technique can accurately determine the triplex stability afforded by base analogues, as opposed to UV melting experiments which often generate melting curves in which the triplex-duplex and duplex-single strand transitions are coincident, thereby preventing accurate determination of the individual thermodynamic steps. These investigations support the findings of Chapter 3, that the bis-amino modified analogue affords higher stability than either 5-propargylamino dU or 2'-aminoethoxy T at both pH 5 and pH 7 (Table 6.1). The technique also allows us to assess the effects of both duplex and triplex specific ligands. Although the melting profiles are usually easy to interpret (naphthylquinoline), some ligands generate multi-phasic profiles and alter the background fluorescence (bis-amidoanthraquinones), thereby complicating the analysis. Keppler *et al*, 1999 concluded that the parallel triplex affinity of the di-substituted amidoanthraquinones decreased in the order 2,7 > 1,8 = 1,5 > 2,6 and that the 1,4 isomer afforded no increase in triplex stability (Table 6.2). The LightCycler data presented in Chapter 5 reflects this order of affinity with the 2,7 isomer demonstrating the greatest stabilising properties and the 1,8 isomer showing slightly higher stabilising properties than the 1,5 isomer. These results are compared with those of Keppler *et al*, 1999 in Table 6.1. Contrary to the footprinting data shown in Chapter 4, analysis with the Roche-LightCycler indicates that β-naphthoflavone stabilises triplex DNA (albeit to a lower degree than that of α-naphthoflavone). This is postulated to be due to differences between intermolecular and intramolecular triplexes.

	pH 5		pH 7	
Base Modification	**Footprint C_{50} Value (μM)**	**Δ Tm (°C)**	**Footprint C_{50} Value (μM)**	**Δ Tm (°C)**
5-Propargylamino dU	8.6 ± 3.8	30.1	/	35.0
2'-Aminoethoxy T	7.9 ± 1.2	28.1	/	33.4
2'-Aminoethoxy-5-propargylamino U	0.13 ± 0.03	37.1	0.5 ± 0.1	41.0

Table 6.1: Shown are the footprinting C_{50} values (μM) for oligonucleotides 4^PU, 4^{AE}T, and 4^{AEP}U. Also shown are the Δ Tm values (°C) of the intramolecular TFO's TB1794, TB1795, and F67449 as determined using the Roche LightCycler. / indicates no footprint detected.

Di-substituted Amidoanthraquinone	**K_L (μM)**	**Δ Tm (°C) Ligand Conc. 1 μM**
2,7	0.17 ± 0.05	15.9
1,5	0.27 ±0.07	7.2
1,8	0.36 ± 0.08	12.2
2,6	1.0 ± 0.4	4.2

Table 6.2: Shown are the apparent dissociation constants (μM) for the interaction of the various anthraquinone derivatives with triplex DNA (reproduced from Keppler *et al*, 1999), and the Δ Tm values of the intramolecular TFO (TB1818) in the presence of the same ligands at a concentration of 1 μM.

The results presented in this thesis show the importance of designing base analogues with positive charges. It is shown that increased triplex stability is afforded by the bis-modified 2'-aminoethoxy-5-propargylamino U analogue, and that the stability is higher than the sum of the individual analogues. Furthermore it is shown that this stability may be pH independent. The stabilising properties of all three analogues is believed to due to the positioning of the positive charge away from the ring structure of the base, enabling it to interact with the negatively charged backbone, dissipating some of the repulsion. Similar substitutions on cytosine derivatives might be expected to produce enhanced triplex stability. However; substitution at the 5 position of cytosine with propargylamino groups may not be useful as this will decrease the pK of N3. However, other cytosine analogues such as 6-oxo-cytosine may be amenable to modification in this way.

The novel high throughput fluorescence method used for assessing triplex and duplex DNA stability should be generally applicable for thermodynamic studies on DNA stability, and is superior to traditional UV melting studies. This technique uses small quantities of sample, is highly sensitive, has high throughput and enables investigation of triplexes which are not accompanied by changes in their UV spectra. This technique is currently being developed for assessing the stability of quadruplex DNA and its stabilisation by ligands.

References.

Agazie, Y.M., Burkholder, G.D., Lee, J.S., (1996) *Biochem. J.* **316**, 461-466

Agrawal, S., Goodchild, J., Civeira, M.P., Thornton, A.H., Sarin, P.S., Zamacnik, P.C., (1988) *Proc. Natl. Acad. Sci. USA* **85**, 7079-7083

Aich, P., Thomas, T.J., Lee, J.S., (2000) *Nucleic Acids Res.* **28**, 2307-2310

Alberts, B., Bray, D., Lewis, J., Raff, M., Roberts, K., Watson, J.D., (1994) *Molecular Biology of The Cell.* **3**rd **Ed.** Garland Publishing, Inc. New York & London.

Alunni-Fabbroni, M., Manfioletti, G., Manzini, G., Xodo, L.E., (1994) *Eur. J. Biochem.* **226**, 831-839

Amosova, O.A., Fresco, J.R., (1999) *Nuc. Acids Res.* **27**, 4632-4635

Anizon, F., Belin, L., Moreau, P., Snacelme, M., Voldoire, A., Prudhomme, M., Ollier, M., Severe, D., Riou, J-F., Bailly, C., Fabbro, D., Meyer, T., (1997) *J. Med. Chem.* **40**, 3456-3465

Arimondo, P.B., Barcelo, F., Sun, J-S., Maurizot, J-C., Garestier, T., Hélène, C., (1998) *Biochemistry* **37**, 16627-16635

Arimondo, P.B., Moreau, P., Boutorine, A., Bailly, C., Prudhomme, M., Sun, J-S., Garestier, T., Hélène, C., (2000) *Bioorg. Med. Chem.* **8**, 777-784

Arimondo, P.B., Bailly, C., Boutorine, A., Moreau, P., Prudhomme, M., Sun, J-S., Garestier, T., Hélène, C., (2001) *Bioconj. Chem.* **12**, 501-509

Arnott, S., Bond, P.J., (1973) *Nature* **244**, 99-101

Arnott, S., Selsing. E.J., (1974) *J. Mol. Biol.* **88**, 509-521

Arnott, S., Bond, P.J., Selsing, E.J., Smith, P.J.C., (1976) *Nucleic Acids Res.* **3**, 2459-2470

Arya, D.P., Coffee Jr., R.L., (2000) *Bioorg. Med. Chem. Lett.* **10**, 1897-1899

Arya, D.P., Coffee Jr., R.L., Willis, B., Abramovitch, A.I., (2001) *J. Am. Chem. Soc.* **123**, 5385-5395

Asensio, J.L., Lane, A.N., Dhesi, J., Bergqvist, S., Brown, T., (1998a) *J. Mol. Biol.* **275**, 811-822

Asensio, J.L., Dosanjh, H.S., Jenkins, T.C., Lane, A.N., (1998b) *Biochemistry* **37**, 15188-15198

Asensio, J.L., Brown, T., Lane, A.N., (1998c) *Structure* **7**, 1-11

Asseline, V., Delarue, M., Lancelot, G., Toulmé, F., Thuong, N.T., Montenay-Garestier,T., Hélène, C., (1984) *Proc. Natl. Acad. Sci. USA* **81**, 3297-3301

Baguley, B.C., Falkenhaug, E-M., (1978) *Nucleic Acids Res.* **5**, 161-171

Bailly, C., Colson, P., Hénichart, J-P., Houssier, C., (1993) *Nucleic Acids Res.* **21**, 3705-3709

Bailly, C., Riou, J-F., Colson, P., Houssier, C., Rodrigues-Pereira, E., Prudhomme, M., (1997) *Biochemistry* **36**, 3917-3929

Baldi, M.I., Benedetti, P., Mattoccia, E., Tocchini-Valentini, G.P., (1980) *Cell* **20**, 461-466

Baran, N., Lapidot, A., Manor, H., (1987) *Mol. Cell. Biol.* **7**, 2636-2640

Bates, P., Laughton, T., Jenkins, T., Capaldi, D., Rosett, P., Reese, C., Neidle, S. (1996) *Nucleic Acids Res.* **24**, 4176-4184

Beal, P., & Dervan, P.B., (1991) *Science* **251**, 1360-1363

Beal, P., & Dervan, P.B., (1992) *Nucleic Acids Res.* **20**, 2773-2776

Bensch, K.G., Malawista, S.E., (1969) *J. Cell Biol.* **40**, 95

Bernardi, A., Ehrlich, S.D., Thiery, J., (1973) *Nature* **246**, 36-40

Bernardi, A., Gaillard, C., Bernardi, G., (1975) *Eur. J. Biochem.* **52**, 451-457

Berressum, R., & Engels, W., (1995) *J. Am. Chem. Soc.* **117**, 1187-1193

Betts, L., Josey, J.A., Veal, J.M., Jordan, S.R., (1995) *Science* **270**, 1838-1841

Bijapur, J., Keppler, M.D., Bergqvist, S., Brown, T., Fox, K.R., (1999) *Nucleic Acids Res.* **27**, 1802-1809

Blommers, M.J.J., Natt, F., Jahnke, W., Cuenoud, B., (1998) *Biochemistry* **37**, 17714-17725

Blume, S.W., Guarcello, V., Zacharias, W., Miller, D.M., (1997) *Nucleic Acids Res.* **25**, 617-625

Boado, R.J., (1995) *Adv. Drug Deliv. Reviews* **15**, 73-107

Boffa, L.C., Morris, P.L., Carpaneto, E.M., Louissaint, M., Allfrey, V.G., (1996) *J.Biol. Chem.* **271**, 13228-13233

Bresloff, J.L., Crothers, D.M., (1981) *Biochemistry* **20**, 3547-3553

Broitman, S., Im, D., Fresco, J., (1987) *Proc. Natl. Acad. Sci. USA* **84**, 5120-5124

Brunar, H., & Dervan, P.B., (1996) *Nucleic Acids Res.* **24**, 1987-1991

Callahan, D.E., Trapane, T.L., Miller, P.S., Ts'o, P.O.P., Kan, L-S., (1991) *Biochemistry* **30**, 1650-1655

Capobianco, M.L., Colonna, F.P., Forni, A., Garbesi, A., Lotti, S., Moretti, I., Samori, B., Tondelli, L., (1991) *Nuc. Acids Res.* **19**, 1695-1698

Cassidy, S.A., Strekowski, L., Wilson, W.D., Fox, K.R., (1994) *Biochemistry* **33**, 15338- 15347

Cassidy, S.A., Strekowski, L., Fox, K.R., (1996) *Nucleic Acids Res.* **24**, 4133-4138

Cassidy, S.A., Slickers, P., Trent, J., Capaldi, D., Roselt, P.,Reese, C., Neidle, S., Fox, K.R., (1997) *Nucleic Acids Res.* **25**, 4891-4898

Cazenave, C., Chevrier, M., Thuong, N.T., Hélène, C., (1987) *Nucleic Acids Res.* **15**, 10507-105012

Chandler, S.P., & Fox, K.R., (1995) *FEBS lett.* **360**, 21-25

Chaturvedi, S., Horn, T., Letsinger, R.L., (1996) *Nucleic Acids Res.* **24**, 2318-2323

Cheng, A-J., & Van Dyke, M.W., (1993) *Nucleic Acids Res.* **21**, 5630-5635

Cherny, D.Y., Belotserkovskii, B.P., Frank-Kamenetskii, M.D., Egholm, M., Buchardt, O., Berg, R.H., Nielsen, P.E., (1993) *Proc. Natl. Acad. Sci. USA* **90**, 1667-1670

Cho, B.P., & Evens, F.E., (1991) *Nucleic Acids Res.* **19**, 1041-1047

Collier, D.A., Mergny, J-L., Thuong, N.T., Hélène, C., (1991) *Nucleic Acids Res.* **19**, 4219-4224

Colocci, N., Distefano, M., Dervan, P.B., (1993) *J. Am. Chem. Soc.* **115**, 4468-4473

Cooney, M., Czernuszewicz, G., Postel, E.H., Flint, S.J., Hogan, M.E., (1988) *Science* **241**, 456-459

Cuenoud, B., Casset, F., Hüsken, D., Natt, F., Wolf, R.M., Altmann, K.H., Martin, P., Moser, H.E., (1998) *Angew. Chem.* **37**, 1288-1291

Dagle, J.M., & Weeks, D.L., (1996) *Nucleic Acids Res.* **24**, 2143-2149

Dagneaux, C., Liquier, J., Taillandier, E., (1995) *Biochemistry* **34**, 16618-16623

Daniel, W.A., Syrek, M., Haduch, A., (1999) *Pol. J. Pharmacol.* **51** 435-442

David-Pfeuty, T., Simon, C., Pantaloni, D., (1979) *J. Biol. Chem.* **254**, 11696-11702

Davison, E.C., & Johnsson, K., (1993) *Nucleosides & Nucleotides* **12**, 237-243

De Clercy, E., Descamps, J., Balzarini, J., Giziewicz, J., Barr, P.J., Robins, M.J., (1983) *J. Med. Chem.* **26**, 661-666

Del los Santos, C., Rosen, M., Patel, D.J., (1989) *Biochemistry* **28**, 7282-7289

Demidov, V.V., Yanilovich, M.V., Belotserkovskii, B.P., Frank-Kamenetskii, M.D., Nielsen, P.E., (1995) *Proc. Natl. Acad. Sci. USA.* **92**, 2637-2641

Dingwall, C., Lomonssoff, G.P., Laskey, R.A., (1981) *Nucleic Acids Res.* **9**, 2659-2673

Drobyshev, A.L., Zasedatelev, A.S., Yershov, G.M., Mirzabekov, A.D., (1999) *Nucleic Acids Res.* **27**, 4100-4105

Drew, H.R., Travers, A.A., (1984) *Cell* **37**, 491-502

Durand, M., Thuong, N.T., Maurizot, J.C., (1994) *Biochime* **76**, 181-186

Durand, M., Maurizot, J.C., (1996) *Biochemistry* **35**, 9133 - 9139

Egholm, M., Buchardt, O., Nielsen, P.E., Berg, R.H., (1992a) *J. Am. Chem. Soc.* **114**, 18950-1897

Egholm, M., Buchardt, O., Nielsen, P.E., Berg, R.H., (1992b) *J. Am. Chem. Soc.* **114**, 9677-9678

Egholm, M., Buchardlt, O., Christensen, L., Behnens, C., Freier, S.M., Driver, D.A., Berg, R.H., Kim, S.K., Norden, B., Nielsen, P.E., (1993) *Nature* **365**, 565-568

Escudé, C., Nguyen, C.H., Mergny, J-L., Sun, J-S., Bisagni, E., Garestier, T., Hélène, C., (1995) *J. Am. Chem. Soc.* **117**, 10212-10219

Escudé, C., Sun, J-S., Nguyen, C.H., Bigagni, E., Montenay-Garestier, T., Hélène, C., (1996) *Biochemistry* **35**, 5735-5740

Escudé, C., Nguyen, C.H., Kukreti, S., Janin, Y., Sun, J-S., Bisagni, E., Montenay-Garestier, T., Hélène, C., (1998) *Proc. Natl. Acad. Sci. USA* **95**, 3591-3596

Faucon, B., mergny, J-L., Hélène, C., (1996) *Nuc. Acids Res.* **24**, 3181-3188

Farber, S, (1948) *N. Engl. J. Med.* **238**, 787-793

Faruqi, A.F., Krawczyk, S.H., Matteucci, M.D., Glazer, P.M., (1997) *Nucleic Acids Res.* **25**, 633-640

Felsenfeld, G., & Rich, A., (1957) *Biochem. Biophys. Acta.* **26**, 457-468

Floris, R., Scaggiante, B., Manzini, G., Quadrifoglio, F., Xodo, L.E., (1999) *Eur. J. Biochem.* **260**, 801-809

Fox, K.R., & Waring, M.J. (1987) *Biochem. Biophys. Acta.* **909**, 145-155

Fox, K.R. & Waring, M.J. (1987) *Nucleic Acids Res.* **15**, 491 - 507

Fox, K.R., (1994) *Nucleic Acids Res.* **22**, 2016-202

Fox, K.R., Polucci, P., Jenkins, T.C., Neidle, S., (1995) *Proc. Natl. Acad. Sci. USA* **92**, 7887-7891

Frantz, J.D., Gilbert, W., (1995) *J. Biol. Chem.* **270**, 9413-9419

Froehler, B.C., & Ricca, D.J., (1992) *J. Am. Chem. Soc.* **114**, 8320-8322

Froehler, B.C., Terhorst, T., Shaw, J-P., McCurdy, S.N., (1992) *Biochemistry* **31**, 1603-1609

Futterman S., (1957) *J. Biol. Chem.* **228**, 1031

Galas, J.D., & Schmitz, A., (1978) *Nucleic Acids Res.* **5**, 3157-3170

Gale, E.F., Cundliffe, E., Reynolds, P.E., Richmond, M.H., Waring, M.J., (1981) *The Molecular Basis of Antibiotic Action* 258-401

Gao, W., Stein, C.A., Cohen, J.S., Dutschman, G.E., Cheng, Y., (1988) *J. Biol. Chem.* **264**, 11521-1152

George, P., Journey, L.J., Goldstein, M.N., (1965) *J. Natl. Cancer Inst. (U.S.)* **35**, 355-375

Gilman, A., Philips, F.S., (1946) *Science* **103**, 409-415

Giovannangeli, C., montenay-Garestier, T., Thuong, N.T., Hélène, C., (1992) *Proc. Natl. Acad. Sci. USA* **89**, 8631-8635

Giovannangeli, C., Perrouault, L., Escaudé, C., Gryaznov, S., Hélène, C., (1996) *J. Mol. Biol.* **261**, 386-398

Glisson, B., Gupta, R., Smallwood, S., Cantu, E., Ross, W., (1985) *proc. Natl. Acad. Sci. USA* **26**, 340-348

Goodchild, J., Porter, R.A., Raper, R.H., Sim, I.S., Upton, R.M., Viney, J., Wadsworth, H.J., (1983) *J. Med. Chem.* **26**, 1252-1257

Gowers, D.M., & Fox, K.R., (1998) *Nucleic Acids Res.* **26**, 3626-3633

Gowers, D.M., & Fox, K.R.,. (1999a) *Nucleic Acids Res.* **27**, 1569-1577

Gowers, D.M., Bijapur, J., Brown, T., Fox, K.R., (1999b) *Biochemistry* **38**, 13747-13758

Gralla, J., & Crothers, D.M., (1973) *J. Mol. Biol.* **78**, 301-319

Greenberg, W.A., Dervan, P.B., (1995) *J. Am. Chem. Soc.* **117**, 5016-5022

Griffin, L., & Dervan, P.B., (1989) *Science* **245**, 967-971

Griffin, L., Kiessling, L., Beal, P., Gillespie, P., Dervan, P.B., (1992) *J. Am. Chem. Soc.* **114**, 7976-7982

Gryaznov, S.M., Lloyd, D.H., (1993) *Nucleic Acids Res.* **21**, 5909-5915

Gryaznov, S.M., Winter, H., (1998) *Nucleic Acids Res.* **26**, 4160-4167

Guieysse, A-L., Praseuth, D., Hélène, C., (1997) *J. Mol. Biol.* **267**, 289-298

Gupta, R., (1983) *Cancer Res.* **43**, 344-351

Hacia, J.G., Wold, B.J., Dervan, P.B., (1994) *Biochemistry* **33**, 5367-5369

Harshman, K.D., Dervan, P.B., (1985) *Nucleic Acids Res.* **13**, 4825-4835

Havre, P.A., Gunther, E., Gasparro, F.P., Glazer, P.M., (1993) *Proc. Natl. Acad. Sci. USA* **90**, 7879-7883

Helmut, B., Dervan, P.B., (1996) *Nucleic Acids Res.* **24**, 1987-1991

Hertzberg, R.P., Dervan, P.B., (1982) *Journ. Amer. Chem. Soc.* **104**, 313-315

Hertzberg, R.P., Dervan, P.B., (1984) *Biochemistry* **23**, 3934-3945

Hogan, M.E., Robertson, M.W., Austin, R.H., (1989) *Proc. Natl. Acad. Sci. USA* **86**, 9273-9277

Horne, D.A., & Dervan, P.B., (1990) *J. Am. Chem. Soc.,* **112**, 2435-2437

Horne, D., & Dervan, P.B., (1991) *Nucleic Acids Res.* **19**, 4963-4965

Hörz, W., Altenburger, W., (1981) *Nucleic Acids Res.* **9**, 2643-2658

Howard, F.B., Miles, H.T., Liu, K., Frazier, J., Raghunathan, G., Sasisekharan, V., (1992) *Biochemistry* **31**, 10671-10677

Hsieh, T-S., Brutlag, D., (1980) *Cell* **21**, 115-121

Ihara, T., Takeda, Y., Jyo, A., (2001) *J. Am. Chem. Soc.* **123**, 1772-1773

Jayaraman, K., Durland, R.H., Roa, T.S., Revankar, G.R., Bodepudi, V., Chaudhary, N., Guy-Caffey, J., (1995) *Nucleosides & Nucleotides* **14**, 951-955

Jayasena, S.D., & Johnston, B.H., (1992$_a$) *Nucleic Acids Res.* **20**, 5279-5288

Jayasena, S.D., & Johnston, B.H., (1992$_b$) *Biochemistry* **31**, 320-327

Jayasena, S.D., & johnston, B.H., (1993) *Biochemistry* **32**, 2800-2807

Jetter, M.C., Hobbs, F.W., (1993) *Biochemistry* **32**, 3249-3254

Ji, J., Hogan, M.E., Gao, X., (1996) *Structure* **4**, 425-434

Jiménez-García, E., Vaquero, A., Espinás, M. L., Soliva, R., Orozco, M., Bernués, J., Azorín, F., (1998) *J. Biol. Chem.* **273**, 24640-24648

Jones, P.A., (2001) *Nature* **409**, 141-144

Joseph, J., Kandala, J.C., Veerpanane, D., Weber, K.T., Guntaka, R.V., (1997) *Nucleic Acids Res.* **25**, 2182-2188

Kan, Y., Armitage, B., Schuster, G.B., (1997) *Biochemistry,* **36**, 1461-1466

Keppler, M.D., Fox, K.R., (1997) *Nucleic Acids Res.* **25**, 4644-4649

Keppler, M.D., (1999) *PhD Thesis*

Keppler, M.D., Read, M.A., Pery, P.J., Trent, J.O., Jenkins, T.C., Reszka, A.P., Neidle, S., Fox, K.R., (1999a) *Eur. J. Biochem.* **263**

Keppler, M.D., Zegrocka, O., Strekowski, L., Fox, K.R., (1999b) *FEBS lett.* **447**, 223-226

Keppler, M.D., McKeen, C.M., Zegrocka, O., Strekowski, L., Brown, T., Fox, K.R., (1999c) *Biochim. Biophys. Acta.* **1447**, 137-145

Keppler, M.D., Neidle, S., Fox, K.R., (2001) *Nucleic Acids Res.* **29**, 1935-1942

Kersten, W., Kersten, H., Szybalski, W., (1986) *Biochemistry* **5**, 236-244

Kibler-Herzog, L., Kell, B., Zon, G., Shinozuka, K., Mizan, S., Wilson, W.D., (1990) *Nucleic Acids Res.* **18**, 3545-3555

Kiessling, L., Griffin, L., Dervan, P.B., (1992) *Biochemistry* **31**, 2829-2834

Kiyama, R., Camerini-Otero, R.D., (1991) *Proc. Natl. Acad. Sci. USA* **88**, 10450-10454

Klevit, R.E., Wemmer, D.E., Reid, B.R., (1986) *Biochemistry* **25**, 3296-3303

Knudsen, H., Nielsen, P.E., (1996) *Nucleic Acids Res.* **24**, 494-500

Koh, J., & Dervan, P.B., (1992) *J. Am. Chem. Soc.* **114**, 1470-1478

Koshlap, K., Gillespie, P., Dervan, P.B., Feigon, J., (1993) *J. Am. Chem. Soc.* **115**, 7908-7909

Krakauer, H., & Sturtevant, J., (1968) *Biopolymers.* **6**, 491-512

Krawczyk, S.H., Milligan, J.F., Wadwani, S., Moulds, C., Froehler, B.C., Matteucci, M.D., (1992) *Proc. Natl. Acad. Sci. USA* **89**, 3761-3767

Kukreti, S., Sun, J-s., Montenay-Garestier, T., Hélène, C., (1997) *Nucleic Acids Res.* **25**, 4264-4270

Lacoste, J., François, J-C., Hélène, C., (1997) *Nucleic Acids Res.* **25**, 1991-1998

Lacroix, L., Lacoste, J., Reddoch, J.F., Mergny, J-L., Levy, D.D., Seidman, M.M., Matteucci, M.D., Glazer, P.M. (1999) *Biochemistry* **38**, 1893-1901

Lacroix, L., Arimondo, P.B., Takasugi, M., Hélène, C., Mergny, J-L., (2000) *Biochem. Biophys. Res. Commun.* **270**, 363-369

Latimer, L.J.P., Hampel, K., Lee, J.S., (1989) *Nucleic Acids Res.* **17**, 1549-1561

Latimer, L.J.P., Payton, N., Forsyth, G., Lee, J.S., (1995) *Biochem. Cell Biol.* **73**, 11-18

Le Doan, T., Perrouault, L., Praseuth, D., Habhoub, N., Decout, J-L., Thuong, N.T., Lhomme, J., Hélène, C., (1987) *Nucleic Acids Res.* **15**, 7749-7760

Lecubin, F., Benhida, R., Fourrey, J.-L., Sun, J-S., (1999) *Tetrahedron Lett.* **40**, 8085-8088

Lee, J.S., Jhonson, D., Margan, A., (1979) *Nucleic Acids Res.* **6**, 3073-3091

Lee, J.S., Woodsworth, M.L., Latimer, L.J.P., Morgan, A.R., (1984) *Nucleic Acids Res.* **12**, 6602-6614.

Lee, J.S., Latimer, L.J.P., Hampel, K.j., (1993) *Biochemistry* **32**, 5591-5597

Lee, M., Chang, D.K., Hartly, J.A., Pon, R.T., Krowicki, K., Lown, J.W., (1988) *Biochemistry* **27**, 445-455

Letai, A., Palladino, M., From, E., Rizzo, V., Fresco, J., (1988) *Biochemistry* **27**, 9180-9112

Leonetti, J.P., Mechti, N., Degols, G., Gagnor, C., Lebleu, B., (1991) *Proc. Natl. Acad. USA* **88**, 2702-2706

Lipsett, M.N., Heppel, L., Bradley, D., (1960) *Biochem. Biophys. Acta.* **41**, 175-177

Lipsett, M.N., (1963) *Biochem. Biophys. Res. Commun.* **11**, 224-231

Lipsett, M.N., (1964) *J. Biol. Chem.* **239**, 1256-1260

Liquier, J., Coffinier, P., Firon, M., Taillandier, E., (1991) *J. Biomol. Struct. Dyn.* **9**, 437-445

Liu, L.F., Liu, C-C., Alberts, B.M., (1980) *Cell* **19**, 697-672

Loke, S.L., Stein, C.A., Zhang, X.H., Mori, K., Nakanishi, M., Subasinghe, C., Cohen, J.S., Neckers, L.M., (1989) *Proc. Natl. Acad. Sci. USA* **86**, 3474-3478

Lyamichev, V., Mirkin, S., Frank-Kamenetskii, M.D., Cantor,C., (1988) *Nucleic Acids Res.* **16**, 2165-2178

Lyamichev, V.I., Frank-Kamenetskii, M.D., Soyfer, V.N., (1990) *Nature* **344**, 568-570

Lyamichev, V., Voloshin, O., Frank-Kamenetskii, M.D., (1991) *Nucleic Acids Res.* **19**, 1633-1638

Macaulay, V.M., Bates, P.J., McLean, M.J., Rowlands, M.G., Jenkins, T.C., Ashworth, A., Neidle, S., (1995) *FEBS lett.* **372**, 222-228

Macaya, R., Wang, E., Schultze, P., Sklenář, Feigon, J., (1992) *J. Mol. Biol.* **225**, 755-773

Malkov, V., Voloshin, O., Rostapshov, V., Jansen, I., Sofyer, V., Frank-Kamenetskii, M.D., (1993) *Nucleic Acids Res.* **21**, 105-111

Manfredi, J.J., Parness, J., Horwitz, S.B., (1982) *J. Cell. Biol.* **94**, 688-696

Marantz, R., Shelanski, M.L., (1970) *J. Cell Biol.* **44**, 234

Marchand, C., Bailly, C., Nguyen, C.H., Bisagni, E., Montenay-Garestier, T., Hélène, C., Waring, M.J., (1996) *Biochemistry* **35**, 5022-5032

Marchand, C., Sun, J-S., Bailly, C., Waring, M.J., Montenay-Garestier, T., Hélène, C., (1998) *Biochemistry* **37**, 13322-13329

Marky, L., & Macgregor, R., (1990) *Biochemistry* **29**, 4805-4811

Matsukara, M., Shinozuka, K., Zon, G., Mitsaya, H., Reitz, M., Cohen, J.S., Broder, S., (1987) *Proc. Natl. Acad. Sci. USA* **84**, 7706-7710

Matteucci, M., Lin, K-Y., Huang, T., Wagner, R., Sternbach, D.D., Mehrotra, M., Besterman, J.M., (1997) *J. Am. Chem. Soc.* **119**, 6939

Mergny, J-L., Collier, D., Rougèe, M., Montenay-Garestier, T., Hélène, C., (1991) *Nucleic Acids Res.* **19**, 1521-1526

Mergny, J.L., Duval-Valentin, G., Nguyen, C.H., Perrouault, L., Faucon, B., Rougee, M., Montenay-Garestier, T., Bisagni, E., Hélène, C., (1992) *Science* **256**, 1681-1684

Michel, J., Toulmé, J-J., Vercauteren, J., Moreau, S., (1996) *Nucleic Acids Res.* **24**, 1127-1135

Michel, J., Gueguen, G., Vercauteren, J., Moreau, S., (1997) *Tetrahedron Lett.* **53**, 8457-8478

Miller, P.S., McParland, K.B., Jayaraman, K., Ts'o, P.O.P., (1981) *Biochemistry* **20**, 1874-1880

Miller, P.S., Bhan, P., Cushman, C.D., Trapane, T.L., (1992) *Biochemistry* **31**, 6788-6793

Milligan, J.F., Krawczyk, S.H., Wadwani, S., Matteucci, M.D., (1993) *Nucleic Acids Res.* **21**, 327-333

Mirkin, S., Lyamichev, V., Drushlyak, K., Dobrynin, V., Frank-Kamenrtskii, K., (1987) *Nature* **330**, 495-497

Morau-Allen, A.A., Cassidy, S.A., Alvarez, J.L.A., Fox, K.R., Brown, T.,Lane, A.N., (1997) *Nucleic Acids Res.* **25**, 1890-1896

Moreau, P., Anizon, F., Sancelme, M., Prudhomme, M., Bailly, C., Carrasco, C., Ollier, M., Sevère, D., Riou, J-F., Fabbro, D., Meyer, T., Aubertin, A-M., (1998) *J. Med. Chem.* **41**, 1631-1640

Morvan, F., Rayner, B., Imbach, J-L., Thenet, S., Bertrand, J-R, Paoletti, J., Malvy, C., Paoletti, C., (1987) *Nucleic Acids Res.* **15**, 3421-3473

Moser, H., & Dervan, P.B., (1987) *Science* **238**, 645-650

Mouscadet, J.F., Ketterle, C., Goulaoic, H., Carteau, S., Subra, F., Le Bret, M., Auclair, C., (1994) *Biochemistry* **33**, 4187-4196

Musso, M., Wang, J.C., Van Dyke, M.W., (1996) *Nucleic Acids Res.* **24**, 4924-4932

Musso, M., Nelson, L.D., Van Dyke, M.W., (1998) *Biochemistry* **37**, 3086-3095

Nakajima, M., Kobayashi, K., Oshima, K., Shimada, N., Tokudome, S., Chiba, K., Yokoi, T., (1999) *Xenobiotica* **29** 885-898

Nelson, E.M., Tewey, K.M., Liu, L.F., (1984) *Proc. Natl. Acad. Sci. USA* **81**, 1361-1365

Nelson, H.C.M., Finch, J.T., Luisi, B.F., Klug, A., (1987) *Nature* **330**, 221-226

Nelson, L.D., Musso, M., Van Dyke, M.W., (2000) *J. Biol. Chem.* **275**, 5573-5581

Nielsen, P.E., Egholm, M., Berg, R.H., Buchardt, O., (1991) *Science* **245**, 1497-1500

Nielsen, P.E., Egholm, M., Buchardt, O., (1994) *J. Mol. Recognit.* **7**, 165-170

Noonberg, S.B., François, J-C., Praseuth, D., Guieysse-Peugot, A-L., Lacoste, J., Montenay-Garestier, T., Hélène, C., (1995) *Nucleic Acids Res.* **23**, 4042-4049

Olivas, W.M., & Maher III, L.J., (1995) *Nucleic Acids Res.* **23**, 1936-1941

Ono, A., Chen, C.N., Kan, L.S., (1991) *Biochemistry* **30**, 9914-9921

Ono, A., Ts'o, P.O.P., Kan, L-S., (1992) *J. Org. Chem.* **57**, 3225-3230

Orson, F.M., Klysik, J., Bergstrom, D.E., Ward, B., Glass, G.A., Hua, P., Kinsey, B.M., (1999) *Nucleic Acids Res.* **27**, 810-816

Osheroff, N., (1989) *Biochemistry* **28**, 6157-6160

Ouali, M., Letellier, R., Adnet, F., Liquier, J., Sun, J-S., Lavery, R., Taillandier, E., (1993) *Biochemistry* **32**, 2098-2103

Parel, S.P., Leumann, C.J., (2001) *Nuc. Acids Res.* **29**, 2260-2267

Phipps, A.K., Tarköy, M., Schulte, P., Feigom, J., (1998) *Biochemistry* **37**, 5820-5830

Pilch, D.S., Levenson, C.,Shafer, R.H., (1991) *Biochemistry* **30**, 6081-6087

Pilch, D.S., Waring, M.J., Sun, J-S., Rougée, M., Nguyen, C.H., Bisagni, E., Garestier, T., Hélène, C., (1993) *J. Mol. Biol.* **232**, 926-946

Pinto, A.L., Lippard, S.J., (1985) *Biochim. Biophys. Acta.* **780**, 167-180

Plum, G.E., Park, Y-W., Singleton, S.F., Dervan, P.B., Breslauer, K.J., (1990) *Proc. Natl. Acad. Sci. USA* **87**, 9436-9440

Pommier, Y., Pourquier, P., Fan, Y., Strumberg, D., (1998) *Biochim Biophys Acta* **1400**, 83-106

Raae, A., & Kleppe, K., (1978) *Biochemistry* **17**, 2939-2942

Radhakrishnan, I., Santos, C., Patel, D., (1991) *J. Mol. Biol.* **221**, 1403-1418

Radhakrishnan, I., Patel, D., Priestly, E., Nash, H., Dervan, P.B., (1993) *Biochemistry* **32**, 11228-11234

Radhakrishnan, I., & Patel, D.J., (1993) *Structure* **1**, 135-152

Radhakrishnan, I., & Patel, D.J., (1994a) *Structure* **2**, 17-32

Radhakrishnan, I., & Patel, D.J., (1994b) *Structure* **2**, 395-405

Raghunathan, G., Miles, H.T., Sasisekharan, V., (1993) *Biochemistry* **32**, 455-462

Raha, M., Wang, G., Seidman, M.M., Glazer, P.M., (1996) *Biochemistry* **93**, 2941-2946

Rajagopal, P., Feigon, J., (1989) *Biochemistry* **28**, 7859-7870

Rao, J.E., Miller, P.S., Craig, N.L., (2000) *Proc. Natl. Acad. Sci. USA* **97**, 3936-3941

Rao, J.E., Craig, N.L., (2001) *J. Mol. Biol.* **307**, 1161-1170

Rau, D.C., Parsegian, V.A., (1992) *Biophys. J.* **61**, 246-259

Read, M., Harrison, R.J., Romagnoli, B., Tanious, F.A., Gowan, S.H., Reszka, A.P., Wilson, W.D., Kelland, L.R., Neidle, S., (2001) *Proc. Natl. Acad. Sci. USA* **98**, 4844-4849

Ren, J., Chaires, J.B., (1999) *Biochemistry* **38**, 16067-16075

Rentzeperis, D., Kupke, D., Marky, L., (1992) *Biopolymers* **32**, 1065-1075

Rhee, S., Han, Z-J., Liu, H., Miles, T., Davies, D.R., (1999) *Biochemistry* **38**, 16810-16815

Riley, M., Maling, B., Chamberlin, M.J., (1966) *J. Mol. Biol.* **20**, 359-389

Roberts, R.W., & Crothers, D.M., (1991) *Proc. Natl. Acad. Sci. USA* **88**, 9397-9401

Roberts, R.W., Crothers, D.M., (1996) *Proc. Natl. Acad. Sci. USA* **93**, 4320-4325

Robles, J., Rajur, S.B., McLaughlin, L.W., (1991) *J. Am. Chem. Soc.* **118**, 5820-5821

Rooney, S.M., Moore, P.D., (1995) *Proc. Natl. Acad. Sci. USA* **92**, 2141-2144

Rosenberg, B., Van Camp, C., Krigas, T., (1965) *Nature* **205**, 698-699

Rougée, M., Faucon, B., Mergny, J.L., Barcelo,F., Giovannangéli, C., Montenay-Garestier, T., Hélène, C., (1992) *Biochemistry* **31**, 9269-9278

Rubin, E., McKee, T., Kool, E., (1993) *J. Am. Chem. Soc.* **115**, 361-362

Safa, A.R., Hamel, E., Felsted, R.L., (1987) *Biochemistry* **26**, 97-102

Sandor, Z., & Bredberg, A., (1994) *Nucleic Acids Res.* **22**, 2051-2056

Sandor, Z., Bredberg, A., (1995) *FEBS Lett.* **374**, 287-291

Sasaki, S., Yamauchi, H., Nagatsugi, F., Takahashi, R., Taniguchi, Y., Maeda, M., (2001) *Tettrahedron Lett.* **42**, 6915-6918

Scaria, P.V., Shafer, R.H., (1991) *J. Biol. Chem.* **226**, 5417-5423

Schiff, P.B., & Horwitz, S.B., (1980) *Proc. Natl. Acad. Sci. USA* **77**, 1561-1565

Schluep, T., & Cooney, C., (1998) *Nucleic Acids Res.* **26**, 4524-2528

Sen, D., & Gilbert, W., (1990) *Nature* **334**, 410-414

Silver, G.C., Sun, J-S., Ngayen, C.H., Boutorine, A.S., Bisagni, E., Hélène, C., (1997) *J. Am. Chem. Soc.* **119**, 263-268

Singleton, S.F., & Dervan, P.B. (1992) *Biochemistry* **31**, 10995-11003

Sofyer, V., Voloshin, O., Malkov, V., Frank-Kamenetskii, M.D., (1992) *Structure & Function* **1** : *Nucleic Acids* 29-41

Sollogoub, M., Dominguez, B., Fox, K.R., Brown, T., (2000) *Chem. Commun.* **2000**, 2315-2316

Stabuli, A.B., Dervan, P.B., (1994) *Nucleic Acids Res.* **22**, 2637-2642

Stein, C.A., Subasinghe, C., Shinozuka, K., Cohen, J.S., (1998) *Nucleic Acids Res.* **16**, 3209-3221

Stilz, H.U., Dervan, P.B., (1993) *Biochemistry* **32**, 2177-2185

Suck, D., Lahm, A., Oefner, C., (1988) *Nature* **332**, 464-468

Summerton, J., & Weller, D., (1997) *Antisense Nucleic Acids Drug Dev.* **7**, 187-195

Sun, J-S., François, J-C., Montenay-Garestier, T., Saison-Behmoaras, T., Roig, V., Thuong, N.T., Hélène, C., (1989) *Proc. Natl. Acad. Sci. USA* **86**, 9198-9202

Sun, J-S., De Bizemont, T., duval-Valentin, G., Montenay-Garestier, T., Hélène, C., (1991) *CR. Acad. Sci. Paris Sér III* **313**, 585-590

Svinarchuk, F., Cherny, D., Debin, A., Delain, E., Malvy, C., (1996) *Nucleic Acids Res.* **24**, 3858-3865

Takasagi, M., Guendouz, A., Chassignol, M., Decoult, J.L., Lhomme, J., Thuong, N.T., Hélène, C., (1991) *Proc. Natl. Acad. Sci. USA* **88**, 5602-5606

Tao, N., Lindsay, S., Rupprecht, A., (1989) *Biopolymers* **28**, 1019-1030

Tewey, K.M., Chen, G.L., Nelson, E.M., Liu, L.F., (1984) *J. Biol. Chem.* **259**, 9182-9187

Thomas, T., & Thomas, T.J., (1993) *Biochemistry* **32**, 14068-14074

Thuong, N.T., & Hélène, C., (1993) *Angew. Chem. Int. Ed. Engl.* **32**, 666-690

Tibanyenda, N., De Brunin, S., Haasnot, C., Van Der Marcel, G., Van Boom, J., Hilbers, C., (1984) *Eur. J. Biochem.* **139**, 19-27

Torigoe, H., (2001) *Biochemistry* **40**, 1063-1069

Tullius, T.D., (1987) *TIBS* **12**, 297-300

Tung, C-H., Breslauer, K.J., Stein, S., (1993) *Nucleic Acids Res.* **21**, 5489-5494

Tyler, B.M., Jansen, K., McCormick, D.J., Douglas, C.L., Boules, M., Stewart, J.A., Zhao, L., Lacy, B., Cusack, B., Fauq, A., Richelson, E., (1999) *Proc. Natl. Acad. Sci. USA* **96**, 7053-7058

Umezawa, H., Maeda, K., Takeuchi, T., Okami, Y., (1966) *J. Antibiot.* **19**, 200-209

Umezawa, H., Ishizuka, M., Iwanaga, J., Takeuchi, T., (1968) *J. Antibiot.* **21**, 592-602

Van Dyke, M.W., Hertzberg, R.P., Dervan, P.B., (1982) *Proc. Natl. Acad. Sci. USA* **79**, 5470-5474

Van Dyke, M.W., & Dervan, P.B., (1984) *Science* **225**, 1122-1127

Van Dyke, M.W., & Dervan, P.B., (1985) *Biochemistry* **22**, 2373-2377

Völker, J., & Klump, H.H., (1994) *Biochemistry* **33**, 13502-13508

Wagner, R.W., Matteucci, M.D., Lewis, J.G., Gutierrez, A.J., Moulds, C., Froehler, B.C., (1993) *Science* **260**, 1510-1513

Wagner, R.W., (1994) *Nature* **372**, 333-335.

Wagner, R.W., Tarköy, M., Schulte, P., Feigon, J., (1998) *Biochemistry* **37**, 5820-5830

Wang, G., Glazer, P.M., (1995) *J. Biol. Chem.* **270**, 22595-22601

Wang, E., Koshlap, K., Gillespe, P., Dervan, P.B., Feigon, J., (1996) *J. Mol. Biol.* **257**, 1052-1069

Wang, J.C., (1996) *Annu. Rev. Biochem.* **65**, 635-692

Waring, M.J., (1965) *J.Mol.Biol.* **13**, 269-282

Waring, M.J., (1966) *Biochim. Biophys. Acta.* **114**, 234-244

Waring, J.M., (1974) *Biochem. J.* **143**, 483-486

Washbrook, E., Fox, K.R., (1994) *Nucleic Acids Res.* **22**, 3977-3982

Watson, J., & Crick, F., (1953) *Nature* **171**, 737-738

Williamson, J.R., Raghuraman, M.K., Cech, T.R., (1989) *Cell* **59**, 871-880

Wilson, W.D., Tanious, F.A., Mizan, S., Yoa, S., Kiselyov, A.S., Zon, G., Strkowski, L., (1993) *Biochemistry* **32**, 10614-10621

Wittung, P., Nielsen, P.E., Norden, B., (1996) *J. Am. Chem. Soc.* **31**, 7049-7054

Wittung, P., Nielsen, P.E., Nordén, B., (1997) *Biochemistry* **36**, 7973-7979

Xiang, G., Soussou, W., McLaughlin, L., (1994) *J. Am. Chem. Soc.* **116**, 11155-11156

Xodo, L.E., Manzini, G., Quadrifoglio, F., Van Der Marcel, G., Boom, J., (1991) *Nucleic Acids Res.* **18**, 3557-3564

Xodo, L.E., Alunni-Fabbroni, M., Manzini, G., Quadrifoglio, F., (1993) *Eur. J. Biochem.* **212**, 395-401

Yoon, K., Hobbs, C., Koch, J., Sardaro, M., Kutny, R., Weis, A., (1992) *Proc. Natl. Acad. Sci. USA* **89**, 3840-3844

Young, S.L., Krawczyk, S.H., Matteucci, M.D., Toole, J.J., (1991) *Proc. Natl. Acad. Sci. USA* **88**, 10023-10026

Zamecnik, P.C., Goodchild, J., Taguchi, Y., Sarin, P.S., (1986) *Proc. Natl. Acad. Sci. USA* **83**, 4143-4146

Zhou-Sun, B.W., Sun, J-S., Gryaznov, S.M., Liquier, J., Garestier, T., Hélène, C., Tailandier, E., (1997) *Nucleic Acids Res.* **25**, 1782

Zimmer, C., (1975) *Progr. Nucl. Acids Res. Mol. Biol.* **15**, 285-311

Zimmer, C., Marck, C., Schneider, C., Guschlbauer, W., (1979) *Nuc. Acids Res.* **6**, 2831-2837